

NEW TRENDS IN SUPRAMOLECULAR CHEMISTRY

EDITED BY

VOLODYMYR I. RYBACHENKO

Supramolecular
Chemistry

Nanotechnology

Self-organization

Molecular
recognition

**NEW TRENDS
IN SUPRAMOLECULAR CHEMISTRY**

Collected research papers

EDITED BY

VOLODYMYR I. RYBACHENKO

DONETSK

«EAST PUBLISHER HOUSE»

2014

УДК 541.1+547

O 80

Reviewers: Opeida I.A. – professor

Grzesiak Piotr – professor

Recommended for printing academic councils of L. Litvinenko Institute Physical Organic and Coal Chemistry National Academy of Science of Ukraine & Faculty of Chemistry Adam Mickiewicz University in Poznań, Poland

O 80 New trends in supramolecular chemistry [collected research papers]

Edited by V.I. Rybachenko.

Donetsk: «East Publisher House»

Ltd, 2014. – 356 p.

ISBN 978-966-317-208-8

Supramolecular chemistry it is interdisciplinary scientific field. The monograph presents various lines of research in the field of nanotechnology, interaction and self-organization of molecules.

Супрамолекулярная химия это междисциплинарное научное поле. В монографии представлены различные направления исследований в области нанотехнологий, взаимодействия и самоорганизации молекул.

УДК 541.1+547

O 80

ISBN 978-966-317-208-8

© Collective of authors, 2014

Contents

List of contributors	5
Supramolecular systems based on lanthanide complexes with modified calix[4]arenes as fluorescent receptors for metal cations	11
<i>Natalya Rusakova, Olga Snurnikova and Ninel Efrushina</i>	
Molecular complexes of carbohydrate-containing metabolites with antibiotics	49
<i>Leonid Yakovishin, Vladimir Grishkovets, Elena Korzh, Grzegorz Schroeder and Volodymyr Rybachenko</i>	
Phenylboronic acids-containing nanoparticles	71
<i>Alicja Pawelko, Agnieszka Adamczyk-Woźniak and Andrzej Sporzyński</i>	
Boronic acids immobilized on diol-functionalized resins	85
<i>Łukasz Włoszczak, Krzysztof M. Borys, Agnieszka Adamczyk-Woźniak and Andrzej Sporzyński</i>	
Electronic structure of the organic compounds and their reactivity in the reactions of radical hydrogen atom tear by HO ₂ • radical	103
<i>A.F. Dmitruk, L.F. Pikula, T.V. Kryuk and Yu.O. Lesishina</i>	
Application of mesoporous silica nanoparticles for drug delivery ...	113
<i>David Lewandowski and Grzegorz Schroeder</i>	
Surface modification of natural halloysite nanotubes. The hybrid materials for nanotechnology	147
<i>Joanna Kurczewska, Agnieszka Michalska, Kajetan Pyrzyński and Grzegorz Schroeder</i>	

Acid-base equilibria in ‘oil-in-water’ microemulsions. The particular case of fluorescein dyes	159
<i>Nikolay O. Mchedlov-Petrossyan, Natalya V. Salamanova and Natalya A. Vodolazkaya</i>	
Functional polymers forming complexes with metal ions	185
<i>Michał Cegłowski and Grzegorz Schroeder</i>	
Application of dilational rheology for analyze the properties of interfacial layers supramolecular systems	205
<i>Svetlana Khil’ko and Volodymyr Rybachenko</i>	
Oligomerization thermodynamics of fatty alcohols and carboxylic acids at the air/water interface. Quantum chemical approach	217
<i>E. S. Fomina, E. A. Belyaeva and Yu. B. Vysotsky</i>	
Inverse phase transfer catalysis in organic synthesis	251
<i>Viktor Anishchenko, Volodymyr Rybachenko, Grzegorz Schroeder, Konstantine Chotiy and Andrey Redko</i>	
Solubilization of carbon nanotubes in water and in organic solvents	281
<i>Grażyna Bartkowiak and Grzegorz Schroeder</i>	
Thin CVD diamond films – synthesis, properties, applications	303
<i>Robert Bogdanowicz</i>	
Design and reactivity of alpha nucleophiles for decontamination reactions: relevance to functionalized surfactants	327
<i>Namrata Singh, Yevgen Karpichev, Kamil Kuca and Kallol K. Ghosh</i>	

List of contributors

Agnieszka Adamczyk-Woźniak

Warsaw University of Technology
Faculty of Chemistry
Noakowskiego 3
00-664 Warsaw, Poland

Viktor Anishchenko

L.M. Litvinenko Institute of physical-Organic and Coal Chemistry
National Academy of Science of Ukraine
Department of Spectrochemical Researches
R. Luxemburg 70
81-134 Donetsk, Ukraine

Grażyna Bartkowiak

Adam Mickiewicz University in Poznań
Faculty of Chemistry
Umultowska 89b
61-614 Poznań, Poland

E. A. Belyaeva

Donetsk National Technical University
58 Artema Str.
83000 Donetsk, Ukraine

Robert Bogdanowicz

Gdansk University of Technology
Faculty of Electronics, Telecommunications and Informatics
Gabriela Narutowicza 11/12
80-233 Gdańsk, Poland

Krzysztof M. Borys

Warsaw University of Technology
Faculty of Chemistry
Noakowskiego 3
00-664 Warsaw, Poland

Michał Ceglowski

Adam Mickiewicz University in Poznań
Faculty of Chemistry
Umultowska 89b
61-614 Poznań, Poland

Konstantine Chotiy

L.M. Litvinenko Institute of physical-Organic and Coal Chemistry
National Academy of Science of Ukraine
Department of Spectrochemical Researches
R. Luxemburg 70
81-134 Donetsk, Ukraine

A.F. Dmitruk

Donetsk National University of Economics and Trade named after
Mykhailo Tugan-Baranovsky
Schersa Str. 31
83050 Donetsk, Ukraine

Ninel Efryushina

A.V. Bogatsky Physico-Chemical Institute NAS of Ukraine
Lustdorfskaya Doroga 86
65080 Odessa, Ukraine

E. S. Fomina

Donetsk National Technical University
Artema Str.
83000 Donetsk, Ukraine

Kallol K. Ghosh

School of Studies in Chemistry
Pt. Ravishankar Shukla University
492010 Raipur (C.G), India

Vladimir Grishkovets

V.I. Vernadsky Taurida National University
Vernadsky Ave. 4
Simferopol 95007, Crimea, Ukraine

Yevgen Karpichev

L.M. Litvinenko Institute of physical-Organic and Coal Chemistry
National Academy of Science of Ukraine
Department of Spectrochemical Researches
R. Luxemburg 70
81-134 Donetsk, Ukraine

Svetlana Khil'ko

L.M. Litvinenko Institute of Physical-Organic and Coal Chemistry
National Academy of Sciences of Ukraine
R. Luxemburg Street 70
Donetsk 83114, Ukraine

Elena Korzh

Sevastopol National Technical University
Universitetskaya Str. 33
Sevastopol 99053, Crimea, Ukraine

T.V. Kryuk

Donetsk National University of Economics and Trade named after
Mykhailo Tugan-Baranovsky
Schersa Str. 31
83050 Donetsk, Ukraine

Kamil Kuca

University of Hradec Kralove
Faculty of Science,
Department of Chemistry
Rokitanskeho 62
50003 Hradec Kralove, Czech Republic

Joanna Kurczewska

Adam Mickiewicz University in Poznań
Faculty of Chemistry
Umultowska 89b
61-614 Poznań, Poland

Yu.O. Lesishina

Donetsk National University of Economics and Trade named after
Mykhailo Tugan-Baranovsky
Schersa Str. 31
83050 Donetsk, Ukraine

Dawid Lewandowski

Adam Mickiewicz University in Poznań
Faculty of Chemistry
Umultowska 89b
61-614 Poznań, Poland

Nikolay O. Mchedlov-Petrossyan

V.N. Karazin Kharkov National University
Svoboda Sq. 4
61022 Kharkov, Ukraine

Agnieszka Michalska

Delta Innovations and Implementation Company
Krupczyn 5
63-140 Dolsk , Poland

Alicja Pawelko

Warsaw University of Technology
Faculty of Chemistry
Noakowskiego 3
00-664 Warsaw, Poland

L.F. Pikula

Donetsk National University of Economics and Trade named after
Mykhailo Tugan-Baranovsky
Schersa Str. 31
83050 Donetsk, Ukraine

Kajetan Pyrzyński

Delta Innovations and Implementation Company
Krupczyn 5
63-140 Dolsk , Poland

Andrey Redko

L.M. Litvinenko Institute of physical-Organic and Coal Chemistry
National Academy of Science of Ukraine,
Department of Spectrochemical Researches
R. Luxemburg 70
81-134 Donetsk, Ukraine

Natalya Rusakova

A.V. Bogatsky Physico-Chemical Institute NAS of Ukraine
Lustdorfskaya Doroga 86
65080 Odessa, Ukraine

Volodymyr Rybachenko

L.M. Litvinenko Institute of physical-Organic and Coal Chemistry
National Academy of Science of Ukraine
Department of Spectrochemical Researches
R. Luxemburg 70
81-134 Donetsk, Ukraine

Natalya V. Salamanova

V.N. Karazin Kharkov National University
Svoboda Sq. 4
61022 Kharkov, Ukraine

Grzegorz Schroeder

Adam Mickiewicz University in Poznań
Faculty of Chemistry
Umultowska 89b
61-614 Poznań, Poland

Namrata Singh

School of Studies in Chemistry
Pt. Ravishankar Shukla University
492010 Raipur (C.G), India

Olga Snurnikova

A.V. Bogatsky Physico-Chemical Institute NAS of Ukraine
Lustdorfskaya Doroga 86
65080 Odessa, Ukraine

Andrzej Sporzyński

Warsaw University of Technology
Faculty of Chemistry
Noakowskiego 3
00-664 Warsaw, Poland

Natalya A. Vodolazkaya

V.N. Karazin Kharkov National University
Svoboda Sq. 4
61022 Kharkov, Ukraine

Yu. B. Vysotsky

Donetsk National Technical University
Artema Str. 58
83000 Donetsk, Ukraine

Łukasz Włoszczak

Warsaw University of Technology
Faculty of Chemistry
Noakowskiego 3
00-664 Warsaw, Poland

Leonid Yakovishin

Sevastopol National Technical University
Universitetskaya Str. 33
Sevastopol, 99053, Crimea, Ukraine

Chapter 1

Supramolecular systems based on lanthanide complexes with modified calix[4]arenes as fluorescent receptors for metal cations

Natalya Rusakova, Olga Snurnikova and Ninel Efryushina
*A.V. Bogatsky Physico-Chemical Institute NAS of Ukraine,
Lustdorfskaya Doroga 86, 65080 Odessa, Ukraine*

The number of publications devoted to polynuclear complexes of lanthanides is steadily increasing. The greatest part of works devoted to heteronuclear complexes of lanthanides with s- and d-elements, in which interest is dictated primarily by their practical application, especially in quantum optics and electronics. The effect of s-metals on the 4f-luminescence was considered in lanthanide-containing compounds that emit in the visible region of the spectrum. As for publications on lanthanide complexes with so-called essential d-elements (copper, zinc, cobalt, nickel, chromium, iron, etc.) the majority of them are devoted to the development of synthetic models of natural ionophores and sensors for biology and medicine. The range of publications that focus on the possibility of using multidentate macrocyclic compounds as a basis for obtaining polynuclear lanthanide complexes is very limited, which determines the prospects of such research. In particular, it is related with the search for new photochromic compounds and approaches for solving the problems of perception of the optical information, including living systems [1-6]. The main advantage of the use of chromophoric macrocyclic ligands compared to acyclic analogs is the presence of already formed molecular cavity preorganized for coordination of lanthanides with appropriate ionic radii, and attached chromophores capable of efficient absorption of the exciting light for sensitization of 4f-luminescence [7-10].

After the publication of van Veggel, dedicated to sensitization of intrinsic luminescence of Nd(III) and Yb(III) in the complexes containing ruthenium bipyridyl and ferrocene, the use of light-absorbing metal complex chromophores as sensitizers of 4f-luminescence has attracted the attention of many research

groups. The term “metal-containing chromophores” have been used until now. A lot of articles were published on the effect of d-metal complex chromophores containing such ions as Pt(II), Ru(II), Re(I), Os(II), Pd(II), Cr(III) on the 4f-luminescence. Their energy levels are in the range of 13000 - 18000 cm^{-1} in most cases, which is favorable for transfer of excitation energy primarily to the resonant levels of lanthanide ions that emit in the infrared region [11-13].

1. Functionalized phenolic-type calix[4]arenes: general characteristics and applications

Calix[n]arenes are macrocyclic products of cyclic oligomerization of phenol with formaldehyde. These compounds are interesting due to the following reasons: the relative ease of preparation, the rigidity of the macrocyclic platform allowing to put binding sites as required, conformational diversity, the opportunity of modification of phenolic groups, aromatic rings and bridged fragments by different functional groups. Calix[n]arenes are compounds in which a modification of one fragment affects all spatial structure of the macrocyclic framework and leads to a change in properties of whole molecule (e.g. complexing, optical, magnetic, etc.) [14-16]. However, the systematic researches in this area are practically not carried out. Furthermore, the calix[n]arene are capable to form inclusion complexes of the “host-guest” type with neutral and charged molecules, thereby they are used for the creation of an effective chelating ligands, extractants, as well as for membrane and phase transfer of low molecular weight substrates such as ions of toxic and heavy metals [17-19].

Polytopic calix[n]arene structure is provided by upper (wider) and lower rims (Fig. 1, a). The inclusive ability of hydrophobic aromatic cavity and coordination properties of substituents on upper and lower rims are used to obtain homo- or heteronuclear complexes and supramolecular assemblies based on them.

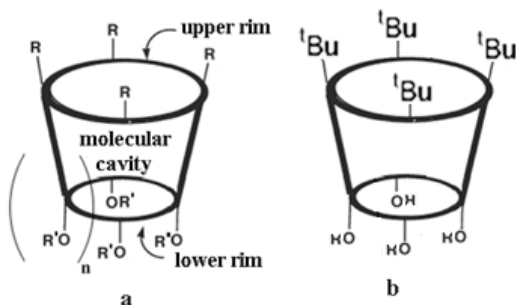


Figure 1. Schematic formula of calix[n]arenes (a, $n=0-5$) and TBC (b)

The size of intramolecular cavity of compounds depends on the number (n) of phenolic fragments, and a set of the donor-acceptor centers depends on number and nature of substituents (R and R') [20]. *p-tert*-Butylcalix[4]arene (TBC, Fig. 1, b) has been studied widely in terms of functionalization with substituents of different nature. Analysis of publications allows selecting three main aspects in modification of calixarene macrocycle. The first one is related to the need to change the size or conformational properties of the ligand cavity, for example, to increase the selectivity in extraction processes [21-23]. The second one provides the increase or the decrease of solubility for bonding substrates containing multiple functional groups, such as amino acids or biopolymers. The third aspect is related with the introduction of additional centers for the coordination of metal ions thus the selectivity of calix[n]arenes increases [24-28].

Besides varying the number of phenol rings, the change in dimensions of the cavity of the macrocycle is achieved by replacing the methylene (-CH₂-) bridge to a silanol (-SiR₂-), sulfur (-S-, -SO-, -SO₂-), oxygen (-CH₂-O-CH₂-) or nitrogen-containing fragments (-CH₂-N-CH₂-), which affects the inclusive ability of cavity for "guests" molecules [14, 29]. In [30, 31] it was shown that the replacement of methylene bridges in TBC on the sulfur atoms increases the size of the macrocyclic cavity in the "cone" conformation from 7.1-7.2 Å to 7.6-7.7 Å and creates new features in chemical behavior and the complexing ability of the ligand. However, the determination of the conformation of macrocycle by ¹H NMR spectra is greatly complicated due to the absence of bridging methylene protons.

One of the earliest examples of modification of *p-tert*-butylcalix[4]arene is the exchange of phenolic protons of lower rim to alkyl radicals. Their introduction increases the inversion barrier and hinders mutual transitions of conformers of ligand [24, 32]. Replacement of four protons on propyl or more bulky groups stabilizes the calix[4]arene molecule in the preferred "cone" conformation. The disadvantage of such functionalization is the decreasing of solubility in polar solvents, which greatly limits the application of the above derivatives.

In addition to conformational features, one of the important properties of calix[4]arenes is their solubility in different environments. Increasing the solubility in water is achieved by functionalization of the upper/lower rims positively (negatively) charged or neutral hydrophilic groups (-N⁺R₃, -SO₃⁻, -NO₂, -COOH, -PO₃H₂). The first example of water-soluble calixarene was tetracarboxy derivative of TBC which solubility in water is 0.5 g per 100 g of water at 298 K [16, 36]. *p*-Tetrasulfocalix[4]arene functionalized with four SO₃⁻ groups at upper rim has the highest solubility in water (7.5 g in 100 g of water) of the presently known synthesized calix[n]arenes [33-37].

Along with the development of synthetic methods of calix[4]arenes with appropriate functional groups to regulate the solubility, studies on the acid-base properties was carried out. This is primarily related to the study of synthetic receptors. Known data [14, 32, 38-41] suggest that due to the spatial structure calix[4]arenes are stronger acids than their monomers and non-cyclic analogues. In [39, 40] acid-base dissociation constants of TBC ($pK_1 = 4-5$; $pK_2 = 11-12$; $pK_3, pK_4 > 14$; Fig. 2, a) were determined. The first dissociation constant of TBC is between the values of medium strength acids and weak acids (compared to the pK of acetic acid, 4.8 ± 0.1), while a *p-tert*-butylphenol ($pK_a = 10.16 \pm 0.05$) and phenol ($pK_a = 9.6 \pm 0.1$) [29] are very weak acids. Unusual properties of one of the phenolic protons (called in the literature “superacidic proton” [14]) were explained by the stabilization of the monoanion, which formed at dissociation of one phenolic group (Fig. 2b). A series of experimental methods and semi-empirical calculations has shown that the oxygen atom of phenolate anion forms strong hydrogen bonds with neighboring OH groups which stabilize the anion and prevent further dissociation of the second OH group, thus explain too high value of pK_2 , compared with non-cyclic analogs. Unusual acidity of the first proton is preserved under the introduction of various substituents on the upper rim (pK_1 (*p*-sulfocalix[4]arene) = 3.08 [40] and pK_1 (*p*-nitrocalix[4]arene) < 0 [39]), and under replacing of methylene bridges in macrocyclic ligand, for example, pK_1 (*p*-tetrasulfothiacalix[4]arene) = 2.18 [41]).

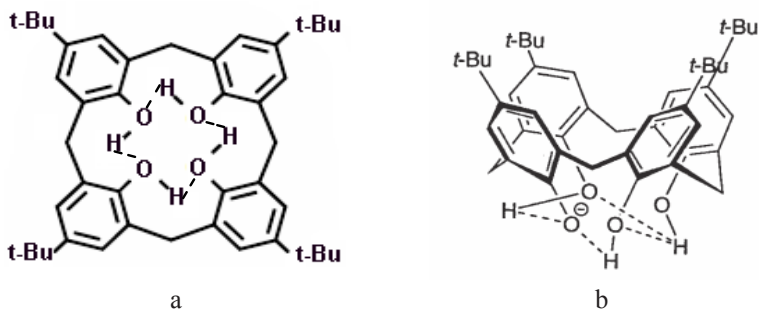


Figure 2. Representation of intramolecular hydrogen bonds in *p-tert*-butylcalix[4]arene (H₄L, a) and its monoanion (H₃L⁻, b)

The nature of the solvent is an important factor that must be considered at determining the dissociation constants of calix[4]arenes. At least two mechanisms of interaction of solvent molecules with calix[4]arenes can be distinguished. The first of them is the participation of solvent molecules in the formation of hydrogen

bonds with the OH groups of the ligand H_4L and its monoanion H_3L^- . The second mechanism involves the formation of inclusion complexes by hydrophobic cavity, which is accompanied by changes in the electron density on the phenolic oxygen atoms. But theory that takes into account both of these mechanisms has not been developed. This is probably due to the acid-base properties of calix[4]arenes in mixed organic or aqueous-organic media, which were used. It should be noted that substituents such as $-NH_2$, $-COOH$, $-PO_3H_2$ also participate in the formation of intermolecular hydrogen bonds similarly to the phenolic groups [42-44].

The X-ray diffraction results for TBC and its derivatives suggest that the calixarenes have the ability to form inclusion complexes (clathrates) with solvent molecules. It was found that calix[4]arenes form inclusion complexes with small organic molecules: acetone [42], acetic acid [47], benzene, toluene, *p*-xylene, anisole [43] due to $CH-\pi$ - and $\pi-\pi$ -interaction [45, 46]. These studies formed the basis of application of calix[n]arene macrocycles (or, as they are often called in the literature, "calixarene platforms") as receptors in "host-guest" chemistry. Thus, the use of TBC for determining cations of metals is rather limited due to poor solubility in water and many organic solvents, low selectivity and strength of binding cations [14, 43, 45-48]. Currently various techniques of TBC modification were developed. However, the most affordable and common method is still selective alkylation OH-groups of the lower rim in the presence of the respective bases (Fig. 3) [49, 50]

After the development of methods for the alkylation on ester derivatives ($R=-CH_3$, $-C_2H_5$, $-C_3H_7$) carboxymethoxy-*p*-*tert*-butylcalix[4]arenes ($R=-CH_2COOH$) were obtained. The first synthesis of tetracarboxy substituted TBC was carried by R. Ungaro in 1983-1985 [14]. The degree of substitution and the predominant conformation of the resulting product are determined by several factors, among which the main role is played by the strength of the base and the nature of its cation.

It is known that 1,2-derived compounds usually are obtained by indirect methods with introducing protecting groups (benzyl, propyl, methyl). The synthesis of only two trisubstituted calix[4]arenes is described in the literature. This indicates that techniques of synthesis of trisubstituted compounds with different nature of substituents are not well developed to date. The effect of sequential introduction of substituents on the physico-chemical, in particular, complexed and spectral-luminescent properties of calix[4]arene studied very limited. In general, analysis of the published data suggests that the substitution of *p*-*tert*-butylcalix[4]arene is carried out mainly by two or four phenol groups (symmetric ligands). The synthesis of asymmetric calix[4]

arenes is less developed and their properties are virtually unexplored. As can be seen from applied synthetic procedure leads to the formation of a mixture of conformational isomers which in its turn, requires multiple purification of the compounds. On the other hand, several methods which are described in the literature involve the introduction of protective groups. The last ones increase the number of synthetic steps and, consequently, lead to lowering of the product yields [51-56].

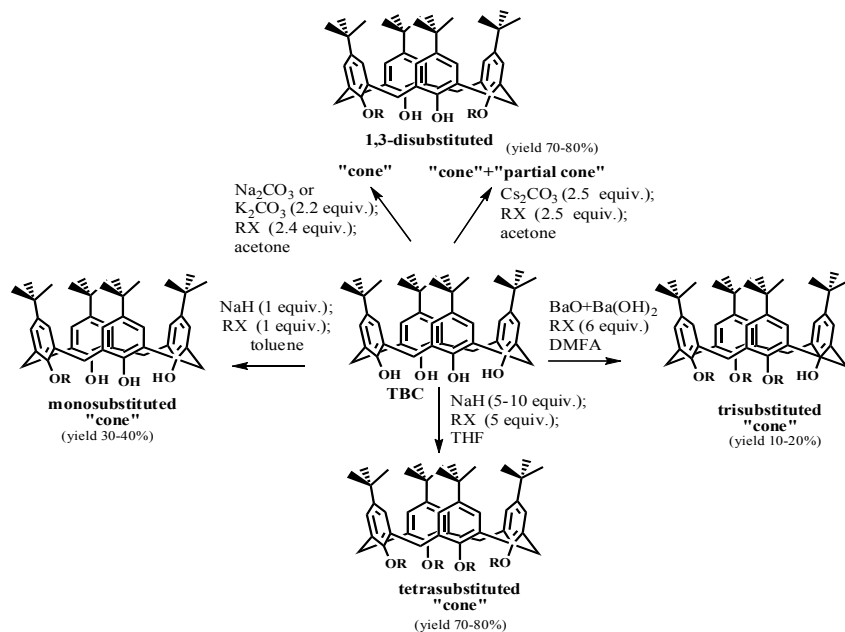


Figure 3. Scheme of synthesis of sequentially substituted *p*-tert-butylcalix[4]arenes

Subsequent development of chemistry of calixarene receptors involves obtaining of modified calix[4]arenes based on appropriate substituted TBC. The most suitable derivatives are carboxylic ligands. The formation of amide or ester bonds allows introducing into the calixarene molecule fragments, which are capable of imparting new properties, such as spectral, coordinational or biological. Thus, it is proved that the amide group makes a double contribution to the formation of complexes. At first, the carbonyl moieties and the oxygen atoms of the ester groups form an intramolecular cavity, which may include

cations. Secondly, the anion coordination with the NH-moiety increases stability of the formed complexes. For example, it was obtained new supramolecular polytopic receptors, based on the carboxyl and amino derivatives of calix[4]arenes, in which calix[4]arene and azacrown ether fragments are separated by spacer groups, (Fig. 4, [14]).

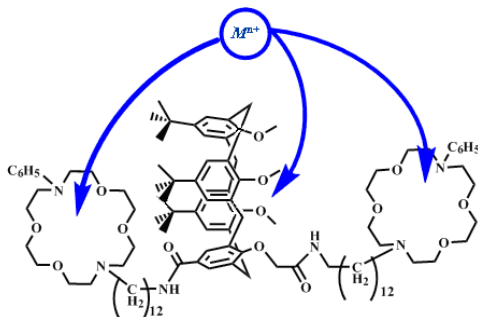


Figure 4. Possible ways of metal cations complexation by calix[4]arene modified with azacrown ether moieties

The next stage in the development of chemistry of functionalized calixarenes was the creation of compounds on their basis, which contain both coordination-active groups and additional chromophoric fragments. Such compounds in the literature are called chromophore or fluorescent sensors or receptors. The receptor consists of an ion-recognizing fragment (an ionophore), the signal part (chromophore/fluorophore) and the bridge between them (the “spacer”, Figure 5).

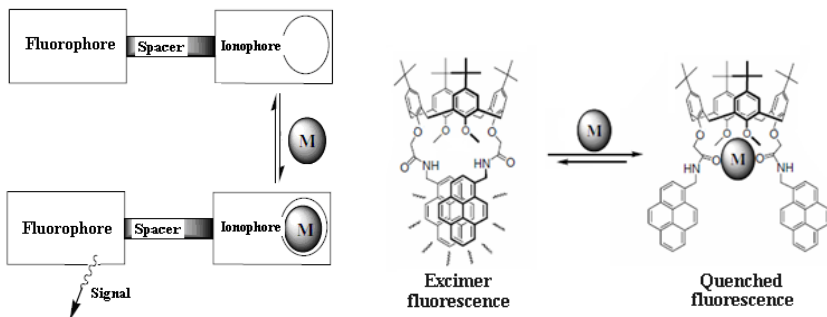


Figure 5. The scheme of action of fluorescent sensor

Chromophoric moiety converts the chemical information obtained by the interaction between the ionophore and the cations (anions) in the optical signal. The mechanism of the photophysical changes occurring at the binding of the ion is associated with a redistribution of the electron density in the molecule as a result of the PET effect («Photoinduced Electron Transfer»). Excitation of the fluorophore (acceptor) allows the electronic transition from ionophore (donor) to the fluorophore causing fluorescence quenching of the latter. After binding the cation to receptor the PET effect is not realized, and the sensor starts to fluoresce.

If fluorophore of sensor in addition to the electron acceptor part also contains an electron donor fragment, it gives so-called PCT-effect («Photoinduced Charge Transfer») due to the interaction of charged fluorophore and ionophore. It leads to batho- or hypsochromic shift of the absorption and emission as well as changes in their characteristics. In disubstituted receptors containing two identical or different fluorophores photochemical changes under the complexation also can be described by FRET-effect («Fluorescence Resonance Energy Transfer») caused by the interaction in pairs of fluorophores in their excited states. As a result of the dipole-dipole interaction of the excited state of the fluorescent donor is transferred to the acceptor and donor returns to its ground state.

Examples of fluorescent sensors based on TBC where as the fluorophores are used conjugated aromatic substituents (naphthalene and pyrene) are shown in Fig. 6.

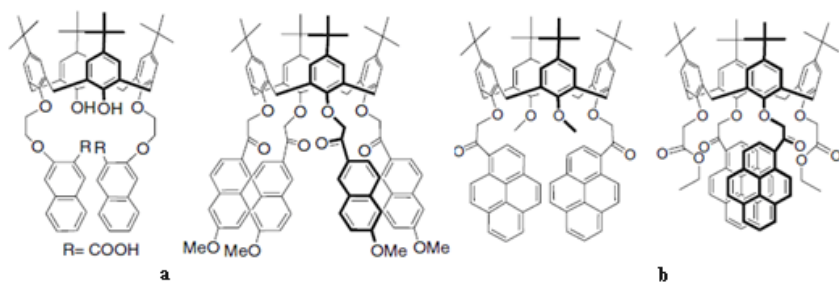


Figure 6. Structures of fluorescent sensors based on TBC with naphthalene (a) and pyrene (b) substituents

The main advantages of these ligands are the sensitivity and the possibility of its application in biological studies. Unsubstituted hydroxyl groups in these ligands serve as an “anchor”, which fix the position of the functional groups of the second pair of substituents. These structures represent so-called molecular

“tweezers” and “tongs” [57-60].

There are the growing number of studies devoted to the calix[4]arenes modified by porphyrins parallel to the research of fluorescent sensors. It is related to the ability of the latter to participate in molecular recognition due to the unique spectral properties [61-69]. Calix[4]arene-porphyrin systems can be classified by molecular design as covalently and non-covalently bound (Fig. 7).

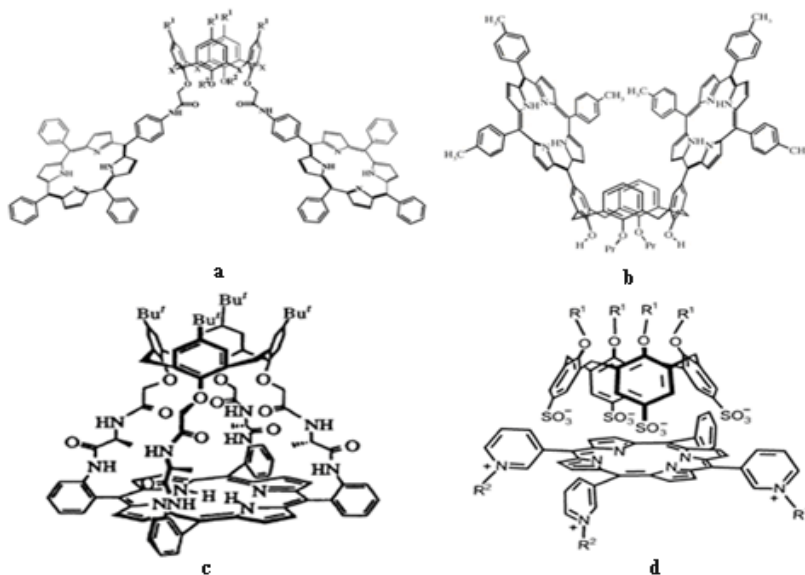


Figure 7. Structures of calix[4]arenes functionalized by porphyrins at the lower (a), upper (b) rim, bound with the several bridges (c) and non-covalent calix[4]arene-porphyrin (d)

Covalently bound calixarene-porphyrins are classified as follows:

1. Calix[4]arenes functionalized with porphyrins at the lower rim (Fig. 7a) [31, 62, 63];
2. Calix[4]arenes functionalized with porphyrins at the upper rim (Fig. 7b) [64, 65];
3. Calix[4]arene-porphyrins linked by several bridges in so-called “cage”- or “sandwich”-like ligands (Fig. 7c) [66].

One of the simplest methods for preparation of covalently bonded systems is the “cross-linking” by amide bond carboxycalix[4]arenes and aminoporphyrin at the lower rim (Fig. 7a). The synthesis is possible with both porphyrins

and porphyrinates of metal. It is a key factor for obtaining the heteronuclear complexes.

Noncovalently binding systems can be referred to ion associates (Fig. 7d), the hallmark of which is the water solubility. The formation of such systems is provided by the presence of charged groups, located on the periphery of the porphyrin macrocycle and at the rim of calixarene. The presence of free porphyrin cavity and a second rim of calixarene makes these polytopic systems interesting in molecular recognition. However, the mutual influence of two macrocycles in calixarene-porphyrin ion associates is not enough studied. In addition, there is no data about heterometallic systems based on these ligands [67-69].

As already mentioned, the directions of possible application of functionalized TBC are very diverse. Lately, they have been actively investigated as antiviral and antibacterial agents. It was found that calix[4]arenes, which are symmetrically disubstituted at lower rim with thiazole fragments have antiviral activity against HIV. The varying of the substituents on the upper rim (*tert*-butyl, phosphonic, sulfonic, carboxy) does not affect on the antiviral activity and only changes the solubility of the compounds in an aqueous medium [70].

Calix[4]arene modified with two bipyridyl groups on the lower rim and four guanidine groups on the upper one exhibits antibacterial activity against some Gram-positive and Gram-negative bacteria comparable to hexamidine but has a lower cytotoxicity [71].

It was found [72] that calix[4]arene tetracarboxy substituted at the lower rim interacts with receptors on the cell membrane of carcinoma and causes their death even at low concentrations (less than 10^{-10} mol/L) and moreover it is non-toxic. The latter indicates that they are effective and promising as anticancer drugs. Study on the biological activity of such compounds has shown that the calix[4]arene macrocycle plays an organizational role holding functional groups that generate antibacterial and antiviral activity at a certain distance in space. The possibility of the additional functionalization of another rim allows enhancing these characteristics and reducing the toxicity of compounds.

The relationship of the chemical structure of calix[4]arene molecules with their biological activity indicates the specific effect of nature of the substituents. The one can suggest that the reasons for the observed differences in biological activity are steric factors which affect the solubility of the compounds, permeability, localization in tissue and interaction with biological structures. However, a systematic research of the biochemical mechanisms involving calix[4]arenes and relationship “structure-bioactivity” was not carried out. It is known, for example, that benzimidazole and its derivatives, particularly complexes with ions of some d-metals (Fe(III), Cu(II), Co(II), Ni(II), Zn(II))

have a broad spectrum of antimicrobial and antifungal activity and are active ingredients of drugs (e.g. omeprazole, astemizole, mebendazole) [73, 74]. However, the biological activity of *p*-*tert*-butylcalix[4]arenes modified benzimidazole fragments at the lower rim and their complexes has not been investigated.

2. Heteronuclear lanthanide-containing complexes

Different variants of structure of polynuclear complexes which contain several central cations both the same and different natures (homo- and heteronuclear complexes) are typically caused by the fact that the polytopic ligand does not fully realize its denticity relative to one ion. Analysis of [75-77] devoted to the methods of synthesis of polynuclear lanthanide-containing compounds allows to select at least two basic requirements for ligands (Fig. 8, [76]).

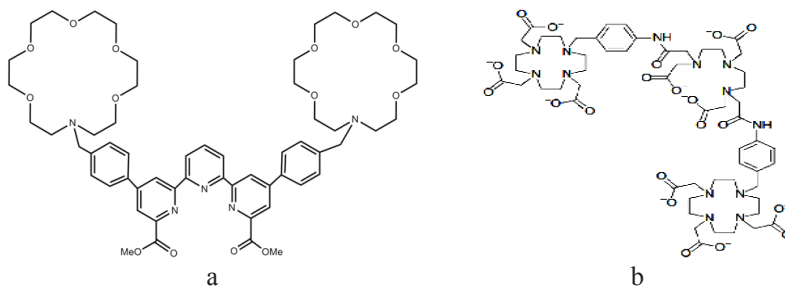


Figure 8. Structures of ligands containing metal chelate cycles based on terpyridine (a) and DTPA modified macrocyclic moieties (b)

Firstly, the number of donor centers must be sufficient for binding several metals. Secondly, their spatial organization must allow formation of a stable coordination structure which can be achieved, for example, if the chelate groups are located at the terminal parts of ligand. In general two synthetic approaches were used for the synthesis of polynuclear compounds in particular lanthanide-containing:

- the synthesis based on mononuclear complexes with vacant donor groups (chelating sites). In this case, mononuclear complexes are «building blocks» for polynuclear. In other words, mononuclear complexes act as ligands. Such methods of synthesis are called «block» or rational design methods [76];
- synthesis of polinuclear complexes based on ligands containing several

individual donor centers able to coordinate two or more metal ion independently. Such methods of synthesis methods are called «self-assembly» in the literature [77].

2.1. Features of formation and spectral-luminescent properties of heteronuclear complexes of lanthanides

«Block» synthesis techniques were widely used for polynuclear complexes of lanthanides and s-elements with ligands that contain modified crown ethers. Undoubted advantage of polytopic ligands is the ability to plan the spatial organization of the complexes. The use of complexes of s- and d-elements as «building blocks» for polynuclear lanthanide-containing compounds is applicable only if the total coordinating capacity of the ligand exceeds the maximum possible coordination number (CN) of the metal ion. Such compounds are, for example, polycarboxylates, polyheterocyclic ligands with chain-like structure, some types of crown ethers and polyazamacrocycles. Thus, free donor atoms may be coordinated to other metals with the implementation of bridging function of ligand. Such synthesis allows obtaining of polynuclear coordination compounds with a specific topology of metal centers, which is undoubtedly one of the main advantages of this method [78-80]. For example, the presence of vacant NN-donor centers in Re(I) complexes with bipyridine (Fig. 9a) and terpyridine ligands (Fig. 9b) allowed to join them with β -diketonate complexes of lanthanides.

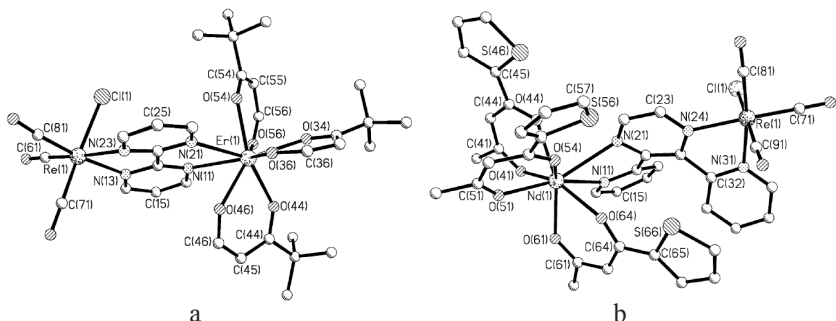


Figure 9. The structures of the Ln(III)–Re(I) complexes based on 2,2'-bipyrimidine (bbp, a) and 2,3-bis-(2-pyridyl)pyrazine (bbpz, b) [81, 82]

In these complexes two metal centers were coupled with diazine bridges of ligand at the distance of 6.23 - 7.47 Å for Re ... Er and Re ... Nd, respectively. The quenching of molecular luminescence was observed in the heteronuclear

compounds $[\text{Re}(\text{CO})_3\text{Cl}(\text{bppz})]$ with maximum at 650 nm, which, according to the authors, shows the energy transfer from donor Re-fragments to the low-lying excited states of Er(III) and Nd(III) ions [81, 82].

In some cases the obtaining of heteronuclear compounds requires additional third stage: joining exo-coordinated metal ions to form supramolecular assemblies [83, 84]. In [84] the synthetic scheme of polynuclear Ln(III) – Pt(II) complexes based on terpyridine derivatives functionalized with alkynyl groups was given (Fig. 10).

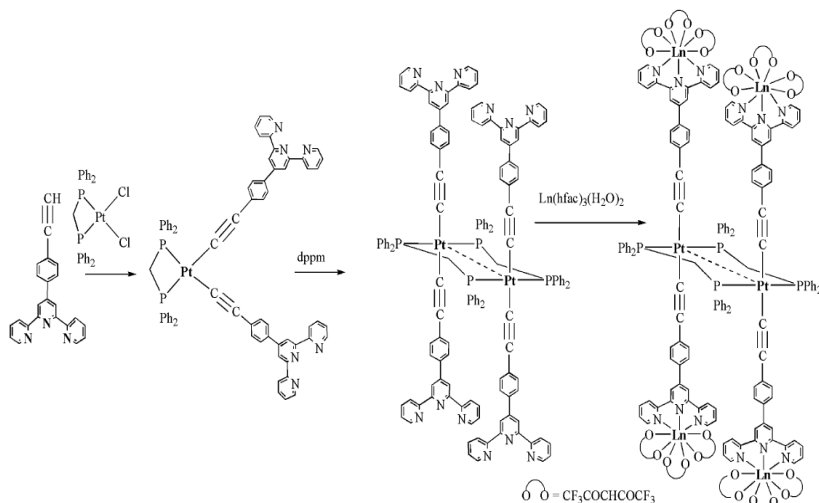


Figure 10. Three-step synthesis scheme of heteronuclear complex $\{\text{Pt}_2(\mu\text{-dppm})_2(\text{C}\equiv\text{CPhpty})_4\}\{\text{Ln}(\text{hfac})_3\}_4$ ($\text{Ln}=\text{Nd}, \text{Eu}, \text{Gd}, \text{Yb}$).

The first step is the reaction of platinum (II) complex with terpyridine derivative with formation of mononuclear complex within a few days. Further continuation of the reaction (the second stage lasts almost a week) leads to the formation of the binuclear complex $\text{Pt}_2(\mu\text{-dppm})_2(\text{C}\equiv\text{CPhpty})_4$. At the third step, lanthanide hexafluoroacetylacetonate solution in dichloromethane was stirred for an hour at room temperature with the resulting platinum “block” to obtain the heteronuclear complex with yield 87 – 92 %. In researches of the structures of europium and ytterbium complexes $\{\text{Pt}_2(\mu\text{-dppm})_2(\text{C}\equiv\text{CPhpty})_4\}\{\text{Ln}(\text{hfac})_3\}_4$ it was showed that the distance Pt...Ln depends on the f-metal and ranges from 14.32 to 14.01 Å (in the case of Nd(III) – 14.01 Å and Yb(III) – 14.08 Å; Fig. 11).

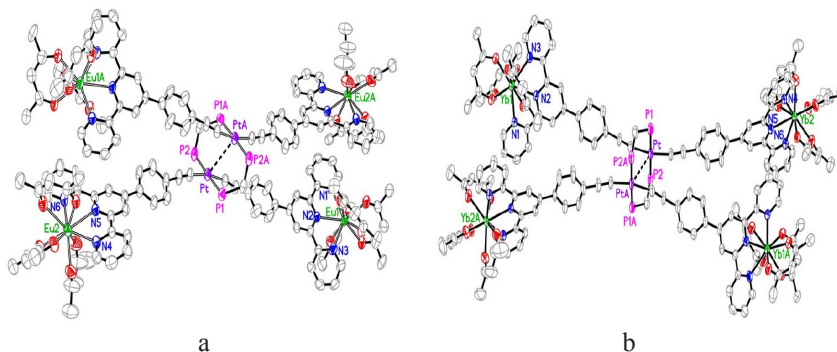


Figure 11. Structures of complexes $\{Pt_2(\mu\text{-dppm})_2(C\equiv CPhtpy)_2\}\text{-}\{Ln(hfac)_3\}_4$ with Eu (III) (a) and Yb (III) (b) ions [84]

In contrast to previous work, sensitized 4f-luminescence of Nd(III), Eu(III) and Yb(III) was registered. The long-wavelength fluorescence band at 500-600 nm that was observed in the initial homonuclear Pt(II) complexes and related to the charge transfer band (CTB), was almost totally quenched in the heteronuclear complexes with Ln(III) ions. Its lifetime (1390 ns for the $[Pt_2Gd_4]$ complex 637 ns for $[Pt_2Yb_4]$ and 4.1 ns for $[Pt_2Nd_4]$) allowed calculating the rate constant of energy transfer Pt \rightarrow Ln. Nd(III)-containing complex is characterized by the greater constant $k_{ET} = 1.02 \cdot 10^7 \text{ c}^{-1}$ due to most effective overlap of the emission spectrum of Pt(II)-containing chromophore with the absorption spectrum of Nd(III) ion, in comparison with Yb(III). In addition, 4f-luminescence of Eu(III) was registered. In this case, the authors suggest that sensitization is not due to CTB, energy transfer occurs from triplet state of organic ligand, which fluorescence is observed at 388 nm (25770 cm^{-1}).

Solvent molecules and counterions have an extremely important role in stabilizing the structure of heteronuclear compounds. They affect both the formation of individual fragments of complexes and various self-assembling processes of supramolecular systems. In some cases, the variation of solvent nature gives the opportunity to control the composition and structure of polynuclear compounds.

In a number of studies special attention is paid to the role of the anions of metal salts. They can act as mono-, bi – and ambidentate ligands and form bridges between two metal atoms. As an example dinuclear Ln(III) – Cu(II) complexes with Schiff base can be considered (Figure 12) [85]. Complexes Ln:Cu:Lig=1:1:1 (Fig. 12a) formed in ethanolic medium, wherein there are coordination of three trifluoroacetate anions and two solvent molecules.

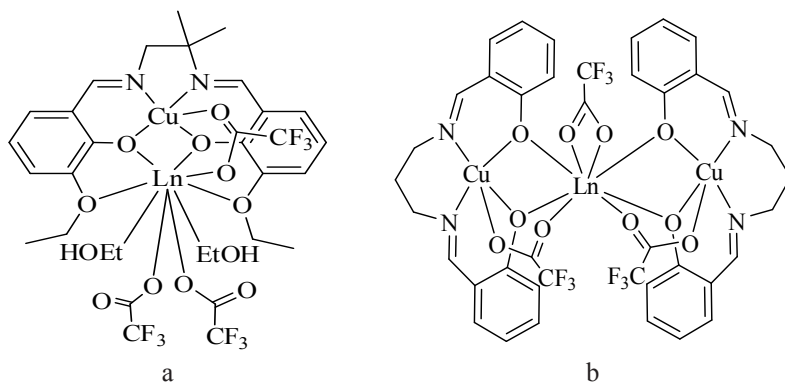


Figure 12. Structures of Ln(III) – Cu(II) heteronuclear complexes with Schiff base obtained in ethanol (a) and acetonitrile (b)

The using of acetonitrile or acetic anhydride as a solvent leads to the formation of the trinuclear complexes Ln:Cu:Lig=1:2:2 and coordination of solvent molecules does not occur (Fig. 12b). Trifluoroacetate ions used in the synthesis, on the one hand, complete a metal coordination sphere neutralizing the positive charge; on the other side they perform the bridging function associating two different metals.

The replacement of one metal ion to another is used in cases where direct obtaining of heteronuclear complexes is not possible. For example mononuclear complex $[\text{Eu}(\text{H}_3\text{L})(\text{NO}_3)(\text{H}_2\text{O})](\text{ClO}_4)_2$ was obtained with cryptand obtained from tris(2-aminoethyl)amine and 2,6-diformyl-4-chlorophenol. Further coordination of d-metal was prevented because of water molecules located in the inner coordination sphere. Their removal was achieved through the use of calcium hydride as dehydrating agent [86]. The results of mass spectrometry experiments showed that calcium ion has sufficient lability to be replaced by d-metals. Heteronuclear complexes $[\text{EuMeL}(\text{DMF})](\text{ClO}_4)_2 \cdot \text{MeCN}$ were obtained by mixing the solutions of block $[\text{EuCaL}(\text{DMF})](\text{ClO}_4)_2$ and d-metal salts, where d-metal ions were Ni(II), Zn(II), Cd(II).

Synthetic procedures that use the processes of spontaneous self-organization include methods of “self-assembly” or “self-organization” [87, 88] and some of their variants, for example, the direct synthesis [89]. The spatial organization of donor atoms as well as conformational flexibility of ligand and dimensions of complexing ions allowing the formation of stable polychelate structure must be considered during such syntheses. Topology of donor centers has been already determined while using the “block” method of synthesis. “Self-organization”

methods have some features in comparison with “block” method: first, the selection of optimal ratios of metal salts and ligands in synthesis, and secondly, the use of inert solvents, which could not act as ligands.

For example, d-f-complexes with helicates containing two different binding sites were prepared: 2-(benzimidazole-oxazolyl)pyridine (L_1) and 2,6-bis(benzimidazolyl)pyridine (L_2) connected by bridging methylene group (Fig. 13, a, b). Similar d-f-complexes were discussed in detail in the works of J.-C. Bunzli and coworkers [90-92]. As tetradentate ligands helicands form mono-, bi- and polynuclear coordination compounds with two- or trivalent ions of p-, d- and f-elements with different composition and molecular structure: pseudo macrocyclic or porphyrin-like, double or triple helix, three-, four- or hexagonal structure, etc. It is assumed that the first donor center selectively binds d-metal ions forming an octahedral coordination environment, while lanthanide ion coordinate exceptionally 2,6-bis-(benzimidazolyl)pyridine moiety with the implementation of coordination number 9. Methylene group prevents simultaneous coordination of two fragments with the same metal.

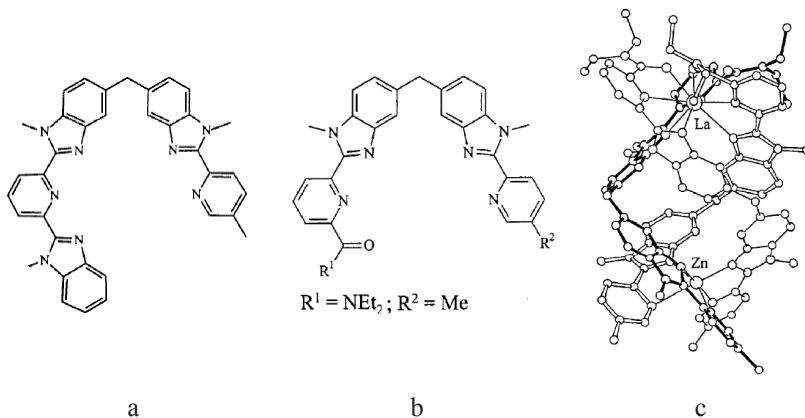


Figure 13. Schematic structure (benzimidazolyl)pyridyl-containing ligands L_1 (a), L_2 (b) and complex $LaZn(L_2)_3$ (c) [91]

Expected heteronuclear complexes with helical structure $LaZn(L_1)_3$ (Fig. 13c) were prepared in acetonitrile at stoichiometric ratio $La:Zn:L = 1:1:3$ and ligand concentration $\geq 10^{-2}$ mol/l; equilibrium concentration of this form in solution exceeds 90 %. Authors [33] concluded that the structure of complexes is determined primarily by complementary functional fragments

to different metals. Despite the considerable affinity of both fragments to binding d-metals, reducing the ligand concentration leads to the formation of complicated mixture of products. At the same time, the substitution of one of the benzimidazolyl fragments to amide or carboxyl group (Fig. 13b) increases the stability of f-block. In this case the selective formation of heteronuclear complex $\text{LaZn}(\text{L}_2)_3$ is observed until the ligand concentration 10^{-4} mol/L. The formation of complexes with different composition ($[\text{Zn}(\text{L}_2)_3]^{2+}$, $[\text{Zn}_2(\text{L}_2)_3]^{4+}$, $[\text{Zn}_2(\text{L}_2)_2]^{4+}$, $[\text{La}(\text{L}_2)_3]^{3+}$, $[\text{La}_2(\text{L}_2)_3]^{6+}$) was observed with further variation of ratios of metal concentrations.

The variety of synthetic approaches that combine both the design of certain “building blocks” and spontaneous self-organization processes were widely used in the recent studies. In such systems the nature of the “second” metal generally determines the structure of the final polynuclear compounds. Typically, it was observed in the case of s-f-complexes when s-metal performs the function of counterion or “stabilizer of the structure”.

For example, bifunctional macrocyclic ligands, which are analogs of Schiff bases, were obtained in [93]. One part of ligands forms donor center N_2O_2 and the second is crown-ether-like cavity O_2O_3 or O_2O_4 which is responsible for coordination of s-metal ion (Fig. 14). Varying the size of macrocycle cavity leads to the possibility to use mononuclear complexes of s- or f-metals as “building blocks”. Ions of alkali or alkaline-earth metals coordinate oxygen atoms of crown ether, while lanthanide ions bind donor atoms of the Schiff base with formation of complexes $[\text{YbNaL}]^{2+}$ or $[\text{LaBaL}]^{3+}$. The presence of the s-metal ions in heteronuclear complexes affects on photophysical and/or relaxation properties of the lanthanide ions, which can be used to create a sensitive sensor systems.

In [1, 5, 76] ligand containing terpyridine moiety for complexation with Eu(III) ions and two azacrown-ether fragments for coordination of potassium ions was studied (Fig. 8a). Excitation of the organic chromophore occurs so-called photoinduced electron transfer: the lone pair of the nitrogen atom moves to the vacant molecular orbital of the aromatic moiety, which leads to quenching of ligand fluorescence. The quantum yield of Eu(III) mononuclear block in methanol solution is 2.6 %. The lone pair is involved in the binding when potassium cations coordinate azacrown ethers fragments, thus, photoinduced process substantially impedes and ϕ_{4f} increases to 46 %. Selective sensors for s-metal ions with programmable luminescence were designed on the basis of this model.

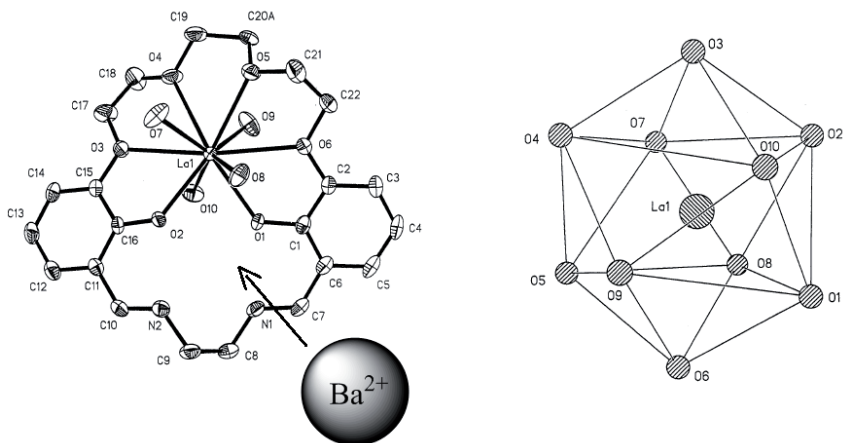


Figure 14. Structure of lanthanum-containing complex with crown-ether-like Schiff base and coordination environment ion Ln (III) (arrow shows further coordination of *s*-metal)

More complicated influence of the nature of “second” metal on the structure of formed complexes and spectral-luminescent properties of lanthanide ions was noted in f-d-complexes compared with s-f-compounds. First of all, this is due to the electronic structure of outer shells. Their completeness/incompleteness determines the specific properties of d-metals such as ability to form coordination compounds with different polyhedron structures, ferromagnetism of some metals, paramagnetism, etc. Therefore, when predicting the photophysical properties of heteronuclear lanthanide compounds it is necessary to consider the basic types of electronic states and transitions for d-metal complexes. Some of them are d-d-transitions (metal-centered transition – MCT), which are significantly affected by the ligand field in the complexes. Metal-ligand charge-transfer band (metal-to-ligand charge transfer – MLCT), i.e. d- π^* -transitions, which are responsible for electron transfer from metal center to π^* -antibonding ligand orbitals, are also characteristic for f-elements. However, the most important process in terms of heteronuclear compounds is the reverse ligand-metal charge transfer (ligand-to-metal-charge-transfer – LMCT), π -d/f-state arising at electron transfer from π - orbitals of the ligand to central metal ion. The contribution of one of these transitions can be varied by replacing atoms as d- and f-metals, using different ligands, introducing of certain substituents in the ligand structure or changing geometry of the complex. Such approaches allow creating new compounds with pre-defined properties.

Metal-metal interactions in f-d-heteronuclear compounds can be divided into three main types: associated with overlapping orbitals, electrostatic and “mechanical” [79].

Overlapping orbitals affect primarily on excitation energy transfer processes. When lanthanide and d-metal ions are close enough mixing of the 4f- and d-orbitals leads to a change in the relaxation time of the electronic states and can either decrease or increase the probability of radiative f-f-transitions. In particular, mixing 4f-orbitals and low-lying states of charge transfer of d-metal causes luminescence quenching if the redox potential of Ln(III) ion is not high (for example, ions Eu(III)). In addition, the excitation energy may be transferred to levels of d-metals with subsequent non-radiative dissipation. Transferring the excitation energy from f- to d-metal was demonstrated for heteronuclear lanthanide compounds with Cr(III), Co(III), Zn(II), Fe(II) ions and various classes of organic ligands.

In one of the fundamental research the problem of mutual influence of Ln(III) and d-metal ions coordination compounds have been studied based on tris(dipicolinates – dipic) lanthanide with general formula $[MeL_x] [Ln(dipic)_3] \cdot nH_2O$ (Ln(III) = Eu, Tb, Nd, Er, Tm; Me = Cr(III), Co(III); L_x – various amines and urea, Fig. 15a, [79, 94]).

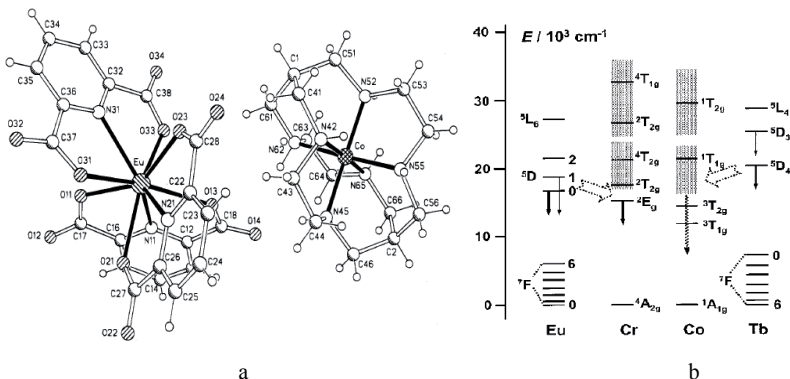


Figure 15. Structure of heteronuclear complexes $[Co(L_x)]-[Eu(dipic)_3] \cdot 13H_2O$ (a) and the energy level diagram of corresponding 4f- and 3d-metals (b) [94]

According to X-ray data Me...Ln distance is in the range 6.5-7.5 Å. Since metal ions are in different parts of complex orbital interaction in this case is completely excluded. Compared with the emission intensity of the

complex $Cs_3[Eu(dipic)_3]$, emission of Eu(III) ions in heteronuclear systems is substantially quenched in the case of Co(III) and Cr(III). That can be explained by energy transfer from excited levels of lanthanides on resonance energy levels of d-metals (Fig. 15b). At the same time, due to the presence of low-lying energy levels of Cr(III) 2E_g this ion has been successfully used for sensibilization of 4f-luminescence in IR-region in solid matrixes containing Nd (III), Er (III) and Tm (III) ions.

Effect of electrostatic interaction between two metals can be demonstrated by Zn(II)-Ln(III), Fe(II)-Ln(III) helicates shown in Fig. 13 [79]. Fe(II) ion is a universal acceptor in pairs with f-metals. This is due to the implementation of two different electronic configurations characterized by optical and magnetic properties, which depend on ligand environment of Fe(II). For complex $[LnFeL_3]^{5+}$ the transition of terms 1A_1 and 5T_2 and thermochromism were observed: the diamagnetic low-spin form is purple at not high temperatures, and the high-spin diamagnetic form has orange coloring at higher temperatures. This is due to intense absorption band of metal-ligand charge transfer at 19000 cm^{-1} , which quenches 4f-luminescence of Eu (III) with the implementation of the transfer $Eu(III) \rightarrow Fe_{1s}(II)$ (Fe...Ln distance about 9 \AA). At the same time, the band of high-spin form has a higher energy ($\approx 22200\text{ cm}^{-1}$) and d-d-transitions in $8800\text{-}11000\text{ cm}^{-1}$ are allowed. The presence of transparent spectral window at $12000\text{-}20000\text{ cm}^{-1}$ in some extent minimizes intramolecular transfer $Eu(III) \rightarrow Fe(II)$. As a consequence, weak 4f-luminescence of Eu(III) is realized in high-spin compound at excitation in absorption region of ligand. The quantum yield is 300 times less than corresponding Zn(II)-Ln(III) complex. Thus, Eu(III) ions can serve as a kind of sensors of spin states of Fe(II) ions.

Zinc (cadmium) complexes are slightly different from the other elements. Their cations have complete d-d-levels, so their compounds are usually fluorescent and for some of them also were observed phosphorescent signals. Such transitions can not only quench 4f-luminescence, but also sensitize it in compounds of lanthanide ions emitting in the near infrared region. This effect is clearly demonstrated in a series of compounds containing d-blocks with Ru(II), Rh(II), Pd(II), Re(I), Pt(II) and nitrogen heterocycles such as bipyridyl, pyrrole and their derivatives as ligands (Fig. 16) [11-13, 77].

Emission caused by charge transfer bands in respective mononuclear complexes were observed in the region of $500\text{-}700\text{ nm}$. This area is optimal for the energy transfer to lanthanide ions with low-lying excited levels, such as Yb (III), Nd (III) and Er(III). The possibility of using visible light excitation makes these compounds promising for biomedical applications due to lack of irradiation of biological tissues with UV light.

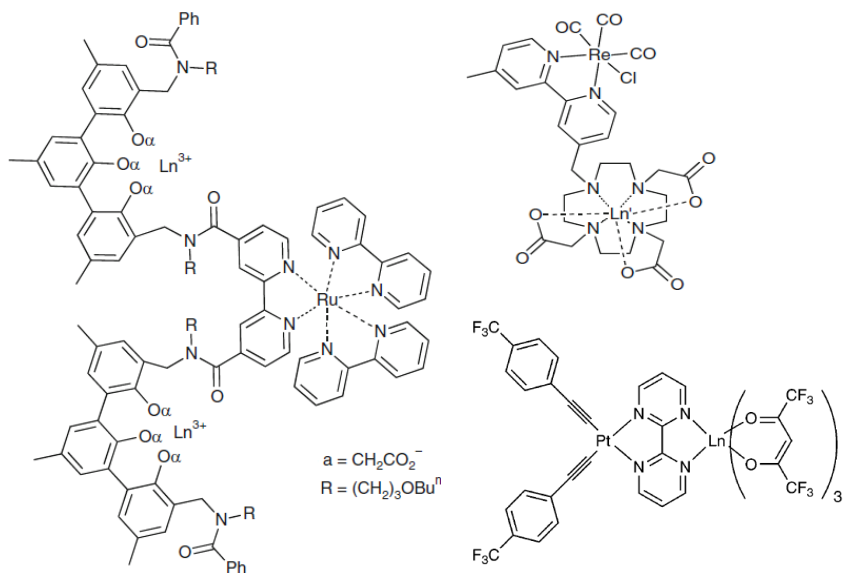


Figure 16. Structures *d-f*-heteronuclear complexes, sensitizing 4*f*-luminescence of Ln(III) in the IR region.

The so-called „mechanical” interactions in heteronuclear complexes can be demonstrated on the example of iron complexes (II), which have been described in [79, 90]. It was found that among Ln(III)-Fe(II) heteronuclear complexes with content of high-spin form at constant temperature depends on radius of lanthanide ion coordinated by neighboring donor centers of ligand. Increasing size of lanthanide ion in $[\text{LnFeL}_3]^{5+}$ imposes some restrictions on expansion of Fe-N bonds, which is necessary for realization of spin-spin transfer.

Analysis of works devoted to synthesis and structure of heteronuclear s- and d-complexes with lanthanides allows emphasizing two main points. First, a key factor in design of such compounds is the selection of ligand containing moieties capable to transfer energy from metal complex chromophore to lanthanide ion. Obviously, this energy transfer will facilitate the presence of π -conjugated system between the donor and acceptor, which imposes certain requirements on the nature of the ligand and the structure of its electron shells. Secondly, prediction of properties of f-d-pairs in complexes, for example, sensitization or quenching of 4*f*-luminescence, is difficult and implies to take into account the mutual influence of many factors, which are not always obvious.

2.2. Homo- and heteronuclear complexes of lanthanide with modified calix[4]arenes

First lanthanide complexes with derivatives of *p-tert*-butylcalix[4]arene were synthesized by J. Harrowfield and coworkers in 1985-1990 [95, 96]. The structure of mono- and dinuclear Eu(III)-containing f-f-compounds were analyzed in solid form and in solution, however, their luminescence characteristics were not investigated. In subsequent works as a circle of functionalized ligands and a number of lanthanide ions has been extended. These research became the basis for further spectral-luminescent studies of lanthanide complexes of calix[4]arenes. One of the features of synthetic techniques for obtaining lanthanide complexes consists in reacting of lanthanide salts and calix[4]arenes in anhydrous solvents or their mixtures, in the presence of triethylamine, which promotes dissociation of phenolic group thereby facilitating complex formation. Chlorides, nitrates and acetates are most commonly used as lanthanide salts. If occurrence of counterions in the inner coordination sphere of the lanthanide is undesirable, trifluoroacetates, trichloroacetates, perchlorates and trifluoromethylsulfonate (triflate) were used.

Lanthanide complexes with TBC substituted at opposite phenolic rings one carboxymethoxy(-CH₂-COOH) and one alkylcarbamoylmethoxy groups (-CH₂-CO-NHR) were obtained in [97] (Fig. 17, a). It was proved that structure of complexes is determined by ionic radius and does not depend on the carbon chain length. Greater ions Ln(III) = La, Eu, Sm form dimeric isomorphous complexes Ln:Lig = 2:2. Lanthanide ion forms the coordination number of eight due to four oxygen atoms of lower rim, oxygen atom of amide group and two μ-O-atom of carboxyl groups of both ligands and oxygen atoms of solvent molecule (Fig. 17, b).

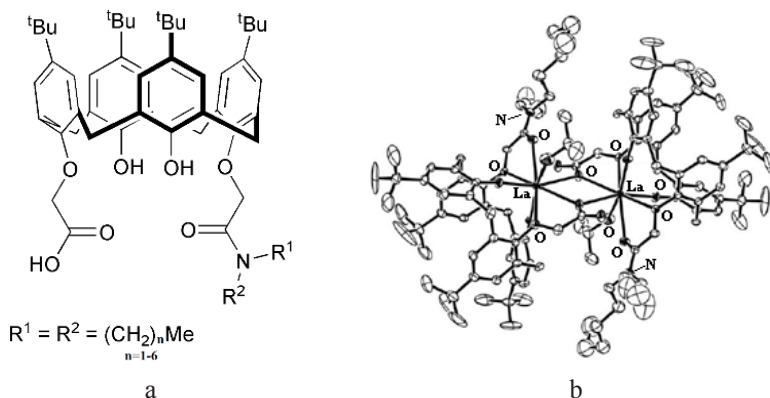


Figure 17. Structure of modified calix[4]arenes (a) and dimeric lanthanide-containing complexes on their basis (b) [97]

Lutetium complexes form the compounds Lu:Lig= 1:1, in which lanthanide coordination polyhedron is formed by four oxygen atoms of lower rim of calixarene, two oxygen atoms of amide and carboxyl groups and one solvent molecule (coordination number = 7). Absence of lanthanide salt counterion in the inner coordination sphere is explained by addition of triethylamine in synthesis, so carboxyl and phenolic groups proton replaced by lanthanide ion forming a neutral complex.

Lanthanide complexes, in which dimerization was not observed, were obtained on the basis of TBC functionalized at lower rim with two (CH₂-CO-NEt₂)-fragments [97]. Coordination sphere was formed by eight oxygen atoms for Sm(III), Yb(III) and Lu(III) ions: four phenolic, two carbonyl of amide substituents and two oxygen atoms of picrate anion (lanthanide picrates were used in synthesis). In the case of La(III) complexes picrate anions are coordinated as monodentate ligand, and inner sphere contains one water molecule. Authors concluded that formation of dimeric complexes is possible only if ligands contain potential bridging donor atoms and at the same time do not contain bulky substituents creating steric hindrance.

Obtaining polynuclear f-f-complexes of calix[4]arenes promotes replacing methylene bridges on sulfide or sulfone groups, which leads to expansion of ligand cavity and appearance of additional coordinating atoms. Polynuclear complex with *p*-*tert*-butylthiacalix[4]arene (L) – [Nd₄(μ₄-OH)(L-4H)₂(DMF)₈-(DMSO)₂](NO₃)₃ (Fig. 18) was obtained in [98].

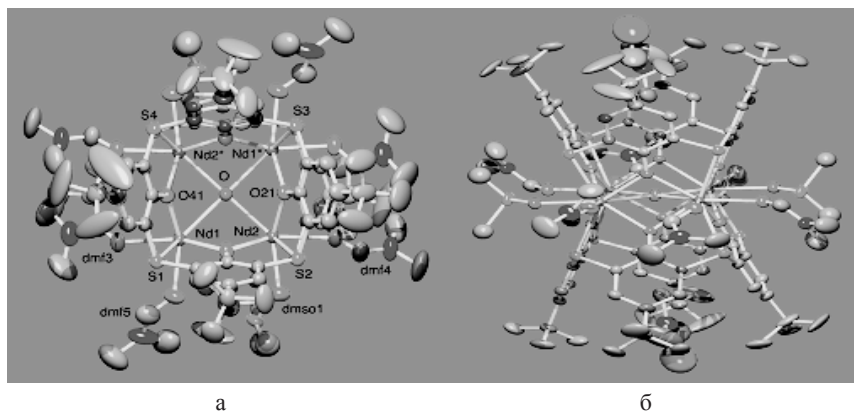


Figure 18. Structure of homotetranuclear complex of *p*-*tert*-butylthiacalix[4]arene with Nd(III) ions: perpendicular view of the complex (a) and along tetrametal plane (b) [98]

Complex contains hydroxyl group, which is coordinated by four neodymium ions at the same time and stabilizes complex reducing electrostatic repulsion between cations. All phenolic groups of ligand are deprotonated; complex particle has charge +3, which is compensated by outer nitrate anions. Complex is symmetrical: every four neodymium ion coordinates oxygen atoms and two sulfur atoms of ligand, oxygen atom of μ_4 -OH-anion and two oxygen atom of solvent molecules (CN = 9). Two DMF molecules are retained in the cavity of each ligand due to CH_3 - π -interactions forming an inclusion complex. The average distance between neodymium ions ($\text{Nd}\dots\text{Nd} - 3.675\text{-}3.689 \text{ \AA}$) is prerequisite for electron interactions, which was confirmed by studies of magnetic susceptibility of complex.

Heteronuclear sandwich-type complex $[\text{Mn}_2[\text{Gd}(\text{CH}_3\text{OH})]_2(\text{OH})\text{L}_2](\text{OH})$ (Fig. 19) was obtained on the basis of this ligand [99]. Dihedral angle between two macrocycles is 14.29° due to the difference in metal cations radii. Manganese (II) cations coordinate four oxygen atoms of phenolic groups of ligands, two sulfur atoms and bridging OH-group, which is located in the center of Mn_2Gd_2 site and coordinated by four cations. Gadolinium ion has CN = 9, that includes four phenolic oxygen atoms, two sulfur atoms, bridging OH-anion and two oxygen atoms of solvent molecules (methanol). It should be noted that all OH-groups of calixarene are deprotonated and complex has a charge +1 which is compensated by outer sphere OH-anion. However, neither in this nor in previous studies spectral properties have not been studied.

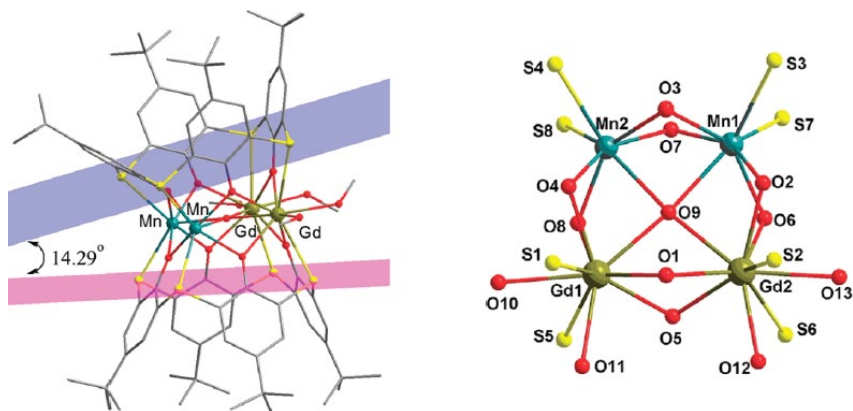


Figure 19. Structure of complex $[\text{Mn}_2[\text{Gd}(\text{CH}_3\text{OH})]_2(\text{OH})\text{L}_2](\text{OH})$ ($\text{L} = p$ -tert-butylthiacalix[4]arene) [99]

One of the few publications devoted to luminescent properties of polynuclear complexes with calixarenes is [100], which describes bi-((*n*-Bu₄N)₂[Ln₂(L)₂(H₂O)₄]) and tetra-homonuclear((*n*-Bu₄N)₄[Ln₄(L)₂(OH)₄(AcO)₄]) complexes of Tb(III), Eu(III) and Gd(III) ion with *p*-*tert*-butylsulfonylcalix[4]arene (H₄L, Fig. 20).

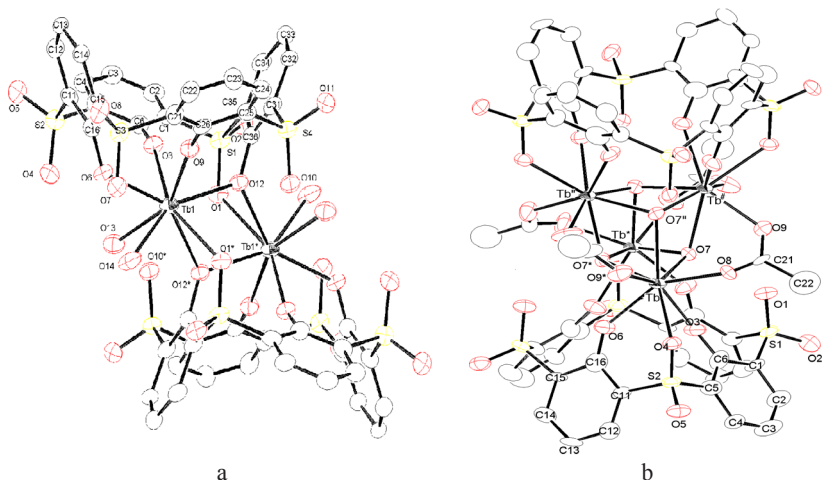


Figure 20. Structures of complexes (*n*-Bu₄N)₂[Tb₂L₂(H₂O)₄] (a) and (*n*-Bu₄N)₄[Tb₄L₂(OH)₄(AcO)₄] (b) [100]

The intense 4f-luminescence was recorded for terbium binuclear compound in solid state at room temperature, while for a similar Eu(III) complex is totally quenched. In tetranuclear systems weak fluorescent signal was recorded for complex of terbium, while for europium compounds 4f-luminescence is intensive enough. This fact was attributed to mutual position of the triplet levels of the ligands (³T*) and excited levels of lanthanides (³D₄ for Tb(III) and ⁵D₁ for Eu(III)) in respective systems, resulting in possible process of energy back transfer from lanthanide ion to ligand (Fig. 21). The article also deals with features 4f-luminescence properties of ions Ln(III) and briefly considered the mechanism of its occurrence in such systems. Since direct excitation of 4f-electrons is not effective, even if quantum efficiency is relatively high, so an alternative way is to use the complex with organic ligands that strongly absorb visible/UV light and are capable of transmitting energy to lanthanide ions (“photoantenna effect”).

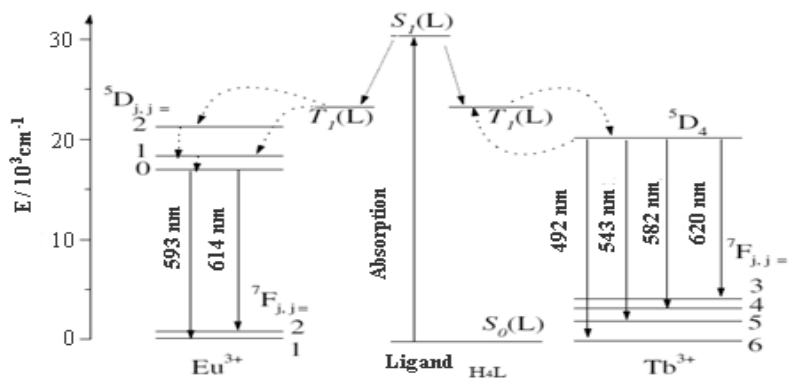


Figure 21. Scheme of intramolecular energy transfer from *p*-*tert*-butylsulfonylcalix[4]arene to excited levels of Tb(III) and Eu(III) ions in the tetranuclear systems

Calix[4]arene H_4L is “photoantenna” which absorbs light, transfers it to Ln(III) ion principally from triplet state of ligand, causing f-emission. Transfer of energy to the excited levels of lanthanide ions can be carried out from singlet state of ligand ($^1S^*$), but this process is considered to be inefficient because of small lifetime. Processes of energy migration from Ln(III) levels can also be initiated by vibrations through states with charge transfer and energy levels of ions of d-elements. Usually simplified energy transfer path for lanthanide compounds is considered $^1S^*$ (ligand) \rightarrow $^3T^*$ (ligand) \rightarrow Ln*. Energy of Tb(III) excited level is 20430-20500 cm^{-1} (5D_4) and Eu (III) – 17250-17500 cm^{-1} (5D_0). The difference between triplet level of organic ligand and resonant 5D_0 level of europium ion $\Delta E(^3T^* - ^5D_0)$ must be in the range 2500 – 3500 cm^{-1} for effective energy transfer, and $2500 < \Delta E(^3T^* - ^5D_4) < 4000$ cm^{-1} for terbium ion. In studied systems for terbium ion it is only 500-800 cm^{-1} which leads to energy back transfer from lanthanide ion to ligand [101].

f-s-Polynuclear complex was obtained on the base of Tb(III)-containing sulthioacalix[4]arene (TCAS) – $Ag_4TbTCAS_2$ (Fig. 22) [102]. Coordination polyhedron of lanthanide ion is a square prism with CN=8 in this compound, which is not characteristic for f-elements. The authors explained that by “mechanical” effect of silver ions, which coordinate bridging sulfur atoms, link together two macrocycle and make pre-organized coordination surrounding of Tb(III) ion. 4f-Luminescence intensity of $Ag_4TbTCAS_2$ is lower than mononuclear complex Tb-TCAS, but quantum yield of luminescence (ϕ_{4f}) is significantly higher (88% for $Ag_4TbTCAS_2$ compared with 16% for Tb-TCAS).

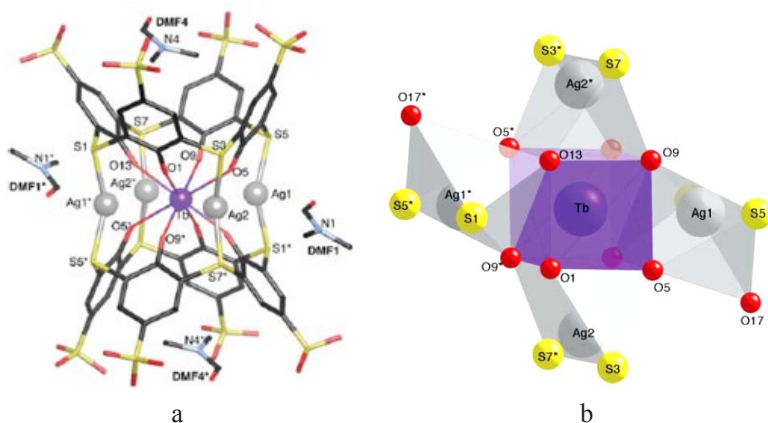


Figure 22. Crystal structure $[Ag_4Tb(TCAS)_2DMF_2]^{9-}$ (a) and coordination environment of the nucleus Ag_4Tb (b) [102]

The increasing of luminescence lifetime of heteronuclear complex to 4.61 ms is due to the coordination of Tb(III) ions with two macrocycles at the same time. Moreover, the presence of four silver ions shields lanthanide ion from the water molecules.

Luminescent properties of d-f-complexes (Me = Ru(II); Ln(III) = Eu, Tb, Nd) with dimeric calix[4]arenes modified on lower rim by amide fragment (Fig. 23a) were studied in [97].

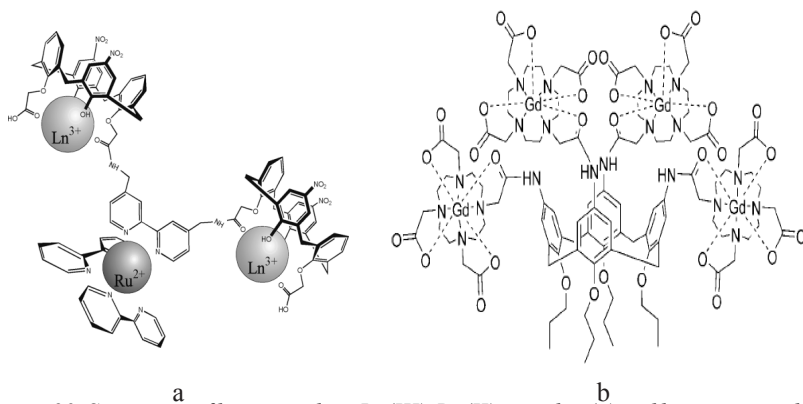


Figure 23. Structures of heteronuclear Ln(III)-Ru(II) complex (a) and homotetranuclear Gd(III) complex with calix[4]arene-DOTA (b)

Luminescence of ruthenium is completely quenched in Nd(III)-Ru(II) compounds. It indicates the efficient energy transfer from excited level metallochromic calix[4]arene moiety to lanthanide ion. At the same time, formation of Tb(III) and Eu(III) adducts leads to increase luminescence and lifetime of Ru(dipy)₃-calix[4]arene fragments.

Particular attention is drawn to practical use of calixarene complexes with lanthanides. For example complexes of gadolinium ions with modified calix[4]arenes are considered as potential contrast agents for magnetic resonance imaging (MRI, Fig. 23b [103]). High solubility in water and significant stability of gadolinium complex are important characteristics for contrast agents.

Water-soluble calix[4]arenes functionalized with phosphorus fragments at lower and/or upper rim are perspective in extraction processes of Ln(III) ions [5, 79, 104]. For example, phosphorus calix[4]arenes included CH₂-, CH(OH)-, CH(NHAr)-, NHC(O)CH₂-, CH₂NHC(Me)₂-spacers between phosphorus and carbon atoms of macrocycle, bi- and tetraphosphonyl acids (-P(O)(OH)₂) obtained by functionalization of lower rim of *p-tert*-butylcalix[4]arene were studied as extraction agents.

Recently increased interest has dedicated to the synthesis, structure and application of hybrid materials containing homo- and heteronuclear lanthanide complexes with calix[4]arenes. These compounds combine rigidity and heat resistance of inorganic matrix and photophysical properties of complexes of lanthanide ions. The presence of covalent bonds between lanthanide complex and inorganic matrix is necessary to achieve high chemical, photo- and thermostability of such systems. Convenient way of covalent binding of calix[4]arenes to inorganic materials is their functionalization with triethoxysilypropyl isocyanate fragments. Hybrid sol-gel materials doped with Tb(III) and Eu(III) complexes of TBC were obtained using such path. It was found that encapsulation of complexes in inorganic matrix leads to reduction of non-radiative energy losses, primarily related to the presence of large number of bonds (OH, CH, etc) quenching 4f-luminescence in solutions. Analogously hybrid materials containing heteronuclear complexes of calix[4]arene with stoichiometric ratio Tb(III):Zn(II) = 1:1 were obtained. Intensity of 4f-luminescence of terbium ions was higher than analogous material containing homonuclear complex [105-108].

Thus, we can conclude that recent interest in calix[n]arenes and their homo- and heteronuclear complexes with Ln(III) ions and other metals has increased significantly. But the works dedicated to heteronuclear complexes with modified calix[4]arenes are still sporadic and researches devoted to the use of these compounds are limited and there is no detailed analysis of “structure-property” dependencies to predicting spectral-luminescent properties of new compounds.

References

1. Bünzli J.-C. Taking advantage of luminescent lanthanide ions / Bünzli J.-C., Piguet C. // *Chem. Soc. Rev.* - 2005. - V. 34, № 12. - P. 1048-1077.
2. Rare earth coordination chemistry: fundamentals and applications / edited by C. Huang. - Chichester: John Wiley & Sons, 2010. - 576 p.
3. Hänninen P. Lanthanide luminescence. Photophysical, analytical and biological aspects. Springer Series on Fluorescence, V. 7 / P. Hänninen, H. Härmä. - Berlin: Springer-Verlag, 2011. - 400 p.
4. The rare earth elements / edited by D.A. Atwood. - Chichester: John Wiley & Sons, 2012. - 696 p.
5. Bünzli J.-C.G. Lanthanide probes in life, chemical and earth sciences. Theory and practice / Bünzli J.-C.G., Choppin G.R. - Amsterdam: Elsevier, 1989. - 432 p.
6. Hemmilä I.A. Applications of fluorescence in immunoassays / Hemmilä I.A. - N.Y.: J.Wiley & Sons, 1991. - 343 p.
7. Korovin Yu.V. Near-infrared luminescence of Yb³⁺, Nd³⁺ and Er³⁺ in complexes with organic dyes / Korovin Yu.V., Rusakova N.V. // *J. Alloys. Compd.* - 2004. - V. 374, № 1-2. - P. 311-314.
8. Korovin Yu.V. Infrared luminescence of lanthanides in complexes with organic dyes / Korovin Yu.V., Rusakova N.V. // *J. Fluorescence.* - 2002. - V. 12, № 2. - P. 159-161.
9. Korovin Yu.V. Luminescence of lanthanide complexes with a chromophoric crown ethers/ Korovin Yu.V., Rusakova N.V., Popkov Yu.A. // *Izvestia RAS. Chem. series* - 2002. - № 12. - P. 2138-2140.
10. Korovin Yu.V. Infrared luminescence of neodymium in complexes with macrocyclic Schiff bases / Korovin Yu.V., Lozitskaya R.N., Rusakova N.V. // *J. General Chem.* - 2003. - V. 73, № 10. - P. 1734-1737.
11. Klink S. Transition metal complexes as photosensitizers for near-infrared lanthanide luminescence / S. Klink, H. Keizer, F. van Veggel // *Angew. Chem. Int. Ed.* - 2000. - V. 39, № 23. - P. 4319-4321.
12. Klink S. Transition metal complexes as a new class of photosensitizers for near-infrared lanthanide luminescence / S. Klink, H. Keizer, H. Hofstraat, F. van Veggel // *Synth. Met.* - 2002. - V. 127, № 1-3. - P. 213-216.
13. Zhu X. Design and synthesis of near-infrared emissive lanthanide complexes based on macrocyclic ligands / Zhu X., Wong W.-K., Wong W.-Y., Yang X. // *Eur. J. Inorg. Chem.* - 2011. - P. 4651-4674.
14. Gutsche C.D. Calixarenes / Gutsche C.D. - Cambridge: Royal Society of Chemistry, 2008. - 276 p.

15. Beer P. Electrochemical molecular recognition: pathways between complexation and signalling / Beer P., Gale P., Chen G. // J. Chem. Soc., Dalton Trans. - 1999. - № 12. - P. 1897-1909.
16. Ikeda A. Novel cavity design using calix[n]areneskeletons: toward molecular recognition and metal binding / Ikeda A., Shinkai S. // Chem. Rev. - 1997. - V. 97, № 5. - P. 1713-1734.
17. Baldini L. Calixarene-based multivalent ligands / Baldini L., Casnati A., Sansone F., Ungaro R. // Chem. Soc. Rev. - 2007. - V. 36, № 2. - P. 254-266.
18. Silva E. Biopharmaceutical applicationa of calixarenes / Silva E., Lazar A.N., Coleman A.W. // J. Drug Del. Sci. Tech. - 2004. - V. 14, № 1. - P. 3-20.
19. Ludwig R. Calixarenes for biochemical recognition and separation / Ludwig R. // Microchim. Acta. - 2005. - V. 152, № 1-2. - P. 1-19.
20. Gutsche C. Calixarenes. 25. Conformations and structures of the products of arylmethylation of calix[4]arenes / Gutsche C., Reddy P. // J. Org. Chem. - 1991. - V. 56, № 15. - P. 4783-4791.
21. O'Neil S. Ion-selective optode membranes using 9-(4-diethylamino-2-octadecanoatestyryl)-acridine acidochromic dye / O'Neil S., Conway S., Twellmeyer J. [et al.] // Anal. Chim. Acta. - 1999. - V. 398, № 1. - P. 1-11.
22. Nguyen T. Solvent extraction of heavy metals with macrocyclic ligands based on calix[4]arenes / Nguyen T., Ludwig R. // New J. Chem. - 1999. - V. 23, № 6. - P. 603-607.
23. Talantova G. Calix[4]arenes with hard donor groups as efficient soft cation extractants. Remarkable extraction selectivity of calix[4]arene N-(X)sulfonylcarboxamides for Hg^{II} / Talantova G., Hwang H., Talantov V., Bartsch R. // J. Chem. Soc., Chem. Commun. - 1998. - № 13. - P. 1329-1330.
24. Arduini A. *p-t*-Butyl-calix[4]arene tetracarboxylic acid. A water soluble calixarene in a cone structure / Arduini A., Pochini A., Reverberi S., Ungaro R. // J. Chem. Soc., Chem. Commun. - 1984. - № 15. - P. 981-982.
25. Gutsche C. Calixarenes. 23. the complexation and catalytic properties of water soluble calixarenes / Gutsche C., Alam I. // Tetrahedron. - 1988. - V. 44, № 15. - P. 4689-4694.
26. Arnaud-Neu F. Cation complexation by chemically modified calixarenes. Part 10. Thioamide derivatives of *p*-tert-butylcalix[4]-, [5]- and [6]-arenes with selectivity for copper, silver, cadmium and

- lead. X-Ray molecular structures of calix[4]arene thioamide–lead(II) and calix[4]arene amide–copper(II) complexes / Arnaud-Neu F., Barrett G., Corry D. [*et al.*] // *J. Chem. Soc., Perkin Trans. 2.* - 1997. - № 3. - P. 575-579.
27. Jung Y. Facile synthesis of *p-tert*-butylthiacalix[4]arene by the reaction of *p-tert*-butylphenol with elemental sulfur in the presence of a base / Kumagi H., Hasegawa M., Miyanari S. [*et al.*] // *Tetrahedron Lett.* - 1997. - V. 38, № 22. - P. 3971-3972.
 28. Lin Y. Synthesis of original capping calixarenes with DTPA fragment / Lin Y., Leydier A., Métay E. [*et al.*] // *J. Incl. Phen. Macrocycl. Chem.* - 2008. - V. 61, № 1-2. - P. 187-193.
 29. König B. Heteroatom-bridged calixarenes / König B., Fonseca H.M. // *Eur. J. Inorg. Chem.* - 2000. - V. 11, № 9. - P. 2303-2310.
 30. Dvorakova H. Partially O-alkylated thiacalix[4]arenes: synthesis, molecular and crystal structures, conformational behavior / Dvorakova H., Lang J., Vlach J. [*et al.*] // *J. Org. Chem.* - 2007. - V. 72, № 19. - P. 7157-7166.
 31. Dudič M. Calixarene-based metalloporphyrins: molecular tweezers for complexation of DABCO / Dudič M., Lhoták P., Petříčková H. [*et al.*] // *Tetrahedron.* - 2003. - V. 59, № 14. - P. 2409-2415.
 32. Gutsche C. Conformational isomers of the ethers and esters of calix[4]arenes / Gutsche C., Dhawan B., Levine J. [*et al.*] // *Tetrahedron.* - 1983. - V. 39, № 3. - P. 409-426.
 33. Shimizu S. Water-soluble calixarenes as new inverse phase-transfer catalysts. Nucleophilic substitution of alkyl and arylalkyl halides in aqueous media / Shimizu S., Kito K., Sasaki Ya., Hirai C. // *J. Chem. Soc., Chem. Commun.* - 1997. - № 17. - P. 1629-1630.
 34. Iki N. A new water-soluble host molecule derived from thiacalixarene / Iki N., Fujimoto T., Miyano S. // *Chem. Lett.* - 1998. - V. 27, № 7. - P. 625-626.
 35. Matulkova I. Synthesis, characterization and extraction behavior of calix[4]arene with four propylene phosphonic acid groups on the lower rim / Matulkova I., Rohovec J. // *Polyhedron.* - 2005. - V. 24, № 2. - P. 311-317.
 36. Gutsche C. The complexation and catalytic properties of water-soluble calixarenes / Gutsche C., Alam I. // *Tetrahedron.* - 1988. - V. 44, № 15. - P. 4689-4691.
 37. Bonal Ch. Binding of inorganic and organic cations by *p*-sulfonato-calix[4]arene in water: a thermodynamic study / Bonal Ch., Israëlli Ya.,

- Morel P., Morel-Desrosiers N. // *J. Chem. Soc., Perkin Trans. 2.* - 2001. - № 7. - P. 1075-1078.
38. Gutsche C. The conformational properties of calix[4]arenes, calix[6]arenes, calix[8]arenes, and oxacalixarenes / Gutsche C., Bauer L. // *J. Am. Chem. Soc.* - 1985. - V. 107, № 21. - P. 6052-6059.
 39. Shinkai S. On the acidity of the hydroxyl groups in calix[4]arenes and the dissociation-dependent conformational change / Shinkai S., Koreishi H., Tsubaki T., Manabe O. // *Chem. Lett.* - 1986. - V. 15, № 8. - P. 1351-1354.
 40. Morohashi N. Thiacalixarenes / Morohashi N., Narumi F., Iki N. [*et al.*] // *Chem. Rev.* - 2006. - V. 106, № 12. - P. 5291-5316.
 41. Matsumiya H. Acid-base properties of sulfur-bridged calix[4]arenes / Matsumiya H., Terazono Y., Iki N., Miyano S. // *J. Chem. Soc., Perkin Trans. 2.* - 2002. - № 6. - P. 1166-1172.
 42. Coruzzi M. Molecular inclusion in functionalized macrocycles. Part 5. The crystal and molecular structure of 25,26,27,28,29-pentahydroxycalix[5]arene-acetone (1 : 2) clathrate / Coruzzi M., Andreetti G., Bocchi V. [*et al.*] // *J. Chem. Soc., Perkin Trans. 2.* - 1982. - № 9. - P. 1133-1138.
 43. Ungaro R. Molecular inclusion in functionalized macrocycles. Part 9. The crystal and molecular structure of p-t-butylcalix[4]arena-anisole (2:1) complex: a new type of cage inclusion compound / Ungaro R., Pochini A., Andreetti J., Domiano P. // *J. Chem. Soc., Perkin Trans. 2.* - 1985. - № 2. - P. 197-201.
 44. Arnaud-Neu F. Cation complexation by chemically modified calixarenes. 5. Protonation constants for calixarene carboxylates and stability constants of their alkali and alkaline-earth complexes / Arnaud-Neu F., Barrett G., Harris S.J. [*et al.*] // *Inorg. Chem.* - 1993. - V. 32, № 12. - P. 2644-2650.
 45. Andreetti G. Molecular inclusion in functionalized macrocycles. Part 6. The crystal and molecular structures of the calix[4]arene from p-(1,1,3,3-tetramethylbutyl)phenol and its 1:1 complex with toluene / Andreetti G., Pochini A., Ungaro R. // *J. Chem. Soc., Perkin Trans. 2.* - 1983. - № 9. - P. 1773-1779.
 46. Hirota M. Theoretical description of the preference of vicinal alkyl/phenyl gauche conformation by molecular mechanics. an alternative interpretation for the CH - π attractive interaction / Hirota M., Sekiya T., Abe K. [*et al.*] // *Tetrahedron.* - 1983. - V. 39, № 19. - P. 3091-3099.
 47. Rizzoli C. Molecular inclusion in functionalized macrocycles 4. the crystal and molecular structure of the cyclo {tetrakis[(5-t-butyl-2-

- acetoxy-1,3-phenylene)methylene}}-acetic acid (1:1) clathrate / Rizzoli C., Andreetti J., Ungaro R., Pochini A. // *J. Mol. Struct.* - 1982. - V. 82, № 1-2. - P. 133-141.
48. Iwamoto K. Conformations and structures of tetra-O-alkyl-*p-tert*-butylcalix[4]arenes / Iwamoto K., Araki K., Shinkai S. // *J. Org. Chem.* - 1991. - V. 56, № 16. - P. 4955-4962.
 49. See K. Calixarenes. 26. Selective esterification and selective ester cleavage of calix[4]arenes / See K., Fronczek F., Watson W. [*et al.*] // *J. Org. Chem.* - 1991. - V. 56, № 26. - P. 7256-7263.
 50. Pitarch M. Conformational control in the synthesis of mixed tetraethers of calix[4]arene. Part 2 / Pitarch M., Browne J., McKervey M. // *Tetrahedron.* - 1997. - V. 53, № 47. - P. 16195-16204.
 51. Ungaro R. New ionizable ligands from *p-t*-butylcalix[4]arene / Ungaro R., Pochini A., Andreetti G. // *J. Incl. Phen. Macrocycl. Chem.* - 1984. - V. 2, № 1-2. - P. 199-206.
 52. Cheriaa N. Synthesis and complexing properties of four imidazolyl acetamido *p-tert*-butylcalix[4]arenes / Cheriaa N., Abidi R., Vicens J. // *J. Incl. Phen. Macrocycl. Chem.* - 2008. - V. 60, № 3-4. - P. 303-312.
 53. Shinkai S. New syntheses and physical properties of *p*-alkylcalix[n]arenes / Shinkai S., Nagasaki T., Iwamoto K. [*et al.*] // *Bull. Chem. Soc. Jpn.* - 1991. - V. 64, № 2. - P. 381-386.
 54. Sorrell T. Synthesis of covalently-linked exo-calix[4]arenes / Sorrell T., Yuan H. // *J. Org. Chem.* - 1997. - V. 62, № 6. - P. 1899-1902.
 55. Biali S. Conformation, inversion barrier, and solvent-induced conformational shift in exo- and endo/exo-calix[4]arenes / Biali S., Böhmer V., Brenn J. [*et al.*] // *J. Org. Chem.* - 1997. - V. 62, № 24. - P. 8350-8360.
 56. Tunstad L. Host-guest complexation. 48. Octol building blocks for cavitands and carcerands / Tunstad L., Tucker J., Dalcanale E. [*et al.*] // *J. Org. Chem.* - 1989. - V. 54, № 6. - P. 1305-1312.
 57. Kim J. Calixarene-derived fluorescent probes / Kim J., Quang D. // *Chem. Rev.* - 2007. - V. 107, № 9. - P. 3780-3799.
 58. Valeur B. Design principles of fluorescent molecular sensors for cation recognition / Valeur B., Leray I. // *Coord. Chem. Rev.* - 2000. - V. 205, № 1. - P. 3-40.
 59. Vance D. Real-time assay of inorganic pyrophosphatase using a high-affinity chelation-enhanced fluorescence chemosensor / Vance D., Czarnik A. // *J. Am. Chem. Soc.* - 1994. - V. 116, № 20. - P. 9397-9398.
 60. Anion receptor chemistry / edited by J.L. Sessler, P.A. Gale, W.-S.

- Cho. - Cambridge: Royal Society of Chemistry, 2006. - 413 p.
61. Mamardashvili N. Zh., Porphyrin-calix[4]arenes / Mamardashvili N. Zh., Koifman O.I. // *Russ. J. Org. Chem.* - 2005. - V. 41, № 6. - P. 787-806.
 62. Mamardashvili G. Supramolecular porphyrin complexes / Mamardashvili G., Mamardashvili N. Zh., Koifman O.I. // *Russ. Chem. Rev.* - 2005. - V. 74, № 8. - C. 765-782.
 63. Dudic M. Synthesis and spectroscopic properties of porphyrin-(thia)calyx[4]arene conjugates / Dudic M., Lhoták P., Stibor I. [*et al.*] // *Tetrahedron.* - 2002. - V. 58, № 27. - P. 5475-5482.
 64. Tsuge A. Binding properties of calixarene-based cofacial bisporphyrins / Tsuge A., Kunimune T., Ikeda Y. [*et al.*] // *Chem. Lett.* - 2010. - V. 39, № 11. - P. 1155-1157.
 65. Baldini L. Molecular acrobatics: self-assembly of calixarene-porphyrin cages / Baldini L., Ballester P., Casnati A. [*et al.*] // *J. Am. Chem. Soc.* - 2003. - V. 125, № 46. - P. 14181-14189.
 66. Nagasaki T. Design and synthesis of a C₄-symmetrical hard-soft ditopic metal receptor by calixarene-porphyrin coupling / Nagasaki T., Fujishima H., Takeuchi M., Shinkai S. // *J. Chem. Soc., Perkin Trans. 1.* - 1995. - № 15. - P. 1883-1888.
 67. Lang K. Photophysical properties and photoinduced electron transfer within "host-guest" complexes of 5,10,15,20-tetrakis(4-N-methylpyridyl)porphyrin with water-soluble calixarenes and cyclodextrins / Lang K., Kubat P., Lhotak P. [*et al.*] // *Photochem. Photobiol.* - 2001. - V. 74, № 4. - P. 558-565.
 68. Fiammengo R. Heme-protein active site models via self-assembly in water / Fiammengo R., Wojciechowski K., Crego-Calama M. [*et al.*] // *Org. Lett.* - 2003. - V. 5, № 19. - P. 3367-3370.
 69. Costanzo L. Calixarene-porphyrin supramolecular complexes: pH-tuning of the complex stoichiometry / Costanzo L., Geremia S., Randaccio L. [*et al.*] // *Angew. Chem. Int. Ed.* - 2001. - V. 40, № 22. - P. 4245-4247.
 70. Mourer M. Synthesis and anti-HIV evaluation of water-soluble calixarene-based bithiazolyl podands / Mourer M., Psychogios N., Laumond G. [*et al.*] // *Bioorg. Med. Chem.* - 2010. - V. 18, № 1. - P. 36-45.
 71. Mourer M. *p*-Guanidinoethyl calixarene and parent phenol derivatives exhibiting antibacterial activities. Synthesis and biological evaluation / Mourer M., Dibama H., Fontanay S. [*et al.*] // *Bioorg. Med. Chem. Lett.*

- 2009. - V. 17, № 15. - P. 5496-5509.
72. Bezouska K. Carboxylated calixarenes bind strongly to CD69 and protect CD69+ killer cells from suicidal death induced by tumor cell surface ligands / Bezouska K., Snajdrova R., Krenek K. [*et al.*] // *Bioorg. Med. Chem.* - 2010. - V. 18, № 4. - P. 1434-1440.
 73. Neelamma M. Synthesis and structural studies on transition metal complexes derived from 4-hydroxy-4-methyl-2-pentanone-1H-benzimidazol-2-yl-hydrazone / Neelamma M., Venkateswar P., Anuradha G. // *E-J. Chem.* - 2011. - V. 8, № 1. - P. 29-36.
 74. Padalkar V. Synthesis, characterization, thermal properties, and antimicrobial activities of 5-(diethylamino)-2-(5-nitro-1H-benzimidazol-2-yl)phenol and its transition metal complexes / Padalkar V., Gupta V., Phatangare K. [*et al.*] // *ISRN Organic Chemistry*. - 2011. - ID 738361.
 75. Tsivadze A.Yu. Thermodynamics and mechanisms of the formation of supramolecules and supramolecular assemblies of s, p, d and f elements: problems and prospects / Tsivadze A.Yu., Ionova G.V., mikhalko V.K., Kostrubov Yu.N. // *Russ. Chem. Rev.* - 2007. - V. 76, № 3. - P. 213-236.
 76. Bünzli J.-C. Benefiting from the unique properties of lanthanide ions / Bünzli J.-C. // *Acc. Chem. Res.* - 2006. - V. 39, № 1. - P. 53-61.
 77. Pope S. Self-assembly of heterobimetallic d-f hybrid complexes: sensitization of lanthanide luminescence by d-block metal-to-ligand charge-transfer excited states / Pope S., Coe B., Faulkner S. [*et al.*] // *J. Amer. Chem. Soc.* - 2004. - V. 126, № 31. - P. 9490-9491.
 78. de Silva A. Switching 'on' the luminescence of one metal ion with another: selectivity characteristics with respect to the emitting and triggering metal / de Silva A., Gunaratne H., Rice T., Stewart S. // *Chem. Commun.* - 1997. - № 19. - P. 1891-1892.
 79. Bünzli J.-C. Lanthanide-containing molecular and supramolecular polymetallic functional assemblies / Bünzli J.-C., Piguet C. // *Chem. Rev.* - 2002. - V. 102, № 6. - P. 1897-1928.
 80. Botta M. Heterodinuclear Ln-Na complexes with an asymmetric macrocyclic compartmental Schiff base / Botta M., Casellato U., Scalco C. [*et al.*] // *Chem. Eur. J.* - 2002. - V. 8, № 17. - P. 3917-3926.
 81. Shavaleev N. Syntheses and structures of mononuclear $\{Re(CO)_3Cl(NN)\}$ 'complex ligands' with a pendant imino-pyridine binding site, and preparation of some heterodinuclear Re(I)-lanthanide(III) complexes / Shavaleev N., Bell Z., Accorsi G., Ward M. // *Inorg. Chim. Acta* - 2003.

- V. 351, № 22. - P. 159-166.
82. Shavaleev N. Syntheses and crystal structures of dinuclear complexes containing d-block and f-block luminophores. Sensitization of NIR luminescence from Yb(III), Nd(III), and Er(III) centers by energy transfer from Re(I)- and Pt(II)-bipyrimidine metal centers / Shavaleev N., Accorsi G., Virgili D. [*et al.*] // *Inorg. Chem.* - 2005. - V. 44, № 2. - P. 61-72.
 83. Piguet C. Isolated d-f pairs in supramolecular complexes with tunable structural and electronic properties / Piguet C., Edder C., Rigault S. [*et al.*] // *J. Chem. Soc., Dalton Trans.* 2000. - № 22. - P. 3999-4006.
 84. Li X.-L. Syntheses, structures, and sensitized lanthanide luminescence by Pt → Ln (Ln = Eu, Nd, Yb) energy transfer for heteronuclear PtLn₂ and Pt₂Ln₄ complexes with a terpyridyl-functionalized alkynyl ligand / Li X.-L., Shi L.-X., Zhang L.-Y. [*et al.*] // *Inorg. Chem.* - 2007. - V. 46, № 25. - P. 10892-10900.
 85. Costes J.-P. Macrocyclic and open-chain Cu^{II}-4f (4f = Gd^{III}, Ce^{III}) complexes with planar diamino chains: structures and magnetic properties / Costes J.-P., Dahan F., Novitchi G. [*et al.*] // *Eur. J. Inorg. Chem.* - 2004. - V. 2004, № 7. - P. 1530-1537.
 86. Chen Q.-Y. Heterodinuclear cryptates [EuML(dmfm)](ClO₄)₂ (M = Ca, Cd, Ni, Zn): tuning the luminescence of europium(III) through the selection of the second metal ion / Chen Q.-Y., Luo Q.-H., Hu X.-L. [*et al.*] // *Chem. Eur. J.* - 2002. - V. 8, № 17. - P. 3984-3990.
 87. dos Santos C. Recent developments in the field of supramolecular lanthanide luminescent sensors and self-assemblies / dos Santos C., Harte A., Quinn S., Gunlaugsson T. // *Coord. Chem. Rev.* - 2008. - V. 252, № 23-24. - P. 2512-2527.
 88. Lawrence D. Self-assembling supramolecular complexes / Lawrence D., Jiang T., Levett M. // *Chem. Rev.* - 1995. - V. 95, № 6. - P. 2229-2260.
 89. Shevchenko D. First heterobimetallic MnII/MII (M=Cu, Ni) complexes with open-chain aliphatic Schiff-base ligands obtained by direct template synthesis / Shevchenko D., Petrusenko S., Kokozay V., Skelton B. // *J. Coord. Chem.* - 2004. - V. 57, № 15. - P. 1287-1298.
 90. Piguet C. Design of luminescent building blocks for supramolecular triple-helical lanthanide complexes / C. Piguet, J.-C. G. Bünzli, G. Bernardinelli // *J. Chem. Soc. Dalton Trans.* - 1995. - № 1. - P. 83-97.
 91. Bünzli J.-C. Self-assembly and photophysical properties of lanthanide

- dinuclear triple-helical complexes / J.-C. Bünzli, G. Bernardinelli, C. Piguet [*et al.*] // J. Amer. Chem. Soc. - 1993. - V. 115, № 18. - P. 8197-8206.
92. Piguet C. Lanthanide podates with predetermined structural and photophysical properties: strongly luminescent self-assembled heterodinuclear d-f complexes with a segmental ligand containing heterocyclic imines and carboxamide binding units / C. Piguet, J.-C. Bünzli, G. Bernardinelli [*et al.*] // J. Amer. Chem. Soc. - 1996. - V. 118, № 28. - P. 6681-6697.
 93. Brianese N. Asymmetric compartmental macrocyclic ligands and related mononuclear and hetero-dinuclear complexes with d- and/or f-metal ions / Brianese N., Casellato U, Tamburini S. [*et al.*] // Inorg. Chim. Acta. - 1999. - V. 293, № 2. - P. 178-194.
 94. Brayshaw P. Synthetic, structural, and spectroscopic studies on solids containing tris(dipicolinato)rare earth anions and transition or main group metal cations / P. Brayshaw, J.-C. Bünzli, P. Froidevaux [*et al.*] // Inorg. Chem. - 1995. - V. 34, № 8. - P. 2068-2076.
 95. Furphy B. Bimetallic lanthanide complexes of the calixarenes: europium(III) and *tert*-butylcalix[8]arene / Furphy B., Harrowfield J., Kepert D. [*et al.*] // Inorg. Chem. - 1987. - V. 26, № 25. - P. 4231-4236.
 96. Harrowfield J. Lanthanide ions as calcium substitutes: a structural comparison of europium and calcium complexes of a ditopic calixarene / Harrowfield J., Ogden M., Richmond W., White A. // J. Chem. Soc., Dalton Trans. - 1991. - № 8. - P. 2153-2160.
 97. Beer P. Acid-amide calixarene ligands for uranyl and lanthanide ions: synthesis, structure, coordination and extraction studies / Beer P., Brindley G., Fox O. [*et al.*] // J. Chem. Soc., Dalton Trans. - 2002. - № 16. - P. 3101-3111.
 98. Bilyk A. A unique rare-earth cluster within a calixarene sandwich: parallels in the chemistry of cyclosiloxanes and calixarenes / Bilyk A., Hall A., Harrowfield J. // Aust. J. Chem. - 2000. - V. 53, № 11-12. - P. 895-898.
 99. Bi Y. A unique Mn₂Gd₂ tetranuclear compound of *p-tert*-butylthiacalix[4]arene / Bi Y., Li Y. // Inorg. Chem. - 2008. - V. 47, № 21. - P. 9733-9735.
 100. Kajiwarra T. Conformation-controlled luminescent properties of lanthanide clusters containing *p-tert*-butylsulfonylcalix[4]arene / Kajiwarra T., Katagiri K., Hasegawa M. [*et al.*] // Inorg. Chem. - 2006. - V. 45, № 13. - P. 4880-4882.
 101. Photoluminescence of solutions / edited by C.A Parker. - Amsterdam-

- London-New York: Elsevier Publishing Co, 1968. - 544 p.
102. Tanaka T. One-step heterogeneous assembly of terbium (III) and silver (I) with thiacalix[4]arene ligands to form a cage including terbium (III) in an octa-oxygen cube / Tanaka T., Iki N., Kajiwara T. [*et al.*] // J. Incl. Phenom. Macrocycl. Chem. - 2009. - V. 64, № 3-4. - P. 379-383.
 103. Schühle D.T. Calix[4]arenes as molecular platforms for magnetic resonance imaging (MRI) contrast agents / Schühle D.T., Schatz J., Laurent S. [*et al.*] // Chem. Eur. J. - 2009. - V. 15, № 13. - P. 3290-3296.
 104. Ramírez F. Physicochemical properties and theoretical modeling of actinide complexes with a *p-tert*-butylcalix[6]arene bearing phosphinoyl pendants. Extraction capability of the calixarene toward f-elements / Ramírez F., Varbanov S., Padilla J., Bünzli J.-C. // J. Phys. Chem. B. - 2008. - V. 112, № 35. - P. 10976-10988.
 105. Yan B. Molecular construction, characterization, and photophysical properties of supramolecular lanthanide-calix[4]arene covalently bonded hybrid systems / B. Yan, Q.-M. Wang, D.-J. Ma // Inorg. Chem. - 2009. - V. 48, № 36 - P. 36-44.
 106. Qiao X.-F. Photoactive binary and ternary lanthanide (Eu^{3+} , Tb^{3+} , Nd^{3+}) hybrids with *p-tert*-butylcalix[4]arene derived Si-O linkages and polymers / X.-F. Qiao, H.-Y. Zhang, B. Yan // Dalton Trans. - 2010. - V. 39. - P. 8882-8892.
 107. Zhang H.-Y. Photoactive ternary $\text{Tb}^{3+}/\text{Zn}^{2+}$ centered hybrids with *p-tert*-butylcalix[4]arene functionalized Si-O bridge and polyvinylpyridine / Zhang H.-Y., Qiao X.-F., Yan B. // Inorg. Chem. Commun. - 2010. - V. 13, № 11. - P. 1231-1233.
 108. Yan B. Novel chemically bonded Tb/Zn hybrid sphere particles: molecular assembly, microstructure and photoluminescence / Yan B., Qian K. // J. Photochem. Photobiol. A. - 2009. - V. 207, № 2-3. - P. 217-223.

Chapter 2

Molecular complexes of carbohydrate-containing metabolites with antibiotics

Leonid Yakovishin¹, Vladimir Grishkovets², Elena Korzh¹, Grzegorz Schroeder³ and Volodymyr Rybachenko⁴

¹ *Sevastopol National Technical University, Universitetskaya Str. 33, Sevastopol, 99053, Crimea, Ukraine*

² *V.I. Vernadsky Taurida National University, Vernadsky Ave. 4, Simferopol, 95007, Crimea, Ukraine*

³ *Adam Mickiewicz University in Poznań, Faculty of Chemistry, Umultowska 89b, 61-614 Poznań, Poland*

⁴ *L.M. Litvinenko Institute of Physical Organic and Coal Chemistry NAS of Ukraine, R. Luxemburg 70, 83114 Donetsk, Ukraine*

Cyclodextrins (CD, Fig. 1) are widely applied to molecular encapsulation of various drugs. The complexes obtained can be used for address delivery, controlled release, solubility increase, spectrum of biological activity expansion, stability improvement, therapeutic doses and side effects reduction [1–6].

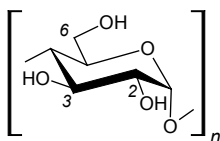


Figure 1. Cyclodextrins (CD): α -cyclodextrin ($n=6$; α -CD), β -cyclodextrin ($n=7$; β -CD) and γ -cyclodextrin ($n=8$; γ -CD).

Plant di- and triterpene glycosides are perspective drug complexants [7–10]. The following complexants are suggested: glycyrrhizic acid (3-*O*- β -*D*-glucuronopyranosyl-(1 \rightarrow 2)-*O*- β -*D*-glucuronopyranoside of glycyrrhetic acid, GA, Fig. 2), which is a dominating triterpene glycoside of *Glycyrrhiza glabra* L.

roots, and its monoammonium salt (glycyram, GC, Fig. 2) [7, 8, 11–14]. GA and GC have solubilizing properties for a range of drugs [15–18].

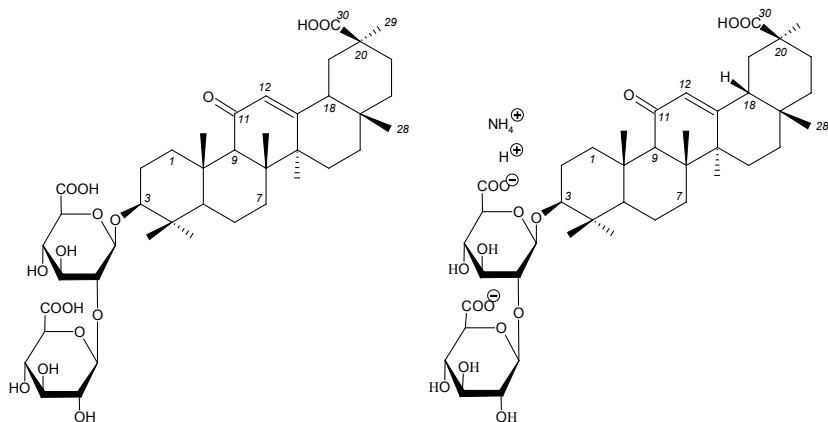


Figure 2. Glycyrrhizic acid (GA) and glycyram (GC).

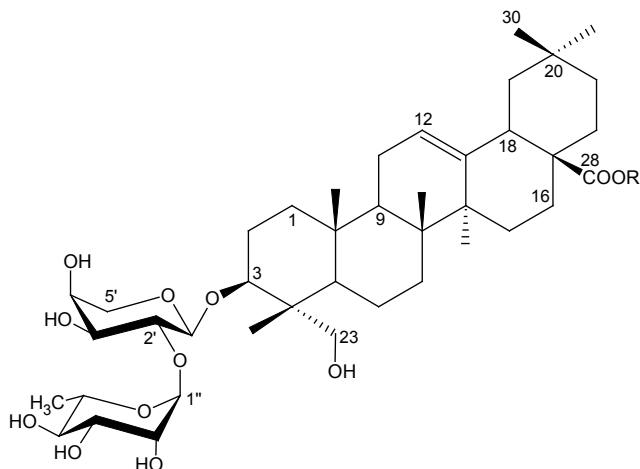


Figure 3. α -Hederin (glycoside 1; R=H) and hederasaponin C (glycoside 2; R= $-\beta\text{Glc}_p-(6\rightarrow1)-\beta\text{Glc}_p-(4\rightarrow1)-\alpha\text{Rha}_p$).

Molecular complexes of ivy triterpene glycosides α -hederin (hederagenin

3-*O*- α -*L*-rhamnopyranosyl-(1 \rightarrow 2)-*O*- α -*L*-arabinopyranoside, glycoside **1**, Fig. 3) and hederasaponin C (hederagenin 3-*O*- α -*L*-rhamnopyranosyl-(1 \rightarrow 2)-*O*- α -*L*-arabinopyranosyl-28-*O*- α -*L*-rhamnopyranosyl-(1 \rightarrow 4)-*O*- β -*D*-glucopyranosyl-(1 \rightarrow 6)-*O*- β -*D*-glucopyranoside, glycoside **2**, Fig. 3) with pharmacones of different nature have been prepared [10].

Clathrate complexes of acanthophylloside, extracted from roots of *Acanthophyllum gypsophyloides*, with prostaglandins are synthesized [7, 14]. Molecular complexes of stevioside and rebaudioside (diterpene glycosides *Stevia rebaudiana* Bertoni (Compositae)) have been studied [7, 9].

Complexes with laevomycetin (chloramphenicol)

Laevomycetin (chloramphenicol, Lev, Fig. 4) is a broad-spectrum antibiotic. It is applied to cure salmonellosis, brucellosis, meningitis, chlamydiosis, typhoid, eye infections, septic wounds and other diseases. But Lev has got a range of side effects. It can toxically affect hematopoietic system, suppress intestinal microflora, cause psychomotor disturbances, confusion of consciousness, delusions, allergic reactions and reduce hearing and eyesight [19].

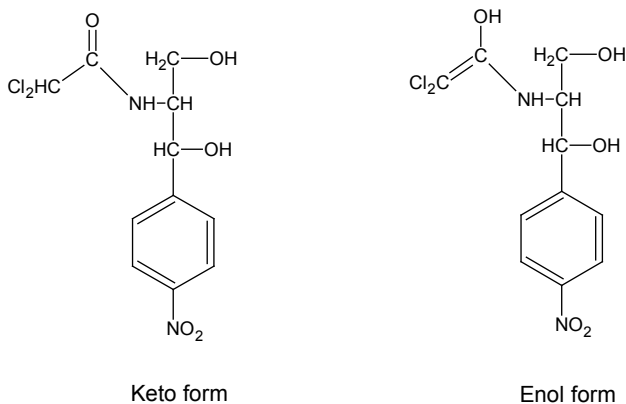


Figure 4. Laevomycetin (chloramphenicol, Lev).

Szabó-Révész P. *et al.* prepared mixtures of Lev and β -CD (Fig. 5) [20] and studied its rheologic parameters [21, 22]. By means of the ^1H NMR method, the complex 1:1 Lev with β -CD was investigated [23]. The antibiotic was discovered to exist in aqueous solution in keto and enol forms with approximate ratio 3:2. Herewith, β -CD makes 1:1 complexes with two tautomeric forms of

Lev. Interaction selectivity was not observed. While complexation, aromatic ring of Lev enters a hydrophobic β -CD cavity, and NO_2 group stands out from the lower torus ring β -CD.

In [24], the results of computer modelling of inclusive complexes of keto and enol forms of Lev with β -CD are given. The complexes in which nitrophenyl fragment of Lev enters β -CD cavity at the side of wide ring are preferable.

Li N.B. *et al.* studied the interaction of Lev with β -CD by means of resonance Rayleigh scattering (RRS). The method was first suggested to define K stability of clathrates. The values of thermodynamic parameters indicate the presence of hydrogen bonds and van der Waals interactions while complexation. A good coincidence of the values of K_s , obtained by RRS and UV-spectroscopy methods, was shown. The temperature increasing, K_s of complexes decrease from 2×10^3 to $3 \times 10^2 \text{ M}^{-1}$ [25].

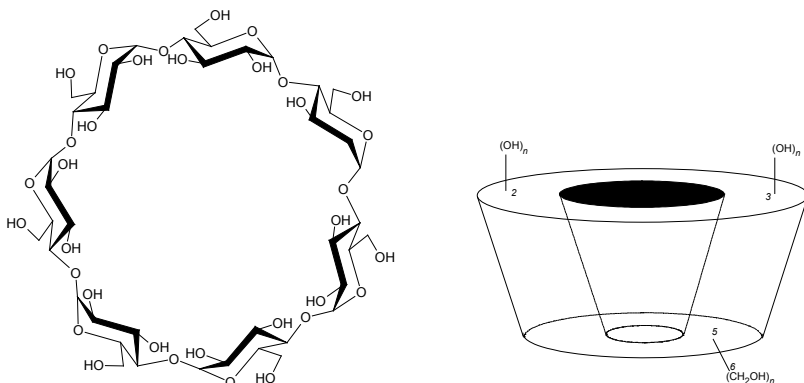


Figure 5. β -Cyclodextrin (β -CD).

The complexes of Lev with modified β -CD were obtained [26–30]. For instance, in [26], the complex of Lev with heptakis (2,6-di-*O*-methyl)- β -CD is reported. It was studied by the method of phase solubility and by different spectral methods. The complex composition is 1:1. K stability of complex, defined by the method of phase solubility, is 493 M^{-1} (293 K). The positions of Lev molecule in internal cavities of heptakis (2,6-di-*O*-methyl)- β -CD and β -CD differ. In the first complex, Lev nitrophenyl group is deeply situated in the cavity at the side of the narrow torus ring. Comparing IR-spectra of individual Lev and heptakis (2,6-di-*O*-methyl)- β -CD, they observed changes in absorption frequencies of aromatic ring and C=O, N–H groups. It indicates their participation in the complexation

process. Absorption bands of NO_2 group do not shift.

Zuorro A. *et al.* reported preparation of complexes of Lev with methyl- and 2-hydroxypropyl- β -CD [27]. Complexes composition is 1:1. On the basis of phase solubility analysis, stability constants K_s were found to equal 259.5 ± 14.0 and $86.3 \pm 4.8 \text{ M}^{-1}$ (under 298 K) respectively. Solubility increase of Lev under interaction with modified β -CD was shown. Besides, the authors studied antibacterial activity of the complexes and suggested to apply them to eye drops preparation. Complexation does not result in Lev biological activity decrease. Herewith, activity of various complexes does not differ substantially.

Complex of Lev with methylated β -CD is constituent in eye drops Clorocil (Oftalder company, Portugal) [29, 30].

Palmitate of Lev makes a complex with 2-hydroxypropyl- β -CD as well [28]. Nevertheless, its composition differs from the one of Lev-hydroxypropyl- β -CD complex. Authors of [28] emphasize on stoichiometry 1:2. They made their conclusions observing A_p -type of phase solubility diagram under 298 K for aqueous solutions. Phase solubility diagrams for Lev- β -CD and Lev-2-hydroxypropyl- β -CD systems are linear of A_L -type. This fact indicates 1:1 complexes formation. K_s of 1:1 complexes of Lev with β -CD and 2-hydroxypropyl- β -CD are 170 and 120 M^{-1} respectively, and for 1:2 complexes of Lev palmitate with β -CD, 2-hydroxypropyl- β -CD are 4500 and 3400 M^{-2} . K_s of complexes with modified β -CD turns to be less, which is a result of steric constraints of complexation caused by oxypropyl groups preventing from molecule-guest penetration into CD cavity.

Complex of tryterpene glycoside from glycyrrhizae GA with Lev was obtained in aqueous-ethanol medium [31–33]. 1:1 Complex was studied by IR- and UV-spectroscopy [31, 33]. It is made up by hydrogen bounds with participation of GA OH and C=O groups. The latter fact is proved by corresponding absorption bands shift to low-frequencies region of IR-spectra [31]. The complex of GA with Lev appeared to be more active than its individual components. It increased mice resistance to infectious diseases and stimulated their immunity [31].

Combined drug Biophenicol, containing Lev and GA, has been made [32]. Complexes of 18-dehydroglycyrrhetic acid (glyderinin, Fig. 6) and its sodium salt with Lev have been prepared [32, 34]. Ointment Glyphenicol, containing 18-dehydroglycyrrhetic acid and Lev, has been made. Its activity surpasses the ointment Levomecol [32]. Complex of Lev with 18-dehydroglycyrrhetic acid, obtained in aqueous-ethanol medium, was described by means of IR- and UV-spectroscopy methods [34].

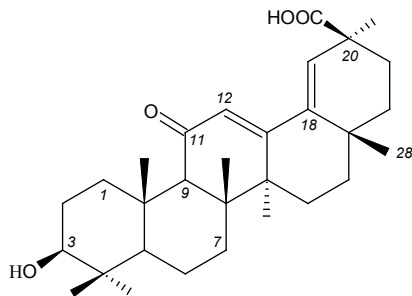


Figure 6. 18-Dehydroglycyrrhetic acid (glyderinin).

By the method of electrospray-ionization mass spectrometry, complexation of Lev with GA was studied [35]. Herewith, in mass spectrum (negative-ion mode) the peaks of ions $[M^{GA}+M^{Lev}-H]^-$ with m/z 1143.29 and $[M^{GA}+M^{Lev}-2H]^{2-}$ with m/z 571.16, corresponding complexation GA with Lev with the ratio 1:1, have been observed. Besides, in mass spectrum, a peak of ion $[M^{GA}+2M^{Lev}-H]^{2-}$ with m/z 732.14 was discovered. Its ratio of components is 1:2.

The method of mass spectrometry (electrospray-ionization) was also applied in [36] to analyze complexation of Lev with glycosides **1** and **2**. In mass spectra, the peaks of ions $[M^1+M^{Lev}-H]^-$ with m/z 1071.7 (I_{rel} 7.4 %), $[M^2+M^{Lev}+H]^+$ with m/z 1545.5 (0.2 %) and $[M^2+M^{Lev}-H]^-$ with m/z 1543.5 (0.1 %), corresponding 1:1 complexes of glycosides **1** and **2** with Lev.

Spectrophotometric study of Lev complexes with GC and glycosides **1** and **2** has been recently carried out in aqueous solutions, and thermodynamic parameters being calculated (Table 1) [37]. Complexes composition is defined by means of isomolar series method. For all the cases the molar ratio ≈ 1.0 is obtained. It corresponds to 1:1 complexes (Fig. 7). Previously, the peaks of ions corresponding to complexes of Lev with glycosides **1** and **2** of the same composition were discovered [36]. Absorption spectrum of isomolar series for Lev–GC mixture has isobestic points at 232 and 268 nm (Fig. 8). With the help of isomolar curves obtained, complex stability constants were calculated by the method [38]. The complex Lev–GC proved to be the most stable one. $K_{Lev \times GC}$ is 2 times more than $K_{Lev \times 1}$, and 4 times more than $K_{Lev \times 2}$.

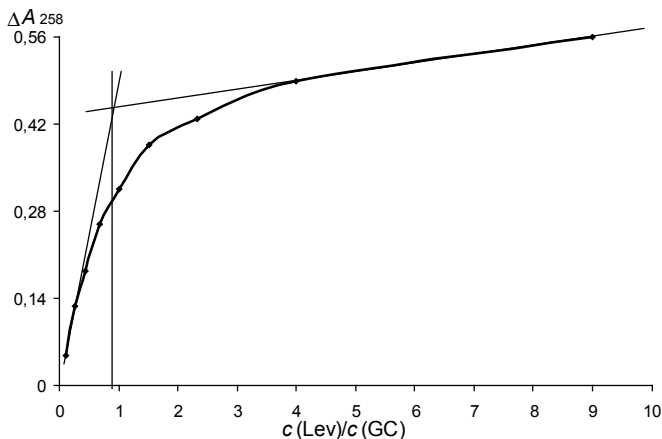


Figure 7. Graph of optical density ΔA against composition ratio in isomolar series under $\lambda=258$ nm: $c(\text{Lev})=10^{-4}$ M, $c(\text{GC})=10^{-4}$ M (pH 7.2).

Table 1. Thermodynamic parameters of Lev complexation with GC and glycosides 1, 2 in aqueous solutions under 20 °C (pH 7.2)

Complex	K , M ⁻¹
Lev×1	4.24×10^4
Lev×2	2.15×10^4
Lev×GC	8.57×10^4

The high stability of complex Lev×GC was explained in [37] with great GC abilities to interact with Lev. Its aglicone and carbohydrate parts contain carboxylic groups. Besides, GC is a salt, and that is why can take part in making ion-molecular hydrogen bond like $-\text{COO}^- \cdots \text{H}-\text{O}-$ and in ion-dipole interactions.

Literature data analysis showed the values K of stability of Lev complexes with triterpene glycosides to be higher than K of stability of Lev complexes with β -CD and with modified β -CD.

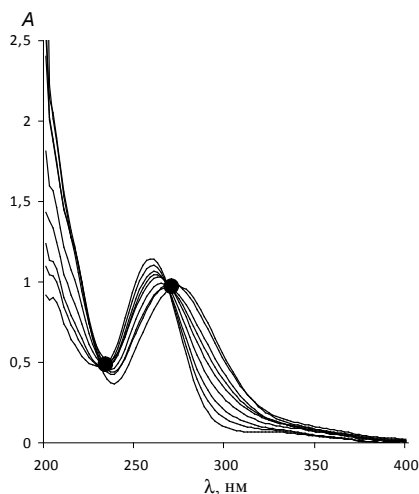


Figure 8. Absorption curves for isomolar series of solutions: $c(\text{Lev})=10^{-4} \text{ M}$, $c(\text{GC})=10^{-4} \text{ M}$ ($\text{pH } 7.2$).

Complexes with anthracycline antibiotics

Anthracycline antibiotics are widely used to cure oncological diseases. But the usage is restricted by their high toxicity [19, 39]. Anthracycline antibiotics include doxorubicin (DOX) and daunorubicin (rubomycin, DAU; Fig. 9), which are traditionally used as hydrochlorides. They have got a high antitumoral activity.

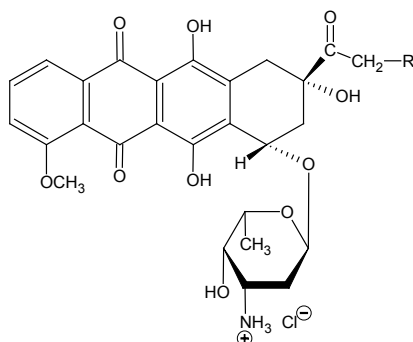


Figure 9. Hydrochlorides of doxorubicin DOX ($R=\text{OH}$) and daunorubicin DAU ($R=\text{H}$).

Anthracycline antibiotics toxicity can be reduced by means of their complexation with various CD. Besides, complexation improves antibiotics solubility. Molecular complexes of DOX with various CD are prepared. Bekers O. *et al.* considered DOX and DAU interaction with α -, β - and γ -CD [40]. The complexes are discovered to make complexes with γ -CD only. The complexation has been studied by different methods (HPLC, circular dichroism measurement, UV- and visible spectroscopy) in aqueous solutions under pH 1.5–10.0. Herewith, under the same temperature and pH, the values of K_s for DOX– γ -CD and DAU– γ -CD complexes are of the same order. The highest K_s are obtained under 25 °C, pH 7.0 (670 and 775 M⁻¹ for DOX and DAU complexes respectively) and 10.0 (713 and 653 M⁻¹ for complexes of DOX and DAU respectively).

Bekers O. *et al.* studied the possibility of DOX and DAU complexation with α -, β - and γ -CD by the methods of NMR ¹H and molecular modelling [41]. Antibiotics complexation with α - and β -CD does not take place. This result confirms the above results obtained by the other methods [40]. Analysis of NMR-spectra showed the aglicone part of DOX and DAU is introduced into an internal cavity, and amino sugar residue can interact with OH-groups of external torus ring of γ -CD (Fig. 10). K_s of the complexes were calculated with the help of a modified equation of Benesi–Hildebrand. They proved to be quite similar, and were equal 345 and 323 M⁻¹ respectively [41].

Besides, Bekers O. *et al.* studied different factors influencing DOX and DAU stability in presence of α -, β - and γ -CD [42]. Antibiotics decomposition in acid medium is discovered to reduce under γ -CD presence only. The presence of α - and β -CD does not affect antibiotics stability either in acid or in alkaline media.

The authors of [43] studied processes of DOX complexation with β - and γ -CD by the methods of NMR ¹H and electronic spectroscopy, circular dichroism measurement, and fluorescent analysis. Complexes K_s are defined. Unlike the authors of [40, 41], Husain N. *et al.* discovered complexation of DOX with β -CD [43]. Under pH 7.1, K_s of complexes β - and γ -CD are 129–210 M⁻¹ and 235–977 M⁻¹ respectively. The values of K_s indicate greater stability of DOX complex with γ -CD, which is caused by a large diameter of its internal cavity. Complexes have 1:1 composition. Besides, Husain N. *et al.* [43] estimated the influence of pH on the value of K_s . The highest values of K_s are obtained under pH 7.1. Under pH 3.6 and 11.0, the values of K_s on the average are equal to 48 and 33 M⁻¹ (for β -CD respectively), as well as 89 and 43 M⁻¹ (for γ -CD respectively).

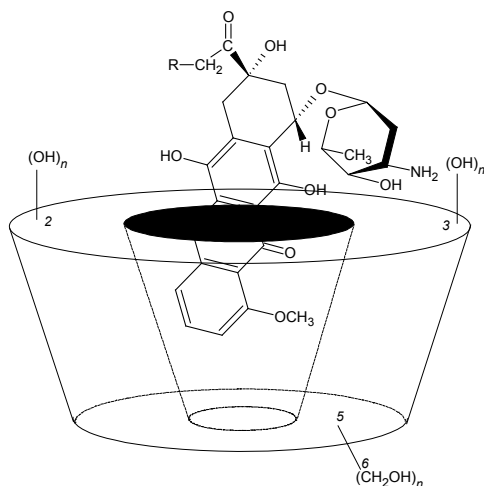


Figure 10. DOX and DAU interaction with β -CD.

By the method of electronic spectroscopy, K_s of complexes of DOX with γ -CD and its hydroxypropyl derivatives under 298 K, are studied [44]. They are 1360 ± 70 and 320 ± 20 M^{-1} respectively. In the previous papers, K_s for complex DOX- γ -CD are given by the values of 1000 M^{-1} [40, 41, 43].

Complexation ability of DOX with α -, β - and γ -CD is studied by the method of electronic spectroscopy. Complexes ability of improvement of DOX cytotoxicity is considered. DOX and β -CD mixture in the greatest degree (for more than 95 %) suppresses vitality of adenocarcinoma cells [45].

2-Hydroxypropyl- β -CD, 2-hydroxypropyl- γ -CD and γ -CD reduced DOX degradation. Modified CD increase DOX solubility rate. Complex of DOX with 2-hydroxypropyl- β -CD turned to be less toxic [46].

The possibility of DOX association with a polymer, obtained by crosslinking of epichlorohydrin with β -CD has been recently considered. The polymer makes nanoparticles of ≈ 15 nm causing DOX dimmers decomposition by complexation. Association constant for 1:1 solution was determined [47].

DOX complexation with new β -CD derivatives mono(6-deoxy-6-(1-1,2,3-triazo-4-yl)-1-propan-3-*O*-(4-methoxyphenyl))- β -CD and mono(6-deoxy-6-thio-(1-propan-3-*O*-(4-methoxyphenyl)))- β -CD has been studied [48]. For 1:1 complexes, in DMSO- H_2O medium, K_s 2.3×10^4 and K_s 3.2×10^5 M^{-1} are calculated respectively. The values K_s of the complexes are considerably greater than of the above-mentioned β -CD complex, obtained in aqueous solution [43].

In DMSO solutions, K_s turned to be considerably less, 121.1 ± 6.2 and 6768 ± 41 M^{-1} respectively.

1:1 Complexes of DAU and DOX hydrochlorides with GA are prepared. Herewith, complex with DAU is stated to be less toxic than the initial antibiotics [49]. Complexes are characterized by UV-spectroscopy. For the complex DAU–GA, IR-spectrum is given. DAU–GA complex is soluble in water, acetone, methanol and ethanol.

Recently, several liposomal transport forms for DOX has been elaborated [50, 51]. DOX– γ -CD complex introduction in pegylated liposomes is considered [52]. The aggregate reduces tumor growth and improves mice survival rate. DOX complex with phospholipid nanosystem, stabilized by trisodium salt of GA, is prepared. It has got a better antitumoral and antimetastatic activity, in comparison with individual DOX [53].

Triterpene glycoside **1** from ivy is known to have antitumoral activity and antimutagenic effect against clastogenicity of DOX [15, 54, 55]. GC improves antitumoral effect of drugs and reduces their toxicity [56].

Paper [57] is dedicated to spectrophotometry research of DOX complexation with GC and with ivy glycosides **1** and **2**, as well as to the definition of K_s of the complexes prepared in aqueous solutions under pH 7.2 (16 °C). Complexes composition 1:1 is defined by the method of isomolar series (the method by Ostromyslensky–Job). For the complexes DOX–**1**, DOX–**2** and DOX–GC, K_s are 4.20×10^5 , 1.56×10^7 and 5.63×10^4 M^{-1} respectively. Absorption spectrum of isomolar series of DOX with GC has got isobestic point at 276 nm (Fig. 11).

In a DOX molecule, OH- and CO-groups, which make hydrogen bounds with carboxylic and hydroxyl groups of GC and glycosides **1** and **2**, are contained. DOX and GC are salts and therefore are involved in ionic interactions by complex formation. High stability of DOX–**2** complex can be explained with a substantial role of hydrophobic interactions of aromatic DOX system and non-polar aglicone part of glycoside **2**, which, unlike glycoside **1** and GC, has got no carboxylic group. Besides, glycoside **2** molecule contains a number of OH-groups, capable of making hydrogen bounds.

K_s of complexes of DOX with CD and their derivatives are discovered to be equal to 10^2 – 10^5 M^{-1} [44, 48]. DOX complexes with human and bovine serum albumin have K_s 1.1×10^4 and 7.8×10^3 M^{-1} respectively [58], with nucleic acid bases, nucleosides and nucleotides – 25 – 380 M^{-1} [59] and with NAD – 190 M^{-1} [59]. In such a way, DOX complexes with triterpene glycosides are quite stable. GC and glycosides **1** and **2** can be treated as its transport systems.

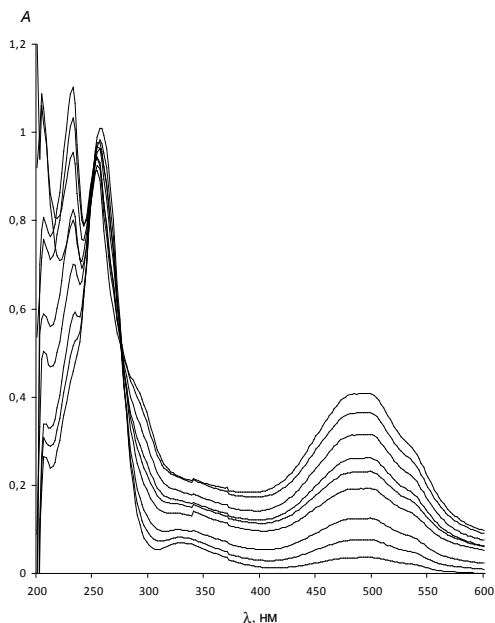


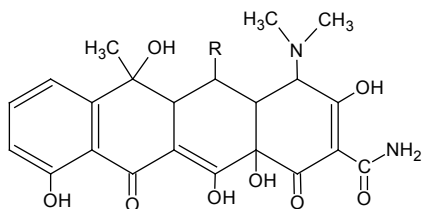
Figure 11. Absorption curves of isomolar series of solutions: $c(\text{DOX})=10^{-4} \text{ M}$, $c(\text{GC})=10^{-4} \text{ M}$ (pH 7.2).

Complexes with tetracyclines

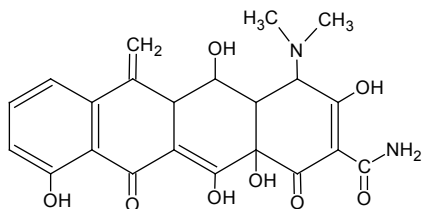
Tetracyclines are antibiotics of broad-spectrum antibiotics. They possess a range of side effects: reduce appetite, sicken, vomit, diarrhea, allergic reactions, photosensitizing etc. Tetracycline (TC), oxytetracycline (OTC), metacycline, doxycycline (DC) and other representatives of tetracyclines have low solubility in aqua [19].

1:1 Complex OTC with GA has been prepared [31]. On the basis of comparison of IR-spectra of complex and individual GA, the conclusion on hydrogen bonds formation is made.

IR-spectrometry is also applied to analyze clathrate of TC hydrochloride with β -CD, formed in aqueous solution [60]. The complex consists of TC molecule and of two molecules of β -CD. Complex stoichiometry is additionally confirmed by NMR-spectroscopy (^1H and NOESY). F.B. de Sousa *et al.* supposed one molecule of β -CD interacts with a TC aromatic ring, and another one is situated at the opposite side of TC (Fig. 13).



TC, OTC



DC

Figure 12. Tetracycline TC ($R=H$), oxytetracycline OTC ($R=OH$) and doxycycline DC.

Dissociation constants of complexes of TC hydrochloride with α - and β -CD are defined by the method of mass-spectrometry with electrospray ionization [61]. 1:1 and 1:2 complexes with α -CD have constants K_s 4.47×10^{-4} and $6.51 \times 10^{-4} \text{ M}^{-1}$ (respectively), and β -CD – 2.26×10^{-4} and $8.57 \times 10^{-4} \text{ M}^{-1}$ (respectively). We can see the values of K_s do not differ considerably.

Nevertheless, in [62] TC was proved to make 1:1 complex with β -CD. They also studied antibacterial activity of mixtures of TC and β -CD, with molar ratios 1:1, 1:2, 1:3 and 1:4 against *Actinobacillus actinomycetemcomitans* and *Porphyromonas gingivalis*. 1:4 Mixture proved to be the most effective against bacteria *P. gingivalis*. Mixtures of 1:1 and 1:2 compositions display the best counteraction against *A. actinomycetemcomitans*.

Biologically active glasses have been considered as delivery systems of TC and TC in 1:1 complex with β -CD [63]. Bacteriostatic activity of glasses with TC and TC- β -CD complex has been discovered. Heptakis (2,6-di-*O*-isobutyl)- β -CD, immobilized on PVC-membrane, has been considered as a sensor for TC determination [64]. Modified β -CD extracts TC from the solution and makes complex with it.

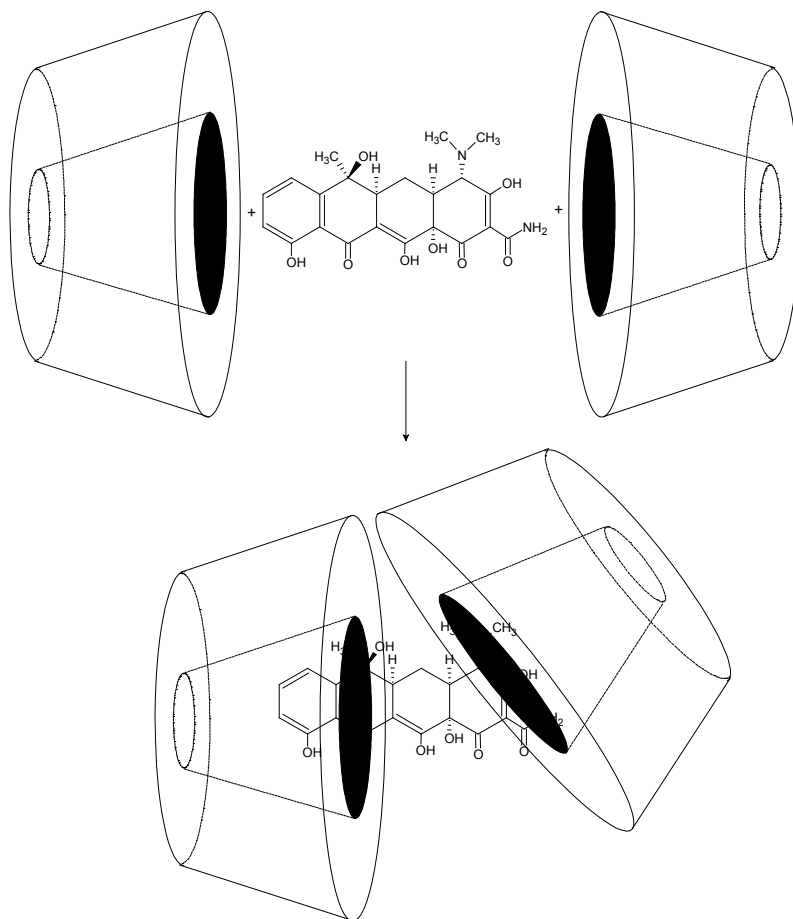


Figure 13. Interaction of TC with β-CD.

Molecular complex of DC with hydroxypropyl-β-CD of 1:1 composition has been prepared. On the basis of phase solubility studies, complex K_s are found to be 31.23 (in aqueous solution) and 120.80 M⁻¹ (in 0.5 % solution of MgCl₂) [65]. Numeric modelling of DC molecular complex with hydroxypropyl-β-CD [66, 67]. Hydroxypropyl-β-CD was used to prepare DC hydrogel [68]. The gel is proved to inhibit neovascularization of rats cornea.

References

1. Steed J.W., Atwood J.L. *Supramolecular chemistry*, Chichester: John Wiley & Sons, Ltd, 2000, 745 p.
2. Challa R., Ahuja A., Ali J., Khar R.K. Cyclodextrins in drug delivery: an updated review, *AAPS Pharm. Sci. Tech.*, 2005, Vol. 6, No. 2, P. E329–E357.
3. Li S., Purdy W.C. Cyclodextrins and their applications in analytical chemistry, *Chem. Rev.*, 1992, Vol. 92, P. 1457–1470.
4. Singh R., Bharti N., Madan J., Hiremath S.N. Characterization of cyclodextrin inclusion complexes – a review, *J. Pharm. Sci. Tech.*, 2010, Vol. 2, P. 171–183.
5. Belikov V.G., Kompantseva E.V., Botezat-Belyi Yu.K. Cyclodextrins and their inclusion compounds with drugs (review), *Pharm. Chem. J.*, 1986, Vol. 20, No. 5, P. 299–306.
6. Uekama K., Hirayama F., Irie T. Cyclodextrin drug carrier systems, *Chem. Rev.*, 1998, Vol. 98, P. 2045–2076.
7. Tolstikova T.G., Tolstikov A.G., Tolstikov G.A. On the way to low-dose drugs, *Vestn. Ross. Acad. Nauk*, 2007, Vol. 77, No. 10, P. 867–874.
8. Tolstikova T.G., Bryzgalov A.O., Sorokina I.V., Ratushnyak A.S., Zapara T.A., Simonova O.G., Tolstikov G.A. To the nature of the effect of glycosidic clathration of pharmacons, *Dokl. Acad. Nauk*, 2007, Vol. 416, No. 1, P. 336–337.
9. Tolstikova T.G., Bryzgalov A.O., Khvostov M.V., Tolstikov G.A. Rebaudioside, a novel agent of glycoside clathration of pharmacons, *Dokl. Biol. Sci.*, 2009, Vol. 426, P. 205–206.
10. Yakovishin L.A., Grishkovets V.I., Schroeder G., Borisenko N.I. Molecular complexation of ivy saponins with some drugs and biologically active substances, in *Functionalized molecules – synthesis, properties and application*, ed. V.I. Rybachenko, Donetsk: Schidnyj vydavnyczyj dim, 2010, 226 p., Chapt. 4, P. 85–103.
11. Tolstikova T.G., Khvostov M.V., Bryzgalov A.O. The complexes of drugs with carbohydrate-containing plant metabolites as pharmacologically promising agents, *Mini Rev. Med. Chem.*, 2009, Vol. 9, No. 11, P. 1317–1328.
12. Polyakov N.E., Leshina T.V. Glycyrrhizic acid as a novel drug delivery vector: synergy of drug transport and efficacy, *Open Conf. Proc. J.*, 2011, Vol. 2, P. 64–72.
13. Dushkin A.V., Tolstikova T.G., Khvostov M.V., Tolstikov G.A. Complexes of polysaccharides and glycyrrhizic acid with drug

- molecules. mechanochemical synthesis and pharmacological activity, in *The complex world of polysaccharides*, ed. D.N. Karunaratn, Publisher: InTech, 2012, 634 p., Chapt. 22, P. 573–602.
14. Tolstikov G.A., Baltina L.A., Grankina V.P., Kondratenko R.M., Tolstikova T.G. *Licorice: biodiversity, chemistry and application in medicine*, Novosibirsk: Geo, 2007, 311 p.
 15. Hostettmann K., Marston A. *Saponins*, Cambridge: Cambridge University Press, 1995, 548 p.
 16. Krasnova T.G., Bashura G.S., Muravev I.A. Research of solubilization of hydrocortisone and prednisolone in aqueous solutions of glycyram, *Pharmacia*, 1978, No. 5, P. 32–35.
 17. Soltész J., Uri J. Solubilisierende Wirkung des monoammoniumglycyrrhizinats auf antibiotika und einige andere stoffe, *Naturwissenschaften*, 1963, Vol. 50, No. 22, P. 691.
 18. Sasaki Y., Mizutani K., Kasai R., Tanaka O. Solubilizing properties of glycyrrhizin and its derivatives solubilization of saikosaponin-a, the saponin of bupleuri radix, *Chem. Pharm. Bull.*, 1988, Vol. 36, P. 3491–3495.
 19. Mashkovskii M.D. *Drugs*, 2 vols., 13th ed. (new), Kharkov: Torsing, 1997, Vol. 2, 592 p.
 20. Szabó-Révész P., Pintye-Hódi K., Miseta M., Selmeczi B. Stabilitätsprüfung von chloramphenicol- β -cyclodextrin-haltigen tabletten, *Pharmazie*, 1988, Vol. 43, No. 8, P. 554–555.
 21. Szabó-Révész P., Pintye-Hódi K., Miseta M., Selmeczi B. Untersuchung des physikalischen gemisches von chloramphenicol- β -cyclodextrin, *Pharm. Ind.*, 1989, Vol. 51, P. 94–97.
 22. Frömring K.-H., Szejtli J. *Cyclodextrins in pharmacy*, Dordrecht: Kluwer Academic Publishers, 1994, 224 p.
 23. Ali S.M., Asmat F., Maheshwari A. NMR spectroscopy of inclusion complex of D-(-)-chloramphenicol with β -cyclodextrin in aqueous solution, *IL FARMACO*, 2004, Vol. 59, P. 835–838.
 24. Fatiha M., Leila L., Eddine K.D., Leila N. Computational investigation of enol/keto chloramphenicol with β -cyclodextrin, *J. Incl. Phenom. Macrocycl. Chem.*, 2013, Vol. 77, No. 1–4, P. 421–427.
 25. Li N.B., Luo H.Q., Liu S.P. Resonance Rayleigh scattering study of the inclusion complexation of chloramphenicol with β -cyclodextrin, *Talanta*, 2005, Vol. 66, No. 2, P. 495–500.
 26. Shi J.-H., Zhou Y.-f. Inclusion interaction of chloramphenicol and heptakis (2,6-di-*O*-methyl)- β -cyclodextrin: Phase solubility and

- spectroscopic methods, *Spectrochim. Acta Part A*, 2011, Vol. 83, P. 570–574.
27. Zuorro A., Fidaleo M., Lavecchia R. Solubility enhancement and antibacterial activity of chloramphenicol included in modified β -cyclodextrins, *Bull. Korean Chem. Soc.*, 2010, Vol. 31, No. 11, P. 3460–3462.
 28. Hirayama F., Usami M., Kimura K., Uekama K. Crystallization and polymorphic transition behavior of chloramphenicol palmitate in 2-hydroxypropyl- β -cyclodextrin matrix, *Eur. J. Pharm. Sci.*, 1997, Vol. 5, P. 23–30.
 29. Loftsson T., Jarho P., Másson M., Järvinen T. Cyclodextrins in drug delivery, *Expert Opin. Drug Deliv.*, 2005, Vol. 2, No. 2, P. 335–351.
 30. Loftsson T., Duchêne D. Cyclodextrins and their pharmaceutical applications, *Int. J. Pharm.*, 2007, Vol. 329, No. 9, P. 1–11.
 31. Kondratenko R.M., Baltina L.A., Mustafina S.R., Ismagilova A.F., Zarudii F.S., Davydova V.A., Bazekin G.V., Suleimanova G.F., Tolstikov G.A. Complex compounds of glycyrrhizic acid with antimicrobial drugs, *Pharm. Chem. J.*, 2003, Vol. 37, No. 9, P. 485–488.
 32. Arystanova T.A., Dzhiembaev B.J., Rakhimov K.D., Ordabaeva S.K., Shukirbekova A.B., Ospanov E.S. Murzakhmetov G.K., Philippovich G.S. Medicinal products based on vegetable raw materials: achievements and prospects, *Papers of Int. res.-pract. conf. "Pharmacy of Kazakhstan: integration of science, education and production"*, Shymkent (Kazakhstan), 15–19 may 2009, Vol. 1, P. 83–86.
 33. Medetbekov B.M., Arystanova T.A., Ordabayeva S.K. New complex compound of the glycyrrhizic acid with antibacterial activity, *Mater. of II Inter. conf. on natural products: chemistry, technology & medicinal perspectives*, Almaty (Kazakhstan), 10–13 oct. 2007, P. 147.
 34. Medetbekov B.M., Ordabaeva S.K., Arystanova T.A., Dzhiembaev B.J. Obtaining a new complex compound of 18-dehydroglycyrrhetic acid, *Papers of Int. res.-pract. conf. "Pharmacy of Kazakhstan: integration of science, education and production"*, Shymkent (Kazakhstan), 15–19 may 2009, Vol. 1, P. 125–127.
 35. Kazmina M.A., Sushkova S.N., Lekar A.V., Borisenko N.I. Complexation process of glycyrrhizic acid and antibiotic chloramphenicol (laevomycesin), *Mater. VIII Int. sci.-techn. conf. "Modern trends in biological physics and chemistry. BPPC – 2012"*, Sevastopol (Ukraine), 23–27 apr. 2012, P. 276–277.
 36. Lekar A.V., Yakovishin L.A., Borisenko S.N., Vetrova E.V., Borisenko

- N.I. Complexation of antibiotic levomycetin (chloroamphenicol) with a-hederin and hederasaponin C under the conditions of electrospray ionization, *J. Analyt. Chem.*, 2011, Vol. 66, No. 14, P. 1437–1440.
37. Yakovishin L.A., Korzh E.N., Degtyar A.D., Klimenko A.V., Spectrophotometry of the supramolecular complexes of ivy and licorice triterpene glycosides with laevomycetin (chloramphenicol), *Ukr. Bioorg. Acta*, 2013, Vol. 11, No. 1, P. 33–36.
 38. Babko A.K. *Physico-chemical analysis of complex compounds in the solutions*, Kiev: Izd-vo AN USSR, 1955, 328 p.
 39. Shevchuk O.O., Posokhova E.A., Sakhno L.A., Nikolaev V.G. Theoretical ground for adsorptive therapy of anthracyclines cardiotoxicity, *Exp. Oncol.*, 2012, Vol. 34, No. 4, P. 314–322.
 40. Bekers O., Beijnen J.H., Otagiri M., Bult A., Underberg W.J. Inclusion complexation of doxorubicin and daunorubicin with cyclodextrins, *J. Pharm. Biomed. Anal.*, 1990, Vol. 8, No. 8–12, P. 671–674.
 41. Bekers O., Kettenes J.J. van den B., Helden S.P.V., Seijkens D., Beijnen J.H., Bulti A., Underberg W.J.M. Inclusion complex formation of anthracycline antibiotics with cyclodextrins; a proton nuclear magnetic resonance and molecular modelling study, *J. Inclusion Phenom. Mol. Recogn. Chem.*, 1991, Vol. 11, No. 2, P. 185–193.
 42. Bekers O., Beijnen J.H., Vis B.J., Suenaga A., Otagiri M., Bult A., Underberg W.J.M. Effect of cyclodextrin complexation on the chemical stability of doxorubicin and daunorubicin in aqueous solutions, *Int. J. Pharm.*, 1991, Vol. 72, No. 2, P. 123-130.
 43. Husain N., Ndou T.T., De La Peña A.M., Warner I.M. Complexation of doxorubicin with β - and γ -cyclodextrins, *Appl. Spectroscop.*, 1992, Vol. 46, No. 4, P. 652–658.
 44. Monnaert V., Betbeder D., Fenart L., Bricout H., Lenfant A.M., Landry C., Cecchelli R., Monflier E., Tilloy S. Effects of γ - and hydroxypropyl- γ -cyclodextrins on the transport of doxorubicin across an in vitro model of blood-brain barrier, *J. Pharmacol. Exp. Ther.*, 2004, Vol. 311, No. 3, P. 1115–1120.
 45. Al-Omar A., Abdou S., De Robertis L., Marsura A., Finance C. Complexation study and anticellular activity enhancement by doxorubicin-cyclodextrin complexes on a multidrug-resistant adenocarcinoma cell line, *Bioorg. Med. Chem. Lett.*, 1999, Vol. 9, No. 8, P. 1115–1120.
 46. Brewster M.E., Loftsson T., Estes K.S., Lin J.-L., Fridriksdottir H., Bodor N. Effect of various cyclodextrins on solution stability and

- dissolution rate of doxorubicin hydrochloride, *Int. J. Pharm.*, 1992, Vol. 79, P. 289–299.
47. Anand R., Manoli F., Manet I., Daoud-Mahammed S., Agostoni V., Gref R., Monti S. β -Cyclodextrin polymer nanoparticles as carriers for doxorubicin and artemisinin: a spectroscopic and photophysical study, *Photochem. Photobiol. Sci.*, 2012, Vol. 11, No. 8, P. 1285–1292.
 48. Swiech O., Mieczkowska A., Chmurski K., Bilewicz R. Intermolecular interactions between doxorubicin and β -cyclodextrin 4-methoxyphenol conjugates, *J. Phys. Chem. B*, 2012, Vol. 116, No. 6, P. 1765–1771.
 49. Baltina L.A., Murinov Y.I., Ismagilova A.F., Davydova V.A., Zarudii F.S., Tolstikov G.A. Synthesis and antitumor activity of complex compounds of β -glycyrrhizic acid with antitumor drug, *Pharm. Chem. J.*, 2001, Vol. 35, No. 11, P. 585–587.
 50. Theodoulou M., Hudis C. Cardiac profiles of liposomal anthracyclines. Greater cardiac safety versus conventional doxorubicin? *Cancer*, 2004, Vol. 100, No. 10, P. 2052–2063.
 51. Zykova M.G., Medvedeva N.V., Torkhovskaya T.I., Tikhonova E.G., Prozorovskii V.N., Zakharova T.S., Ipatova O.M. Influence of doxorubicin inclusion into phospholipid nanoformulation on its antitumor activity in mice: increased efficiency for resistant tumor model, *Exp. Oncol.*, 2012, Vol. 34, No. 4, P. 323–326.
 52. Arima H., Hagiwara Y., Hirayama F., Uekama K. Enhancement of antitumor effect of doxorubicin by its complexation with gamma-cyclodextrin in pegylated liposomes, *J. Drug Target*, 2006, Vol. 14, No. 4, P. 225–232.
 53. Ipatova O.M., Zykova M.G., Torkhovskaya T.I., Medvedeva N.V., Prozorovsky V.N. Possibility for use of phospholipid nanosystem with glycyrrhizic acid (“Phosphogliv”) for optimization of drugs: doxorubicin and budesonide as examples, *Biomed. Khim.*, 2009, Vol. 55, No. 2, P. 185–194.
 54. Amara-Mokrane Y.A., Lehucher-Michel M.P., Balansard G., Dumenil G., Botta A. Protective effects of α -hederin, chlorophyllin and ascorbic acid towards the induction of micronuclei by doxorubicin in cultured human lymphocytes, *Mutagenesis*, 1996, Vol. 11, No. 2, P. 161–167.
 55. Villani P., Orsière T., Sari-Minodier I., Bouvenot G, Botta A. Etude in vitro de l’activité antimutagène de l’alphahédérine, *Ann. Biol. Clin.*, 2001, Vol. 59, No. 3, P. 285–289.
 56. Pavlova S.I, Uteshev B.S., Sergeev A.B. Licorice root: possible mechanisms of antitoxicant, anticarcinogen, and antitumor properties

- (a Review), *Pharm. Chem. J.*, 2003, Vol. 37, No. 6, P. 314–317.
57. Yakovishin L.A., Grishkovets V.I., Korzh E.N., Klimentenko A.V., Degtyar A.D., Kuchmenko O.B. Molecular complexation of ivy and licorice saponins with doxorubicin, *Abstr. Xth Intern. symp. on the chemistry of natural compounds*, Tashkent–Bukhara (Uzbekistan), 21–23 nov. 2013, P. 309.
 58. Agudelo D., Bourassa P., Bruneau J., Bérubé G., Asselin É., Tajmir-Riahi H.-A. Probing the binding sites of antibiotic drugs doxorubicin and *N*-(trifluoroacetyl) doxorubicin with human and bovine serum albumins, *PLoS ONE*, 2012, Vol. 7, No. 8, e43814, P. 1–13.
 59. Dalmark M., Johansen P. Molecular association between doxorubicin (adriamycin) and DNA-derived bases, nucleosides, nucleotides, other aromatic compounds, and proteins in aqueous solution, *Mol. Pharmacol.*, 1982, Vol. 22, No. 1, P. 158–165.
 60. Sousa de F.B., Oliveira M.F., Lula I.S., Sansiviero M.T.C., Cortés M.E., Sinisterra R.D. Study of inclusion compound in solution involving tetracycline and β -cyclodextrin by FTIR-ATR, *Vibr. Spectrosc.*, 2008, Vol. 46, No. 1, P. 57–62.
 61. Zhang H., Zhang H., Jin W., Ding L. Determination of dissociation constants of cyclodextrin-ligand inclusion complexes by electrospray ionization mass spectrometry, *Eur. J. Mass. Spectrom.*, 2006, Vol. 12, No. 5, P.291–299.
 62. Oliveira H.F.D. *Nanoagregados baseados em ciclodextrinas em associação com a tetraciclina: caracterização físico-química e avaliação antimicrobiana*, Dissertação apresentada à banca examinadora como requisito parcial para a obtenção do grau de mestre em odontologia, Belo Horizonte, 2007, 80 f.
 63. Domingues Z.R., Cortés M.E., Gomes T.A., Diniz H.F., Freitas C.S., Gomes J.B., Faria A.M., Sinisterra R.D. Bioactive glass as a drug delivery system of tetracycline and tetracycline associated with beta-cyclodextrin, *Biomaterials*, 2004, Vol.25, No. 2, P. 327–333.
 64. Yang R.-H., Wang K.-M., Xiao D., Yang X.-H., Zhang L.-D. A selective sensing membrane for the determination of tetracycline with heptakis (2,6-di-*O*-isobutyl)- β -cyclodextrin as the substrate, *Microchem. J.*, 2000, Vol. 64, No. 3, P. 213–220.
 65. He Z.-x., Wang Z.-h., Zhang H.-h., Pan X., Su W.-r., Liang D., Wu C.-b. Doxycycline and hydroxypropyl- β -cyclodextrin complex in poloxamer thermal sensitive hydrogel for ophthalmic delivery, *Acta Pharm. Sin. B*, 2011, Vol. 1, No. 4, P. 254–260.

66. Wang Z., He Z., Zhang L., Zhang H., Zhang M., Wen X., Quan G., Huang X., Pan X., Wu C. Optimization of a doxycycline hydroxypropyl- β -cyclodextrin inclusion complex based on computational modeling, *Acta Pharm. Sin. B*, 2013, Vol. 3, No. 2, P. 130–139.
67. Zhang H., Chen M., He Z., Wang Z., Zhang M., He Z., Wan Q., Liang D., Repka M.A., Wu C. Molecular modeling-based inclusion mechanism and stability studies of doxycycline and hydroxypropyl- β -cyclodextrin complex for ophthalmic delivery, *AAPS Pharm. Sci. Tech.*, 2013, Vol. 14, No. 1, P. 10–18.
68. Su W., Li Z., Lin M., Li Y., He Z., Wu C., Liang D. The effect of doxycycline temperature-sensitive hydrogel on inhibiting the corneal neovascularization induced by BFGF in rats, *Graefes Arch. Clin. Exp. Ophthalmol.*, 2011, Vol. 249, No. 3, P. 421–427.

Chapter 3

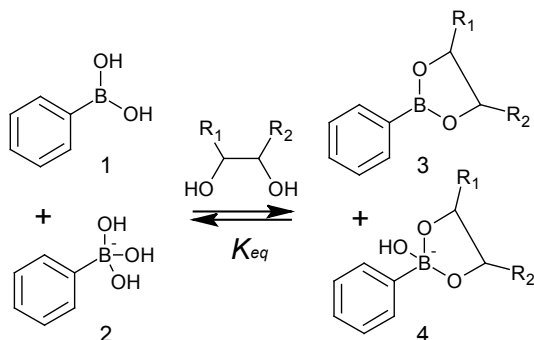
Phenylboronic acids-containing nanoparticles

Alicja Pawełko, Agnieszka Adamczyk-Woźniak and Andrzej Sporzyński
*Warsaw University of Technology, Faculty of Chemistry,
 Noakowskiego 3, 00-664 Warsaw, Poland*

Introduction

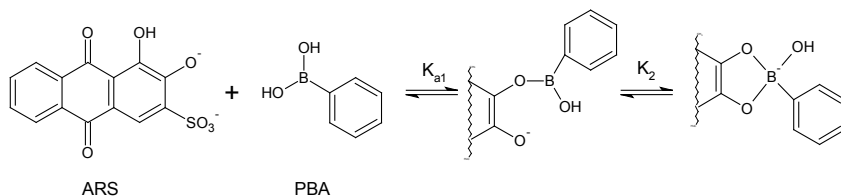
Phenylboronic acids (PBAs) have been widely investigated in variety of chemical and biomedical applications but their most important value is biologically important analytes sensing. Bioresponsive compounds which form reversible covalent bond with 1,2- or 1,3- diols have attracted scientists' interest for decades [1, 2, 3]. Sugars [4, 5], dopamine [6, 7] and glycoproteins [7] can be detected by boronic acids which form complexes with multihydroxy compounds. Selective D-glucose binding receptors are significantly important due to diabetes mellitus. This disease is projected to be the seventh major cause of death in the world by the year 2030. Boronic acids bind carbohydrates with reversible covalent bond. They reveal potential medical application as non-invasive glucose receptors.

Phenylboronic acids exist in two forms neutral – trigonal (**1**, **3**) and anionic – tetragonal form (**2**, **4**), which are in equilibrium in water (Scheme 1) [2, 8].



Scheme 1. Equilibrium of phenylboronic acids and their esters.

The anionic PBAs form glucose-boronate complexes and hence shift the equilibrium in aqueous media to form **4** (Scheme 1). Neutral boronate adducts were considered as unstable [8]. Tomsho and Benkovic proved that both trigonal and tetragonal PBA form esters with model diol – Alizarin Red S (Scheme 2).



Scheme 2. Binding ARS with PBA at near-neutral pH [9].

Polymer matrix loaded with insulin has been widely investigated [10, 11]. Self-assembled macromolecular structures can work as nanocarriers for triggered drug delivery [12]. Such vehicles can show increased activity due to multivalency and provide longer circulation time in the body [13]. Complex system combining polymer as a drug nanocarrier and boronic acid moiety as a glucose receptor seems to be perfect solution to detect carbohydrates and to allow controlled drug release.

The wide variety of boronic acids containing materials [14, 15] such as gels [10, 16], hydrogels [17-22], microgels [23-27], nanogels [28], homopolymers [29], block copolymers [29-36], glycopolymers [37-39] have been used to obtain glucose-sensitive systems. In this review, we addressed the development of nanoparticles containing boronic acid moiety and different ways to tune their response to biologically important polyols.

Hydrogels, microgels, nanogels

Glucose concentration can be analyzed by volumetric changes of hydrogel matrix. Swelling pressure measurements [21], optical [19] and fluorescence sensors can be used to study sugar response. PBA immobilized on polymerized crystalline colloidal arrays (PCCA) enable monitoring sugar concentration by measuring changes in volume (Fig. 1) [17].

Another group of hydrogels are zwitterionic glucose-sensitive hydrogels (GSHs) i.e. AAM/3-APB/DMApAA/BIS. GSHs displayed very good results in *ex vivo* blood plasma. Hydrogel swelling was observed to be five times faster at 37 °C than at room temperature (~20 °C) [18]. On the other hand, Horkay *et al.* proved with chemomechanical sensor that zwitterionic hydrogel shrinks upon

glucose and swells upon fructose binding (Fig. 1) [21]. The chemical structure of the immobilized PBAs was found to be the most influential factor that causes volumetric change of hydrogels.

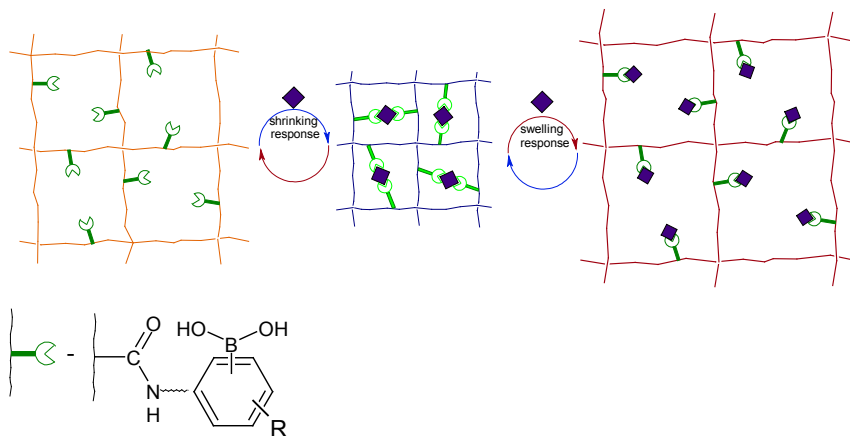
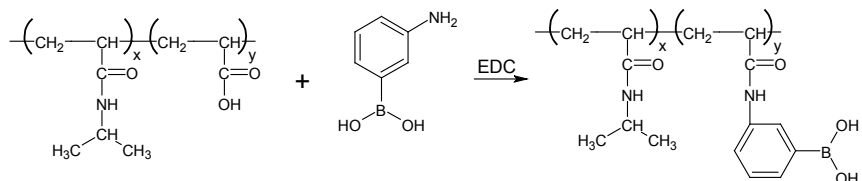


Figure 1. Esterification of PBA-modified hydrogel with glucose and the shrinking/swelling behavior of hydrogel volume of PCCA [17].

Poly(*N*-isopropylacrylamide) (PNIPAM) microgels with PBA moieties reveal reversible swelling/deswelling responses to glucose as well [23]. The esterification reaction of PBA groups incorporated into PNIPAM can be studied by turbidity. Swelling effect of glucose binding by poly(*N*-isopropylacrylamide-*co*-3-acrylamidophenylboronic acid) (P(NIPAM-AAPBA)) (Scheme 3) is observed within 10^2 s [25].



Scheme 3. Synthesis of P(NIPAM-AAPBA) microgels.

Derivatives of *N*-alkylacrylamides were synthesized by copolymerization reaction with 4-(1,6-dioxo-2,5-diaza-7-oxamyl)phenylboronic acid (DDOPBA)

and cross-linkers such as *N,N'*-methylenebis(acrylamide) (BIS) or ethylene glycol dimethacrylate (EGDMA) (Fig. 2) [24].

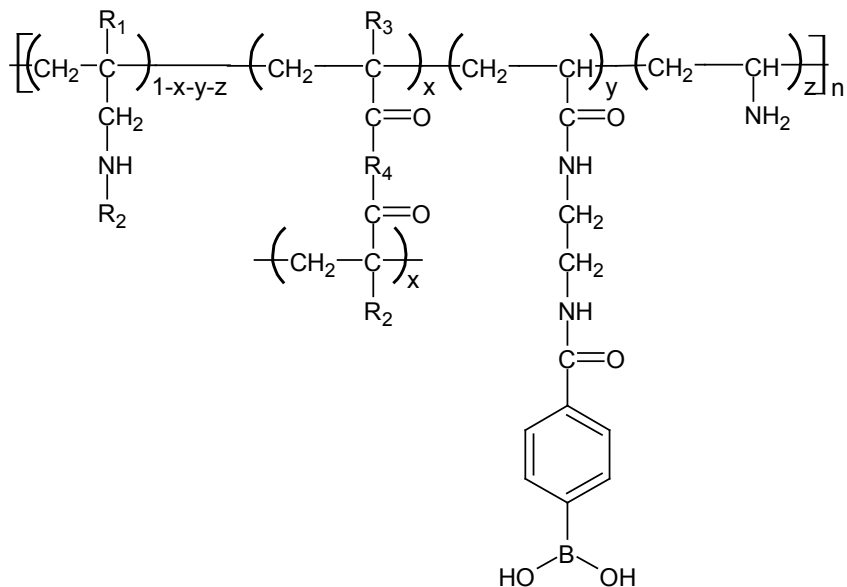


Figure 2. General structure of *N*-alkylacrylamides [24].

PBA modifications in polymer change the volume phase transition temperature (VPTT) of microgel. The VPTT decreases with increasing number of PBA groups. According to the applications in physiological conditions, VPTT should be above 37 °C. From group of *N*-alkylacrylamides polymers based on i.e. *N*-isopropylacrylamide (NIPAM), *N*-isopropylmethacrylamide (NIPMAM), and *N*-ethylmethacrylamide (NEMAM), only PNEMAM shows such a characteristic [24]. Selective glucose receptors are based on shrinkage of microgels with EGDMA cross-linkers which form bis-boronate complexes. Monobidentate form occurs under higher glucose concentrations, whereas fructose binding caused monotonous swelling.

Fluorescent response to glucose within polymer nanoparticles was designed by Zenkl *et al.* Donor (*N*-fluoresceinacrylamide) and acceptor (acryloylpiperazinyl sulforhodamine B Isomer I and Isomer II) were in close distance inside nanosphere without any presence of sugar. Glucose or fructose binding caused swelling response of the sensor which extended the space between molecules (Fig. 3) [26].

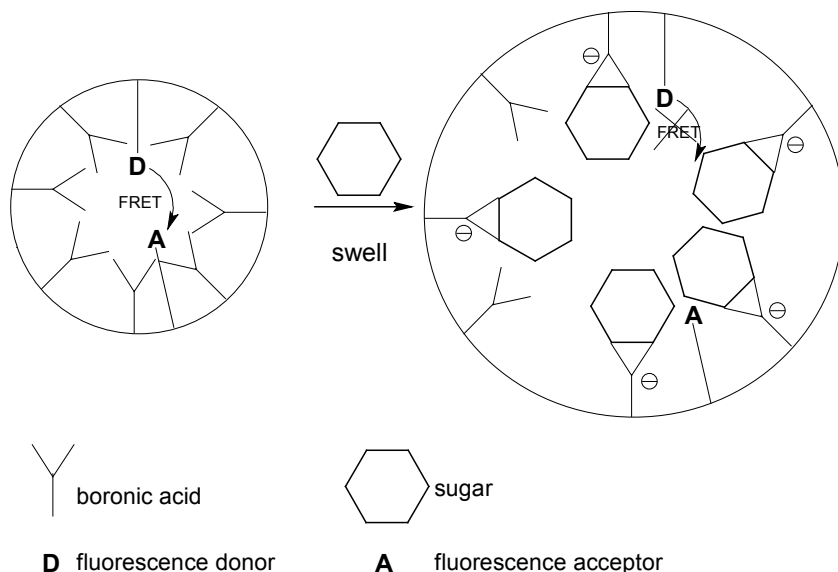


Figure 3. Fluorescent response to sugar [26].

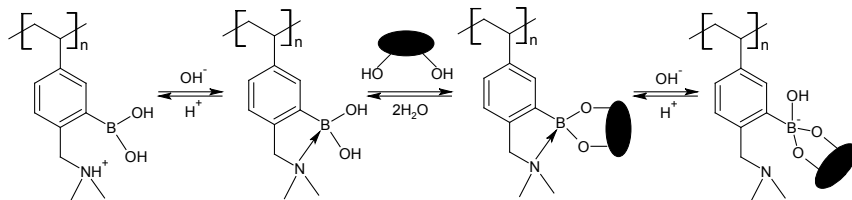
Controlled release of insulin from nanocarrier can be tuned by glucose concentration. A biocompatible nanogel with a core-shell structure was synthesized by copolymerization of pentaerythritol tetra(3-mercaptopropionate), poly(ethylene glycol) diacrylate, methoxyl poly(ethylene glycol) acrylate and *N*-acryloyl-3-aminophenylboronic acid. The hydrodynamic radius (R_H) increased and the insulin delivery was faster with the higher concentration of glucose in solution [28].

Light scattering is a useful technic to investigate interactions of PBA-modified microgels with carbohydrates. Changes in light scattering intensity enable to prove shrinking/swelling responses of microgels to sugar concentration [23].

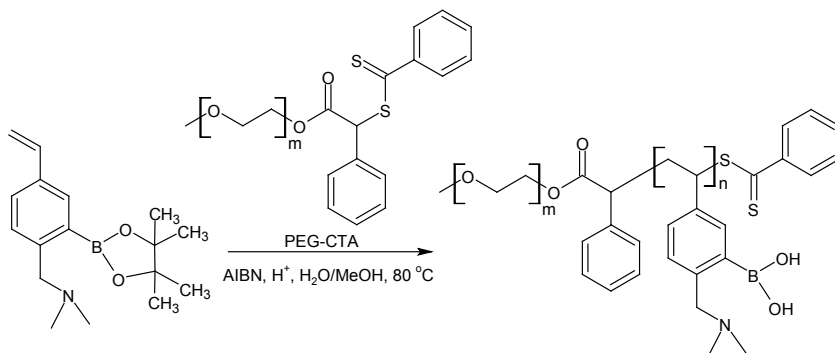
Homopolymers and block copolymers

Homopolymer is a macromolecule which comprises identical monomer units, whereas, block copolymer consists of two or more monomers which form alternating blocks. Sugar-responsive homopolymer was obtained by radical addition-fragmentation chain transfer (RAFT) polymerization of a Wulff-type monomer. Aminomethyl substituent at *ortho* position of phenylboronic acids

decreased pK_a of compounds and enhanced polyols binding at neutral pH (Scheme 4 and 5).



Scheme 4. Interaction of homopolymer with sugar at different pH [29].



Scheme 5. Synthesis of Wulff-type block copolymer by RAFT [29].

Both homopolymer (Scheme 4) and block copolymer (Scheme 5) formed soluble esters with D-fructose and D-glucose in pH range 7.4-7.8.

Nanoparticles obtained by self-assembled block copolymers (complex polymeric micelles – CPMs) reveal potential medical application as nanocarriers for triggered drug delivery. Glucose and pH responsive micelles of poly(ethylene glycol)-block-poly(acrylic acid-*co*-acrylamidophenylboronic acid) PEG-*b*-(PAA-*co*-PAAPBA)] were synthesized and analyzed by ^{11}B magic-angle spinning nuclear magnetic resonance (^{11}B MAS NMR) by Wang *et al.* [31, 32]. Interactions between carboxylate anion and PBA can cause shift of boron atom toward tetragonal form and enhance sugar binding at physiological pH. Insulin was loaded to a hydrophobic, sugar-sensitive core, and nanoparticles were stabilized by hydrophilic PEG shell (Fig. 4).

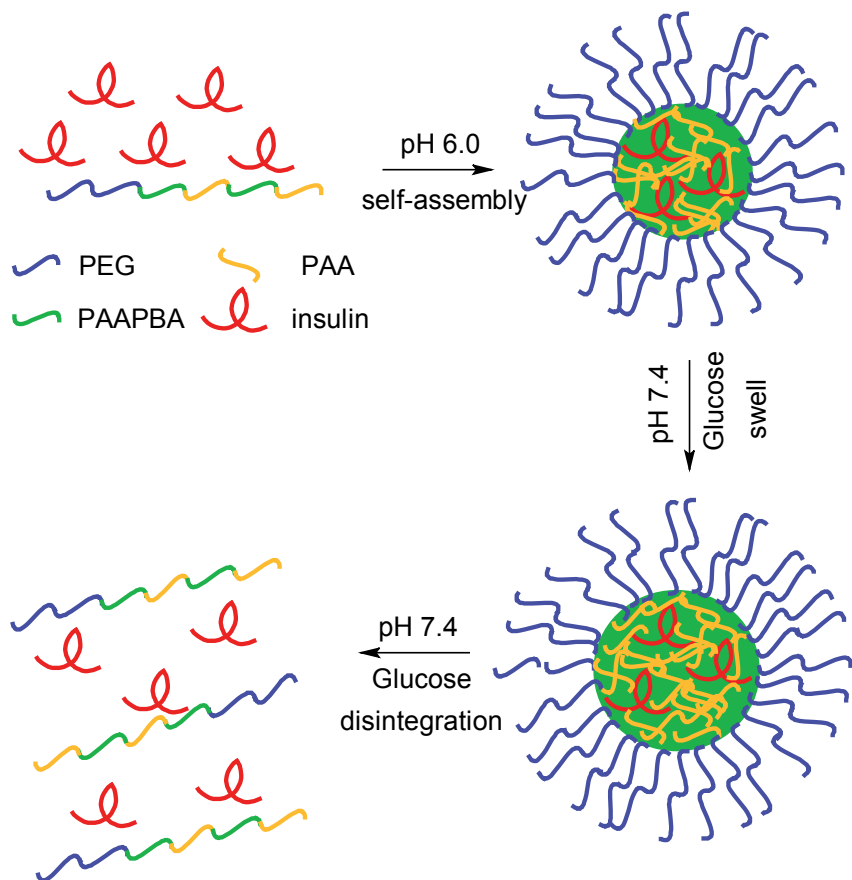


Figure 4. Glucose-responsive system [31].

Nanoparticles self-assembled from poly(3-acrylamidophenylboronic acid)-*b*-poly (*N*-isopropylacrylamide) (PAPBA-*b*-PNIPAM) (**1**, Fig. 5) sensitive to temperature, sugar concentration and pH have been designed by Roy *et al.* [35, 36]. At $\text{pH} < \text{p}K_a$ of phenylboronic acid and absence of sugar polymeric micelles consist of PAPBA core and PNIPAM shell, whereas, at temperature $> 32^\circ\text{C}$ they form PNIPAM core and PAPBA shell structure (Fig. 6).

Both nanoaggregates of PAPBA-*b*-PNIPAM (**5**) and PDMA-*b*-PAEBB (**6**, Fig. 5) dissociate after increasing pH above the $\text{p}K_a$ of phenylboronic acid or at neutral pH after addition of glucose.

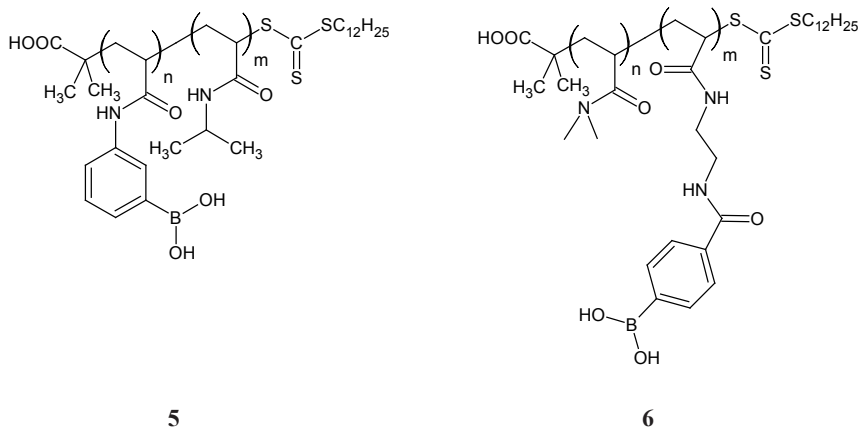


Figure 5. Structure of poly(3-acrylamidophenylboronic acid)-*b*-poly(*N*-isopropylacrylamide) (PAPBA-*b*-PNIPAM) (**5**) [35] and poly(*N,N*-dimethylacrylamide)-*b*-poly(*N*-(2-acryloylamino-ethyl)-4-boronobenzamide) (PDMA-*b*-PAEBB) (**6**) [36].

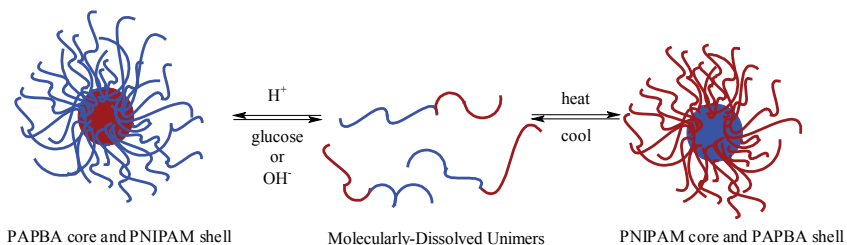
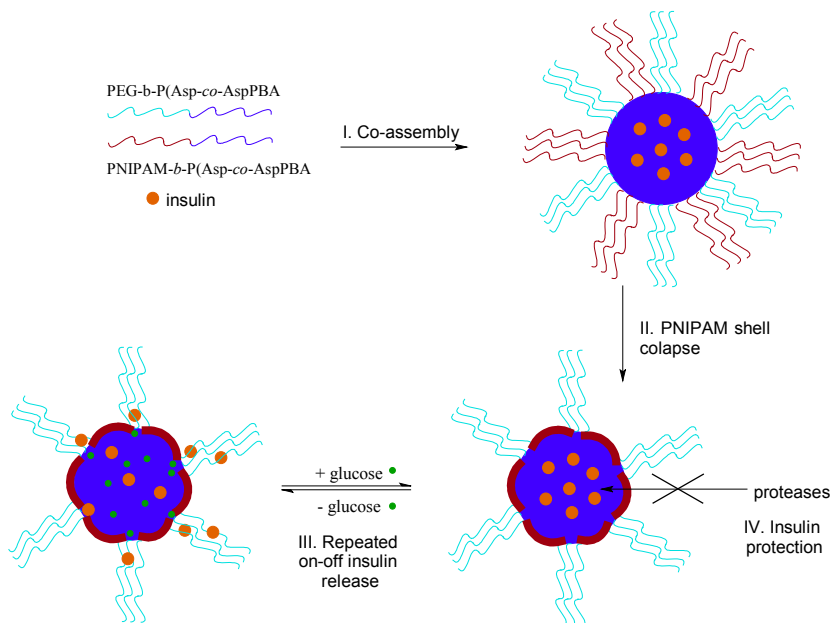


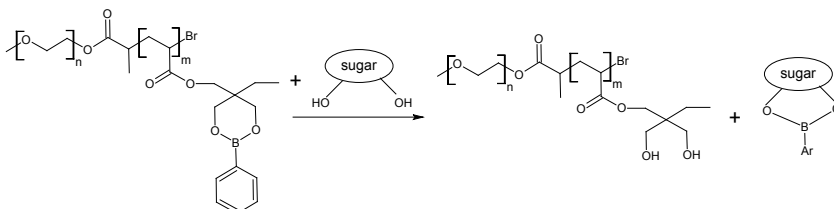
Figure 6. Tuning response of PAPBA-*b*-PNIPAM to temperature, sugar concentration and pH [35].

Complex micelles of poly(ethylene glycol)-*b*-poly(aspartic acid-*co*-aspartamido-phenylboronic acid) (PEG-*b*-P(Asp-*co*-AspPBA)) and poly(*N*-isopropylacrylamide)-*b*-poly(aspartic acid-*co*-aspartamidophenylboronic acid) (PNIPAM-*b*-P(Asp-*co*-AspPBA)) were prepared. The same hydrophobic block [P(Asp-*co*-AspPBA)] of two polymers was used to form core and different hydrophilic blocks (PEG and PNIPAM) were used to obtain collapsed shell of PNIPAM at 37 °C, above lower critical solution temperature (LCST). Collapsed PNIPAM membrane protected insulin loaded core of CPMs from proteases (Scheme 6) [30].



Scheme 6. Protected insulin delivery system of CPM of (PEG-*b*-P(Asp-*co*-AspPBA)) and (PNIPAM-*b*-P(Asp-*co*-AspPBA)) [30].

Atom transfer radical polymerization (ATRP) was used to achieve amphiphilic poly(ethylene glycol)-*block*-poly[(2-phenylboronic esters-1,3-dioxane-5-ethyl) methyl-acrylate] (MPEG5000-*block*-PBDEMA). Nanoparticles swelled upon presence of sugar as a result of changes in polymer polarity (Scheme 7). Double hydrophilic polymer was obtained by transesterification reaction of phenylboronic acid with sugar [33, 34].



Scheme 7. Transfer of polymer polarity from amphiphilic to double hydrophilic [33].

Glycopolymers

Glycopolymers contain carbohydrates in their molecules. They can be utilized in targeted drug delivery and synthesis of biocompatible materials. Triblock copolymer poly(acrylic acid-*co*-acrylamidophenylboronic acid)-*block*-poly(2-acryloxyethyl galactose)-*block*-poly(acrylic acid-*co*-acrylamidophenylboronic acid) (((PAA-*co*-PAAPBA)-*b*-)2PAEG) was designed to form insulin loaded nanoparticles. Nanocarriers were sensitive to pH value and presence of glucose. The hydrodynamic diameter increased with increasing glucose concentration. Insulin release profile showed that 17% of the hormone was detached from surface of nanoparticles in the absence of glucose, compared to 40% and 60% of insulin delivery in solution comprising glucose [36].

Complex micelles of poly(ethyleneglycol)-*block*-poly(acrylic acid-*co*-acrylamidophenylboronic acid) PEG-*b*-P(AA-*co*-APBA) and poly(acrylic acid-*co*-acrylglicosamine) (P(AA-*co*-AGA)) were fabricated. Lower pK_a of PBA occurred upon PBA complexation with glycopolymer [38, 39].

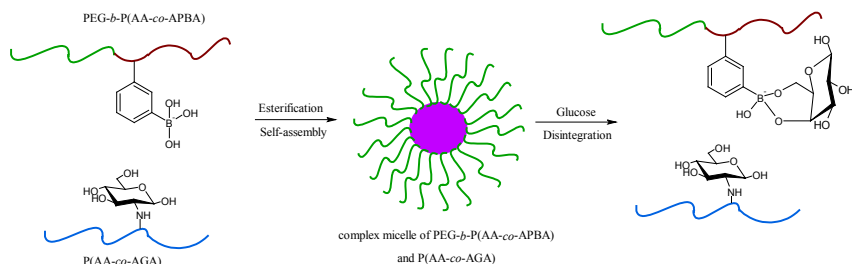
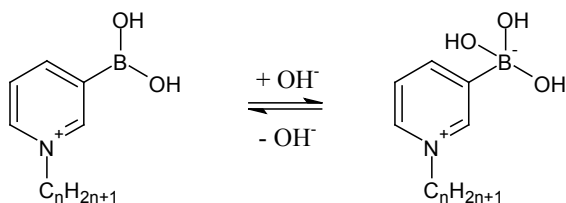


Figure 7. Formation and disintegration of PEG-*b*-P(AA-*co*-APBA)/(P(AA-*co*-AGA)) micelles [39].

PBA nanoparticles

N-alkyl-3-boronopyridinium salts form vesicular micelles in aqueous media [14, 15].



Scheme 8. Equilibrium of *N*-alkylpyridiniumboronic acids [15].

The introduction of boronic acid moiety into surfactant molecule changes its properties i.e. critical aggregation concentration (CAC) as well as minimum required area per molecule effectiveness. Savsunenko *et al.* obtained first self-assembled micelles of *N*-alkylpyridiniumboronic acids. This new type of receptors can detect sugars at low concentrations at physiological pH.

All the described phenylboronic acids-containing nanoparticles are promising receptors for sensing biologically important polyols. Tuned response of designed systems has been achieved by pH, sugar concentration or temperature. Sugar responsive behavior has potential application in medical treatment of diabetes mellitus.

Acknowledgement

This work has been supported by the European Union in the framework of European Social Fund through the Warsaw University of Technology Development Programme by the scholarship awarded by the Center of Advanced Studies for Alicja Pawełko.

References

1. H. G. Kuivila, A. H. Keough, E. J. Soboczanski, *J. Org. Chem.* **1954**, *19*, 780-783.
2. G. Springsteen, B. Wang, *Tetrahedron*, **2002**, *58*, 5291-5300.
3. Z. Guo, I. Shin, J. Yoon, *Chem. Soc. Rev.*, **2013**, *42*, 8106-8121.
4. J. Yan, G. Springsteen, S. Deeter, B. Wang, *Tetrahedron*, **2004**, *60*, 11205-11209.
5. A. Adamczyk-Woźniak, K. M. Borys, I. D. Madura, A. Pawełko, E. Tomecka, K. Żukowski, *New J. Chem.*, **2013**, *37*, 188-194.
6. S. M. Strawbridge, S. J. Green, J. H. R. Tucker, *Chem. Commun.*, **2000**, 2393-2394.
7. L. Liu, N. Xia, Y. Xing, D. Deng, *Int. J. Electrochem. Sci.*, **2013**, *8*, 11161-11174.
8. J. P. Lorand, J. O. Edwards, *J. Org. Chem.*, 1958, *24*, 769.
9. J. W. Tomsho, S. J. Benkovic, *J. Org. Chem.*, **2012**, *77*, 2098-2106.
10. K. Kataoka, H. Miyazaki, M. Bunya, T. Okano, Y. Sakurai, *J. Am. Chem. Soc.*, **1998**, *120*, 12694-12695.
11. M. G. Li, W. L. Lu, J. C. Wang, X. Zhang, X. Q. Wang, A. P. Zheng, Q. Zhang, *Int. J. Pharm.*, **2007**, *329*, 182-191.
12. A. Harada, K. Kataoka, *Prog. Polym. Sci.*, **2006**, *31*, 949-982.
13. L. W. Seymour, R. Duncan, J. Strohal, J. Kopeček, *J. Biomed. Mater.*

- Res., **1987**, *21*, 1341-1358.
14. O. Savsunenko, H. Matondo, Y. Karpichev, V. Poinsoot, A. Popov, I. Rico-Lattes, A. Lattes, *J. Surfact. Deterg.*, **2012**, *15*, 345-350.
 15. O. Savsunenko, H. Matondo, S. Franceschi-Messant, E. Perez, A. F. Popov, I. Rico-Lattes, A. Lattes, Y. Karpichev, *Langmuir*, **2013**, *29*, 3207-3213.
 16. A. Matsumoto, T. Ishii, J. Nishida, H. Matsumoto, K. Kataoka, Y. Miyahara, *Angew. Chem. Int. Ed.*, **2012**, *51*, 2124-2128.
 17. C. Zhang, M. D. Losego, P. V. Braun, *Chem. Mater.*, **2013**, *25*, 3239-3250.
 18. S. Tierney, D. R. Hjelm, B. T. Stokke, *Anal. Chem.*, **2008**, *80*, 5086-5093.
 19. S. Tierney, B. M. H. Falch, D. R. Hjelm, B. T. Stokke, *Anal. Chem.*, **2009**, *81*, 3630-3636.
 20. S. Tierney, S. Volden, B. T. Stokke, *Biosensors and Bioelectronics*, **2009**, *24*, 2034-2039.
 21. F. Horkay, S.H. Cho, P. Tathireddy, L. Rieth, F. Solzbacher, J. Magda, *Sensors and Actuators B*, **2011**, *160*, 1363-1371.
 22. J. Magda, S. Cho, S. Streitmatter, T. Jevremovic, *Polymer Degradation and Stability*, **2014**, *99*, 219-222.
 23. T. Hoare, R. Pelton, *Macromolecules*, **2007**, *40*, 670-678.
 24. C. Ancla, V. Lapeyre, I. Gosse, B. Catargi, V. Ravaine, *Langmuir*, **2011**, *27*, 12693-12701.
 25. S. Xing, Y. Guan, Y. Zhang, *Macromolecules*, **2011**, *44*, 4479-4486.
 26. G. Zenkl, T. Mayr, I. Klimant, *Macromol. Biosci.*, **2008**, *8*, 146-152.
 27. P. Liu, Q. Luo, Y. Guan, Y. Zhang, *Polymer*, **2010**, *51*, 2668-2675.
 28. L. Zhao, C. Xiao, J. Dinga, P. He, I. Tanga, X. Pang, X. Zhuanga, X. Chen, *Acta Biomater.*, **2013**, *9*, 6535-6543.
 29. K. T. Kim, J. Cornelissen, R. Nolte, J. van Hest, *J. Am. Chem. Soc.*, **2009**, *131*, 13908-13909.
 30. G. Liu, R. Ma, J. Ren, Z. Li, H. Zhang, Z. Zhang, Y. An, L. Shi, *Soft Matter*, **2013**, *9*, 1636-1644.
 31. B. Wang, R. Ma, G. Liu, Y. Li, X. Liu, Y. An, L. Shi, *Langmuir*, **2009**, *25*, 12522-12528.
 32. B. Wang, R. Ma, G. Liu, X. Liu, Y. Gao, J. Shen, Y. An, L. Shi, *Macromol. Rapid Commun.*, **2010**, *31*, 1628-1634.
 33. Y. Yao, X. Wang, T. Tan, J. Yang, *Soft Matter*, **2011**, *7*, 7948-7951.
 34. Y. Yao, L. Zhao, J. Yang, J. Yang, *Biomacromolecules*, **2012**, *13*, 1837-1844.

35. D. Roy, J. N. Cambre, B. S. Sumerlin, *Chem. Commun.*, **2009**, 2106-2108.
36. D. Roy, B. S. Sumerlin, *ACS Macro Lett.*, **2012**, *1*, 529-532.
37. Y. Wang, X. Zhang, Y. Han, C. Cheng, C. Li, *Carbohydrate Polymers*, **2012**, *89*, 124-131.
38. H. Yang, X. Sun, G. Liu, R. Ma, Z. Li, Y. An, L. Shi, *Soft Matter*, **2013**, *9*, 8589-8599.
39. R. Ma, H. Yang, Z. Li, G. Liu, X. Sun, X. Liu, Y. An, L. Shi, *Biomacromolecules*, **2012**, *13*, 3409-3417.

Chapter 4

Boronic acids immobilized on diol-functionalized resins

Łukasz Włoszczak, Krzysztof M. Borys, Agnieszka Adamczyk-Woźniak
and Andrzej Sporzyński
*Warsaw University of Technology, Faculty of Chemistry,
Noakowskiego 3, 00-664 Warsaw, Poland*

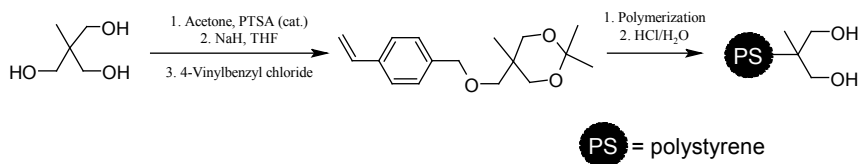
Introduction

Introduced by Merrifield in the early sixties, solid-phase synthesis (SPS) became a powerful tool in organic chemistry. Its original use to prepare peptides was the major application of SPS for almost thirty years [1]. From the point of view of medicinal chemistry, however, the use of peptides was limited as they generally cannot be taken orally and do not have sufficient plasma half-life [2]. To sustain the synthetic importance of SPS, its use had to be extended to the preparation of non-peptidic drugs. It was not until 1992 that Ellman and Bunin developed a method for expedient SPS of 1,4-benzodiazepine derivatives [3]. Their findings opened new pathways in the synthesis and biological evaluation of potentially bioactive compounds, as the method was invaluable in terms of preparing libraries of structurally diverse derivatives of the lead compounds. Today, solid-phase reactions play a significant role in parallel synthesis and combinatorial chemistry, primarily in the area of pharmaceutical chemistry [4,5].

Due to a growing interest in the chemistry of boronic acids, a lot of effort has been made in recent years to develop the SPS methodologies that involve linking the boronic compounds to solid supports by means of the $B(OH)_2$ group. Such concept gives access to the previously unknown boronic acid derivatives as well as broadens the scope of their synthetic applications. This work reviews the reported achievements in immobilization of boronic acids onto diol-functionalized resins and solid-phase derivatization of boronic acids. The use of solid-phase support in metal catalyzed reactions as well as in separating (scavenging [6]) boronic acids from post-reaction mixture is also described.

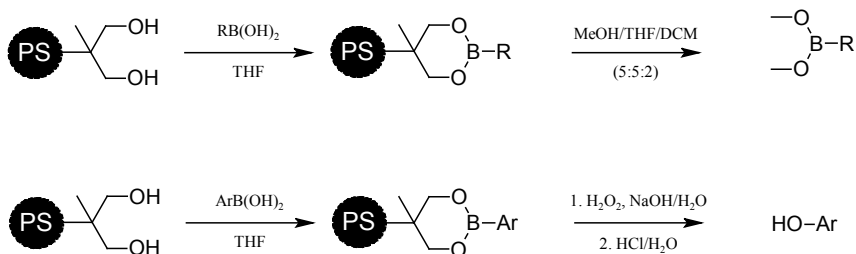
Diol-functionalized resins for immobilization of boronic acids

Carboni *et al.* developed a method for attaching boronic acids to a macroporous polymer bearing 1,3-diol groups [7]. The solid support was obtained in a five-step procedure (Scheme 1), starting from 1,1,1-tris(hydroxymethyl) ethane. The monomer was prepared in three steps, involving acid-catalyzed acetalization with acetone, deprotonation of the remaining free hydroxyl group with sodium hydride, followed by ether formation with 4-vinylbenzyl chloride. Polymerization was carried out in an aqueous solution using azobisisobutyronitrile (AIBN) as initiator, poly(diallyldimethylammonium chloride) as stabilizer and 2-ethyl-hexanol as solvent. Hydrolysis enabled to afford deprotected 1,3-diol-functionalized polystyrene solid support (PSS).



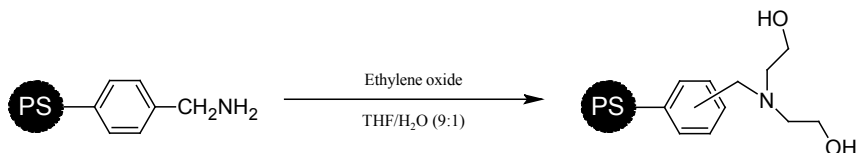
Scheme 1. Synthesis of a 1,3-diol-functionalized PSS.

Optimal conditions for immobilization and cleavage of boronic acids were determined by varying different reaction parameters (Scheme 2). The highest yields of immobilization were observed when refluxing the diol resin and a boronic acid in tetrahydrofuran (THF). The most efficient cleavage was performed in the mixture of methanol (MeOH), THF and dichloromethane (DCM). Due to the use of MeOH, the post-cleavage filtrate contained the corresponding methyl esters of boronic acids. Various alkyl- and aryl-substituted boronic acids were investigated, the yields varying significantly, depending on the group attached to boronic acid moiety, e.g. 50% for 1-decen-1-yl, 80% for 1-decyl, 55% for 2-MeO-C₆H₄ and 75% for 3-NH₂-C₆H₄. All boronic acids obtained in the course of cleavage were of high purity (90-99%). Additionally, the authors showed an alternative way of arylboronic acids' cleavage that lead to the corresponding phenols, using a mixture of hydrogen peroxide and sodium hydroxide which triggered oxidation reaction. The peroxides that are present in THF can also react with boronic acids this way. Because of that, all procedures involving immobilized boronic acids require freshly distilled THF. The alternative way of cleavage could extend the scope of small organic molecules produced utilizing SPS.



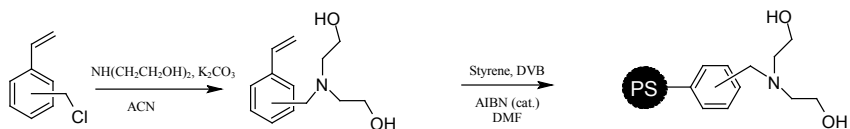
Scheme 2. Immobilization and cleavage of alkyl- and arylboronic acids on the 1,3-diol resin.

The most frequently used resin in boron-based linking methodologies has become *N,N*-diethanolaminomethyl polystyrene (DEAM-PS), first synthesized by Hall *et al.* [8] The original method for its preparation featured the reaction of aminomethylated polystyrene (AM-PS) with the excess of ethylene oxide in a mixture of THF and H₂O (Scheme 3).



Scheme 3. Synthesis of DEAM-PS from AM-PS.

Another approach to the preparation of DEAM-PS was proposed by Arimori *et al.* [9]. The synthesis starts from functionalization of 4-vinylbenzyl chloride with diethanolamine in the presence of a base in acetonitrile (ACN). Afterwards, the prepared monomer is co-polymerized with divinylbenzene (DVB) and styrene to afford DEAM-PS (Scheme 4). Such approach can be optimized using different co-monomers in order to increase the loading capacity of the resin and enhance its physical properties. In this method the size of the beads can be controlled by the addition of surfactants as well as by adjustment of stirring speed. Cross-linking is controlled by the amount of DVB.



Scheme 4. Synthesis of DEAM-PS from 4-vinylbenzyl chloride.

Initial studies on the immobilization of arylboronic acids on DEAM-PS were carried out using 4-tolylboronic acid as a model compound [8]. The most suitable solvents were found to be THF, toluene and DCM (>95% yields). Dimethylformamide (DMF) and diethyl ether were almost as effective (87% and 90%, respectively). Methanol gave significantly lower yield (53%), partly because of an anticipated rival transesterification reaction [10], and partly because of a poor swelling of polystyrene resins in polar solvents [11].

DEAM-PS couples arylboronic acid in almost equimolar amount. Neither excess of reagent nor heating is required. These advantages as well as higher yields of immobilization compared to 1,3-diol resins are considered to be benefits of the formation of a nitrogen–boron bond (Figure 1).

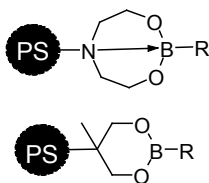
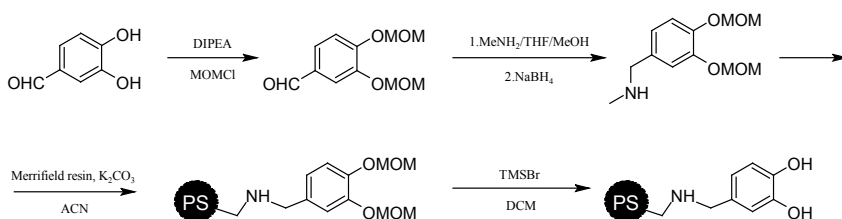


Figure 1. Nitrogen-boron bonding in the boronated DEAM-PS versus the boronated 1,3-diol resin.

Cleavage of boronic acids from DEAM-PS is usually carried out with a THF/H₂O/acetic acid mixture (9:0.5:0.5 v/v ratio), while for the acid-sensitive compounds a prolonged exposure to THF/H₂O mixture (9:1 ratio) can be applied. DEAM-PS can be regenerated by vigorous stirring in a basic solution (CH₂Cl₂:Et₃N in 3:1 ratio) with only slight loss of loading capacity.

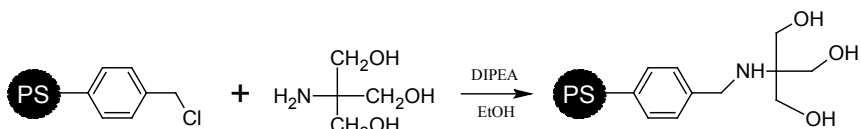
Another example of a solid support for immobilization of boronic acids is catechol-functionalized polystyrene. For this purpose it was first used by Yang *et al.* [12] In terms of immobilization, the catechol polymer is slightly more efficient than the 1,3-diol-functionalized resin and less efficient than DEAM-PS (immobilization yields varying from 67% to 75% in THF). Its synthesis

starts with protection of the hydroxyl groups of 3,4-dihydroxybenzaldehyde, executed by treatment with methoxymethyl chloride (MOMCl) in the presence of diisopropylethylamine (DIPEA). The next step was reductive amination with methylamine, followed by attaching the obtained amine to Merrifield resin in the presence of a strong base in ACN. Deprotection of methoxymethyl groups was carried out with trimethylsilyl bromide in DCM (Scheme 5). Immobilization reactions of boronic acids were performed in THF. Noteworthy, heating significantly increased the immobilization yields. Cleavage mixture was identical to the one applied for DEAM-PS by Hall *et al.*



Scheme 5. Synthesis of the catechol-functionalized polystyrene. TMS = trimethylsilyl.

Good results were obtained with triol-functionalized resins, first prepared by Liu *et al.* [13]. It can be produced from Merrifield resin and 2-amino-2-(hydroxymethyl)-1,3-propanediol (trometamol) in the presence of DIPEA in EtOH (Scheme 6).



Scheme 6. Synthesis of the triol resin.

The triol resin is efficient in immobilizing arylboronic acids in THF, DCM and ethyl acetate at room temperature (yields from 84% to 90% in THF). Liu *et al.* also attempted to immobilize arylboronic acids from aqueous solutions. However, poor yields were obtained, mostly due to the fact that polystyrene is a hydrophobic, polarizable material and its swelling is poor in alkanes, protic solvents or water. Yields of immobilization in basic aqueous and basic methanol solutions were varying from 17% to 68%, the highest one being observed for 4-tolylboronic

acid in 1M NaOH/MeOH. The triol resin, contrary to DEAM-PS, can be thus utilized in immobilization from a basic environment (under the same conditions, 4-tolylboronic acid was immobilized on DEAM-PS in 41% yield).

The reported average loading capacities for the discussed resins are as follows:

- ca. 1 mmol/g for the 1,3-diol-functionalized polymer [7],
- 0.92 mmol/g [8] to 1.54 mmol/g [9] for DEAM-PS (depending on the method of preparation),
- 0.97 mmol/g for the catechol polymer [12],
- 1.1 mmol/g for the triol resin [13].

An interesting alternative for polystyrene solid supports is posed by polyglycerols (PGs), commercially available polyhydroxylic dendritic polymers. Hebel and Haag showed that a series of four boronic acids - phenylboronic acid, 2-trifluoromethylphenylboronic acid, 3-nitrophenylboronic acid and 2-thienylboronic acid could be successfully immobilized onto dendritic PG [14]. Immobilization occurs at room temperature almost quantitatively (>95%), though molecular sieves are required to drive the process to completion. In case of 2-thienylboronic acid heating was additionally required. Interestingly, the average molecular weight of PG was found to significantly influence the rate of immobilization [14].

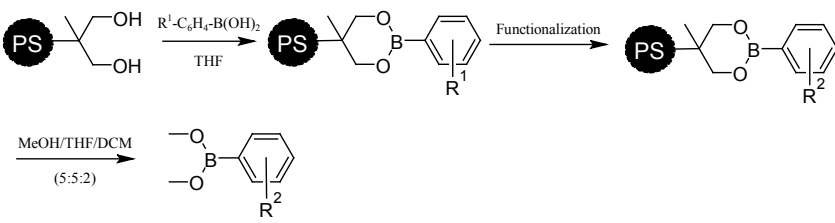
Solid-phase derivatization of functionalized arylboronic acids

Following immobilization, functional groups of the immobilized boronic acids can be subjected to various synthetic transformations. In the literature, such functionalizations were carried out solely on arylboronic derivatives. Although it is possible to immobilize alkylboronic acids, no works on their modification after immobilization have been reported.

Functionalization of arylboronic acids immobilized on the 1,3-diol resin could be achieved with moderate yields (54% to 67%, Table 1) [7]. Due to the cleavage procedure involving methanol, all the transformed boronic compounds were afforded as methyl esters.

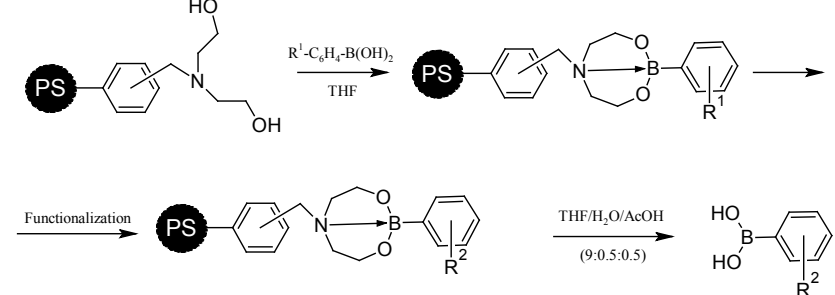
Higher yields of functionalization were obtained with arylboronic species bound to DEAM-PS resin. The transformations involved reductive amination, anilide synthesis, amide formation, ureas synthesis and substitution reactions (Table 2) [15]. Only *para*- and *meta*-substituted arylboronic acids gave satisfactory yields in the anilide, amide and ureas syntheses as well as in substitution reactions. For unexplained reasons, *ortho*-substituted substrates suffer from premature cleavage in the course of these reactions. To the contrary, only *ortho*-substituted substrates were surprisingly reported to give reasonable yields in reductive amination reactions.

Table 1. Arylboronic acids bound to 1,3-diol resin: immobilization, functionalization and cleavage.



R ¹	Functionalization	Solvent	R ²	Yield (%)
3-NH ₂	Propionyl chloride, pyridine	DCM	3-NHCOEt	63
3-NH ₂	4-Toluenesulfonyl chloride, DIPEA	DCM	3-NHSO ₂ Tol	54
3-NH ₂	Phenylisocyanate	DCM	3-NHC(O)NHPh	59
4-CO ₂ H	1. SOCl ₂ 2. <i>n</i> -BuOH, pyridine	Toluene	4-CO ₂ Bu	65
4-CH ₂ OH	Propionyl chloride, (<i>i</i> -Pr) ₂ NEt	DCM	4-CH ₂ O(O)CEt	54
4-CHO	Pinacol allylboronate	DCM	4-CH(OH)-Allyl	67

Table 2. Arylboronic acids bound to DEAM-PS: immobilization, functionalization, cleavage. PyBOP = Benzotriazol-1-yl-oxytripyrrolidinophosphonium hexafluorophosphate, Fmoc = Fluorenylmethyloxycarbonyl, NMP = *N*-Methyl-2-pyrrolidone.

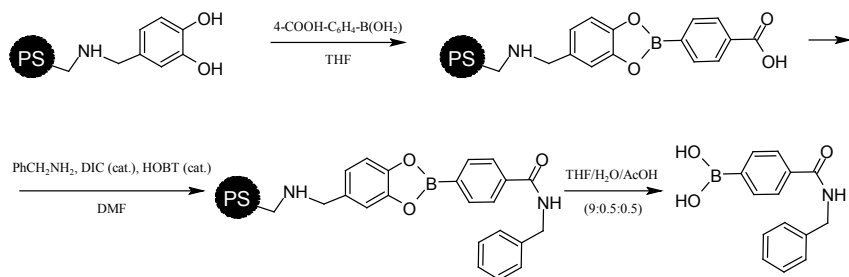


R ¹	Functionalization	Solvent	R ²	Yield (%)
3-CH ₂ Br	NH ₂ CH ₂ Ph	NMP	3-CH ₂ NHCH ₂ Ph	69
3-CH ₂ Br	NH ₂ CH ₂ CH(CH ₃) ₂	NMP	3-CH ₂ NHCH ₂ CH(CH ₃) ₂	50

R¹	Functionalization	Solvent	R²	Yield (%)
3-CH ₂ Br	HN(CH ₂ CH ₂) ₂ O	NMP	3-CH ₂ N(CH ₂ CH ₂) ₂ O	85
3-CH ₂ Br	CH ₃ NHCH ₂ Ph	NMP	3-CH ₂ N(CH ₂)CH ₂ Ph	75
4-CH ₂ Br	NH ₂ CH ₂ Ph	NMP	4-CH ₂ NHCH ₂ Ph	69
4-CH ₂ Br	NH ₂ CH ₂ CH(CH ₃) ₂	NMP	4-CH ₂ NHCH ₂ CH(CH ₃) ₂	53
4-CH ₂ Br	HN(CH ₂ CH ₂) ₂ O	NMP	4-CH ₂ N(CH ₂ CH ₂) ₂ O	98
4-CH ₂ Br	CH ₃ NHCH ₂ Ph	NMP	4-CH ₂ N(CH ₂)CH ₂ Ph	94
2-CHO	NH ₂ CH ₂ Ph, NaBH ₄	THF	2-CH ₂ NHCH ₂ Ph	66
2-CHO	NH ₂ CH ₂ CH(CH ₃) ₂ , NaBH ₄	THF	2-CH ₂ NHCH ₂ CH(CH ₃) ₂	55
2-CHO	NH ₂ (CH ₂) ₃ Ph, NaBH ₄	THF	2-CH ₂ NH(CH ₂) ₃ Ph	62
2-CHO	NH ₂ (CH ₂) ₃ CH ₃ , NaBH ₄	THF	2-CH ₂ NH(CH ₂) ₃ CH ₃	73
3-COOH	NH ₂ (CH ₂) ₃ Ph, DIC, HOBT/H ₂ O	NMP or DMF	3-CONH(CH ₂) ₃ Ph	57
3-COOH	NH ₂ CH(CH ₃) ₂ , DIC, HOBT/H ₂ O	NMP or DMF	3-CONHCH(CH ₃) ₂	60
3-COOH	NH ₂ (CH ₂) ₃ CH ₃ , DIC, HOBT/H ₂ O	NMP or DMF	3-CONH(CH ₂) ₃ CH ₃	56
3-COOH	NH ₂ Ph, PyBOP, DIPEA	DMF	3-CONHPh	82
3-COOH	NH(Et) ₂ , DIC, HOBT/ H ₂ O	NMP or DMF	3-CON(Et) ₂	77
3-COOH	NH(<i>n</i> -Bu) ₂ , DIC, HOBT/H ₂ O	NMP or DMF	3-CON(Bu) ₂	79
3-COOH	NH(CH ₂ Ph) ₂ , DIC, HOBT/H ₂ O	NMP or DMF	3-CON(CH ₂ Ph) ₂	60
4-COOH	NH ₂ (CH ₂) ₃ Ph, PyBOP, DIPEA	DMF	4-CONH(CH ₂) ₃ Ph	65
4-COOH	NH ₂ CH(CH ₃) ₂ , PyBOP, DIPEA	DMF	4-CONHCH(CH ₃) ₂	81

R¹	Functionalization	Solvent	R²	Yield (%)
4-COOH	NH ₂ (CH ₂) ₃ CH ₃ , DIC, HOBT/H ₂ O	NMP or DMF	4-CONH(CH ₂) ₃ CH ₃	64
4-COOH	NH ₂ Ph, DIC, HOBT/H ₂ O	NMP or DMF	4-CONHPh	67
4-COOH	NH(Et) ₂ , DIC, HOBT/H ₂ O	NMP or DMF	4-CON(Et) ₂	59
4-COOH	NH(<i>n</i> -Bu) ₂ , DIC, HOBT/H ₂ O	NMP or DMF	4-CON(Bu) ₂	53
4-COOH	NH(CH ₂ Ph) ₂ , PyBOP, DIPEA	DMF	4-CON(CH ₂ Ph) ₂	70
4-COOH	NH ₂ (CH ₂) ₂ NEt ₂ , DIC, HOBT/H ₂ O	NMP or DMF	4-CONH(CH ₂) ₂ NEt ₂	70
2-NH ₂	CH ₃ CH ₂ CO ₂ H, PyBOP, DIPEA	NMP	NHCOCH ₂ CH ₃	61
2-NH ₂	PhCO ₂ H, PyBOP, DIPEA	NMP	NHCOPh	60
3-NH ₂	CH ₃ CH ₂ CO ₂ H, DIC, HOBT/H ₂ O	DMF	NHCOCH ₂ CH ₃	42
3-NH ₂	PhCO ₂ H, DIC, HOBT/H ₂ O	DMF	NHCOPh	52
3-NH ₂	CH ₃ CH ₂ CO ₂ H, PyBOP, DIPEA	NMP	NHCOCH ₂ CH ₃	72
3-NH ₂	PhCO ₂ H, PyBOP, DIPEA	NMP	NHCOPh	82
3-NH ₂	CH ₂ =CHCH ₂ CH ₂ CO ₂ H, PyBOP, DIPEA	NMP	NHCOCH ₂ CH ₂ CH=CH ₂	70
3-NH ₂	PhCCCO ₂ H, PyBOP, DIPEA	NMP	NHCOCCPh	75
3-NH ₂	FmocNH(CH ₃)(S)CHCO ₂ H, PyBOP, DIPEA	NMP	NHCOR(S)CH(CH ₃)NHFmoc	51

R ¹	Functionalization	Solvent	R ²	Yield (%)
4-NH ₂	CH ₃ CH ₂ CO ₂ H, PyBOP, DIPEA	NMP	NHCOCH ₂ CH ₃	61
4-NH ₂	PhCO ₂ H, PyBOP, DIPEA	NMP	NHCOPh	46
3-NH ₂	(CH ₃) ₂ CHNCO	DCM	NHCONHCH(CH ₃) ₂	66
3-NH ₂	PhNCO	DCM	NHCONHPh	79
3-NH ₂	(4-MeO-C ₆ H ₄)NCO	DCM	NHCONH-(4-MeO-C ₆ H ₄)	82
3-NH ₂	(4-NO ₂ -C ₆ H ₄)NCO	DCM	NHCONH-(4-NO ₂ -C ₆ H ₄)	80
3-NH ₂	PhNCS	DCM	NHCSNHPh	85
4-NH ₂	(CH ₃) ₂ CHNCO	DCM	NHCONHCH(CH ₃) ₂	65
4-NH ₂	PhNCO	DCM	NHCONHPh	85
4-NH ₂	(4-MeO-C ₆ H ₄)NCO	DCM	NHCONH-(4-MeO-C ₆ H ₄)	88
4-NH ₂	(4-NO ₂ -C ₆ H ₄)NCO	DCM	NHCONH-(4-NO ₂ -C ₆ H ₄)	92



Scheme 7. Synthesis of 4-(benzyl carbamoyl)phenylboronic acid using the catechol-functionalized polystyrene.

Only a few solid-phase reactions have been developed for other resins than DEAM-PS. No reactions have been reported for the triol resin and only one for the catechol polymer [12]. The reaction of 4-carboxyphenylboronic acid immobilized on the catechol resin with benzylamine was carried out in

the presence of diisopropylcarbodiimide (DIC) and 1-hydroxybenzotriazole (HOBT) in DMF as a solvent (Scheme 8). The resulting 4-(benzylcarbamoyl) phenylboronic acid was afforded in 53% yield.

Use of solid supports for boronic acids in metal-catalyzed reactions

Transition metal-promoted couplings are among the most popular reactions for the formation of new carbon-carbon bonds within organic molecules. With the palladium-catalyzed Suzuki-Miyaura cross-coupling regarded as one of the most popular synthetic applications of boronic acids and their derivatives [16], it was clear that metal-catalyzed reactions would be investigated in the context of SPS.

Pourbaix *et al.* applied Suzuki cross-coupling as a cleavage protocol for a series of boronic acids bound to a 1,3-diol resin [17]. The reactions were carried out by treating an immobilized arylboronic acid with an excess of 4-iodomethoxybenzene in the presence of a palladium catalyst: ([1,1'-bis(diphenylphosphino)ferrocene] dichloropalladium(II), Pd(dppf)Cl₂) and a base in a polar aprotic solvent. A new C-C bond is consequently formed, affording a biaryl product (Table 3). The desired biaryls were frequently detached from the resin along with the products of boronic acid homocoupling. Because of that, all post-cleavage mixtures had to be further subjected to flash chromatography on silica gel.

Table 3. Suzuki cross-coupling of 4-iodomethoxybenzene with arylboronic acids immobilized on 1,3-diol resin.

R ¹	Yield (%)
H	67
3-NO ₂	60
3-NHCOEt	75
4-NHCH ₂ Ph	53
4-C(O)N(CH ₂ Ph)CH(ⁱ Pr)C(O)NHCH ₂ Ph	45

The conditions for arylation of aldehydes developed by Miyaura *et al.* [18] were successfully adopted by Pourbaix *et al.* [17] for the solid-phase transformations. Immobilized arylboronic acid is reacted with an aromatic aldehyde in the presence of (acetylacetonato)dicarbonylrhodium(I) Rh(acac)(CO)₂ and (diphenylphosphino)ferrocene (dppf) (Table 4).

Table 4. Arylation of aromatic aldehydes with arylboronic acids immobilized on 1,3-diol resin. DME = dimethoxyethane.

R ¹	R ²	Yield (%)
CH ₃	H	62
CH ₃	Cl	43
CH ₃	CF ₃	63
CH ₃	CN	81
H	CN	56

The pure products were isolated in moderate yields. Increase in the amount of the starting aldehyde was found to decrease the yield of the desired alcohol. Noteworthy, a 1,3-diol-functionalized resin was utilized also for removal of the starting aldehyde remaining in the post-reaction mixture [19].

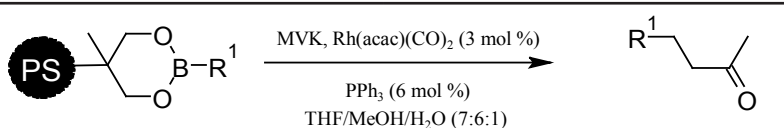
Solid support functionalized with 1,3-diol groups was also found to be useful for the nucleophilic 1,4-addition of alkyl or aryl groups to enones (Table 5). Reaction of a resin-bound alkyl-/arylboronic acid with methyl vinyl ketone (MVK) in the presence of Rh(acac)(CO)₂ and triphenylphosphine afforded β-functionalized ketones in moderate yields.

DEAM-PS resin was also successfully employed in palladium-catalyzed reactions for the preparation of unsymmetrical biaryl compounds [20], as well as bi(hetero)aryl compounds [21].

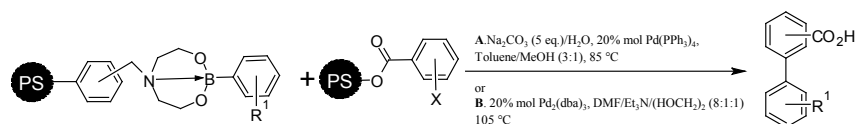
Gravel *et al.* presented a strategy for the synthesis of biaryl species *via* a resin-to-resin Suzuki coupling, both under aqueous and anhydrous conditions [20]. In both cases, the resin with the immobilized boronic acid is used in excess. The presence of a base and a palladium catalyst is required, which is common

for all Suzuki couplings. The feature distinguishing these two methods is of course the solvent system, with special emphasis put on the solid phase-transfer agent. This agent allows the boronic acid to be cleaved from DEAM-PS and then transferred to the iodoarene-bearing resin. Aqueous conditions feature the use of a toluene/methanol mixture with water as the solid phase-transfer agent, while the anhydrous method involves DMF with ethylene glycol (Scheme 8). Coupling products were isolated in good to excellent yields (75%-quantitative).

Table 5. Nucleophilic 1,4-addition of immobilized boronic acids to enones

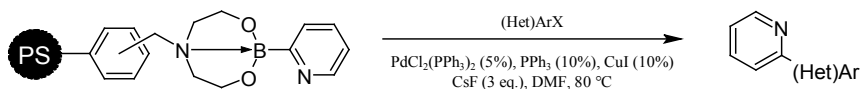


R ¹	Yield (%)
Ph	60
4-MeC ₆ H ₄	47
1-hexenyl	55



Scheme 8. General concept of the resin-to-resin Suzuki coupling leading to biaryls. dba = dibenzylideneacetone.

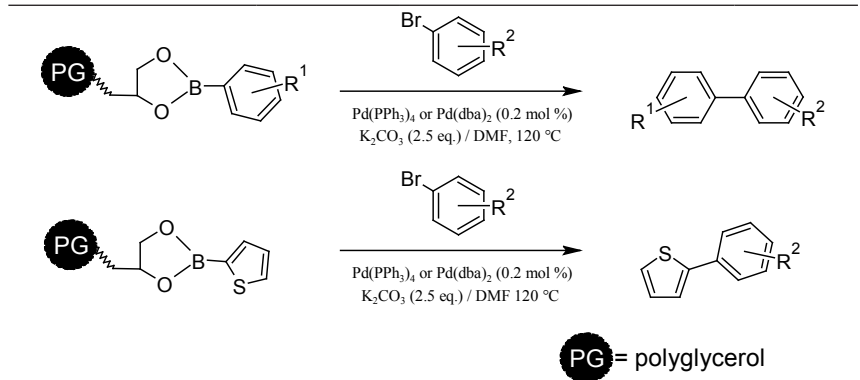
First approach to the Suzuki coupling-based SPS of bi(hetero)aryls (namely pyridylarenes and pyridylheteroarenes) was proposed by Gros *et al.* [21]. 2-Pyridylboronic acid bound to DEAM-PS was reacted with aromatic and heteroaromatic halides (Scheme 9). Only slight excess of halide was needed. Reactions were catalyzed by bis(triphenylphosphine)palladium (II) dichloride PdCl₂(PPh₃)₂, accompanied with an additive of the phosphine ligand (PPh₃). Out of three tested bases: Et₃N, K₂CO₃ and CsF, the most efficient proved to be CsF. Addition of CuI gave meaningful increase in reaction efficiency, preventing the homocoupling process. Reactions were carried in DMF as a solvent. The products were obtained in moderate to good yields (50% to 87%).



Scheme 9. Coupling of DEAM-PS-bound 2-pyridylboronic acid with (hetero)aromatic halides. X = Br; I.

Also boronic acids immobilized on polyglycerols were employed in Suzuki couplings (Table 6) [14]. The biaryl compounds were obtained in the reaction with an aryl halide, K_2CO_3 and $\text{Pd}_2(\text{dba})_3$ in DMF. When the reaction was complete, DMF was substituted with toluene for the separation protocol in which ultrafiltration and precipitation were used to purify the products.

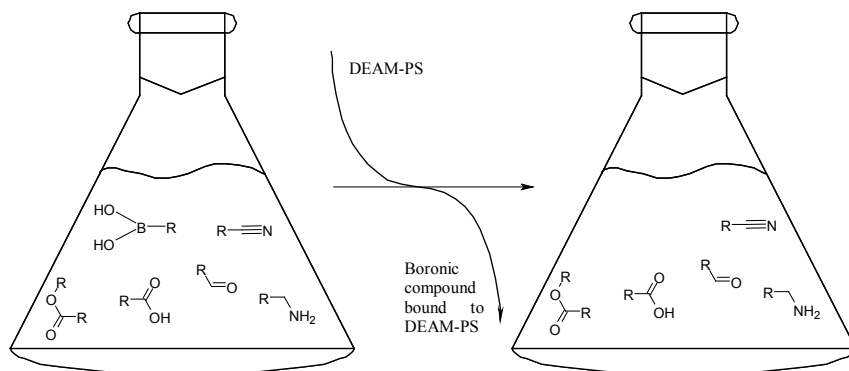
Table 6. Suzuki couplings performed with boronic acids immobilized on PG supports.



Boronic Acid	R ¹	R ²	Catalyst	Yield (%)
Phenylboronic acid	H	4-OCH ₃	Pd(PPh ₃) ₄	88
Phenylboronic acid	H	4-C(O)CH ₃	Pd(PPh ₃) ₄	84
Phenylboronic acid	2-CF ₃	4-OCH ₃	Pd(PPh ₃) ₄	89
Phenylboronic acid	2-CF ₃	4-C(O)CH ₃	Pd(dba) ₂	91
Phenylboronic acid	3-NO ₂	4-OCH ₃	Pd(PPh ₃) ₄	86
Phenylboronic acid	3-NO ₂	4-C(O)CH ₃	Pd(dba) ₂	91
2-Thienylboronic acid	-	4-OCH ₃	Pd(PPh ₃) ₄	90
2-Thienylboronic acid	-	4-C(O)CH ₃	Pd(dba) ₂	88

Scavenging boronic acids with diol-functionalized resins

One of the biggest issues in operating boronic acids as reagents in organic synthesis is isolating them from the post-reaction mixtures. Diol resins may be useful in solving this problem. As a matter of fact, scavenging of boronic acids with DEAM-PS may be considered one of the most interesting application of diol resins. By addition of DEAM-PS to a mixture, stirring for several hours, followed by removal of the resin by filtration, the immobilized boronic acids can be removed from the reaction mixture (Scheme 10) [22]. The efficiency of scavenging is highly dependent on the structure of the boronic acid and on the solvent applied.



Scheme 10. Scavenging of boronic acids from a post-reaction mixture with the use of DEAM-PS.

Hence, performing Suzuki coupling without the need for aqueous work-up or column chromatography was made possible owing to the use of DEAM-PS resin.

Lan *et al.* proposed a polymer-supported carbonate (tetraalkylammonium carbonate resin) as a scavenger for boronic acids [22]. However, the experiments performed by Vickerstaffe *et al.* proved that it was not sufficiently effective in this process [23]. They found excess boronic acid contaminating the desired product after Suzuki coupling. To purify it, evaporation of the reaction mixture, followed by redissolving in DMF and then incubation with DEAM-PS was needed.

Remarkably, the scavenging applications of DEAM-PS are not limited to the removal of boronic acids. Tsukamoto *et al.* employed DEAM-PS resin for the work-up of a Suzuki coupling reaction mixture, separating boronic acids along with palladium catalyst [24]. The authors reported that DEAM-PS scavenged

99.4% of the used palladium catalyst ($\text{Pd}(\text{PPh}_3)_4$). The diethanolamine moiety in DEAM-PS was found to be essential for scavenging: non-functionalized cross-linked polystyrene scavenged (by adsorption) only 49.5% of the catalyst.

Acknowledgements

Krzysztof M. Borys acknowledges the Ministry of Science and Higher Education of Poland for financial support within the framework of “Diamentowy Grant” programme (grant No. DIA/2013/42).

References

1. Merrifield, R. B. Solid phase peptide synthesis. I. The synthesis of tetrapeptide. *J. Am. Chem. Soc.* **1963**, *85*, 2149-2154.
2. Banga A. J. Therapeutic peptides and proteins; Taylor & Francis: New York, **2006**.
3. Bunin, B. A.; Ellman, J. A. A general and expedient method for the solid-phase synthesis of 1,4-benzodiazepine derivatives. *J. Am. Chem. Soc.* **1992**, *114*, 10997-10998.
4. Dolle, R. E.; Bourdonnec, B.; Goodman, A. J.; Morales, G. A.; Thomas, C. J.; Zhang, W. Comprehensive survey of chemical libraries for drug discovery and chemical biology: 2008. *J. Comb. Chem.* **2009**, *11*, 739-789.
5. Kennedy, J. P.; Williams, L.; Bridges, T. M.; Daniels, R. N.; Weaver, D.; Lindsley, C. W. Application of combinatorial chemistry science on modern drug discovery. *J. Comb. Chem.* **2008**, *10*, 345-354.
6. Tzschucke, C. C.; Markert, C.; Bannwarth, W.; Roller, S.; Hebel, A.; Haag, R. Modern separation techniques for the efficient workup in organic synthesis. *Angew. Chem. Int. Ed.* **2002**, *41*, 3964-4000.
7. Carboni, B.; Pourbaix, C.; Carreaux, F.; Deleuze, H.; Maillard, B. Boronic ester as a linker system for solid phase synthesis. *Tetrahedron Lett.* **1999**, *40*, 7979-7983.
8. Hall, D. G.; Taylor, J.; Gravel, M. *N,N*-diethanolaminomethyl polystyrene: an efficient solid support to immobilize boronic acids. *Angew. Chem. Int. Ed.* **1999**, *38*, 3064-3066.
9. Arimori, S.; Hartley, J. H.; Bell, M. L.; Oh, C. S.; James T. D. ‘Tailored’ polymers for supported syntheses using boronic acids. *Tetrahedron Lett.* **2000**, *41*, 10291-10294.
10. Matteson, D. S. Stereodirected synthesis with organoboranes; Springer: Berlin, **1995**.

11. Santini, R.; Griffith, M. C.; Qi, M. A measure of solvent effects on swelling of resins for solid phase organic synthesis. *Tetrahedron Lett.* **1998**, *39*, 8951-8954.
12. Yang, W.; Gao, X.; Springsteen, G.; Wang, B. Catechol pendant polystyrene for solid-phase synthesis. *Tetrahedron Lett.* **2002**, *43*, 6339-6342.
13. Liu, L. F.; Wan, S. B.; Jiang, T. First preparation of a novel polyol resin for purifying arylboronic acids. *Chin. Chem. Lett.* **2012**, *23*, 993-995.
14. Hebel, A.; Haag, R. Polyglycerol as a high-loading support for boronic acids with application in solution-phase Suzuki cross-couplings. *J. Org. Chem.* **2002**, *67*, 9452-9455.
15. Gravel, M.; Thompson, K. A.; Zak, M.; Bérubé, C.; Hall, D. G. Universal solid-phase approach for the immobilization, derivatization, and resin-to-resin transfer reactions of boronic acids. *J. Org. Chem.* **2002**, *67*, 3-5.
16. Lennox, A. J. J.; Lloyd-Jones, G. C. Selection of boron reagents for Suzuki-Miyaura coupling. *Chem. Soc. Rev.* **2014**, *43*, 412-443.
17. Pourbaix, C.; Carreaux, F.; Carboni, B. Metal-catalyzed release of supported boronic acids C—C bond formation. *Org. Lett.* **2001**, *3*, 803-805.
18. Sakai, M.; Ueda, M.; Miyaura, N. Rhodium-catalyzed addition of organoboronic acids to aldehydes. *Angew. Chem. Int. Ed.* **1998**, *37*, 3279-3281.
19. Chamoin, S.; Houldsworth, S.; Kruse, C. G.; Iwema Bakker, W.; Snieckus, V. The Suzuki-Miyaura cross coupling reactions on solid support. Link to solution phase directed *ortho* metalation. The Leznoff acetal linker approach to biaryl and heterobiaryl aldehydes. *Tetrahedron Lett.* **1998**, *39*, 4179-4182.
20. Gravel, M.; Bérubé, C. D.; Hall, D. G. Resin-to-resin Suzuki coupling of solid supported arylboronic acids. *J. Comb. Chem.* **2000**, *2*, 228-231.
21. Gros, P.; Doudouh, A.; Fort, Y. New polystyrene-supported stable source of 2-pyridylboron reagent for Suzuki couplings in combinatorial chemistry. *Tetrahedron Lett.* **2004**, *45*, 6239-6241.
22. Lan, P.; Berta, D.; Porco, Jr, J. A.; South, M. S.; Parlow, J. J. Polymer-assisted solution-phase (PASP) Suzuki couplings employing an anthracene-tagged palladium catalyst. *J. Org. Chem.* **2003**, *68*, 9678-9686.
23. Vickerstaffe, E.; Villard, A.; Ladlow, M.; Ley, S. V. Chromatography-free Suzuki reactions using a polymer-assisted solution-phase (PASP) approach. *Synlett* **2007**, *8*, 1251-1254.

24. Tsukamoto, H.; Suzuki, T.; Sato, M.; Kondo, Y. Chromatography-free Pd-catalyzed deprotection of allyl ethers using PS-DEAM as a scavenger of boronic acids and Pd catalyst. *Tetrahedron Lett.* **2007**, *48*, 8438-8441.

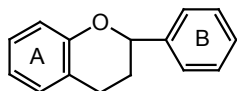
Chapter 5

Electronic structure of the organic compounds and their reactivity in the reactions of radical hydrogen atom tear by HO₂[•] radical

A.F. Dmitruk, L.F. Pikula, T.V. Kryuk and Yu.O. Lesishina
*Donetsk National University of Economics and Trade named after
Mykhailo Tugan-Baranovsky, Schersa Str. 31, 83050 Donetsk, Ukraine*

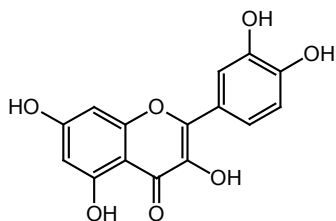
The highly-active free radicals are formed constantly in the living organism during the oxidation of lipids, proteins and nucleic acids creating conditions for the development of many different diseases. Substances that neutralize these reactive particles – antioxidants – are produced, to some extent, by the cell, but most of them are delivered with the food, especially of plant origin. The forecasting of the antioxidant activity of different substances depending on their structure is thus an extremely important goal.

Analysis of the latest research and publications showed that the oxidation inhibitors (InH), contained in the food, are related primarily to different types of phenolic compounds [1]. Primarily, these are flavonoids (formulas I-III), hydroxy acids and their derivatives (formula IV, V), polyphenols (formula VI, VII). Heterocyclic compounds containing nitrogen (mainly B vitamins, formula VIII, IX) and oxygen (E vitamins, the formula X) also have high antioxidant effect.

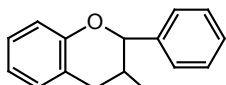


(I)

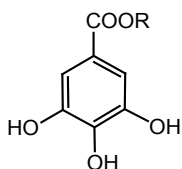
I – a general formula of flavonoids,
rings A and B may contain a
different number of OH-groups



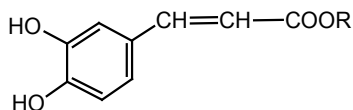
(II) II – quercetin –
an antioxidant of tea, hops, onion,
black currants, blackberries;



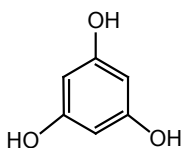
(III) III – catechin – antioxidant
strawberry, peach);



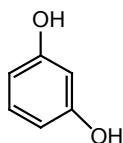
(IV) IV – gallic acid derivatives
(R – H, alkyl radical) are part of
the plants of tea;



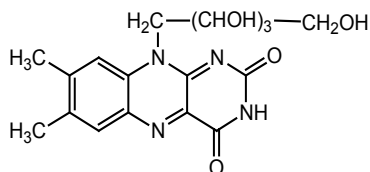
(V) V – caffeic acid derivatives (R –
H, alkyl radical) are contained in
the stone fruit;



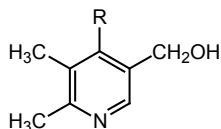
(VI) VI – phloroglucinol – the
component of the citrus fruits;



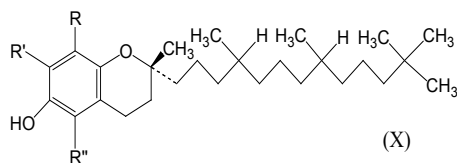
(VII) VII – resorcinol – is a part of citrus
fruit plants;



(VIII) VIII – riboflavin (vitamin B₂) – is
a part of the green leaf vegetables,
legumes;

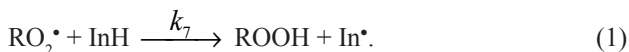


(IX) IX – the general formula of
vitamins B₆ (R= –CHO, –CH₂NH₂,
–CH₂OH) – components of green
pepper, wheat, dry yeast;



X – the total formula of tocopherols – derivatives of the tocol ($R=R'=R''=H$), which are found in vegetable oils.

All these compounds possessing reducing properties and easily react with peroxy radicals thus breaking the natural oxidation chain:



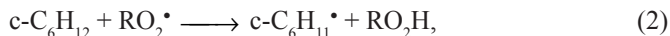
The rate constant of the reaction (1) is a quantitative measure of the antioxidant activity of the inhibitor [2]. While the rate constant of hydrogen abstraction by peroxy radicals can be calculated for the individual chemical compounds, most natural antioxidants present a complex mixture of substances, which is difficult to separate.

A number of comprehensive studies of the kinetics of the reaction (1) have been conducted to date. The hydrocarbons of various structures and inhibitors, representing a variety of aromatic compounds with OH- and NH-groups analogous to natural antioxidants have been studied in this reaction.

The aim of this study was to investigate the effect of the features of the chemical structure of antioxidants on the reactivity of X-H bonds (where X is or N) towards oxidation.

The most complete information about the electronic structure of chemical compounds can be obtained by quantum-chemical methods. Here, we performed such studies using SCF approach within the restricted Hartree-Fock molecular orbitals theory, at PM3 approximation [3], as implemented in MOPAC 93 [4]. Geometry optimization was carried out in all degrees of freedom of the molecules (i.e., (3N-6) variables). The optimization was performed until the the gradient $< 0.1 \text{ kcal}/(\text{mol}\cdot\text{\AA})$ is reached and frequency calculations were used to confirm that the optimized structure in the minimum (by lack of imaginary frequencies).

In order to study the electronic nature of the transition state of the reaction (1), we have scanned the surface of the potential energy along the reaction coordinate for the reaction:



where RO_2^\bullet – cyclohexyl peroxy radical.

The localization of the transition state (TS) of the reaction (2) was carried out in the approximation PM3 Unrestricted Hartree-Fock method. The starting geometry of the saddle point has been found by the method proposed in [3]. The saddle point on the potential energy surface corresponding to the TS, has been localized by Bartel method, realized in MOPAC 93. This saddle point was tested as follow. We performed a numerical harmonic vibrational analysis by calculation of the mass-weighted Hessian and obtained frequencies and forms of normal vibrations, one of which is imaginary and corresponds to the mode of the antisymmetric $C \leftrightarrow H \leftrightarrow O$ vibration of atoms of the reaction center. Besides the reaction coordinate was built in mass-weighted Cartesian coordinates using the method of the internal reaction coordinate as showed on Figure 1.

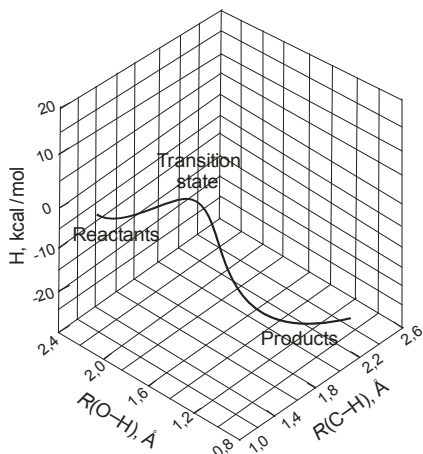


Figure 1. Reaction(2) coordinate

Primary disturbance (equal to the quantum of vibrational energy) in the direction of the normal coordinate and reversible disturbance in the opposite direction to the normal coordinate has been applied. Thus, the internal reaction's coordinate was built from the transition state along the way down the reaction channels in both directions until the reactants and reaction products.

Figure 1 shows that the transition state actually connects the reactants and products. The reduction of the potential energy of the system is monotonic in both directions on the way from the TS. The values of the calculated parameters of the transition state of the reaction (2): the imaginary frequency (ν^*I), the relative increase of the length of C-H and O-H bonds in the transition state (ΔR), the total square of deformation of the bond lengths in the reactants and products in relation to the transition state (r^*), the total electronic charge on the fragments of TS are shown in the Table 1.

Table 1. The values of the calculated parameters of the transition state of the reaction (2)

ν^*I , [cm^{-1}]	$\Delta R_{\text{C-H}}$, [\AA]	$\Delta R_{\text{O-H}}$, [\AA]	r^* , [\AA^2]		Electronic charge on the fragments of TS		
			Reactants	Products	c-C ₆ H ₁₁	H	O ₂ R
1683	0.1119	0.2433	0.01	20.04	0.022	0.110	-0.132

As follows from the results, the transition state of the reaction is very close geometrically to the structure of the reactants and far away from products. This is evidenced by the small deformation of the TS structure from the structure of the reagents and a large deformation from the structure of the products. Most notable is the fact that the transition state of the reaction is polarized, i.e. the transfer of the electron density from the molecule containing the C–H bond to the peroxy radical is observed. Thus, the reaction proceeds by the donor-acceptor mechanism, where the oxidize molecule is an electron donor, and the peroxy radical is an acceptor.

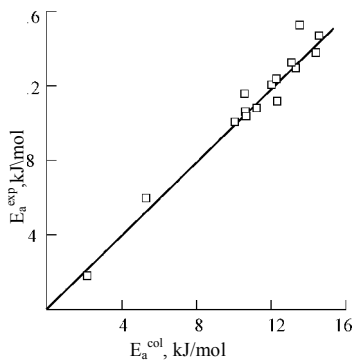


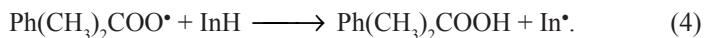
Figure 2. The relationship between the experimental values of the activation energy and values of the activation energy calculated from equation (3), for the hydrogen abstraction by peroxy radical.

It should be expected that there is a functional dependence between the electron-donor properties of the molecule (ionization energy, electron-charge distribution on the atoms of the reaction center) and the ability of the molecule to oxidize. The authors of [3] obtained a correlation as showed on Figure 2, which connect the activation energy of the reaction with the parameters of the electronic structure of the following reagents: c-C₆H₁₂, PhCH₃, PhC₂H₅, PhCH(CH₃)₂, 1,4-(CH₃)₂C₆H₄, 1,4-(C₂H₅)₂C₆H₄, 1,4-(*iso*-C₃H₇)₂C₆H₄, Ph₂CH₂, PhCHO for molecules containing reactive C–H bond. These dependences are obtained by the equation:

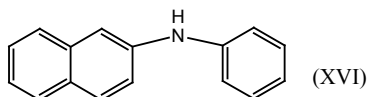
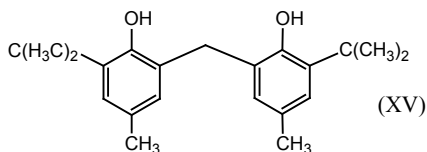
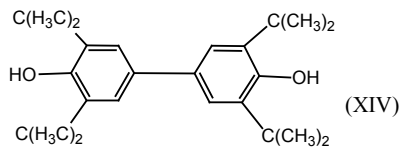
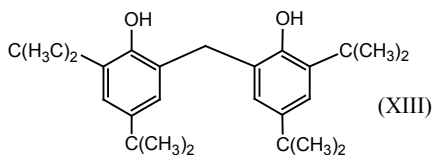
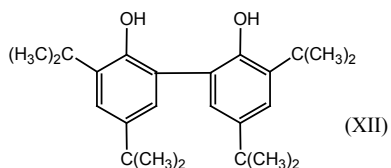
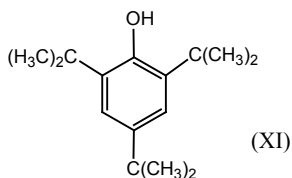
$$E_a = 925.1 + 485.6 \cdot F_O - (78.1 \cdot F_H + 1.0 \cdot \delta_{\text{cyk}}), \quad (3)$$

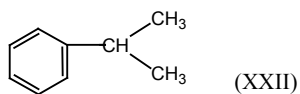
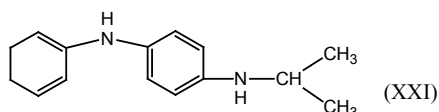
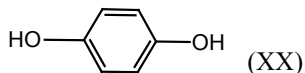
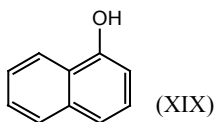
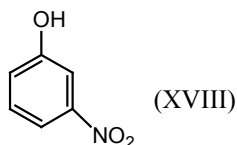
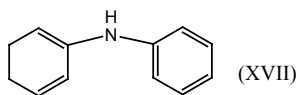
where Q_H , Q_O – electronic charges on the atoms of the reaction center H and O, respectively; I_{RH} , I_{RO_2} – ionization potential of the molecule and peroxy radical; $F_O = (Q_O/I_{RO_2})^{1/2}$ and $F_H = (Q_H/I_{RH})$; $\delta_{\text{cyk}} = 0$ or 1 (depending on the presence or absence of a saturated cycle).

These results allow us to suggest that similar dependence should be observed for compounds with a more reactive X–H bond. Based on this assumption, we calculated the electronic structure of a number of aromatic amines and phenols, for which the experimental values of the reaction rate constants at 60°C are known [4].



Following aromatic phenols and amines have been used as InH:





The results of the quantum-chemical calculations of these compounds are given in Table 2.

It should be noted in general, that the hydrogen abstraction from the X-H bond leads to radicals centered on the atom X. Radicals in which the unpaired electron is centered on C, O or N atoms are quite different the spin density localized on these atoms. Therefore, the oxidative capacity of molecules containing X-H bond will be determined not only by the electron-donating ability of the molecule, but also by the stability of the forming radical. Accounting for this fact it was possible to obtain an equation relating the logarithm of the rate constant of reaction (4) with the electronic parameters of the reactants and reaction products:

$$\lg k = (24.3 \pm 2.0) - (102.1 \pm 10.4)F_H - (19.1 \pm 1.7)\rho_X + (1.1 \pm 0.2)n_{XH}, \quad (5)$$

where ρ_X – the spin density on the atom X forming radical, n_{XH} – the number of reactive X-H bonds. Multiple correlation coefficient is 0.97 and the standard error is 0.4.

Table 2. Values of the enthalpy of formation ($\Delta H_{f,298}$), ionization potential (I), the charges on the H atom of the tearing X-H bond (Q_H) and the value of the spin density (ρ_X) on the atom X of the formed radical $In\bullet$ by the reaction of (5)

Number of the substance	$\Delta H_{f,298}$, kcal/mol	I , eV	Q_H	ρ_X
1	2	3	4	5
XI	-79,20	8,74	0,2111	0,2797
XII	-115,83	8,46	0,2111	0,2882
XIII	-129,90	8,65	0,2070	0,2999
XIV	-111,36	8,21	0,2164	0,2853
XV	-101,65	8,73	0,2065	0,3009
XVI	67,75	8,33	0,0508	0,6724
XVII	50,50	8,60	0,049	0,6840
XVIII	-30,14	9,99	0,2042	0,3608
XIX	-3,28	8,54	0,1994	0,2573
XX	-66,25	8,75	0,1953	0,3192
XXI	35,91	8,20	0,0482	0,6770
XXII	5,35	9,44	0,0659	0,9098

Our results demonstrate that the ability of molecules to act as antioxidantants is determined first by their electron-donor properties, and, second, by a stability of the radical formed in the breaking of the X-H bond.

References

1. Filatova I.A., Kolesnov A.Yu. Importance of the phenolic compounds of fruits and berries in the prevention of diseases // Food Industry – 2000. – № 8. – P.35–37.
2. Denisov Ye.T., Sarkisov O.M., Liechtenstein G.I. Chemical Kinetics. – M.: Chemistry, 2000. – 568 p.
3. Opeyda I.A., Dmitruk A.F., Zarechnaya O.M. The reactivity of the C–H

- bond of organic molecules with different structures in the reactions of hydrogen atom abstraction by peroxy radicals // Theoretical and experiment. Chem. – 1997. – Vol. 33. – № 1. – P. 6-11.
4. Dewar M.J.S., Zoebisch E.G., Hedy E.F., Stewart J.J.P. Ground states of molecules. 25. PM3 an improved version of the MNDO semiempirical SCF - MO method // J. Am. Chem. Soc. - 1985. - Vol.10, № 7. - P.3902-3912.
 5. Shlyapnikov Yu.A., Kiryushkin S.G., Marin A.P. Antioxidative stabilization of polymers. M.: Chemistry, 1986. – 256 p.

Chapter 6

Application of mesoporous silica nanoparticles for drug delivery

Dawid Lewandowski and Grzegorz Schroeder
*Adam Mickiewicz University in Poznań, Faculty of Chemistry,
Umultowska 89b, 61-614 Poznań*

1. Introduction

Since the discovery of the MCM-41s silicas in 1992, the synthesis of mesoporous silica materials has developed rapidly. The best known families of mesoporous silicas include MCM-n¹, MSU-n (Michigan State University silica)², KIT-1 (Korean Institute of Technology)³, SBA-n (Santa Barbara amorphous silica)⁴, IBN (Institute of Bioengineering and Nanotechnology)⁵, FDU-n (Fudan University)⁶, KSW silicas⁷, FSM⁸ and HMS⁹ silicas. Each of them has its own unique advantages and disadvantages, and all have found a variety of applications.

Mesoporous nanoparticles have been found particularly interesting from the point of view of applications in medicine because of their increased mechanical strength, chemical stability, tunable particle size, uniform and tunable pore sizes, high surface areas, large pore volumes, two functional surfaces – an internal one in the pores and an external one on the exterior particle surface, porous structure enabling controlled cargo delivery, biocompatibility and higher resistance to microbial attack comparing to their organic (polymeric) equivalents¹⁰. Additionally, the silica matrix protects entrapped molecules against denaturation or enzymatic degradation induced by external pH and temperature¹¹.

Multiple nanocomponents with diagnostic and therapeutic functions can be combined into a single nanosystem. These systems follow on the concept of a “theranostic” device, in which both diagnostic and therapeutic functions can be administered in a single dose¹².

2. Synthesis and surface properties of the mesoporous silica nanoparticles

2.1. General synthetic approaches

According to the International Union of Pure and Applied Chemistry (IUPAC), a mesoporous material is defined as a porous material with pore diameters between 2 and 50 nm.

There are three main synthetic routes to the synthesis of mesoporous silica nanoparticles. The first one, the so-called “modified Stöber method”, involves the condensation of silicon source (TEOS, TMOS, etc.) in a basic medium in the presence of a cationic structure directing agent¹³, which yields monodisperse spherical particles with sizes in the 50-200 nm range, containing pores of about 2 nm in diameter. More useful in plant-scale is the use of the spray-drying process¹⁴. This method involves spraying a homogenized precursor solution containing the inorganic compounds and relevant additives within a specially designed chamber at above the boiling point of the solvent. The particle size is determined mainly by the droplet size sprayed into a chamber, however diameters below 250 nm are difficult to achieve and the particle size distribution is poor¹⁵. Another method for the production of nanoparticles is microemulsion process. This approach has been used for synthesis of metallic nanoparticles¹⁶ as well as magnetic and superconductor nanoparticles¹⁷. Microemulsions are produced spontaneously without the need for mechanical agitation, making it a rather simple technique. The technique is useful for large-scale production and uses relatively simple and inexpensive equipment that result in high yields with homogenous particle size distribution¹⁸.

Two main approaches have been used to avoid secondary aggregation during the synthesis: a) carrying out the synthesis in highly diluted solutions and b) the use of particle growth quenchers. Performing the synthesis under dilute conditions gives reproducible results for producing monodisperse particles in the laboratory scale, but up-scaling of the synthesis may become difficult. In this case, the use of particle growth quenchers, like non-ionic surfactants or polymers^{19,20}, fluorocarbon-based cationic surfactants²¹, triethanolamine²², propanetriol²³ etc. is an alternative.

The last step of all synthetic approaches is the surfactant removal and it leads to two-dimensional hexagonal organization of cylindrical mesopores typical of MCM-41-type materials¹. Elimination of the structure directing agent is normally carried out by solvent extraction, as calcination can lead to inter-particle condensation. Thermal decomposition can also lead to decomposition of organic moieties incorporated during the co-condensation reactions, which normally is undesired. Dialysis has also been shown to be an attractive method for surfactant removal in the case of very small nanoparticles (<20 nm), which

otherwise tend to aggregate irreversibly during repeated centrifugation and re-dispersion cycles²⁴.

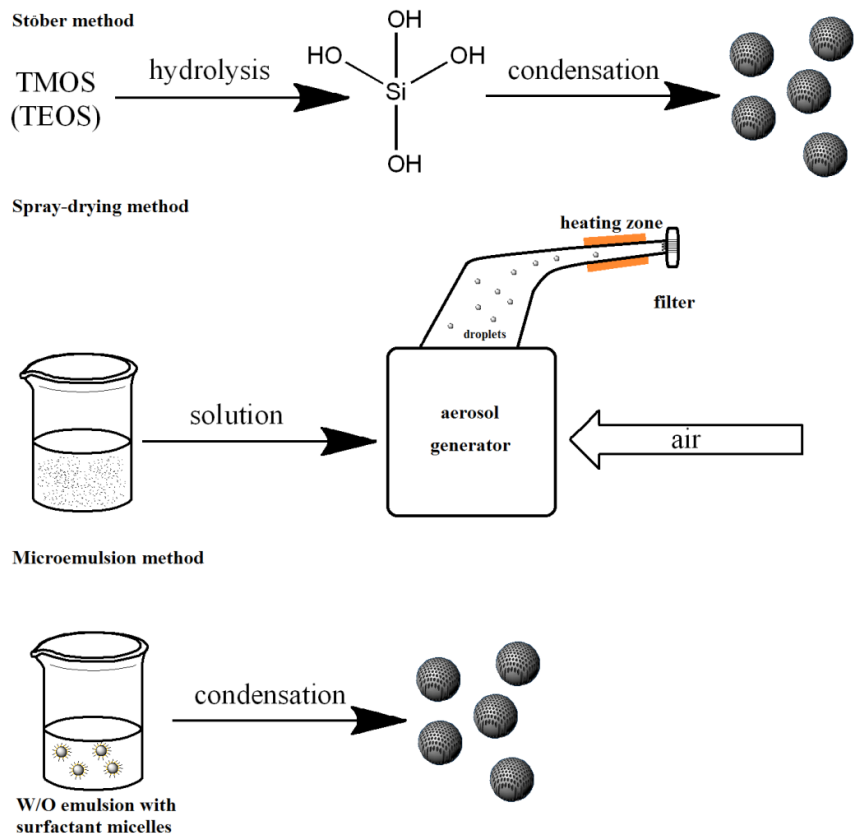


Figure 1. General synthetic approaches to the synthesis of mesoporous silica nanoparticles.

2.2. Surface properties and characterization

Nanoparticles are often defined as materials with two or three dimensions between 1 and 100 nm and showing specific properties related to their size, shape and chemical composition. Indeed, it is generally assumed that the size of nanoparticles allows them to easily enter and pass through tissues, cells and organelles as this size is comparable to that of many biological molecules and structures.

Native mesoporous silica nanoparticles typically have a high surface concentration of silanol groups (approximately 5 per nm², measured using the proton-deuterium exchange method²⁵), especially when not calcined, and the process of the particles drying can easily lead to formation of siloxane bridges between the particles. Surface silanol groups show different acidic properties, for example SBA-15 silica analyzed by Rosenholm *et al.*²⁶ is characterized by two different pK_a values. One pK_a of 8.2 describes the Si-(OH)₂ groups that represent over 80% of all silanol moieties covering the silica nanoparticles surface. The other 18% of Si-(OH) groups are characterized by pK_a near 2.0. These two pK_a values result in silica's negative charge in most biological systems (≈ 7.4 in physiological pH and lower than 7.0 under most pathological conditions)²⁷.

The surface functional organic groups, which can be attached to the surface through the post-synthetic grafting process or by using the co-condensation method, are employed to fulfill specific tasks in medical applications²⁸: a) to increase the host-guest affinity when drugs are adsorbed in the mesoporous channels to enhance drug adsorption and/or slow down drug release rates, b) to chemically graft functional molecules inside or outside the pores, c) to control the surface electrical charge of particles, d) to link nanogates at the mesopore entrances to prevent premature release of entrapped cargo.

Characterization of unloaded mesoporous silica usually means specification of its chemical composition and pore network structure. Spectroscopic methods, such as nuclear magnetic resonance spectroscopy, Raman spectroscopy and Fourier transformation infrared spectroscopy have been widely used to characterize the chemical groups on the surfaces of these materials. High surface area and the high number of attached species make its characterization relatively easy although heterogeneity of the surface can complicate interpretation of results.

The pore structure is often characterized by electron microscopy imaging (transmission electron microscopy (TEM) or SEM) or nitrogen sorption measurements. Imaging methods provide valuable information about the morphology of the pores, unobtainable by other methods. Nitrogen sorption measurements give statistically strong results for pore sizes and can also characterize the pore volume and surface area of the materials. It also informs about pore blocking effects when reduction in pore diameter and pore volume is observed. Mesoporous structures can also be characterized by a few other methods such as mercury intrusion porosimetry, thermoporometry and NMR cryoporometry²⁹.

X-ray diffraction (XRD) is frequently used for characterization of ordered mesoporous silica materials. Although the pore walls consist of amorphous

silica, the pore order gives rise to a diffraction pattern following the Babinet's principle. XRD provides information about the regularity of the structure and the mean distance between adjacent pore centers. This repeat distance along with the pore diameter can be used to determine the pore wall thickness.

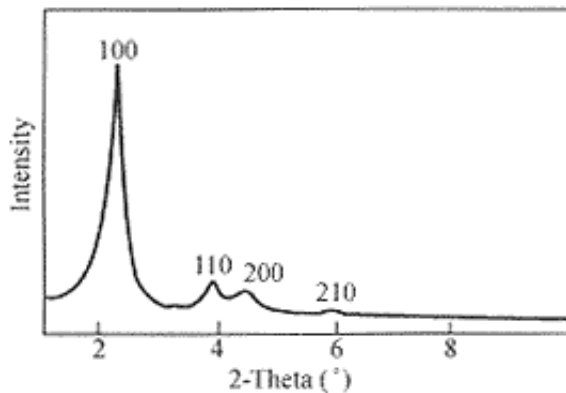


Figure 2. Typical XRD pattern of MCM-41 mesoporous silica.

Particle size and morphology can also play a role in drug delivery applications. Particle size is typically characterized by different techniques, e.g. imaging, sieving, dynamic light scattering and laser diffraction²⁹. Particle morphology characterization relies mostly on imaging by optical or electron microscopy methods.

The characterization of drug loaded carriers is connected with drug-carrier interactions, the amount and physical characteristics of the loaded drug. Drug-carrier interactions can be determined with FTIR or by determining the adsorption isotherms of the model adsorbate (drug), which can provide important information about the possible sorption mechanism - chemisorption or physisorption.

Measuring the drug loading degree of the carrier includes extraction and thermogravimetry (TG) as the most commonly applied methods. In extraction, drug is released from the carrier and the drug concentration in the medium to which it has been released is measured by UV/VIS spectroscopy or other techniques. High performance liquid chromatography (HPLC) is frequently used for drug concentration assay since it is also able to provide information about the possible degradation of the cargo molecules. While using the extraction method, care should be taken that all of the cargo material has been extracted from the

silica; quite often the release is incomplete. In TG, the weight of the sample is measured as a function of temperature. The mass of the loaded drug can be calculated because the thermal decomposition of the organic drug takes place at lower temperatures than the degradation of the carrier²⁹.

Knowledge of the state of the drug in the mesoporous carrier is of the utmost importance. A poorly soluble drug located on the external surface of the carrier particle can inhibit or block the release of the drug from the pores by forming crystallites larger than the molecules inside the pores. This is usually characterized by XRD and differential scanning calorimeter (DSC). Both methods can be used to detect crystalline phases and size of the crystallites in the loaded materials. An advantage of DSC in this context is that it is more sensitive to detection of material of small crystallite size. In addition, pycnometry, nitrogen sorption and NMR can be used to obtain information about the loaded drugs²⁹.

3. Biocompatibility and toxicology issues

The term “biocompatible” means that the nanoparticles must display limited toxicity to the organism at their effective dose, they must be able to accomplish their function without interference from the organism’s defense mechanisms, and they must be able to circulate sufficiently long to perform their intended task – they should not be eliminated or undergo hydrolysis under biological conditions and the targeting or imaging groups attached to their surface, as well as the drug inside the pores, have to remain associated with the nanoparticles until it reaches its target site in order for the targeting/delivery to be efficient. A key requirement for intravenously administered nanotherapeutics is that they are able to circulate in the bloodstream for >2 hours; if they are filtered out by the liver or the kidneys they cannot make it to the intended site of action³⁰. Shape, size and charge are all factors in determining how long a given nanoparticle will circulate before being absorbed by the cells and, after performing its task, eliminated by the liver, kidneys or spleen. The cellular uptake and distribution of the mesoporous silica nanoparticles can be studied by attaching fluorescent dye molecules (e.g. fluorescein isothiocyanate and Rhodamine B) to them, to permit visualization of the particles by fluorescence and confocal microscopy³¹.

3.1. Factors influencing the cytotoxicity of mesoporous silica nanoparticles

Several articles have reported the influence of size dependent cellular uptake and toxicity, but the results have not proved whether larger or smaller particles are more toxic. For human monocyte-derived dendritic cells, the so-called size effect holds which means that larger micron sized silica particles (2.5 μm) are

more toxic than smaller submicron (270 nm) sized ones. Moreover, for particles of either size the toxicity increased with increasing concentration³². Size effect can also be observed when human endothelial cells are used with amorphous silica particles. Silica particles below 20 nm were much more toxic than those of 104 and 335 nm in size. These larger particles showed very little toxic effects³³. The use of particles from the submicron range below 500 nm is recommended as they are easily taken up by the cell through endocytosis and can be seen localised in the lysosomes of the cell³⁴. In another study, Mou and co-workers synthesized ordered monodispersed mesoporous silica nanoparticles of uniform sizes in the range from 30 to 280 nm (most of which had hexagonally ordered structures, except for the 30-nm sized particles, which had predominantly worm-like mesostructures), and they then investigated their uptake by HeLa cells. While the cell proliferation and viability were found to be unchanged at a dosage of 100 µg/mL for all the silica particles despite their differences in size, their cellular uptakes varied with sizes in the order of 50 > 30 > 110 > 170 nm³⁵. These results clearly indicate that endocytosis of silica particles is virtually a complicated process, determined by many more factors than just the particle size of the mesoporous silicas. Also their *in vivo* biodistribution is influenced by the surface charge and size. To date, only a few authors have addressed the influence of these parameters on *in vivo* behavior of these potential drug carriers. Mesoporous nanoparticles in the size range of 50–100 nm possessing a relative positive charge have been shown to mainly be targeted to the liver after intravenous injections³⁶ while 50–200 nm non-porous silica particles were shown to be cleared to urine and bile over time, in a size dependent manner³⁷. Smaller particles were preferably cleared by the urine and bile, whereas larger particles were trapped by macrophages and accumulated in the liver and spleen where they remained up to 4 weeks after injection. 130–180 nm mesoporous silicon particles were shown to be cleared from the body within 4 weeks after intravenous injections³⁸. It was contributed to disintegration of the particles followed by renal clearance.

Particle cytotoxicity is also influenced by the surface charge. Cationically modified silica nanoparticles exhibit lower cytotoxicity in cellular assays than non-functionalized ones³⁹. In the case of mesoporous silica nanoparticles, no significant cell death was observed to have been caused by amino-functionalized particles, indicating that positively charged amines reduce the toxicity of mesoporous silica in *in vitro* conditions. As-synthesized particles with negative surface charge in physiological conditions, influenced the cell growth with a recovery of cell viability over time, while exposure to amino-functionalized particles was not shown to induce a noticeable cell death until longer incubation

when a high dosage of $200 \mu\text{g}\cdot\text{mL}^{-1}$ was applied. Also Pasqua *et al.*⁴⁰ have found that unmodified mesoporous silica was more cytotoxic than thiol- or amino-functionalized silica.

Nanoparticles of different morphologies interacted differently with cell membranes that are the first physical barriers that need to be penetrated by silica particles. This hypothesis was tested and confirmed in several experimental papers. Huang *et al.*⁴¹ showed different cellular uptakes and subsequent cellular responses to mesoporous silica nanoparticles with three different aspect ratios. The particles of the aspect ratios 1:1, 2:1, and 4:1, with dimensions ranging from $100 \times 100 \text{ nm}$ to $100 \times 450 \text{ nm}$ and of surface areas ranging from 791 to $1169 \text{ m}^2\cdot\text{g}^{-1}$ were all efficiently ingested by A375 human melanoma cells via encapsulation within endosomes, while the particles with higher aspect ratios entered the cells faster than those with lower aspect ratios. Moreover, the particles with higher aspect ratios destroyed the cytoskeleton of the cells and induced more cytotoxicity in a dose-dependent manner. The mesoporous silica-treated cells also expressed less melanoma adhesion proteins comparing to the untreated cells. The particles with higher aspect ratios resulted in much less protein expression, although they did not influence the levels of mRNA concentrations, suggesting that some damage to protein translation or post-translational modification was dependent on the shapes of the mesoporous silica nanoparticles. General conclusions about the effect of shapes of silica particles on cells cannot be easily drawn and require consideration of several other parameters including cell type and material composition.

3.2. Factors influencing the biodistribution and the hemolytic activity

As yet no detailed analyses of biodistribution of differently charged mesoporous silica nanoparticles have been made. Generally, negatively charged surfaces should be less bioreactive avoiding cellular interactions that can give rise to unspecific toxicity. Positively charged particles are expected to be more prone to interact with the reticuloendothelial system (RES) and induce an immune response. High absolute charge, either positive or negative, is prone to disable the so-called “stealth” properties of any particle⁴², by increasing the protein adsorption (opsonization) on the particles, a property known to be induced also by hydrophobicity. Critical evaluation of how electrostatic charge of mesoporous silica nanoparticles affects biodistribution is needed to avoid accumulation in healthy organs, disruption of biological membranes and undesired activation of immune response.

Protein adsorption to the mesoporous silica nanoparticles under physiological conditions is an important problem that must be avoided because it would

decrease the targetability of the particles, as well as increase the recognition of the particles as foreign by the body defense mechanisms, which would lead to their rapid removal from the blood circulation. In addition, protein adsorption onto the silica's surface may also influence its toxicity. The PEGylation (PEG-functionalization) of nanoparticles has been frequently used as a general and effective approach to reduce the nonspecific binding of nanoparticles to blood proteins and macrophages. This reduction is caused by the steric hindrance and repulsion effects of PEG chains against blood proteins and macrophages, which are closely correlated to the PEG molecular weight, surface chain density and conformation²⁸.

The effect of mesoporous silica materials on hemolytic activity is important in order to understand how the materials will interact with blood. Lin and Haynes have found significant effects of silica particles size, porosity and dosage on the hemolytic activity. They reported that mesoporous silica nanoparticles with ordered structures show lower activity compared with the solid nonporous particles of similar size because of the smaller amount of silanol groups on the external surface. The addition of poly-ethylene glycol (PEG) coatings can help to overcome the hemolysis⁴³. Hemolytic assays have recently been made with hollow mesoporous silica. Again, at low dosages (up to $1600\mu\text{g}\cdot\text{ml}^{-1}$) these hollow mesoporous silica showed no effect on the activity of the red blood cells⁴⁴. He *et al.* obtained similar results, that is they reported a significant influence of PEGylated particles on the nonspecific serum binding and proved that these particles showed significantly reduced hemolysis rate compared to non PEGylated particles⁴⁵. Tang *et al.* tested the *in vivo* effect of differently shaped and PEGylated MSNs on blood, hematology and serum biochemical indicators in 1 day and 18 days after the intravenous administration of MSNs⁴⁶. All hematology markers, such as RBC, HGB, HCT, MCV, MCH, MCHC, PLT and WBC, took values mostly within the normal ranges and did not show significant trends of toxicity of all tested samples, indicating the excellent biocompatibility in hematology.

Due to the leaky vasculature and poorly operational lymph system of tumors, nanoparticles can exit the blood vessels and accumulate at the tumor site by passive targeting *via* the enhanced permeability and retention (EPR) effect. The diffusion rate in the extracellular spaces of the tumor is determined by the size and the surface charge of the particles. Small particles easily diffuse out and in of the tumor vasculature and within the tumor interstitium and the active concentration of the drug carrier at the tumor site might be low. Free movement is also affected by surface charge and negatively charged or weakly positively charged particles in the 50–150 nm range easily pass through the tumor tissue⁴⁷.

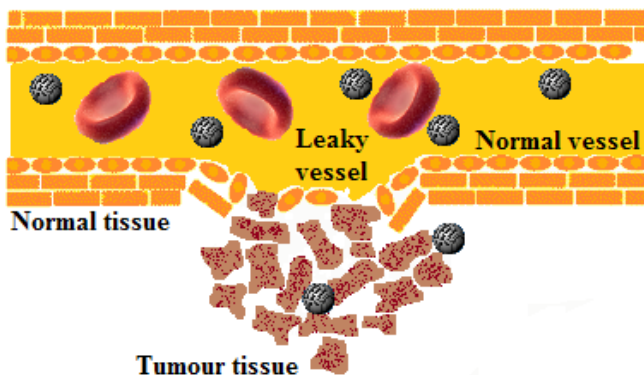


Figure 3. Scheme presenting enhanced permeability and retention effect in tumour tissues.

3.3. Elimination of mesoporous silica nanoparticles and their degradation in biological environment

Once the mesoporous silica nanoparticles have reached their target, it is important to know the kinetics of the particles removal from the cells. It is clear that the extracellular dissolution kinetics is different, probably much faster, than that of the intracellular one due to the limited liquid volume inside the cell, but this topic remains the focus of future studies⁴⁸.

Although only a few authors have studied the phenomenon of exocytosis of nanoparticles, there have been some reports on exocytosis of mesoporous silica nanoparticles in different cell lines. Slowing *et al.*⁴⁹ have studied the exocytosis of particles by normal (HUVEC) and cancerous (HeLa) cells and reported two interesting findings. The first is that, the particles were found to be ingested by the cells and reached a constant intracellular amount within 2 h, indicating the attainment of a balance between the rates of endocytosis and exocytosis of the particles (or equilibrium) in 2 h of incubation time. The second is that the exocytosis as well as transcytosis of mesoporous silica nanoparticles were found to be much more efficient in healthy HUVEC cells than in malignant HeLa cells.

Etienne and Walcarius⁵⁰ have studied the dissolution of mesoporous silica in water as a function of pH, both for as-synthesized silica and amino-functionalized one, and showed that amino-functionalized silica dissolved at a faster rate than pure silica particles under biologically relevant pH conditions. For the aminosilane functionalized particles as much as 2/3 of the amino-groups were already found in the supernatant 4h into the experiment, after which the concentration of amino species in solution reached a plateau. Thus, not all amino-functions were dissolved in solution, but clearly factors such as particle

surface charge could be expected to have dramatically influenced the process. He *et al.*⁵¹ have reported a three-stage degradation behavior of mesoporous silica nanoparticles in simulated body fluid. Also this study revealed rapid initial bulk degradation, followed by the deposition of calcium/magnesium silicate layer, which drastically reduced (or counteracted) the degradation rate, similarly to the observations of Onida *et al.*⁵². The third stage involved a maintained slow diffusion of dissolved silica species detected as free Si, whereas the whole sample was degraded after 15 days when immersed in an aqueous solution at a concentration of 0.5 mg*ml⁻¹. Importantly, the particle morphology remained intact after 24h even though hollowing out and enlargement of the mesopores was clearly observed.

Suspended silica is known to be adsorbed or excreted by the body. Several reports have supported elimination of MSNs through renal excretion. Mamaeva *et al.* have shown quite rapid renal clearance of particles (250–350 nm) injected both intravenously and peritumorally with a peak at 42–72 h depending on the functionalization. PEI functionalized particles were more rapidly eliminated than folate tagged particles⁵³. He *et al.* have shown that differently modified amorphous silica nanoparticles (OH-Si, COOH-Si and PEG-Si) with a size of approximately 45 nm were all partly excreted through the urine⁵⁴.

Mesoporous silica nanoparticles have also been reported to be eliminated by hepatobiliary route although that process appeared to be slower and showed a peak at 4 days after intravenous injection⁵⁵. Lo and coworkers have studied the effect of the surface charge on the two proposed elimination routes of mesoporous silica nanoparticles and found that particles (size 50–100 nm) with high positive charge showed rapid hepatobiliary excretion and reached the peak of excretion at 2 days post injection⁵⁶. Although both particles were sequestered by the liver, the one with the higher charge could have been more opsonized by serum proteins and thus more amenable to hepatobiliary excretion into the gastrointestinal tract. In conclusion, this shows that the surface charge regulates the rate of excretion.

4. Application of mesoporous silica nanoparticles in drug delivery systems

4.1. General methods for preparation of drug delivery systems

In general there are two main approaches to incorporate a drug or diagnostic entity in a nanoparticle³⁰: to stick it to the surface of a silica nanoparticle, or to encapsulate it in a porous nanostructure. These approaches can be illustrated by the two methods of carrying goods on ships in the macroscopic world: we either stack the cargo on the deck of a barge or we place it in the closed container of a tanker. As with shipping in a macroscopic world, the solution

chosen to carry a nanocargo depends on the characteristics of the cargo and the delivery requirements. A reactive or antigenic drug should be isolated from the environment in some sort of container vessel until it reaches its “port,” whereas an imaging agent attached to the external surface of a barge-like vessel can be more readily accessed and more rapidly released in response to physiological stimuli.

One concept that does not translate well to the macroscopic shipping analogy, is the carrying capacity. For a macroscopic sphere, many more molecules can be contained in the inner volume than can be adsorbed on the surface. As the sphere gets smaller, the space available to load a drug in the interior volume decreases with the sphere radius to the third power and on the surface with its radius squared. That is why when the diameter of the sphere approaches the molecular dimensions, more molecules can be placed on the surface than can be contained in the inner volume.

Table 1. Comparison of the number of molecules trapped inside of a sphere and adsorbed on its surface at different radii values. The volume occupied by a single molecule assumed to be 2 nm^3 ($1 \text{ nm} \times 1 \text{ nm} \times 2 \text{ nm}$) and the surface - 1 nm^2 ($1 \text{ nm} \times 1 \text{ nm}$)

Sphere radius	Number of molecules trapped inside the sphere (N_i)	Number of molecules adsorbed on the external and internal sphere surface (N_s)	$N_i:N_s$ ratio
1 m	$2.618 \cdot 10^{26}$	$6.284 \cdot 10^{18}$	$4.166 \cdot 10^7$
1 mm	$2.618 \cdot 10^{17}$	$6.284 \cdot 10^{12}$	$4.166 \cdot 10^4$
100 nm	$2.618 \cdot 10^5$	$6.284 \cdot 10^4$	4.166

Nevertheless, nanoparticles of a size equal to 100 nm or more, with an empty interior, the so-called hollow mesoporous silica spheres, are known to store more cargo than conventional mesoporous silicas thanks to their voids inside the shells and mesoporous channels at the shells providing accessibility without blocking (channels in conventional mesoporous silica are much longer and can be easily blocked by molecules occupying pore entrances). Despite lower surface area ($436 \text{ m}^2 \cdot \text{g}^{-1}$) relative to that of MCM-41 ($1152 \text{ m}^2 \cdot \text{g}^{-1}$) hollow mesoporous spheres can deliver as much cargo as conventional mesoporous silicas ($302 \text{ mg} \cdot \text{g}^{-1}$ for hollow mesoporous silica and $358 \text{ mg} \cdot \text{g}^{-1}$ for MCM-41)⁵⁷. When surface areas are comparable, the hollow mesoporous silica’s capacity is even much larger than that of MCM-41 ($1133 \pm 52.4 \text{ mg} \cdot \text{g}^{-1}$ of ibuprofen adsorbed by hollow mesoporous silica and $337 \text{ mg} \cdot \text{g}^{-1}$ by MCM-41)⁵⁸.

Until now, simple surface adsorption has been used much more often

than encapsulation of a cargo in the hollow mesoporous silica spheres. A few procedures for loading a cargo onto the silica's surface have been proposed. In the method of incipient wetness impregnation, a very concentrated drug solution is used to obtain a high loading degree, where the drug concentration is usually close to its solubility limit. Capillary action draws the solution into the pores together with the drug molecules. The interactions between the cargo molecules and the silica particle usually include hydrogen bonding and electrostatic interactions.

The impregnation method is preferred when only small amounts of the drug are available. It is easy to determine the amount of the loaded drug in advance, but a disadvantage of the method is the difficulty to control the uniformity of the drug distribution. Moreover, the residual drug can recrystallize on the external surface of mesoporous materials after repeatable solvent evaporation.

In the melt method, a physical mixture of drug and mesoporous carrier is heated above the melting point of the drug. To some extent, this method can be considered as a special case of the impregnation method. However, many drugs cannot withstand melting without degradation. In addition, the drug molecules loaded from melt are distributed less homogeneously on the pore surfaces if the molten drug has high viscosity. In this case most of the drug molecules pack on the surface close to the pore opening and can undergo recrystallization. Thus, the drug materials loaded from the melt have a bit slower release rate. However, if the molten drug has low viscosity such as ibuprofen, the effect of the drug loading method on the physical state and release profile of the drug is minor²⁹

Controlled release systems based on mesoporous silica nanoparticles are more useful than simple, unmodified silicas loaded with drug molecules. They have been developed by applying mechanical controls over the pore openings. First, polymers that are either adsorbed or covalently bonded to the surface of the silica particles have served as a mechanized controlled release system⁵⁹. Under their "close" condition, the polymer chains tightly wrap around the particle surface, each blocking multiple pore openings. Then the polymers are induced by certain stimuli to undergo swelling or coiling so that the pore openings are re-exposed and cargo is released through the unblocked pores. The second method to achieve controllable release is to form chemical bonds directly over the pore openings so that they can later be cleaved upon stimulation⁶⁰. The third way to mechanically block the pores is to attach bulky groups such as Au or CdS nanocrystals over the pore openings⁶¹. These bulky groups serve as gatekeepers for the encapsulated cargo. Removal of the bulky blocking groups *via* chemical methods initiates cargo release.

Targeting is especially relevant in the context of cancer therapies, as most of

the commonly used anticancer drugs have serious side-effects due to unspecific action on healthy cells. The selectivity is a key ability of the nanoparticles to be internalized by the targeted cell population. Active targeting requires the knowledge of which receptors are overexpressed on the outer cell membrane for a given cancer type. Different moieties, such as peptides, antibodies or more simple molecules, such as folic acid can be attached to the silica surface and used as targeting agents. The folate receptor has been found to be overexpressed on the surface of several cancer cell types, such as ovarian, endometrial, colorectal, breast, lung, renal cell carcinoma, brain metastases derived from epithelial cancer, and neuroendocrine carcinoma^{62,63}.

4.2. Factors influencing the adsorption and release of cargo molecules

There are many physicochemical parameters affecting adsorption and release of cargo from mesoporous silicas: pore size, particle size and morphology, pore structure, pore volume, surface area, surface functionalization, pH at which the adsorption is carried out, molecule's polarity and surface polarity⁶⁴.

The maximum loading degree, i.e., the ratio of the drug mass to the total mass of the drug loaded carrier when the pores are totally filled, can be estimated on the basis of the pore volume of mesoporous carriers and the packing density of the payload drug. However, the ultimate density of the drug is difficult to estimate as it usually differs from the density of the crystalline drug. Loading degrees as high as 60 wt.% can be obtained for the carriers with very high porosity. As the inorganic mesoporous carriers are denser than the organic drugs, the loading degrees higher than 60 wt.% is difficult to obtain. The loading method also affects the loading degree obtained, the packing of the molecules in the pores as well as their distribution in the carrier. This naturally affects the release kinetics; the more disordered the structure, the faster the release is taking place²⁹.

The drug molecules physically adsorbed on the surfaces of mesoporous materials from organic solvents form multilayers or (typically) monolayers can be modeled using a Langmuir adsorption isotherm⁶⁵. Monolayer adsorption onto the pore walls has also been observed for proteins from aqueous solutions⁶⁶. In the case of a monolayer, the loading capacity increases with increasing the surface area⁶⁵. Thus, the pore volume of the materials has no effect on the drug loading.²⁹ For more hydrophilic drugs, the pH-matching in aqueous solvent can be used to reach higher drug loading levels than possible from organic media⁶⁷. Many studies have highlighted the possibility of using these kinds of specific interactions between the drug and functional groups present on the pore wall also for controlling the drug release process. In most cases, the vast majority of

the groups present on the silica surface even functionalized mesoporous particles are still silanol groups, while the influence of the silanol groups on the overall surface chemistry of the pore surface should not be underestimated⁶⁷.

The pore size is crucial for drug loading because the mesopores act as molecular sieves and in this way they can determine the size of molecules that can be loaded into the carrier materials. Generally, the ratio of pore diameter/drug molecule size should be >1 so that the pores will be accessible for drug molecules. Furthermore, the ratio should be greater than 3 if the full use of surface area and high drug loading is desired. Horcajada *et al.*⁶⁸ have prepared mesoporous MCM-41 with different pore sizes by using surfactant molecules with different lengths of alkyl chain and subsequently studied the effect of pore size on drug loading. After immersing mesoporous MCM-41 in a hexane solution with ibuprofen (molecule size $1.0 \text{ nm} \times 0.5 \text{ nm}$), more ibuprofen molecules were loaded into the carrier with the pore size of 3.6 nm (loading degree of 19 wt.%) than in that with the pore size of 2.5 nm (11 wt.%).

Pore size affects also the possibility of drug crystallization, which influences the drug solubility. In the classical theory of homogenous nucleation, crystal growth proceeds spontaneously once a critical nucleation size is reached⁶⁹. If, however, the spatial constraints of a capillary are imposed on the clusters of molecules before they reach the critical size, nucleation and growth will be prevented and the system will exist in an intrinsically noncrystalline state. Mesoporous materials have pores with diameters lower than the critical nucleation size of many popular drugs, so they have been used to increase their solubility. Solubility improvement was observed for a wide range of compounds such as carbamazepine⁷⁰, danazol⁷⁰, cinnarizine⁷⁰, diazepam⁷⁰, indomethacin^{70,71}, griseofulvin⁷⁰, ketoconazole⁷⁰, phenylbutazone⁷⁰, nifedipine⁷⁰, fenofibrate^{70,72}, telmisartan⁷³, glibenclimide⁷⁴ and carvedilol⁷⁵. Wang *et al.* have encapsulated poorly water soluble drug, telmisartan, into mesoporous silica nanoparticles and mesoporous silica microparticles to test the oral drug delivery potentials of mesoporous particles in beagle dogs⁷⁶. After the administration of drugs by gavage, the mean plasma drug concentrations were determined by HPLC. After the pharmacokinetic calculations, they found that the relative bioavailabilities of telmisartan-loaded nano- and microparticles were $154.4 \pm 28.4\%$ and $129.1 \pm 15.6\%$, respectively, of commercial product Micardis. This research demonstrated the significant potential of using mesoporous particles to promote drug dissolution and drug permeability, thus to enhance the oral bioavailability of drugs.

The loading and release efficiencies of the particles are also affected by the electrostatic interactions between the cargo molecules and the silica surface^{77,78}. Various studies using silica materials as adsorbents have shown that the maximum

adsorption of protein occurs at or near the isoelectric (pI) point of the protein. For example, myoglobin, cytochrome c (cyt c) and bovine serum albumin (BSA) have been shown to have a higher adsorption capacity onto the materials at a pH equal or less than the pI point of the protein⁶⁶.

For adsorption to take place in the solution state, the chemical potential of the drug in the solution must be the same as the chemical potential of drug adsorbed on the surface of silica at equilibrium. The same is true for the solvent molecules as well. Depending on the collective properties of the silica surface, solvent, and drug compound, a competitive interaction with the silica surface between solvent and drug molecules can be expected. Charnay *et al.*⁷⁹ and Fernandez-Nunez *et al.*⁸⁰ have studied the effect of solvent polarity on the capacity of ibuprofen inclusion in MCM-41 and SBA-15 silicas. The amount of ibuprofen adsorbed showed an inverse trend with the polarity of the solvent. The less polar solvent the greater amount of ibuprofen adsorbed on both MCM-41 and SBA-15.

Dissolution rate depends on the volume of dissolution media, hydrodynamic conditions, and amount of drug present, among other factors. The volumes of the dissolution media used by various investigators reporting controlled release were between 10 and 100mL^{52,81,82}. Because hydrodynamic conditions were not clearly specified, local supersaturation may have resulted in precipitation, followed by slow dissolution of precipitated drug into the bulk medium. Sustained release might be an outcome of slow dissolution from the crystallized drug. On the other hand, if the pore diameter of SiO₂ is similar to the dimensions of drug molecules, the diffusion of the molecules out of pores during dissolution can be kinetically hindered due to collisions between the drug and water molecules or the drug molecules and the pore wall. On the basis of this explanation, microporous SiO₂ with 0.4-nm mean pore diameter has been synthesized to develop controlled release formulations of ibuprofen⁸³ and chlorhexidine⁸⁴. In addition, if the lengths of the pores are sufficiently long, the formulation may provide sustained release because of the diffusion path length.

4.3. Examples of drug delivery systems triggered by different stimuli

Generally, the release of poorly soluble drugs can be fitted with Higuchi or Korsmeyer–Peppas model:

$$Q = K_H * \sqrt{t} \quad (1)$$

$$F = \left(\frac{M_t}{M} \right) = K_m t^n \quad (2)$$

In the Higuchi equation (1), Q is the cumulative amount of drug released at time t and K_H is the Higuchi constant. In the Korsmeyer-Peppas equation (2), F is the fraction of drug released at time t , M_t is the amount of drug released at time t , M is the total amount of the loaded drug in mesoporous carriers, K_m is the kinetic constant and n is the release constant. If n equals to $1/2$ in the Korsmeyer-Peppas equation, both of the models describe diffusion controlled release.

The Higuchi equation is used to describe the release of cargo molecules from an insoluble carrier. Fitting with Higuchi equation suggests that the drug release is limited by diffusion process. Unlike bioactive polymer-based drug carriers, the mesoporous materials are mostly prepared with inorganic compounds that are insoluble in aqueous solutions under biological condition, so the Higuchi equation could also be applied to the mesoporous silica materials to explain the drug release kinetics. The Korsmeyer–Peppas equation is a more comprehensive way to describe the drug release kinetics from the mesoporous carriers, which is indicated by the parameter n in Eq. (2)²⁹.

Table 2. Examples of biologically active compounds that have already been released from unmodified or modified mesoporous silicas^{85,29}

MCM-41
ibuprofen, vancomycin, gentamycin, acetylsalicylic acid, sodium alendronate, camptothecin, atenolol, cytochrome C, bovine serum albumin, paclitaxel, vitamin-B ₂ , calcein, safranin O, cAMP, carvedilol, fenofibrate, indomethacin, telmisartan
FSM
taxol, flurbiprofen
SBA-15
gentamycin, amoxicillin, erythromycin, sodium alendronate, L-tryptophan, bovine serum albumin, nimodipine, ezetimibe, fenofibrate, glibenclamide, indomethacin, itraconazole, telmisartan, griseofulvin
MCM-48
erythromycin
hollow mesoporous nanoparticles
fluorescein, propidium iodide
other
atazanavir

4.3.1. Release from the unmodified particles

The effect of incorporation of three poorly soluble drugs from BSC class II (ibuprofen and griseofulvin) and class IV (furosemide) into mesoporous silicon microparticles⁸⁶ on their solubility and release was studied. After loading the cargo, the dissolution of these model drugs was clearly improved and the pH dependence of the dissolution was reduced. The drugs loaded into the unmodified mesoporous silicas show very fast initial drug release profiles; i.e., 50% of the loaded itraconazole was dissolved within 3 min and more than 80% of the drug was dissolved after 5 min compared to only 14% solution of pure itraconazole.

Ibuprofen is probably the most extensively studied hydrophobic drug in the applications involving adsorption in matrices of mesoporous silicas^{65,77,87}. The loading capacity and the release rate of ibuprofen from these materials have been proved to be affected by the surface area, pore diameter and surface functionalization⁸⁸⁻⁹⁰.

The *in vitro* applications of unmodified mesoporous silicas to deliver hydrophobic anti-cancer drugs, namely camptothecin and paclitaxel, to human cancer cells have been studied^{91,92}. A suspension of camptothecin loaded particles in phosphate buffer saline (PBS) was added to a human pancreatic cancer cell culture PANC-1. The uptake of the mesoporous silica was confirmed by the fluorescence from the fluorescein isothiocyanate (FITC) labeled particles within the cells. The cytotoxic efficacy of the camptothecin-loaded silica is similar to that of the DMSO dissolved camptothecin, and much higher than the cytotoxicity of the PBS suspension of camptothecin.

Balkus *et al.* have reported lysozyme immobilisation within MCM-41 matrices. This study highlighted the importance of silica pore size to encapsulate the enzyme. But, MCM-41 could not encapsulate a biomolecule with a size greater than 40 kDa⁹³. On the other hand, SBA-15 with larger pore sizes (5–30 nm) could encapsulate various larger proteins. Unfortunately, the amount of larger protein such as bovine serum albumin⁹⁴ adsorbed in SBA-15 materials (pore sizes 6.8 nm) was small.

Sun *et al.* have been able to perform highly accelerated lysozymes adsorption by enlarging the conventional SBA-15 pore. They synthesized a material with ordered large mesopores with a pore size of 13 nm. Adsorption of enzymes reached equilibrium after 10 min as compared to hours needed to reach equilibrium in the conventional SBA-15. They could confirm that most of the lysozymes were within the pores.

4.3.2. Release from modified particles

Fujiwara and co-workers have introduced light-responsive mesoporous silica

systems from which the release of the cargo could be controlled through the photo-controlled and reversible intermolecular dimerization of coumarin derivatives attached to the pore outlets⁹⁵. The same group has developed a controlled storage and release system by attaching azobenzene groups to the mesopore outlets. The release was promoted by simultaneous irradiation with UV and visible light, which made the azobenzene molecules act as both impellers and gatekeepers. Other light-operated systems, developed by Zink and co-workers⁹⁶, uses differences in binding affinity between β -CD and both isomers (*cis*- and *trans*-) of azobenzene. Irradiation with 351 nm light causes the isomerisation of azobenzene to the *cis* conformation and therefore pore uncapping. Another example of light-sensitive systems includes Au nanoparticles anchored to the surface through thioundecyl-tetraethyleneglycoester-nitrobenzylethyltrimethylammonium bromide (TUNA). Upon UV irradiation TUNA would lead to the negatively charged thioundecyltetraethyleneglycolcarboxylate (TUEC), leading to the dissociation of the Au NPs from the surface due to charge repulsion⁹⁷. Lin and co-workers have loaded the mesopores of mercaptopropyl-functionalized silica with sulforhodamine 101 and the cargo molecules were entrapped by the presence of Ru(bpy)₂(PPh₃)-moieties, coordinated to mercaptopropyl functional groups⁹⁸. Upon irradiation with visible light, Ru-S coordination bond was cleaved, triggering the release of capping species and loaded molecules.

The pH-sensitive supramolecular nanovalves with the N-methylbenzimidazole stalks have the ability to bind β -CD strongly at pH 7.4⁹⁹, trapping dye or drug molecules inside the mesopores of silica. Upon entering an endosomal compartment at pH < 6, N-methylbenzimidazole becomes protonated and β -CD cap dissociates, allowing the cargo molecules to be released from the silica. Meng and co-workers¹⁰⁰ have loaded mesoporous silica with either Hoechst 33342 to cause nuclear staining in human differentiated myeloid cells (THP-1) or anticancer drug doxorubicin to induce cell apoptosis in squamous carcinoma (KB-31) cells. Cyclodextrin and polyethyleneimine complexes have been used by Kim and co-workers to achieve a pH-dependent cargo release. Calcein molecules were first loaded into pores and then cyclodextrin/polyethyleneimine inclusion complexes were attached onto the surface of mesoporous silica nanoparticles. Due to the size of these compounds the cargo is protected until polypseudorotaxane is split. In acidic conditions, the cyclodextrin complex can be broken and hence the cargo can be released.

Magnetic field can also be used as external stimulus to trigger the release of molecules – it can guide the drug delivery systems to the desired location, hold them until the therapy is complete, and then remove them. Chen *et al.*¹⁰¹ have recently reported the capping of mesoporous silica with Fe₃O₄ magnetic nanoparticles. To

achieve this, silica was first functionalized with 3-aminopropyltrimethoxysilane and then loaded with camptothecin. The mesopore entrances were covalently capped through amidation of the 3-aminopropyltrimethoxysilane bound at the pore surface with *meso*-2,3-dimercaptosuccinic acid functionalized superparamagnetic iron oxide nanoparticles with an average diameter of 5.6 nm. When a magnetic trigger was applied, the Fe₃O₄ caps were removed due to the cleavage of chemical bonds and this subsequently led to a fast-responsive drug release. Also some rattle-type particles with large hollow interior spaces, functional cores and mesoporous silica shells have been prepared. Shi and co-workers¹⁰² have prepared a series of rattle-type Fe₃O₄/Fe₂O₃@mSiO₂ hollow ellipsoids/spheres with a single or double mesoporous silica shell and loaded them with doxycycline (DOX). The excellent blood compatibility and the greater cytotoxicity of doxycycline loaded nanospheres than free doxycycline to induce MCF-7 cell death indicate that the Fe₃O₄@mSiO₂ nanocapsules are excellent anticancer drug carriers for diagnosis and chemotherapy applications.

It is known that the local temperature in many tumours is slightly higher than normal body temperature. This is why a temperature-sensitive delivery system able to release its cargo only at temperatures higher than 37°C, but preserving the drugs entrapped while in blood, is required. Thermo-sensitive polymers, such as poly(N-isopropylacrylamide) (PNIPAM) and its derivatives have been used in the design of thermo-responsive release systems, reported in the recent years^{103,104}. PNIPAM changes its conformation responding to temperature in aqueous environments. Its chains are hydrated below the lower critical solution temperature (LCST) of 32°C and occupy more space near the pore entrances and this is what prevents the departure of the cargo loaded inside the mesopore channels. Increasing the temperature above the LCST dehydrates the polymer chains, collapses PNIPAM's conformation and opens the pores resulting in a release of the cargo. Increasing the LCST under physiological conditions would be desirable for biomedical applications and this can be achieved by modifying the polymer composition by copolymerization with other monomers (such as acrylamide¹⁰⁵ or N-isopropylmethacrylamide¹⁰⁶). Baeza *et al.* created a novel nanodevice based on mesoporous silica with iron oxide nanoparticles inside the matrix and decorated on the outer surface with a thermo-responsive copolymer of poly(ethylenimine)-β-poly(N-isopropylacrylamide) that was able to deliver small molecules or proteins in response to an alternating magnetic field or temperature¹⁰⁷. Other thermo-responsive systems that have been already prepared involve double-stranded DNA sequences attached to the pore openings of mesoporous silica melting at certain temperatures¹⁰⁸ or octadecyl chains interacting with a hydrophobic layer made of paraffin that melts at certain

temperature, specific for different paraffins¹⁰⁹.

Another stimulus that can be used in controlled delivery systems is the redox potential. Different redox potential-responsive systems have been developed until now. They use various gatekeepers, such as CdS¹¹⁰, Au¹¹¹ or Fe₃O₄¹¹² nanoparticles or organic molecules such as cross-linked poly(N-acryloxysuccinimide)¹¹³, collagen¹¹⁴ or cyclodextrin¹¹⁵, covalently attached to the silica through disulphide links. These caps can be removed by cleaving such links using disulphide-reducing agents, such as mercaptoethanol or dithiothreitol. Redox potential is an important stimulus as in most tumor cells the level of intracellular glutathione, a natural reducer, is 100-1000-fold higher than in the extracellular space.

Biomolecules are internal stimuli that can be used to trigger cargo release. Enzyme-responsive systems can be represented by cyclodextrin-capped mesoporous silica attached on the silica surface thanks to “click chemistry” reactions. The addition of α -amylase catalyzed the hydrolysis and allowed the release of calcein trapped inside the pores¹¹⁶. Another example of such systems can be the one prepared by Martínez-Máñez and co-workers. They described the capping of mesoporous silica with lactose and the selective uncapping in the presence of enzyme β -D-galactosidase¹¹⁷. The same group developed multi-enzyme-responsive capped mesoporous silica containing amide and urea links to block the pores. The addition of amidase and urease triggered the cargo release. Amidase induced an immediate, but not complete release and urease allowed a near total cargo release that was delayed in time¹¹⁸. Glucose-responsive systems can be used in the treatment of diabetes. Zhao *et al.*¹¹⁹ have reported a double delivery system for both insulin and cyclic adenosine monophosphate (that activates Ca²⁺ channels of pancreas beta cells stimulating insulin secretion) with precise control over the sequence of release. cAMPs gluconic acid-modified insulin proteins were immobilized on the outermost surface of phenylboronic acid-functionalized silica particles *via* reversible covalent bonding. Modified insulin also served as caps to encapsulate cAMP molecules inside the mesoporous channels. Phenylboronic acid forms much more stable cyclic esters with the adjacent diols of saccharides than with acyclic diols. Thus, the presence of saccharides induced the release of modified insulin and cAMP trapped inside the pores. Examples of very interesting biomolecules-responsive systems include antigen-responsive reported by Climent *et al.*¹²⁰, where hapten-modified surface of the mesoporous silica is covered by antibody nanoscopic caps that can recognize a certain hapten releasing the cargo after displacement reaction, or aptamer-target-responsive system containing aptamers (single stranded, short oligonucleotide sequences that can bind specific targets with high affinity and specificity) releasing the cargo upon detection of certain guest molecules (i.e. ATP¹²¹).

4.3.3. Modified mesoporous silica nanosystems against cancer multidrug resistance

Nanoparticle-mediated delivery of a single cancer drug often serves as proof of concept. A clinically relevant alternative approach is to combine therapeutic agents targeting specific survival mechanisms of cancer cells with classical anticancer drugs. One of the problems, with potential to be solved by co-delivery of several compounds, is cancer multidrug resistance (MDR) which is a major cause of therapy failure in cancer patients. Design of a drug delivery system might be tailored to overcome MDR by focusing on the ability for targeted delivery of different cargos to combine circumvention of MDR mechanisms with chemotherapy. We want to underline that the problem of MDR in general is far from being resolved, but the attempts made to overlap it with nanoparticle drug delivery are worth considering¹²².

Although the mechanisms of MDR are multifaceted, they can be roughly classified as pharmacological and cellular. Pharmacological MDR mechanism employs different circumstances resulting in therapeutically insufficient drug dosage, such as inadequate infusion, influence of tumor microenvironment, pharmacokinetics in the plasma and others. Cellular mechanisms, simply classified into pump and non-pump, such as ABC-transporters, apoptosis signaling pathways, and DNA repair pathways may be switched on and off during the development of a drug-resistant phenotype and are potentially “druggable”. Many of these challenges could be overcome by using drug carriers.

For example, a combination of mesoporous silica, an anticancer drug (DOX or cisplatin (CIS)), a suppressor drug resistance (siRNA targeted to MRP1 transporter or BCL2 mRNA), and a tumor targeting moiety (LHRH peptide) has been used and revealed enhanced anticancer activity when compared to that of free drug mixtures¹²³.

A different approach to overcome drug resistance has been investigated by Huang *et al.*¹²⁴, who studied DOX attached to the surface through a pH-sensitive linker, hydrazone bonds, to provide sustained and proportionate release of DOX and its effectiveness against human uterine sarcoma MES-SA/DOX-resistant tumor cell line was tested. Its uptake and activity were higher than those of free doxycycline and doxycycline combined with verapamil (the inhibitor of drug efflux pump protein).

Another modification of pH-responsive silica nanoparticles able to overcome drug resistance has been published by He *et al.*¹²⁵ Their nanoparticles consisted of silica still containing the surfactant, cetyltrimethylammoniumbromide (CTAB), and doxycycline. The surfactant was used as a chemosensitizer for overcoming the multidrug resistance and enhancing the drug efficiency. The cytotoxicity of

these particles was tested on MCF-7 and MCF-7/ADR cell lines and composite mesoporous silica was shown to increase the MCF-7/ADR intracellular accessibility to doxycycline and presented much higher drug efficiencies *in vitro* against both cell lines compared to that of the free drug.

Dual stimuli-responsive systems are those able to respond to two stimuli, either in an independent or in a synergistic fashion. Martínez-Máñez *et al.*¹²⁶ attached suitable polyamines to the silica surface to obtain pH sensitive and anion-controllable gate-like ensembles capable of controlling the release of a ruthenium dye trapped inside the mesoporous matrix. To achieve this goal, they varied the pH value and content of certain anions in the release medium.

Acknowledgements

This work was partially supported from the funds of National Science Centre (grant no. 2011/03/B/ST5/01573).

References

1. Kresge, C. T.; Leonowicz, M. E.; Roth, W. J.; Vartuli, J. C.; Beck, J. S., Ordered mesoporous molecular sieves synthesized by a liquid-crystal template mechanism, *Nature* **1992**, *359*, 710.
2. Bagshaw, S. A.; Prouzet, E.; Pinnavaia, T. J., Templating of Mesoporous Molecular Sieves by Nonionic Polyethylene Oxide Surfactants, *Science* **1995**, *269*, 1242.
3. Ryoo, R.; Kim, J. M.; Ko, C. H.; Shin, C. H., Disordered Molecular Sieve with Branched Mesoporous Channel Network, *The Journal of Physical Chemistry* **1996**, *100*, 17718.
4. Zhao, D.; Feng, J.; Huo, Q.; Melosh, N.; Fredrickson, G. H.; Chmelka, B. F.; Stucky, G. D., Triblock Copolymer Syntheses of Mesoporous Silica with Periodic 50 to 300 Angstrom Pores, *Science* **1998**, *279*, 548.
5. Han, Y.; Ying, J. Y., Generalized Fluorocarbon-Surfactant-Mediated Synthesis of Nanoparticles with Various Mesoporous Structures, *Angewandte Chemie International Edition* **2005**, *44*, 288.
6. Huo, Q.; Margolese, D. I.; Ciesla, U.; Feng, P.; Gier, T. E.; Sieger, P.; Leon, R.; Petroff, P. M.; Schuth, F.; Stucky, G. D., Generalized synthesis of periodic surfactant/inorganic composite materials, *Nature* **1994**, *368*, 317.
7. Shigeno, T.; Nagao, M.; Kimura, T.; Kuroda, K., Direct Silylation of a Mesostructured Precursor for Novel Mesoporous Silica KSW-2, *Langmuir* **2002**, *18*, 8102.

8. Inagaki, S.; Fukushima, Y.; Kuroda, K., Synthesis of highly ordered mesoporous materials from a layered polysilicate, *Journal of the Chemical Society, Chemical Communications* **1993**, 680.
9. Zhang, W.; Pauly, T. R.; Pinnavaia, T. J., Tailoring the Framework and Textural Mesopores of HMS Molecular Sieves through an Electrically Neutral (S⁰I⁰) Assembly Pathway, *Chemistry of Materials* **1997**, *9*, 2491.
10. Avnir, D.; Coradin, T.; Lev, O.; Livage, J., Recent bio-applications of sol-gel materials, *Journal of Materials Chemistry* **2006**, *16*, 1013.
11. Gill, I., Bio-doped Nanocomposite Polymers: Sol–Gel Bioencapsulates, *Chemistry of Materials* **2001**, *13*, 3404.
12. Bromley, A. *Theranostics: the influence of diagnostics on pharmaceutical therapy*; P. J. B. Publications: Richmond, 2000.
13. Grün, M.; Lauer, I.; Unger, K. K., The synthesis of micrometer- and submicrometer-size spheres of ordered mesoporous oxide MCM-41, *Advanced Materials* **1997**, *9*, 254.
14. Vasiliev, P. O.; Faure, B.; Ng, J. B. S.; Bergström, L., Colloidal aspects relating to direct incorporation of TiO₂ nanoparticles into mesoporous spheres by an aerosol-assisted process, *Journal of Colloid and Interface Science* **2008**, *319*, 144.
15. Trommelen, A. M.; Crosby, E. J., Evaporation and drying of drops in superheated vapors, *AIChE Journal* **1970**, *16*, 857.
16. Kishida, M.; Fujita, T.; Umakoshi, K.; Ishiyama, J.; Nagata, H.; Wakabayashi, K., Novel preparation of metal-supported catalysts by colloidal microparticles in a water-in-oil microemulsion; catalytic hydrogenation of carbon dioxide, *Journal of the Chemical Society, Chemical Communications* **1995**, 763.
17. Pileni, M.; Fendler, J. H. *Nanoparticles and Nanostructured Films*; Wiley-VCH: New York, 1998.
18. Vestal, C. R.; Zhang, Z. J., Synthesis of CoCrFeO₄ Nanoparticles Using Microemulsion Methods and Size-Dependent Studies of Their Magnetic Properties, *Chemistry of Materials* **2002**, *14*, 3817.
19. Mizutani, M.; Yamada, Y.; Nakamura, T.; Yano, K., Anomalous Pore Expansion of Highly Monodispersed Mesoporous Silica Spheres and Its Application to the Synthesis of Porous Ferromagnetic Composite, *Chemistry of Materials* **2008**, *20*, 4777.
20. Suzuki, K.; Ikari, K.; Imai, H., Synthesis of Silica Nanoparticles Having a Well-Ordered Mesostructure Using a Double Surfactant System, *Journal of the American Chemical Society* **2003**, *126*, 462.

21. Gao, F.; Botella, P.; Corma, A.; Blesa, J.; Dong, L., Monodispersed Mesoporous Silica Nanoparticles with Very Large Pores for Enhanced Adsorption and Release of DNA, *The Journal of Physical Chemistry B* **2009**, *113*, 1796.
22. Möller, K.; Kobler, J.; Bein, T., Colloidal Suspensions of Nanometer-Sized Mesoporous Silica, *Advanced Functional Materials* **2007**, *17*, 605.
23. He, Q.; Cui, X.; Cui, F.; Guo, L.; Shi, J., Size-controlled synthesis of monodispersed mesoporous silica nano-spheres under a neutral condition, *Microporous and Mesoporous Materials* **2009**, *117*, 609.
24. Urata, C.; Aoyama, Y.; Tonegawa, A.; Yamauchi, Y.; Kuroda, K., Dialysis process for the removal of surfactants to form colloidal mesoporous silica nanoparticles, *Chemical Communications* **2009**, 5094.
25. Zhuravlev, L. T., The surface chemistry of amorphous silica. Zhuravlev model, *Colloids and Surfaces A: Physicochemical and Engineering Aspects* **2000**, *173*, 1.
26. Rosenholm, J. M.; Czuryzkiewicz, T.; Kleitz, F.; Rosenholm, J. B.; Lindén, M., On the Nature of the Brønsted Acidic Groups on Native and Functionalized Mesoporous Siliceous SBA-15 as Studied by Benzylamine Adsorption from Solution, *Langmuir* **2007**, *23*, 4315.
27. Asefa, T.; Tao, Z., Biocompatibility of Mesoporous Silica Nanoparticles, *Chemical Research in Toxicology* **2012**, *25*, 2265.
28. Colilla, M.; Gonzalez, B.; Vallet-Regi, M., Mesoporous silica nanoparticles for the design of smart delivery nanodevices, *Biomaterials Science* **2013**, *1*, 114.
29. Xu, W.; Riikonen, J.; Lehto, V.-P., Mesoporous systems for poorly soluble drugs, *International Journal of Pharmaceutics* **2013**, *453*, 181.
30. Sailor, M. J.; Park, J.-H., Hybrid Nanoparticles for Detection and Treatment of Cancer, *Advanced Materials* **2012**, *24*, 3779.
31. Li, Z.; Barnes, J. C.; Bosoy, A.; Stoddart, J. F.; Zink, J. I., Mesoporous silica nanoparticles in biomedical applications, *Chem. Soc. Rev.* **2012**, *41*, 2590.
32. Vallhov, H.; Gabrielsson, S.; Strømme, M.; Scheynius, A.; Garcia-Bennett, A. E., Mesoporous Silica Particles Induce Size Dependent Effects on Human Dendritic Cells, *Nano Letters* **2007**, *7*, 3576.
33. Napierska, D.; Thomassen, L. C. J.; Rabolli, V.; Lison, D.; Gonzalez, L.; Kirsch-Volders, M.; Martens, J. A.; Hoet, P. H., Size-Dependent Cytotoxicity of Monodisperse Silica Nanoparticles in Human Endothelial Cells, *Small* **2009**, *5*, 846.

34. Qianjun, H.; Zhiwen, Z.; Yu, G.; Jianlin, S.; Yaping, L., Intracellular localization and cytotoxicity of spherical mesoporous silica nano-/micro-particles, *Small* **2009**, *5*, 2722.
35. Lu, F.; Wu, S.-H.; Hung, Y.; Mou, C.-Y., Size Effect on Cell Uptake in Well-Suspended, Uniform Mesoporous Silica Nanoparticles, *Small* **2009**, *5*, 1408.
36. Lee, C.-H.; Cheng, S.-H.; Wang, Y.-J.; Chen, Y.-C.; Chen, N.-T.; Souris, J.; Chen, C.-T.; Mou, C.-Y.; Yang, C.-S.; Lo, L.-W., Near-Infrared Mesoporous Silica Nanoparticles for Optical Imaging: Characterization and In Vivo Biodistribution, *Advanced Functional Materials* **2009**, *19*, 215.
37. Cho, M.; Cho, W.-S.; Choi, M.; Kim, S. J.; Han, B. S.; Kim, S. H.; Kim, H. O.; Sheen, Y. Y.; Jeong, J., The impact of size on tissue distribution and elimination by single intravenous injection of silica nanoparticles, *Toxicology Letters* **2009**, *189*, 177.
38. Park, J.-H.; Gu, L.; Maltzahn, G. V.; Ruoslahti, E.; Bhatia, S. N.; Sailor, M. J., Biodegradable luminescent porous silicon nanoparticles for in vivo applications, *Nat. Mater.* **2009**, *8*, 331.
39. Tao, Z.; Toms, B. B.; Goodisman, J.; Asefa, T., Mesoporosity and Functional Group Dependent Endocytosis and Cytotoxicity of Silica Nanomaterials, *Chemical Research in Toxicology* **2009**, *22*, 1869.
40. Di Pasqua, A. J.; Sharma, K. K.; Shi, Y.-L.; Toms, B. B.; Ouellette, W.; Dabrowiak, J. C.; Asefa, T., Cytotoxicity of mesoporous silica nanomaterials, *Journal of Inorganic Biochemistry* **2008**, *102*, 1416.
41. Huang, X.; Teng, X.; Chen, D.; Tang, F.; He, J., The effect of the shape of mesoporous silica nanoparticles on cellular uptake and cell function, *Biomaterials* **2010**, *31*, 438.
42. Verma, A.; Stellacci, F., Effect of Surface Properties on Nanoparticle–Cell Interactions, *Small* **2010**, *6*, 12.
43. Lin, Y.-S.; Haynes, C. L., Impacts of Mesoporous Silica Nanoparticle Size, Pore Ordering, and Pore Integrity on Hemolytic Activity, *Journal of the American Chemical Society* **2010**, *132*, 4834.
44. Chen, Y.; Chen, H.; Guo, L.; He, Q.; Chen, F.; Zhou, J.; Feng, J.; Shi, J., Hollow/Rattle-Type Mesoporous Nanostructures by a Structural Difference-Based Selective Etching Strategy, *ACS Nano* **2009**, *4*, 529.
45. He, Q.; Zhang, J.; Shi, J.; Zhu, Z.; Zhang, L.; Bu, W.; Guo, L.; Chen, Y., The effect of PEGylation of mesoporous silica nanoparticles on nonspecific binding of serum proteins and cellular responses, *Biomaterials* **2010**, *31*, 1085.

46. Huang, X.; Li, L.; Liu, T.; Hao, N.; Liu, H.; Chen, D.; Tang, F., The Shape Effect of Mesoporous Silica Nanoparticles on Biodistribution, Clearance, and Biocompatibility in Vivo, *ACS Nano* **2011**, *5*, 5390.
47. Davis, M. E.; Chen, Z.; Shin, D. M., Nanoparticle therapeutics: An emerging treatment modality for cancer, *Nat. Rev. Drug Discovery* **2008**, *7*, 771.
48. Rosenholm, J. M.; Sahlgren, C.; Linden, M., Towards multifunctional, targeted drug delivery systems using mesoporous silica nanoparticles - opportunities & challenges, *Nanoscale* **2010**, *2*, 1870.
49. Slowing, I. I.; Vivero-Escoto, J. L.; Zhao, Y.; Kandel, K.; Peeraphatdit, C.; Trewyn, B. G.; Lin, V. S. Y., Exocytosis of Mesoporous Silica Nanoparticles from Mammalian Cells: From Asymmetric Cell-to-Cell Transfer to Protein Harvesting, *Small* **2011**, *7*, 1526.
50. Etienne, M.; Walcarius, A., Analytical investigation of the chemical reactivity and stability of aminopropyl-grafted silica in aqueous medium, *Talanta* **2003**, *59*, 1173.
51. He, Q.; Shi, J.; Zhu, M.; Chen, Y.; Chen, F., The three-stage in vitro degradation behavior of mesoporous silica in simulated body fluid, *Microporous and Mesoporous Materials* **2010**, *131*, 314.
52. Mortera, R.; Fiorilli, S.; Garrone, E.; Verné, E.; Onida, B., Pores occlusion in MCM-41 spheres immersed in SBF and the effect on ibuprofen delivery kinetics: A quantitative model, *Chemical Engineering Journal* **2010**, *156*, 184.
53. Mamaeva, V.; Rosenholm, J. M.; Bate-Eya, L. T.; Bergman, L.; Peuhu, E.; Duchanoy, A.; Fortelius, L. E.; Landor, S.; Toivola, D. M.; Linden, M.; Sahlgren, C., Mesoporous Silica Nanoparticles as Drug Delivery Systems for Targeted Inhibition of Notch Signaling in Cancer, *Mol Ther* **2011**, *19*, 1538.
54. He, X.; Nie, H.; Wang, K.; Tan, W.; Wu, X.; Zhang, P., In Vivo Study of Biodistribution and Urinary Excretion of Surface-Modified Silica Nanoparticles, *Analytical Chemistry* **2008**, *80*, 9597.
55. Lu, J.; Liong, M.; Li, Z.; Zink, J. I.; Tamanoi, F., Biocompatibility, Biodistribution, and Drug-Delivery Efficiency of Mesoporous Silica Nanoparticles for Cancer Therapy in Animals, *Small* **2010**, *6*, 1794.
56. Souris, J. S.; Lee, C.-H.; Cheng, S.-H.; Chen, C.-T.; Yang, C.-S.; Ho, J.-a. A.; Mou, C.-Y.; Lo, L.-W., Surface charge-mediated rapid hepatobiliary excretion of mesoporous silica nanoparticles, *Biomaterials* **2010**, *31*, 5564.
57. Zhao, W.; Chen, H.; Li, Y.; Li, L.; Lang, M.; Shi, J., Uniform Rattle-

- type Hollow Magnetic Mesoporous Spheres as Drug Delivery Carriers and their Sustained-Release Property, *Advanced Functional Materials* **2008**, *18*, 2780.
58. Zhu, Y.; Shi, J.; Shen, W.; Chen, H.; Dong, X.; Ruan, M., Preparation of novel mesoporous silica spheres and their sustained-release property, *Nanotechnology* **2005**, *16*, 2633.
 59. Fu, Q.; Rao, G. V.-R.; Ista, L. K.; Wu, Y.; Andrzejewski, B. P.; Sklar, L. A.; Ward, T. L.; Lopez, G. P., Control of molecular transport through stimuli-responsive ordered mesoporous materials, *Adv. Mater* **2003**, *15*, 1262.
 60. Mal, N. K.; Fujiwara, M.; Tanaka, Y.; Taguchi, T.; Matsukata, M., Photo-switched storage and release of guest molecules in the pore void of coumarin-modified MCM-41, *Chem. Mater.* **2003**, *15*, 3385.
 61. Vivero-Escoto, J. L.; Slowing, I. I.; Trewyn, B. G.; Lin, V. S.-Y., Mesoporous silica nanoparticles for intracellular controlled drug delivery, *Small* **2010**, *6*, 1952.
 62. Sudimack, J.; Lee, R. J., Targeted drug delivery via the folate receptor, *Advanced Drug Delivery Reviews* **2000**, *41*, 147.
 63. Elnakat, H.; Ratnam, M., Distribution, functionality and gene regulation of folate receptor isoforms: implications in targeted therapy, *Advanced Drug Delivery Reviews* **2004**, *56*, 1067.
 64. Lewandowski, D.; Schroeder, G. In *From molecules to functional architecture - Supramolecular interactions*; Rybachenko, V. I., Ed.; East Publisher House: Donetsk, 2012, p 229.
 65. Andersson, J.; Rosenholm, J.; Areva, S.; Linden, M., Influences of material characteristics on ibuprofen drug loading and release profiles from ordered micro- and mesoporous silica matrices, *Chem. Mater.* **2004**, *16*, 4160.
 66. Vinu, A.; Murugesan, V.; Tangermann, O.; Hartmann, M., Adsorption of Cytochrome c on Mesoporous Molecular Sieves: Influence of pH, Pore Diameter, and Aluminum Incorporation, *Chemistry of Materials* **2004**, *16*, 3056.
 67. Rosenholm, J. M.; Lindén, M., Towards establishing structure–activity relationships for mesoporous silica in drug delivery applications, *Journal of Controlled Release* **2008**, *128*, 157.
 68. Horcajada, P.; Rámila, A.; Pérez-Pariente, J.; Vallet, R.; amp; x, M., Influence of pore size of MCM-41 matrices on drug delivery rate, *Microporous and Mesoporous Materials* **2004**, *68*, 105.
 69. Klafter, J.; Drake, J. M. *Molecular dynamics in restricted geometries*;

- 1st ed. New York City ed.; Wiley: New York 1989.
70. Van Speybroeck, M.; Barillaro, V.; Thi, T. D.; Mellaerts, R.; Martens, J.; Van Humbeeck, J.; Vermant, J.; Annaert, P.; Van den Mooter, G.; Augustijns, P., Ordered mesoporous silica material SBA-15: A broad-spectrum formulation platform for poorly soluble drugs, *Journal of Pharmaceutical Sciences* **2009**, *98*, 2648.
 71. Limmell, T.; Santos, H. A.; Mäkilä, E.; Heikkilä, T.; Salonen, J.; Murzin, D. Y.; Kumar, N.; Laaksonen, T.; Peltonen, L.; Hirvonen, J., Drug delivery formulations of ordered and nonordered mesoporous silica: Comparison of three drug loading methods, *Journal of Pharmaceutical Sciences* **2011**, *100*, 3294.
 72. Van Speybroeck, M.; Mellaerts, R.; Mols, R.; Thi, T. D.; Martens, J. A.; Van Humbeeck, J.; Annaert, P.; Van den Mooter, G.; Augustijns, P., Enhanced absorption of the poorly soluble drug fenofibrate by tuning its release rate from ordered mesoporous silica, *European Journal of Pharmaceutical Sciences* **2010**, *41*, 623.
 73. Zhang, Y.; Jiang, T.; Zhang, Q.; Wang, S., Inclusion of telmisartan in mesocellular foam nanoparticles: Drug loading and release property, *European Journal of Pharmaceutics and Biopharmaceutics* **2010**, *76*, 17.
 74. van Speybroeck, M.; Mellaerts, R.; Thi, T. D.; Martens, J. A.; Van Humbeeck, J.; Annaert, P.; Van den Mooter, G.; Augustijns, P., Preventing release in the acidic environment of the stomach via occlusion in ordered mesoporous silica enhances the absorption of poorly soluble weakly acidic drugs, *Journal of Pharmaceutical Sciences* **2011**, *100*, 4864.
 75. Planinšek, O.; Kovačič, B.; Vrečer, F., Carvedilol dissolution improvement by preparation of solid dispersions with porous silica, *International Journal of Pharmaceutics* **2011**, *406*, 41.
 76. Zhang, Y.; Wang, J.; Bai, X.; Jiang, T.; Zhang, Q.; Wang, S., Mesoporous Silica Nanoparticles for Increasing the Oral Bioavailability and Permeation of Poorly Water Soluble Drugs, *Molecular Pharmaceutics* **2012**, *9*, 505.
 77. Munoz, B.; Ramila, A.; Perez-Pariente, J.; Diaz, I.; Vallet-Regi, M., MCM-41 organic modification as drug delivery rate regulator, *Chem. Mater.* **2003**, *15*, 500.
 78. Chung, T. H.; Wu, S. H.; Yao, M.; Lu, C. W.; Lin, Y. S.; Hung, Y.; Mou, C. Y.; Chen, Y. C.; Huang, D. M., The effect of surface charge on the uptake and biological function of mesoporous silica nanoparticles in

- 3T3-L1 cells and human mesenchymal stem cells, *Biomaterials* **2007**, *28*, 2959.
79. Charnay, C.; Bégu, S.; Tourné-Péteilh, C.; Nicole, L.; Lerner, D. A.; Devoisselle, J. M., Inclusion of ibuprofen in mesoporous templated silica: drug loading and release property, *European Journal of Pharmaceutics and Biopharmaceutics* **2004**, *57*, 533.
80. Fernández-Núñez, M.; Zorrilla, D.; Montes, A.; Mosquera, M. J., Ibuprofen Loading in Surfactant-Templated Silica: Role of the Solvent According to the Polarizable Continuum Model, *The Journal of Physical Chemistry A* **2009**, *113*, 11367.
81. Aiello, R.; Cavallaro, G.; Giammona, G.; Pasqua, L.; Pierro, P.; Testa, F. In *Studies in Surface Science and Catalysis*; R. Aiello, G. G., Testa, F., Eds.; Elsevier: 2002; Vol. Volume 142, p 1165.
82. Wang, G.; Otuonye, A. N.; Blair, E. A.; Denton, K.; Tao, Z.; Asefa, T., Functionalized mesoporous materials for adsorption and release of different drug molecules: A comparative study, *Journal of Solid State Chemistry* **2009**, *182*, 1649.
83. Aerts, C. A.; Verraedt, E.; Depla, A.; Follens, L.; Froyen, L.; Van Humbeeck, J.; Augustijns, P.; Van den Mooter, G.; Mellaerts, R.; Martens, J. A., Potential of amorphous microporous silica for ibuprofen controlled release, *International Journal of Pharmaceutics* **2010**, *397*, 84.
84. Verraedt, E.; Pendela, M.; Adams, E.; Hoogmartens, J.; Martens, J. A., Controlled release of chlorhexidine from amorphous microporous silica, *Journal of Controlled Release* **2010**, *142*, 47.
85. Papat, A.; Hartono, S. B.; Stahr, F.; Liu, J.; Qiao, S. Z.; Qing Lu, G., Mesoporous silica nanoparticles for bioadsorption, enzyme immobilisation, and delivery carriers, *Nanoscale* **2011**, *3*, 2801.
86. Salonen, J.; Laitinen, L.; Kaukonen, A. M.; Tuura, J.; Björkqvist, M.; Heikkilä, T.; Vähä-Heikkilä, K.; Hirvonen, J.; Lehto, V. P., Mesoporous silicon microparticles for oral drug delivery: Loading and release of five model drugs, *Journal of Controlled Release* **2005**, *108*, 362.
87. Vallet-Regi, M.; Ramila, A.; Real, R. P. d.; Perez-Pariente, J., A new property of MCM-41: Drug delivery system, *Chem. Mater.* **2001**, *13*, 308.
88. Qu, F. Y.; Zhu, G. S.; Lin, H. W.; Zhang, W. M.; Sun, J. Y.; Li, S. G.; Qiu, S. L., A controlled release of ibuprofen by systematically tailoring the morphology of mesoporous silica materials, *J. Solid State Chem.* **2006**, *179*, 2027.

89. Horcajada, P.; A., R.; Gerard, F.; M., V.-R., Influence of superficial organic modification of MCM-41 matrices on drug delivery rate, *Solid State Sci.* **2006**, *8*, 1243.
90. Manzano, M.; Aina, V.; Arean, C. O.; Balas, F.; Cauda, V.; Colilla, M. R.; Delgado, M.; M., V.-R., Studies on MCM-41 mesoporous silica for drug delivery: Effect of particle morphology and amine functionalization, *Chem. Eng. J.* **2008**, *137*, 30.
91. Lu, J.; Liong, M.; Zink, J. I.; Tamanoi, F., Multifunctional inorganic nanoparticles for imaging, targeting, and drug delivery, *Small* **2007**, *3*, 1341.
92. Lu, J.; Liong, M.; Sherman, S.; Xia, T.; Kovochich, M.; Nel, A.; Zink, J.; Tamanoi, F., Mesoporous Silica Nanoparticles for Cancer Therapy: Energy-Dependent Cellular Uptake and Delivery of Paclitaxel to Cancer Cells, *Nanobiotechnol* **2007**, *3*, 89.
93. Díaz, J. F.; Balkus Jr, K. J., Enzyme immobilization in MCM-41 molecular sieve, *Journal of Molecular Catalysis B: Enzymatic* **1996**, *2*, 115.
94. Yiu, H. H. P.; Botting, C. H.; Botting, N. P.; Wright, P. A., Size selective protein adsorption on thiol-functionalised SBA-15 mesoporous molecular sieve, *Physical Chemistry Chemical Physics* **2001**, *3*, 2983.
95. Mal, N. K.; Fujiwara, M.; Tanaka, Y., Photocontrolled reversible release of guest molecules from coumarin-modified mesoporous silica, *Nature* **2003**, *421*, 350.
96. Ferris, D. P.; Zhao, Y.-L.; Khashab, N. M.; Khatib, H. A.; Stoddart, J. F.; Zink, J. I., Light-Operated Mechanized Nanoparticles, *Journal of the American Chemical Society* **2009**, *131*, 1686.
97. Vivero-Escoto, J. L.; Slowing, I. I.; Wu, C.-W.; Lin, V. S. Y., Photoinduced Intracellular Controlled Release Drug Delivery in Human Cells by Gold-Capped Mesoporous Silica Nanosphere, *Journal of the American Chemical Society* **2009**, *131*, 3462.
98. Knezevic, N. Z.; Trewyn, B. G.; Lin, V. S. Y., Functionalized mesoporous silica nanoparticle-based visible light responsive controlled release delivery system, *Chemical Communications* **2011**, *47*, 2817.
99. Meng, H.; Xue, M.; Xia, T.; Zhao, Y.-L.; Tamanoi, F.; Stoddart, J. F.; Zink, J. I.; Nel, A. E., Autonomous in Vitro Anticancer Drug Release from Mesoporous Silica Nanoparticles by pH-Sensitive Nanovalves, *Journal of the American Chemical Society* **2010**, *132*, 12690.
100. Park, C.; Oh, K.; Lee, S. C.; Kim, C., Controlled Release of Guest Molecules from Mesoporous Silica Particles Based on a pH-Responsive

- Polypseudorotaxane Motif, *Angewandte Chemie International Edition* **2007**, *46*, 1455.
101. Chen, P.-J.; Hu, S.-H.; Hsiao, C.-S.; Chen, Y.-Y.; Liu, D.-M.; Chen, S.-Y., Multifunctional magnetically removable nanogated lids of Fe₃O₄-capped mesoporous silica nanoparticles for intracellular controlled release and MR imaging, *Journal of Materials Chemistry* **2011**, *21*, 2535.
 102. Chen, Y.; Chen, H.; Zeng, D.; Tian, Y.; Chen, F.; Feng, J.; Shi, J., Core/Shell Structured Hollow Mesoporous Nanocapsules: A Potential Platform for Simultaneous Cell Imaging and Anticancer Drug Delivery, *ACS Nano* **2010**, *4*, 6001.
 103. Park, J.-H.; Lee, Y.-H.; Oh, S.-G., Preparation of Thermosensitive PNIPAm-Grafted Mesoporous Silica Particles, *Macromolecular Chemistry and Physics* **2007**, *208*, 2419.
 104. Zhu, S.; Zhou, Z.; Zhang, D.; Jin, C.; Li, Z., Design and synthesis of delivery system based on SBA-15 with magnetic particles formed in situ and thermo-sensitive PNIPAA as controlled switch, *Microporous and Mesoporous Materials* **2007**, *106*, 56.
 105. Zintchenko, A.; Ogris, M.; Wagner, E., Temperature Dependent Gene Expression Induced by PNIPAM-Based Copolymers: Potential of Hyperthermia in Gene Transfer, *Bioconjugate Chemistry* **2006**, *17*, 766.
 106. Keerl, M.; Smirnovas, V.; Winter, R.; Richtering, W., Copolymer Microgels from Mono- and Disubstituted Acrylamides: Phase Behavior and Hydrogen Bonds, *Macromolecules* **2008**, *41*, 6830.
 107. Baeza, A.; Guisasaola, E.; Ruiz-Hernández, E.; Vallet-Regí, M., Magnetically Triggered Multidrug Release by Hybrid Mesoporous Silica Nanoparticles, *Chemistry of Materials* **2012**, *24*, 517.
 108. Schlossbauer, A.; Warncke, S.; Gramlich, P. M. E.; Kecht, J.; Manetto, A.; Carell, T.; Bein, T., A Programmable DNA-Based Molecular Valve for Colloidal Mesoporous Silica, *Angewandte Chemie International Edition* **2010**, *49*, 4734.
 109. Aznar, E.; Mondragón, L.; Ros-Lis, J. V.; Sancenón, F.; Marcos, M. D.; Martínez-Mañez, R.; Soto, J.; Pérez-Payá, E.; Amorós, P., Finely Tuned Temperature-Controlled Cargo Release Using Paraffin-Capped Mesoporous Silica Nanoparticles, *Angewandte Chemie International Edition* **2011**, *50*, 11172.
 110. Lai, C.-Y.; Trewyn, B. G.; Jeftinija, D. M.; Jeftinija, K.; Xu, S.; Jeftinija, S.; Lin, V. S. Y., A Mesoporous Silica Nanosphere-Based Carrier System with Chemically Removable CdS Nanoparticle Caps for

- Stimuli-Responsive Controlled Release of Neurotransmitters and Drug Molecules, *Journal of the American Chemical Society* **2003**, *125*, 4451.
111. Torney, F.; Trewyn, B. G.; Lin, V. S.-Y.; Wang, K., Mesoporous silica nanoparticles deliver DNA and chemicals into plants, *Nat. Nanotechnol.* **2007**, *2*, 295.
112. Giri, S.; Trewyn, B. G.; Stellmaker, M. P.; Lin, V. S. Y., Stimuli-Responsive Controlled-Release Delivery System Based on Mesoporous Silica Nanorods Capped with Magnetic Nanoparticles, *Angewandte Chemie International Edition* **2005**, *44*, 5038.
113. Liu, R.; Zhao, X.; Wu, T.; Feng, P., Tunable Redox-Responsive Hybrid Nanogated Ensembles, *Journal of the American Chemical Society* **2008**, *130*, 14418.
114. Luo, Z.; Cai, K.; Hu, Y.; Zhao, L.; Liu, P.; Duan, L.; Yang, W., Mesoporous Silica Nanoparticles End-Capped with Collagen: Redox-Responsive Nanoreservoirs for Targeted Drug Delivery, *Angewandte Chemie International Edition* **2011**, *50*, 640.
115. Kim, H.; Kim, S.; Park, C.; Lee, H.; Park, H. J.; Kim, C., Glutathione-Induced Intracellular Release of Guests from Mesoporous Silica Nanocontainers with Cyclodextrin Gatekeepers, *Advanced Materials* **2010**, *22*, 4280.
116. Park, C.; Kim, H.; Kim, S.; Kim, C., Enzyme Responsive Nanocontainers with Cyclodextrin Gatekeepers and Synergistic Effects in Release of Guests, *Journal of the American Chemical Society* **2009**, *131*, 16614.
117. Bernardos, A.; Aznar, E.; Marcos, M. D.; Martínez-Máñez, R.; Sancenón, F.; Soto, J.; Barat, J. M.; Amorós, P., Enzyme-Responsive Controlled Release Using Mesoporous Silica Supports Capped with Lactose, *Angewandte Chemie International Edition* **2009**, *48*, 5884.
118. Agostini, A.; Mondragón, L.; Coll, C.; Aznar, E.; Marcos, M. D.; Martínez-Máñez, R.; Sancenón, F.; Soto, J.; Pérez-Payá, E.; Amorós, P., Dual Enzyme-Triggered Controlled Release on Capped Nanometric Silica Mesoporous Supports, *ChemistryOpen* **2012**, *1*, 17.
119. Zhao, Y.; Trewyn, B. G.; Slowing, I. I.; Lin, V. S. Y., Mesoporous Silica Nanoparticle-Based Double Drug Delivery System for Glucose-Responsive Controlled Release of Insulin and Cyclic AMP, *Journal of the American Chemical Society* **2009**, *131*, 8398.
120. Climent, E.; Bernardos, A.; Martínez-Máñez, R. n.; Maquieira, A.; Marcos, M. D.; Pastor-Navarro, N.; Puchades, R.; Sancenón, F. I.; Soto, J.; Amorós, P., Controlled Delivery Systems Using Antibody-Capped Mesoporous Nanocontainers, *Journal of the American Chemical*

- Society* **2009**, *131*, 14075.
121. Zhu, C.-L.; Lu, C.-H.; Song, X.-Y.; Yang, H.-H.; Wang, X.-R., Bioresponsive Controlled Release Using Mesoporous Silica Nanoparticles Capped with Aptamer-Based Molecular Gate, *Journal of the American Chemical Society* **2011**, *133*, 1278.
 122. Mamaeva, V.; Sahlgren, C.; Lindén, M., Mesoporous silica nanoparticles in medicine—Recent advances, *Advanced Drug Delivery Reviews* **2013**, *65*, 689.
 123. Taratula, O.; Garbuzenko, O. B.; Chen, A. M.; Minko, T., Innovative strategy for treatment of lung cancer: targeted nanotechnology-based inhalation co-delivery of anticancer drugs and siRNA, *Journal of Drug Targeting* **2011**, *19*, 900.
 124. Huang, I.-P.; Sun, S.-P.; Cheng, S.-H.; Lee, C.-H.; Wu, C.-Y.; Yang, C.-S.; Lo, L.-W.; Lai, Y.-K., Enhanced Chemotherapy of Cancer Using pH-Sensitive Mesoporous Silica Nanoparticles to Antagonize P-Glycoprotein-Mediated Drug Resistance, *Molecular Cancer Therapeutics* **2011**, *10*, 761.
 125. He, Q.; Gao, Y.; Zhang, L.; Zhang, Z.; Gao, F.; Ji, X.; Li, Y.; Shi, J., A pH-responsive mesoporous silica nanoparticles-based multi-drug delivery system for overcoming multi-drug resistance, *Biomaterials* **2011**, *32*, 7711.
 126. Casasús, R.; Climent, E.; Marcos, M. D.; Martínez-Mañez, R.; Sancenón, F.; Soto, J.; Amorós, P.; Cano, J.; Ruiz, E., Dual Aperture Control on pH- and Anion-Driven Supramolecular Nanoscopic Hybrid Gate-like Ensembles, *Journal of the American Chemical Society* **2008**, *130*, 1903.

Chapter 7

Surface modification of natural halloysite nanotubes. The hybrid materials for nanotechnology

Joanna Kurczewska¹, Agnieszka Michalska², Kajetan Pyrzyński²
and Grzegorz Schroeder¹

¹ Adam Mickiewicz University in Poznań, Faculty of Chemistry,
Umultowska 89b, 61-614 Poznań, Poland

² Delta Innovations and Implementation Company, Krupczyn 5,
63-140 Dolsk, Poland

1. Definition of hybrid materials

Continuous development of technology generates a desire to receive more and newer materials. This is due to the fact that the commonly used traditional materials (metals, ceramics, plastics) are not able to meet certain expectations and technological requirements. One commonly used solution is the mixing of materials to produce composite systems having improved properties than the individual components. Furthermore, reducing the size of the inorganic fragments (molecular, nanoscale) allows to obtain a much more homogeneous materials with new properties. The beginning of industrial production of multicomponent systems is associated with the development of sol-gel process. Especially silicon based sol-gel method has allowed the production of a huge amount of inorganic-organic systems.

There are a variety of systems defined as hybrid materials. General definition assumes that a hybrid material is composed of two different components linked at the molecular level (Figure 1). Usually one of the components is of inorganic and the other of organic nature. Depending on interaction between components of hybrid materials, they are divided into two classes. *Class I* refers to materials with weak interactions between two phases (van der Waals; hydrogen bonding; weak electrostatic interactions). *Class II* refers to materials with strong interactions between the components (covalent bonding), [1,2].

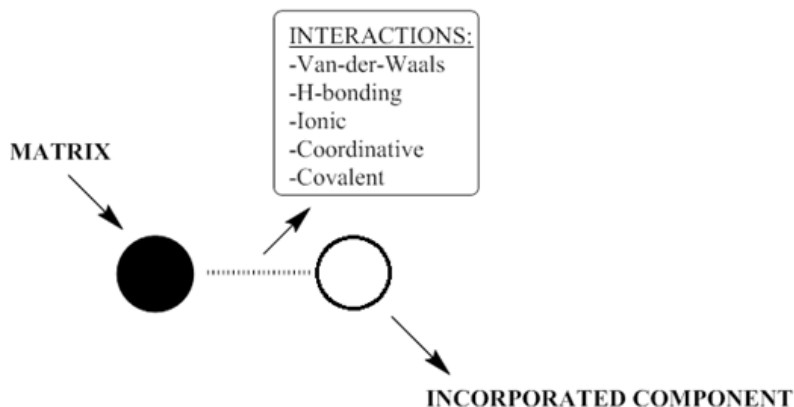


Figure 1. Schematic representation of hybrid material

2. Methods of surface modification

The formation of hybrid materials requires the synthesis of chemical compounds having substituents able to form covalent, ionic or non-covalent bonding with matrix surface. A monolayer of chemical molecules significantly modifies properties of a surface. Especially bifunctional molecules, having two types of terminal groups, are preferred for such type of modification because they are able to form chemical bonding with matrix surface as well as they are linkers to create successive layers. Deposition of the active compounds on the surface of the matrix (metal, polymer, metallic oxide,...) may be carried out using a variety of techniques (adsorption, chemical grafting, modification, functionalization,...). Chemical grafting relates to chemical modification of a surface or a polymer by single reactive molecules or by a formation of active spaces at a surface, which can be further applied for deposition of molecules (self-organization) or polymerization. This method is useful whenever the aim is to change the properties of part of the material. Functionalization is a type of chemical modification and it involves incorporation of functional groups (a few %) to macromolecules, which results in different chemical reactivity of a surface or polymer. It can be accomplished using halogenation, hydrogenation, epoxidation, chlorosulfonation etc. Immobilization, in turn, refers to the attachment of a soluble compound to insoluble matrix under certain conditions. This process utilizes the micro-encapsulation, adsorption, physical entrapment within the structure of the matrix and formation of covalent bonds [3,4].

3. Structure of halloysite

Hybrid materials can be constructed on the basis of different inorganic matrices, including tubular nanomaterials (SiO_2 , TiO_2 , ZrO_2 , CeO_2 ,...). However many of them are unattractive because of their toxicity or/and high costs. On the other hand clay nanotubes are characterized by biocompatibility and relatively low cost.

Halloysite of structural formula $\text{Al}_2\text{Si}_2\text{O}_5(\text{OH})_4 \cdot n\text{H}_2\text{O}$ is a natural kaolinite mineral, having rolled aluminosilicate sheets (Figure 2). It is chemically similar to kaolin (1:1 dioctahedral layer), but with different morphology (kaolin is characterized by plate-like structure). Halloysite contains additional water monolayer between the adjacent layers. This monolayer refers to so called halloysite-10 Å ($n=2$). Heating halloysite dehydrates it to halloysite-7 Å ($n=0$). Naturally occurring halloysite consists of first of all SiO_2 and Al_2O_3 , but also could contain Fe_2O_3 , K_2O , TiO_2 , CaO , MgO . Therefore the color of the mineral can be different (yellowish, brown, greenish) depending on its origin.

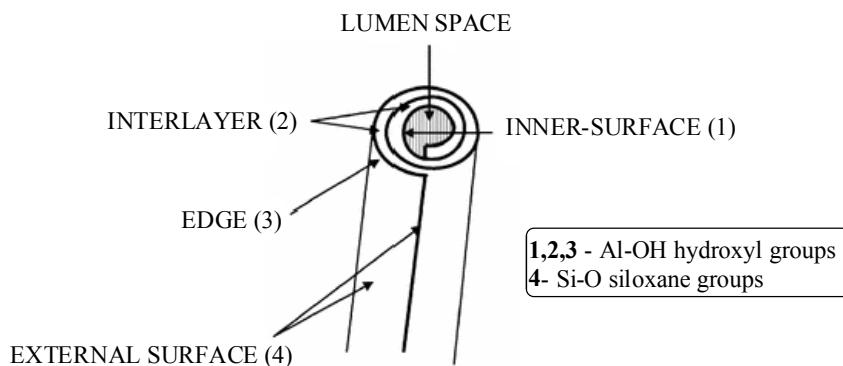


Figure 2. Scheme of halloysite structure

A halloysite wall contains 15-20 bilayers (aluminum and silicon oxides). Alumina layer is at the inner surface, while the silica layer at the outer surface of the tube. Outer surface is negatively charged, while inner lumen surface is positively charged in the pH range 2-8. This enables selective modifications because anionic species can be entrapped into lumen, while cationic units can be immobilized on the surface [5,6].

4. Selected examples of halloysite surface modification

Halloysite surface groups have only weak interactions with guest molecules (hydrogen bonding; van-der-Waals forces). This can be overcome by modification of the mineral surface, which should result in stronger binding of guest molecules. Commonly used method is based on modification with organosilane with specific functional groups. The surface of halloysite functionalized with 3-aminopropyltriethoxysilane [7] (Figure 3) was used for loading of different molecules. Yuan *et al.* [8] applied it for loading and release of model dye – anionic Orange II. The dye loading of the functionalized halloysite was 32% greater than that of the unmodified sample. Tan *et al.* [9] applied APTES-halloysite for the loading of ibuprofen. In case of unmodified halloysite, the bioactive molecule was weakly anchored by hydrogen bonding. The presence of amine groups in APTES, mostly in the internal lumen surface, resulted in strong anchoring of ibuprofen by electrostatic interactions (carboxyl groups of ibuprofen and protonated aminopropyl groups of grafted APTES). Zhang *et al.* [10] prepared nanocomposites by deposition of palladium (Pd) nanoparticles on the surface of APTES-halloysite. They compared the catalytic properties of halloysite nanotubes (HNTs), Pd/HNTs and Pd/APTES-HNTs in the hydrogenation of styrene to ethylbenzene. The distributions of Pd nanoparticles deposited on APTES-HNTs are much more uniform and palladium particles show a higher catalytic activity compared to those deposited on unmodified HNTs. Liu *et al.* [11] obtained more advanced material – APTES-HNTs@reduced graphene oxide composite for waste water treatment and energy storage.

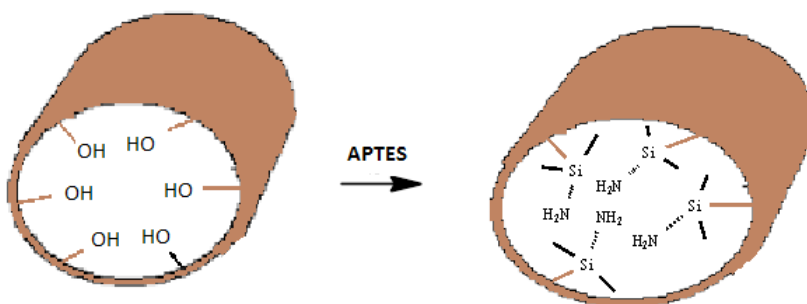


Figure 3. Functionalization of halloysite with 3-Aminopropyltriethoxysilane (APTES)

It was already mentioned that the organosilanes with terminal functional groups can be also linkers for incorporating of other molecules. The silanization

procedure is commonly used for inorganic supports with surface hydroxyl groups. Analogous procedure is applied for functionalization of HNTs. He *et al.* [12] found HNTs modified with *N*-2-Pyridylsuccinamic acid (Figure 4a) suitable for solid-phase extraction of lead(II). The adsorption capacity of the sorbent was much better compared with other more expensive adsorbents. Murexide (Figure 4b) functionalization HNTs were applied for separation and preconcentration of Pd(II) ions [13]. In both examples, APTES-HNTs are intermediate products providing free amine groups that participate in further chemical reactions.

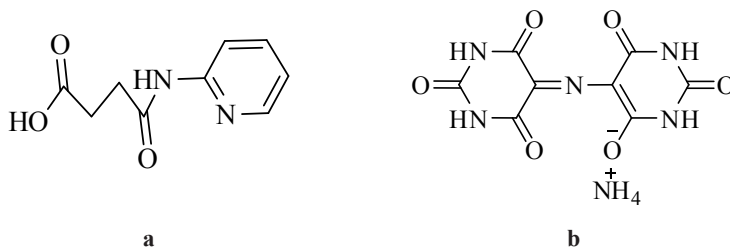


Figure 4. Structural formulas of (a) *N*-2-Pyridylsuccinamic acid; (b) Murexide

The interesting properties of HNTs are observed after their modification with the surfactant of hexadecyltrimethylammonium (HDTMA) salts. In case of hydrophobic organic contaminants (*e.g.* naphthalene) the adsorption process depends on the arrangement of the surfactant cations. Lee *et al.* [14] found that at high surface coverage, HDTMA formed clusters and despite high loadings of surfactant, naphthalene adsorption was unsatisfactory. Bromide ammonium salt was also used by Jinhua *et al.* [15] for adsorption of chromium(VI). Positively charged surface of modified HNTs should allow adsorption of HCrO_4^- and $\text{Cr}_2\text{O}_7^{2-}$ anions. The modified HNTs were used as adsorbent for Cr(VI) removal from its aqueous solution and they exhibited rapid adsorption rate for chromates, and approached to 90% of the maximum adsorption capacity within 5 min. The effects of pH and ionic strength on the adsorption capacity were also investigated, which showed the adsorption capacity of the adsorbent decreased significantly with the increase of ionic strength and pH. Chromium(VI) could be adsorbed using other modified HNTs. Jingimn *et al.* [16] modified the mineral surface with 3-mercaptopropyltrimethoxysilane (SH-HNTs). Massaro *et al.* [17] grafted HNTs with the same silane by a microwave irradiation. This time however, the material was used as a support for palladium particles and further tested as a catalyst in the Suzuki reaction between phenylboronic acid and some aryl halide.

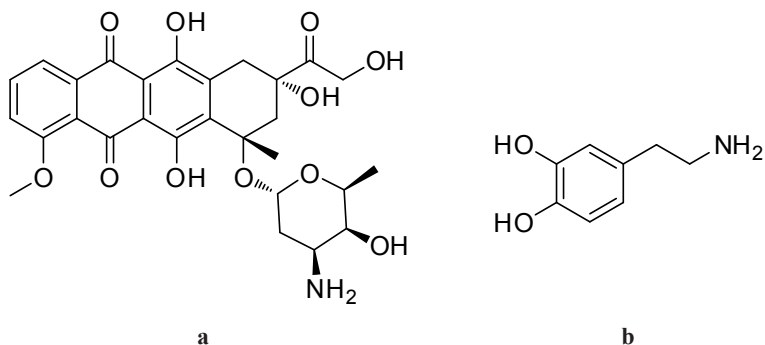


Figure 5. Structural formulas of (a) Doxorubicin (DOX); (b) Dopamine (DP)

Very promising results are also obtained after functionalization of HNTs with bioactive compounds. Lee *et al.* [18] synthesized DNA-wrapped HNTs and applied it as a doxorubicin, effective anticancer drug, (Figure 5a) delivery carrier. DNA plays two different functions in this system: it makes HNTs water-dispersible and it is a platform for loading DOX. On the other hand dopamine (Figure 5b) modified HNTs can be suitable tool for enzyme immobilization [19]. Analogously like with DNA, dopamine forms polymer coating, making HNTs suitable for biomacromolecule immobilization. It was proved that DP-HNTs showed an excellent capacity for selected enzyme loading.

Natural halloysite clay nanotubes are described by Lvow *et al.* [20] as inorganic reinforcing materials for polymers. Loading these tubes' 15-nm diameter lumens with chemical agents, including bioactive molecules (self-healing, anticorrosion, antimicrobial agents, proteins, DNA, drugs, etc.), and doping them into polymers allows a controlled sustained release, providing these nanocomposites with new smart properties. Typically, addition of 5% halloysite synergistically increases polymer strength on 30–70%, enhances composite adhesivity and adds new functions due to triggered release of needed chemicals. Halloysite is biocompatible “green” material and its simple processing combined with low cost make it a perspective additive for polymeric biocomposites.

The functionalization of halloysite nanotube was performed also by grafting hyperbranched (co)polymers via surfaceinitiated self-condensing vinyl (co) polymerization [21]. Zou *et al.* [22] used tea polyphenols (TPs) as a reductant. Ag nanoparticles (AgNPs) supported on halloysite nanotubes (HNTs) were simply and greenly synthesized for the photocatalytic decomposition of methylene blue (MB). HNTs were initially functionalized by N- β -aminoethyl- γ -aminopropyl trimethoxysilane (AEAPTMS) to introduce amino groups to form N-HNTs to

fasten the AgNPs; then AgNPs were synthesized and 'anchored' on the surface of the HNTs. The photocatalytic activity of the as-prepared AgNPs@N-HNTs catalyst was evaluated by decomposition of MB. The results showed that the prepared catalyst exhibited excellent catalytic activity and high adsorption capability to MB.

Zhang *et al.* [23] prepared well-dispersed epoxy resin/halloysite nanotubes composites by functionalization of the HNTs surfaces using polyamidoamine generation-3 (HNTs-G3.0). A series of modified halloysite nanotubes with different generations of dendritic polyamidoamine (PAMAM) were prepared via a divergent synthetic process by repeating the Michael addition of methyl acrylate to superficial amino groups and the amidation of the resulting esters with ethylenediamine. The impact strength and fracture toughness (K_{IC}) of composites with polyamidoamine generation-3 grafted HNTs were about 160 and 20 % higher than the values of functionalization halloysite nanotube system.

The grafting of natural halloysite nanotubes (HNT) with aminosilanes exhibiting two (DAS) and three (TAS) amino groups has been investigated by Barrientos-Ramírez *et al.* [24] and compared to the physisorption of both silanes on halloysite nanotubes. Halloysite nanotubes were used as solid supports for the heterogeneous Atom Transfer Polymerization of methyl methacrylate (MMA) into poly(methylmethacrylate) (PMMA) using CuBr as catalyst. Silane grafted on the nanoclay acts both as a ligand those bonds to CuBr and as a catalyst for the heterogeneous MMA polymerization. Grafting of halloysite nanotubes with DAS produced a polymer with polydispersities similar to those produced by the physically adsorbed diaminosilane catalyst, but conversion percentages were lower and a poorer control over the polymerization reaction was achieved. Grafting of halloysite nanotubes with TAS had a detrimental effect on the control of the polymerization reaction and a loss of catalytic activity due to the immobilization of the copper catalyst.

Furthermore halloysite clay nanotubes were selectively modified by adsorbing perfluoroalkylated anionic surfactants at the inner surface. The modified nanotubes formed kinetically stable dispersions due to the enhanced electrostatic repulsions exercised between the particles. It was proved that the modified nanotubes can be used as non-foaming oxygen nanocontainers in aqueous media [25].

Albdiry *et al.* [26] presented investigation studies of the structure/property relationship of thermosetting unsaturated polyester (UPE) filled with pristine halloysite (HNT) and vinyltrimethoxysilane-treated halloysite nanotubes (s-HNT) nanocomposites. The introduction of HNT or s-HNT up to 5 wt.% induced higher mechanical properties and improved fracture toughness

associated with a shift in toughening mechanisms from a highly brittle fracture for neat UPE into matrix shear yielding and zone shielding mechanisms with the presence of halloysite particles in the nanocomposite.

5. Conclusions

Halloysite nanotubes, with specific characteristics, may find applications in a number of areas. There are numerous examples of hybrid materials based on HNTs and it is difficult to discuss all of them. Although it is worth mentioning the main areas where such materials can be extremely effective [27, 28]. HNTs can form anticorrosion coatings or release in controlled way corrosion inhibitors (e.g. benzotriazole) entrapped in their tubes. There are many articles describing their excellent results for thermal resistance. Polymer (e.g. poly(propylene)/polyethylene)/HNT nanocomposites are characterized by increased thermal stability and flame retardancy. Probably it is a result of tubular structure of mineral, which is a barrier for heat and mass transport, as well as the presence of iron in tubes. HNTs can also act as nanoreactors or nanotemplates to prepare nanoparticles, nanowires, nanocoatings etc. Furthermore it is also a catalytic support in polymerization and biological processes.

Moreover the material has a great potential for medical applications. As it is capable of entrapping both hydrophilic and hydrophobic agents, it can be used as drug delivery system. Compared with other supports like carbon nanotubes, it is less expensive and has large surface area (better control of loading and elution profile). It is also suitable in protecting environment, acting as sorbent for different contaminants (dyes; heavy metals).

Plenty of new structural and functional hybrid materials based on HNTs should not be surprising. Due to their characteristics (nano-sized lumen, large surface area), no toxicity, low cost, high availability, we can expect more and more interesting research results and new areas of applications of this extremely interesting material.

Acknowledgements

The authors would like to thank The National Science Center of Poland (Grant No. 2011/03/B/ST5/01573) for financial support.

References

1. *“Hybrid Materials: Synthesis, Characterization, and Applications”*, G. Kicelbick, Ed.; Wiley-VCH, **2007**, ISBN: 9783527312993;
2. *“Functional Hybrid Materials”*, P. Gómez-Romero, C. Sanchez (Eds.),

- Wiley-VCH, **2003**, ISBN-10: 3527304843;
3. E.F. Vansant, P. Van Der Voort, K.C. Vrancken, “*Characterization and Chemical Modification of the Silica Surface*”, Elsevier Science B.V., 1995, ISBN: 0444819282;
 4. “*Fundamental and applied aspects of chemically modified surfaces*”, J.P. Blitz, C.B. Little (Eds.), Woodhead Publishing, **1999**, ISBN: 1 855738228;
 5. “*Chemistry of clays and clay minerals*”, Newman, A. C. D., Ed.; Longman Scientific and Technical: Harlow, **1987**, ISBN: 0582301149;
 6. R. Kamble, M. Ghag, S. Gaikawad, B.K. Panda, “Halloysite Nanotubes and Applications: A Review”, *J. Adv. Scient. Res.* **2012**, 3(2) 25-29;
 7. P. Yuan, P.D. Southon, Z. Liu, M.E.R. Green, J.M. Hook, S.J. Antill, C.J. Kepert, “Functionalization of Halloysite Clay Nanotubes by Grafting with γ -Aminopropyltriethoxysilane”, *J. Phys. Chem. C*, **2008**, 112, 15742-15751;
 8. P. Yuan, P. D. Southon, Z. Liu, C. J. Kepert, “Organosilane functionalization of halloysite nanotubes for enhanced loading and controlled release”, *Nanotechnology* **2012**, 23 (37) 375705;
 9. D. Tan, P. Yuan, F. Annabi-Bergaya, H. Yu, D. Liu, H. Liu, H. He, “Natural halloysite nanotubes as mesoporous carriers for loading of ibuprofen”, *Micropor. Mesopor. Mat.* **2013**, 179, 89-98;
 10. Yi Zhang, X. He, J. Ouyang, H. Yang, “Palladium nanoparticles deposited on silanized halloysite nanotubes: synthesis, characterization and enhanced catalytic property”, *Sci. Rep.* **2013**, 3, 2948;
 11. Y. Liu, X. Jiang, B. Li, X. Zhang, T. Liu, X. Yan, J. Ding, Q. Caib, J. Zhang, “Halloysite nanotubes@reduced graphene oxide composite for removal of dyes from water and as supercapacitors”, *J. Mater. Chem. A*, **2014**, Advance Article; 10.1039/C3TA14594H
 12. Q. He, D. Yang, X. Deng, Q. Wu, R. Li, Y. Zhai, L. Zhang, “Preparation, characterization and application of *N*-2-Pyridylsuccinamic acid-functionalized halloysite nanotubes for solid-phase extraction of Pb(II)”, *Water Res.* **2013**, 47, 3976-3983;
 13. R. Li, Q. He, Z. Hu, S. Zhang, L. Zhang, X. Chang, “Highly selective solid-phase extraction of trace Pd(II) by murexide functionalized halloysite nanotubes”. *Anal. Chim. Acta* **2012**, 713, 136-144;
 14. S.Y. Lee, S. J. Kim, “Adsorption of naphthalene by HDTMA modified kaolinite and halloysite”, *Appl. Clay Sci.* **2002**, 22 (1-2), 55-63;
 15. W. Jinhua, Z. Xiang, Z. Bing, Z. Yafei, Z. Rui, L. Jindum, C. Rongfeng, “Rapid adsorption of Cr(VI) on modified halloysite nanotubes”,

- Desalination* **2010**, 259, 22-28;
16. D. Jingmin, J. Wang, B. Zhang, Y. Zhao, J. Liu, "Cr(VI) adsorption on Mercaptopropyl-functionalized halloysite nanotubes", *Frusen. Environ. Bull.* **2010**, 19 (12), 2783-2787;
 17. M. Massaro, S. Riela, G. Cavallaro, M. Gruttadauria, S. Milioto, R. Noto, G. Lazzara, „Eco-friendly functionalization of natural halloysite clay nanotube with ionic liquids by microwave irradiation for Suzuki coupling reaction”, *J. Orgmet. Chem.* **2014**, 749, 410-415;
 18. Y. Lee, G.E. Jung, S.J. Cho, K.E. Geckeler, H. Fuchs, "Cellular interactions of doxorubicin-loaded DNA-modified halloysite nanotubes", *Nanoscale* **2013**, 5, 8577-8585;
 19. C. Chao, J. Liu, J. Wang, Y. Zhang, B. Zhang, Y. Zhang, X. Xiang, R. Chen, "Surface modification of halloysite nanotubes with dopamine for enzyme immobilization", *Appl. Mater. Interfaces* **2013**, 5, 10559-10564;
 20. Y. Lvov, E. Abdullayev, "Functional polymer–clay nanotube composites with sustained release of chemical agents", *Prog. Polym. Sci.*, **2013**, 38, 1690-1719;
 21. B. Mu, M. Zhao, P. Liu, "Halloysite nanotubes grafted hyperbranched (co)polymers via surface-initiated self-condensing vinyl (co) polymerization", *J. Nanopart. Res.*, 2008, 13, 831-838;
 22. M. Zou, M. Du, H. Zhu, C. Xu, Y. Fu, "Green synthesis of halloysite nanotubes supported Ag nanoparticles for photocatalytic decomposition of methylene blue", *J. Phys. D: Appl. Phys.*, **2012**, 45, 325302;
 23. J. Zhang, D. Zhang, A. Zhang, Z. Jia, D. Jia, "Dendritic polyamidoamine-grafted halloysite nanotubes for fabricating toughened epoxy composites", *Iran. Polym. J.* **2013**, 22, 501-510;
 24. S. Barrientos-Ramírez, G. Montes de Oca-Ramírez, E.V. Ramos-Fernández, A. Sepúlveda-Escribano, M.M. Pastor-Blas, A. González-Montielb, "Surface modification of natural halloysite clay nanotubes with aminosilanes. Application as catalyst supports in the atom transfer radical polymerization of methyl methacrylate", *Appl. Catal. A: General*, 2011, 406, 22-33;
 25. G. Cavallaro, G. Lazzara, S. Milioto, G. Palmisano, F. Parisi, "Halloysite nanotube with fluorinated lumen: Non-foaming nanocontainer for storage and controlled release of oxygen in aqueous media", *J. Colloid Interface Sci.*, **2014**, 417, 66-71;
 26. M.T. Albdiry, B.F. Yousif, "Role of silanized halloysite nanotubes on structural, mechanical properties and fracture toughness of thermoset

- nanocomposites”, *Mater. Des.*, **2014**, 57, 279–288;
27. D. Rawtani, Y.K. Agrawal, “Multifarious applications of halloysite nanotubes: a review”, *Rev. Adv. Mater. Sci.* **2012**, 30, 282-295;
28. M. Du, B. Guo, D. Jia, “Newly emerging applications of halloysite nanotubes: a review”, *Polym. Int.* **2010**, 59, 574-582.

Chapter 8

Acid-base equilibria in ‘oil-in-water’ microemulsions. The particular case of fluorescein dyes

Nikolay O. Mchedlov-Petrosyan, Natalya V. Salamanova,
and Natalya A. Vodolazkaya
*V.N. Karazin Kharkov National University, Svoboda Sq. 4,
61022 Kharkov, Ukraine*

1. Introduction

An increasing use of organized solutions in different branches of chemistry [1–13] calls for extending the concepts of ionic equilibria in these media. Lyophilic systems, that is, thermodynamically stable dispersions with well-reproducible properties, are probably most suitable for analytical chemistry and molecular spectroscopy. In addition to typical lyophilic dispersions, such as micellar solutions of colloidal surfactants in water, these systems include microemulsions usually formed by a colloidal surfactant, a hydrocarbon, and an alcohol, which possess limited solubility in water [1, 3, 5, 8, 14].

Protolytic equilibria in microemulsions have been studied less comprehensively than those in micellar solutions of surfactants. The corresponding publications are few in number [13, 15–22], as compared with the vast literature devoted to acid-base reactions in micellar solutions of surfactants. (See, for instance, some reviews [13, 23–25]).

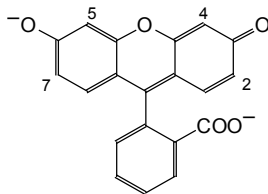
In order to fill up this gap, we decided to gain insight into the properties of microemulsions as media for such processes.

Our previous studies were devoted to determination of the parameters of ionic equilibria of a set of acid-base indicators in microemulsions stabilized by cationic, anionic, and non-ionic surfactants. In these colloidal systems, sulfonephthaleins, azo-dyes and some other common acid-base indicators, as well as solvatochromic Reichardt’s betaine dyes have been studied [20–22].

This work was aimed to systematic study of protolytic behavior of three widely used hydroxyxanthene luminophores, namely fluorescein and its 2,4,5,7-tetrabromo- and 2,4,5,7-tetraiodo derivatives (eosin and erythrosin,

respectively), in microemulsions of ‘oil-in-water’ type. Earlier we have already studied a set of hydroxyxanthene dyes in cationic surfactant-based microemulsions at high ionic strength of the aqueous phase [26, 27] and in reversed AOT-base water-in-oil microemulsions [27–29]. Basing on the results obtained, we have chosen the direct microemulsions ‘benzene – pentanol-1 – surfactant – water’ based on cationic, anionic, and non-ionic surfactants, under identical conditions. Following surfactants were used: cetyltrimethylammonium bromide, CTAB, sodium *n*-dodecylsulfate, SDS, and non-ionic surfactant Tween 80, TW 80.

Fluorescein dyes are widely used in analytical chemistry and neighboring fields, first of all owing to their unique fluorescent properties. The structure of fluorescein dianion is shown below:



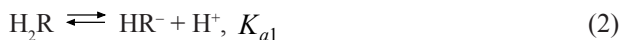
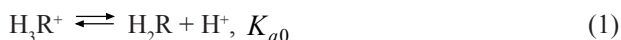
These dyes are applied for optical sensing of O_2 , CO_2 , H_2S , sulfur-containing organic compounds [30–34], as pH-sensors, including fiber-optical systems [32, 35–37], in biochemistry [38–45], as tracers for hydrological investigations [46]. These compounds are now intensively utilized in nanochemistry [47, 48] and as guest molecules in supramolecular chemistry [49, 50], as fluorescent dyes in molecular beacons [51], for imaging nitric oxide production [52, 53], etc. The spectral and acid-base behavior of the dyes in the presence of surfactants was examined [54, 57]. In some cases, the hydrophobic representatives of this family of dyes, bearing one or two long hydrocarbon chains [25, 42, 54, 55, 57–62], possess some advantages as compared with the parent compounds, e.g., in optical sensors [61], two-phase indicators [58, 59], for studying lyophilic colloidal systems [25, 42, 54, 55, 57, 60], etc. The fluorescent properties of fluorescein and its derivatives are recently used for creation of ratiometric fluorescent pH and temperature probes based on hydrophilic block copolymers [63] and for turn-on fluorescent detection of tartrazine in the presence of graphene oxide [64].

Most often, application of hydroxyxanthenes is connected primarily with embedding them into non-aqueous environments. So far the latter were modeled either by water-organic mixtures, or by micellar solutions of surfactants. In microemulsions, the particle diameter of the dispersed phase is usually larger as compared with common surfactant micelles, and the nanodroplets are considered

as swollen surfactant micelles [14]. Hence, microemulsions can be regarded as a transition step from surfactant micelles to organic solvents. On the other hand, microemulsions can be considered as reduced models of more complex objects, such as suspensions of phospholipid liposomes, polymer films, Langmuir–Blodgett multilayers, and sol-gel systems doped by surfactants.

Throughout the last decade, hydroxyxanthene dyes have been increasingly utilized in organic solvents. Thus, fluorescein was proposed for oxygen and carbon dioxide monitoring in dimethylformamide and dimethylsulfoxide solutions [30, 65]; some new studies are devoted to fluorescence lifetimes of fluorescein dianion [66] and to spectral properties of fluorescein monoanion [39] in organic media. Consequently, a further development of knowledge about the influence of non-aqueous media on the interconversions of the various prototropic forms of these substances is necessary.

The study of protolytic equilibria and visible spectra of organic dyes is a touchstone for research of the influence of microenvironment on the properties and reactivity of these substances. Acid-base ionization of fluorescein dyes in solution occurs stepwise [24, 26–29, 67–70]:



The detailed scheme of protolytic equilibria includes several tautomers of molecules and monoanions (Fig. 1). The most intensive absorption and fluorescence in the visible portion of the spectrum possesses the dianion **7**, and (in the case of substances with electron-acceptor substituents in the xanthene nuclei) also the monoanion **6b,c**. The latter tautomer is atypical for the parent compound fluorescein, but some traces of species **6a** may be detected in non-hydrogen bond donor solvents [70]. Until now, mono- and dianions possessing lactic structures are detected only in the case of nitro-substituted fluoresceins, e.g., for 2,4,5,7-tetranitrofluorescein [69].

Previously we have studied the protolytic equilibria of fluorescein and its derivatives in micellar solutions of surfactants [60, 71–74], in solutions of water-soluble dendrimers [75], in aqueous dispersions of CTAB-modified silica nanoparticles [76], in Langmuir–Blodgett films [77], and in aqueous solutions in the presence of β -cyclodextrin [78] and cationic calixarenes [79, 80].

A comparison of the obtained results with the parameters of protolytic

equilibrium in water and micellar solutions of the corresponding surfactants will enable us to predict the effect of microemulsions on organic reagents, which will provide a more rational use of this type of organized solutions in analytical chemistry.

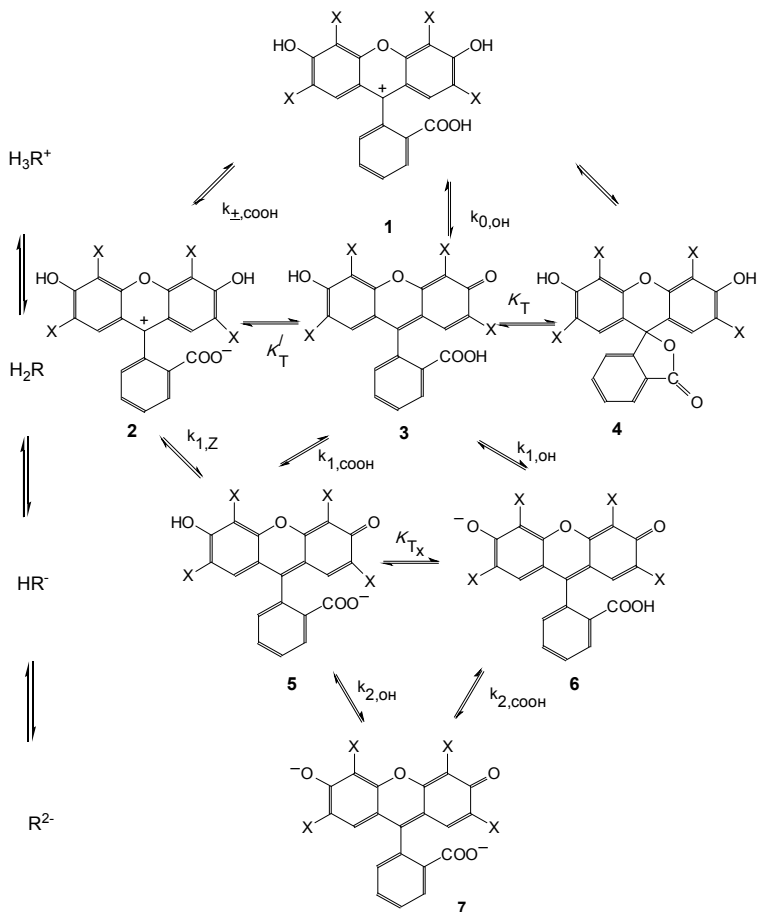


Figure 1. Protolytic conversions of hydroxyxanthenes; fluorescein ($X = H$): **1a-7a**, 2,4,5,7-tetrabromofluorescein (eosin) ($X = Br$): **1b-7b**, and 2,4,5,7-tetraiodofluorescein (erythrosin) ($X = I$): **1c-7c**

$$K_T = a_4/a_3; K_T^I = a_2/a_3; K_T^{II} = K_T / K_T^I = a_4/a_2; K_T^X = a_6/a_5; k_{\pm,COOH} = ha_2 / a_1;$$

$$k_{0,OH} = ha_3 / a_1; k_{1,Z} = ha_5 / a_2; k_{1,COOH} = ha_5 / a_3; k_{1,OH} = ha_6 / a_3; k_{2,OH} = ha_7 / a_5;$$

$$k_{2,COOH} = ha_7 / a_6.$$

A key characteristic of an indicator in organized solutions is the so-called 'apparent' ionization constant, K_a^{app} [13, 20–26, 71–74]:

$$pK_a^{app} = \text{pH} + \log\{[\text{HB}^z]/[\text{B}^{z-1}]\} \quad (4)$$

Here z and $(z-1)$ are charges of the conjugated indicator species ($\text{HB}^z \rightleftharpoons \text{B}^{z-1} + \text{H}^+$). We define the corresponding K_a^{app} constant as $K_{a(1-z)}^{app}$. The ratio of the equilibrium concentrations of these species can be derived from electronic absorption, while the pH values of the bulk (continuous, aqueous) phase are determined as a rule by using the glass electrode in a cell with liquid junction.

2. Experimental

2.1. Materials

The samples of xanthene dyes used in the present study were purified by re-precipitation or/and by column chromatography. Their purity was checked previously [26, 28, 29, 67, 68], and was additionally controlled by fluorescence excitation spectra of their aqueous alkaline solutions. Phosphoric and hydrochloric acids and potassium chloride were of analytical grade, stock CH_3COOH solutions were prepared from glacial acetic acid, the sample of sodium tetraborate was twice re-crystallized. The stock NaOH solution, prepared from saturated carbonate-free sodium hydroxide solution using CO_2 -free water, was kept protected from atmosphere and standardized using potassium biphthalate. CTAB (99 % purity) and TW 80 were from Sigma, the sample of SDS (98.1 % purity) was from Merck. Organic solvents were of analytical grade. Pentanol-1 was purified by standard procedure; the absence of aldehydes was checked by the UV-spectra.

2.2. Apparatus

Absorption spectra of dye solutions were measured using SF-46 apparatus (Russia), with optical path length $l = 1$ to 5 cm. The absorbance of reference solutions containing all the components except dyes was close to that of water. Fluorescence spectra were registered by Hitachi F 4010 fluorometer in the Laboratory of Professor A. O. Doroshenko, Kharkov National University. The results of zeta-potential determinations mentioned in this paper were obtained by Dr. L. V. Kutuzova in the Laboratory of Professor M. Ballauff, University of Bayreuth, Germany, as described previously [76, 79, 80]. The pH measurements of the bulk (aqueous) phase were performed at $25.0 \pm 0.1^\circ\text{C}$ on a P 37-1 potentiometer and pH-121 pH-meter equipped with ESL-63-07 glass electrode

reversible to H^+ ions and an $Ag/AgCl$ reference electrode in a cell with liquid junction (1 M KCl). Standard buffer solutions (pH 1.68, 4.01, 6.86, and 9.18) were used for cell calibration. The experimental uncertainty in the measured pH value did not exceed 0.02 pH unit (standard deviation).

2.2. Procedure

Stock microemulsions based on cationic surfactant were prepared by mixing 0.0047 mole of CTAB or CPC with 2.3 ml of pentanol-1, then 0.43 cm^3 of benzene and, finally, 5.5 cm^3 of H_2O were added [21, 22]. In the case of anionic microemulsions, 1.417 g of SDS were mixed with 3.46 cm^3 of alcohol, then 1.87 cm^3 of benzene and 22.7 cm^3 of H_2O were added; in the case of non-ionic microemulsions, the above quantities were as follows: 14.65 g (TW 80), 5.1 cm^3 (pentanol-1), 2.0 cm^3 (C_6H_6), and 11.85 cm^3 (H_2O) [21]. Working solutions were prepared by dilution of stock solutions with water, with addition of buffer components and aliquots of stock dye solutions, and made up to required volume at 25 °C. The volume fraction, φ , of organic phase in working solutions was calculated taking into account the amount of water in the stock microemulsion.

The pH values were varied as a rule applying buffer solutions. Acetate and phosphate buffer solutions were obtained by mixing required amounts of the stock acid solutions and the standard NaOH solution. Borax was used for creating higher pH values. The HCl solutions were used at $pH < 3.5$ and diluted NaOH at pH around 12. In all the cases, the ionic strength of aqueous solutions, I , was maintained constant ($= 0.05$ M) by additions of calculated amounts of KCl. Only at pH below 1.3, the ionic strength was higher, especially in the case of fluorescein.

The pK_a^{app} values were determined at $\varphi = 0.013$ vis-spectroscopically by the standard procedure [13, 20–29, 60, 71–74]. The systems under study contained 4.9 mole of pentanol-1 and 1 mole of benzene per 1 mole of CTAB, 9.3 mol of pentanol-1 and 2 mole of benzene per 1 mole of TW 80, and 6.5 and 4.3 mole of pentanol-1 and benzene per 1 mole of SDS, respectively; this corresponds to the stability region of the studied microemulsions [21, 22].

Stock aqueous solutions of dyes were prepared with small addition of NaOH. The working concentrations of dyes, C , were as a rule $(6$ to $20) \times 10^{-6}$ M during pK_a^{app} determination and $(3-4) \times 10^{-6}$ M at emission spectra measurements; in the case of fluorescein the H_2R spectra were measured at dye concentration 2×10^{-5} M.

The instrumental pH values of aqueous buffer solutions as a rule stay practically unchanged after organic phase adding; alterations observed in some cases are, probably, due to the partial binding of the buffer components by the

nanodroplets. However, from our previous studies it follows that in these cases the determined values of pK_a^a of indicators insignificantly differ from those obtained in other buffer systems [81]. Hence, the indicator ratio demonstrates stable response to the bulk pH value.

3. Results and discussion

3.1. Determination of apparent ionization constants

The pK_a^{app} values of the three dyes are determined in each of the three colloidal systems. Several representative pH-dependences of absorbances are depicted in Figure 2.

The stepwise ionization constants are calculated by using the dependences of A vs. pH at a fixed wave length and constant total dye concentration and optical path [Eq. (5)]:

$$A = \frac{A_{H_3R^+} h^3 + A_{H_2R} h^2 K_{a0}^{app} + A_{HR^-} h K_{a0}^{app} K_{a1}^{app} + A_{R^{2-}} K_{a0}^{app} K_{a1}^{app} K_{a2}^{app}}{h^3 + h^2 K_{a0}^{app} + h K_{a0}^{app} K_{a1}^{app} + K_{a0}^{app} K_{a1}^{app} K_{a2}^{app}} \quad (5)$$

Here A is the absorbance at the current pH value, $A_{R^{2-}}$, A_{HR^-} , A_{H_2R} and $A_{H_3R^+}$ are absorbances under conditions of complete conversion of the dye into the corresponding form, $h \equiv 10^{-pH}$. In the case of eosin and erythrosin, the pK_{a0}^{app} values lie in the far acidic region and are not determined here, and hence it is possible to simplify Eq. (5). Moreover, for fluorescein in cationic and non-ionic microemulsions, the pK_{a0}^{app} value can be estimated separately from pK_{a1}^{app} and pK_{a2}^{app} . For calculations of the pK_{a1}^{app} and pK_{a2}^{app} values of a dye in a given system, at least 15 solutions with various pH values at $I = 0.05$ M and not less than 12 wavelengths within the visible region are used. For determination of pK_{a0}^{app} value of fluorescein in non-ionic microemulsion, working solutions pH values within the range 1.30–2.40 are utilized; 4 wavelengths in the region of λ_{max} of cationic species, H_3R^+ , are used as analytical positions. The spectra at HCl concentrations 2 M and 3 M coincide, which allows regarding their absorbances as $A_{H_3R^+}$ values. In cationic microemulsions, the interval of working pH was 1.29–1.85; $I = 0.05$ M. And again, the spectrum of H_3R^+ species was obtained at high hydrochloride concentrations: the spectra of fluorescein at 2.0 M and 4.0 M of HCl coincide.

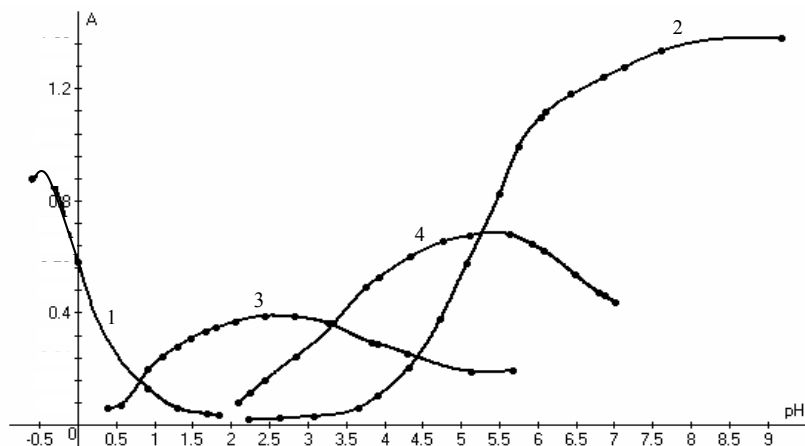


Figure 2. Plots of absorbance against pH: 1 – fluorescein, $C = 2.03 \times 10^{-5} \text{ M}$, $\lambda = 440 \text{ nm}$, 2 – fluorescein, $C = 2.03 \times 10^{-5} \text{ M}$, $\lambda = 490 \text{ nm}$, 3 – eosin, $C = 5.94 \times 10^{-6} \text{ M}$, $\lambda = 540 \text{ nm}$, 4 – erythrosin, $C = 7.56 \times 10^{-6} \text{ M}$, $\lambda = 550 \text{ nm}$; curves 1-3: microemulsions with CTAB, curve 4 – microemulsion with TW 80; all the data are re-calculated to optical path length 1 cm.

In a general case, the A_{HR^-} values are unavailable for direct measurements and are to be calculated jointly with the $\text{p}K_a^{\text{app}}$ values. The $A_{\text{R}^{2-}}$ values and first approximation of $A_{\text{H}_2\text{R}}$ values are obtained directly at suitable pH. The calculations were carried out using the CLINP program [82]. The $\text{p}K_a^{\text{app}}$ values are presented in Table 1.

3.2. The treatment of apparent ionization constants: electrostatic approach

The differences between apparent value in micellar solution or in microemulsion, $\text{p}K_a^{\text{app}}$, and the ‘aqueous’ value, $\text{p}K_a^w$, of the same indicator can be explained in terms of electrostatic theory [13, 24, 25].

The $\text{p}K_a^{\text{app}}$ value of the indicator couple $\text{HB}^z/\text{B}^{z-1}$ depends on the electrostatic surface potential Ψ of nanodroplets and on other equilibrium parameters [Eq. (6)]:

$$\text{p}K_a^{\text{app}} = \text{p}K_a^w + \log \frac{\gamma_{\text{B}}}{\gamma_{\text{HB}}} + \log \frac{f_{\text{B}}^m}{f_{\text{HB}}^m} - \frac{\Psi F}{2.303RT} - \log \frac{1 + P_{\text{B}}^{-1}(\varphi^{-1} - 1)}{1 + P_{\text{HB}}^{-1}(\varphi^{-1} - 1)} \quad (6)$$

Here pK_a^w is the thermodynamic value of pK_a in water, γ_i are the transfer activity coefficients of the corresponding species from water to the pseudophase, f_i^m are the concentration activity coefficients of the species bound by the pseudophase, Ψ is the electrical potential of the Stern layer, F is the Faraday constant, R is the gas constant, and T is absolute temperature. At $T = 298.15$ K, $2.303RT/F = 59.16$ mV.

Table 1. Indices of the apparent ionization constants values of hydroxyxanthene dyes in microemulsions; $\varphi = 0.013$, $I = 0.05$ M, 25 °C.

Fluorescein			Eosin		Erythrosin	
pK_{a0}^{app}	pK_{a1}^{app}	pK_{a2}^{app}	pK_{a1}^{app}	pK_{a2}^{app}	pK_{a1}^{app}	pK_{a2}^{app}
<u>Benzene – n-C₃H₁₁OH –CTAB</u>						
-0.03 ± 0.04^a	4.49 ± 0.03^a	5.62 ± 0.08^a	1.14 ± 0.08	3.69 ± 0.06	1.60 ± 0.07	4.03 ± 0.08
<u>Benzene – n-C₃H₁₁OH –TW 80</u>						
0.31 ± 0.07	6.46 ± 0.06	7.08 ± 0.04	3.64 ± 0.07	6.17 ± 0.04	3.47 ± 0.05	6.44 ± 0.04
<u>Benzene – n-C₃H₁₁OH – SDS</u>						
2.61 ± 0.04	5.53 ± 0.14	6.62 ± 0.07	3.57 ± 0.10	5.15 ± 0.10	4.41 ± 0.10	5.48 ± 0.10
<u>None (water, $I = 0.05$ M)</u>						
2.22^b	4.37^b	6.55^b	2.73^b	3.50^b	$\approx 3.8^b$	$\approx 4.8^b$

^a In analogous system, with CPC instead of CTAB, $pK_{a0}^{app} = 0.19 \pm 0.03$, $pK_{a1}^{app} = 4.34 \pm 0.02$, $pK_{a2}^{app} = 5.51 \pm 0.04$ [83]. ^b From ref. [29].

The ratio of the bulk (aqueous) and dispersed phases, v_w/v_m , is equal to $(\varphi^{-1} - 1)$. Taking into account high electrolyte concentration in the Stern layer, it is reasonable to regard the ratio f_B^m / f_{HB}^m as being close to unity [13, 24, 25]. The P_i are the partition constants of the corresponding species, i , between the bulk phase and the pseudophase. Thermodynamic P_i value is equal to the ratio of activities in corresponding phases ($P_i = a_i^m / a_i^w$). Taking into account the (possible) charge of the dye species the electrical potential of the nanodroplet/water interface, one obtains the following expression:

$$P_i = \gamma_i^{-1} e^{-z_i \Psi F / RT} \quad (7)$$

The value of the interfacial charge of the pseudophase is substantial. So, for the SDS-based system, the zeta-potential was estimated as $\zeta = -66 \pm 3$ mV;

for the earlier studied system benzene – *n*-pentanol – CPC [21, 22, 83, 84], $\zeta = +25 \pm 5$ mV. The size of the droplets in these two dispersions appeared to be surprisingly small, 4.4 and 4.85 nm, respectively, while for microemulsions of *n*-hexane, stabilized by *n*-pentanol and a non-ionic surfactant Triton X-100, the diameters are 9.6 and 16.6 nm for $\phi = 0.013$ and 0.129, respectively. (All data were determined in the presence 0.05 M NaCl.)

From Eq. (6) it is evident that the values ($\Delta pK_a^{app} = pK_a^{app} - pK_a^w$) in the given dye/microemulsion system depend on the completeness of binding and on the solvation character of bound species in the pseudophase. In the expression for the apparent pK_a^{app} value under conditions of practically complete binding of the indicator couple HB^2/B^{2-} , the last logarithmic term in Eq. (6) disappears.

3.3. Vis spectra of ionic and molecular species: structure and tautomerism

Having the K_{a1}^{app} and K_{a2}^{app} values (Table 1) made it possible to calculate the absorbances of HR^- ions at various wavelengths, and in such way to obtain the spectra of these species [Eq. (8)]:

$$A_{HR^-} = A + (A - A_{H_2R})h(K_{a1}^{app})^{-1} + (A - A_{R^{2-}})h^{-1}K_{a2}^{app}, \quad (8)$$

where A is absorbance at the current pH value. The interval $pK_{a1}^{app} \leq \text{pH} \leq pK_{a2}^{app}$ is used. The A_{HR^-} values, obtained jointly with the K_{a1}^{app} at analytical wavelength, are refined in the same manner. The ϵ_{HR^-} values are calculated using the A_{HR^-} values: $\epsilon_{HR^-} = A_{HR^-} l^{-1} C^{-1}$.

The A_{H_2R} values are, in turn, calculated by using Eq. (7), in order to avoid any influence of traces of intensely colored ions (H_3R^+ , HR^- and R^{2-}) on the spectra of the neutral forms:

$$A_{H_2R} = A + (A - A_{H_3R^+})hK_{a0}^{app-1} + (A - A_{HR^-})h^{-1}K_{a1}^{app}. \quad (9)$$

The molar absorptivities of neutral species are calculated as $\epsilon_{H_2R} = A_{H_2R} l^{-1} C^{-1}$. The spectra of individual ionic and molecular species of fluorescein, singled out in such manner, are typified in Figures 3–5. The λ_{max} values of hydroxyxanthene ions in microemulsions are compiled in Table 2.

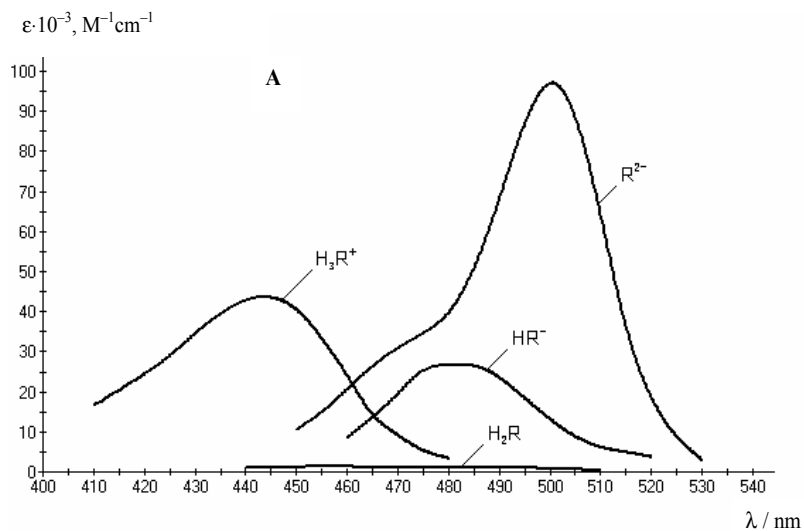


Figure 3. The absorption spectra of the equilibrium forms of fluorescein in the CTAB-based microemulsion.

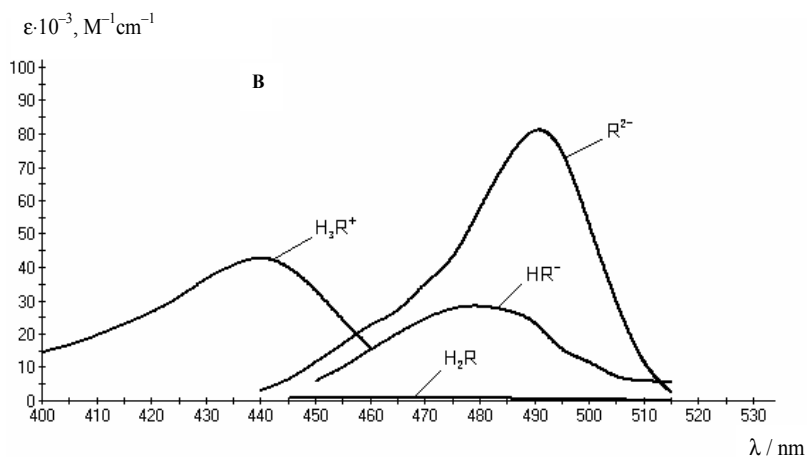


Figure 4. The absorption spectra of the equilibrium forms of fluorescein in the TW 80 based microemulsion.

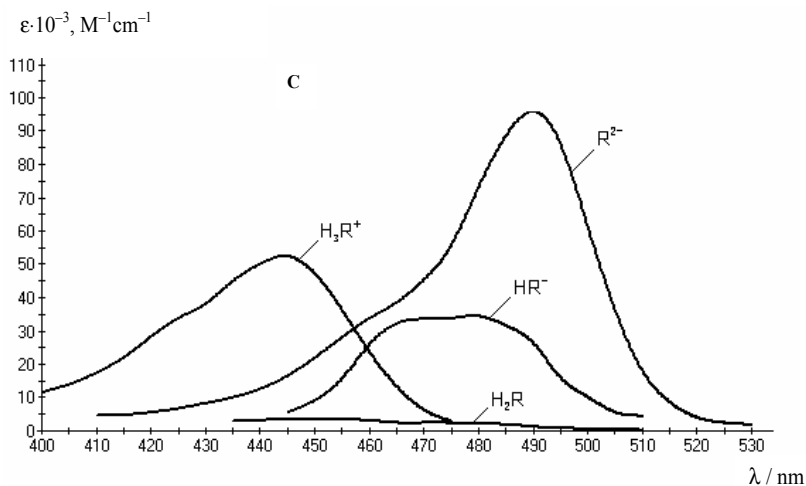


Figure 5. The absorption spectra of the equilibrium forms of fluorescein in the SDS-based microemulsion.

Table 2. The λ_{\max} /nm values of hydroxyxanthene ions in microemulsions; $\varphi = 0.013$.

	Water	Microemulsions		
		Benzene – $n\text{-C}_5\text{H}_{11}\text{OH} - \text{CTAB}$	Benzene – $n\text{-C}_5\text{H}_{11}\text{OH} - \text{TW 80}$	Benzene – $n\text{-C}_5\text{H}_{11}\text{OH} - \text{SDS}$
Fluorescein, H_3R^+	437	440	440	445
HR^-	455, 475	480	480	480
R^{2-}	490	500	490	490
Eosin, HR^-	517–519	540	540	525
R^{2-}	514–515	525	525	515
Erythrosin, HR^-	530	545	545	530
R^{2-}	525	532	533	525

The results for eosin and erythrosin are exemplified in Figures 6 and 7.

According to the main extrathermodynamic assumption, taken as a basis for studying tautomerism [24, 26–29, 67–76, 78–80, 85] and being confirmed by numerous published data [40, 55, 86–90], the spectra of species of types (3) and

(5) (Scheme 1) for the given dye are similar, and the ϵ_{\max} values may be taken as equal. The same is the case for the species of types (2) and (1).

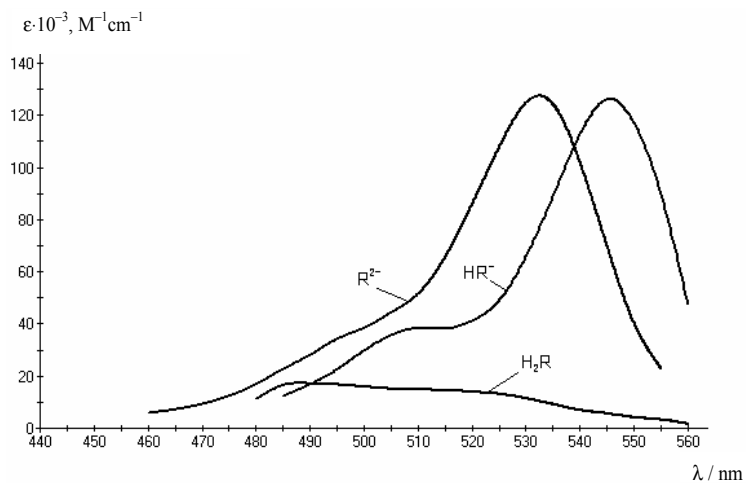


Figure 6. The absorption spectra of the equilibrium forms of erythrosin in the CTAB-based microemulsion.

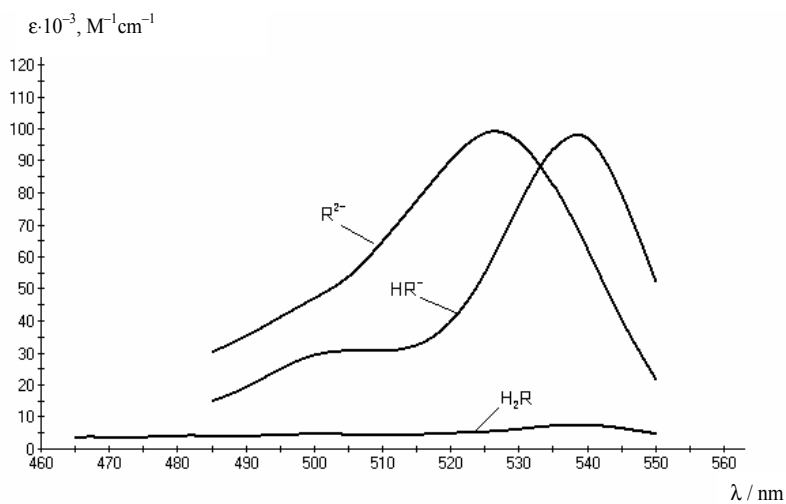


Figure 7. The absorption spectra of the equilibrium forms of eosin in the TW 80-based microemulsion.

The ionization of the carboxylic group in the 2' position ($\text{COOH} \rightarrow \text{COO}^-$) seriously affects only the charged xanthene chromophore, leading to blue shift of species (7) band as compared with the tautomer (6) band [24, 26–29, 67–71, 74, 91]. This experimental fact was confirmed by quantum-chemical calculations [92].

Hence, monoanions HR^- of eosin and erythrosin exist in microemulsions (Figs. 6 and 7) as tautomers (6b) and (6c), correspondingly, whereas the HR^- ion of fluorescein (Figs. 3–5) exists as tautomer (5a), like in other liquid media studied earlier. This is in agreement with sharp increase in the acidity of hydroxyl groups in the presence of two *ortho*-halogen substituents. Really, from Figure 1 it follows: $K_{T_x} = k_{1,\text{OH}} / k_{1,\text{COOH}}$. For unsubstituted fluorescein in water, $\text{p}k_{1,\text{OH}} = 6.3$, $\text{p}k_{1,\text{COOH}} = 3.5$, hence $K_{T_x} = 0.0016$. In the case of eosin in water, $\text{p}k_{1,\text{OH}} = 2.4$, $\text{p}k_{1,\text{COOH}} \approx 3.5$, and $K_{T_x} \approx 12$.

For fluorescein molecules H_2R in microemulsions, the total decrease in absorptivity as compared with the spectrum in water (where $\epsilon = 13.9 \times 10^3$ at 437 nm and $\epsilon = 3 \times 10^3$ to 4×10^3 within the range of 470–485 nm) and the disappearance of the band with λ_{max} near 440 nm (Fig. 8) indicate a distinct shift of tautomeric equilibrium towards the colorless lactone (4a) accompanied by absence of zwitter-ion (2a), just as in micellar systems [24, 26–29, 71–74], solutions of dendrimers [75], cyclodextrins [78], calixarenes [79, 80], and in organic solvents [24, 27, 67, 68, 70].

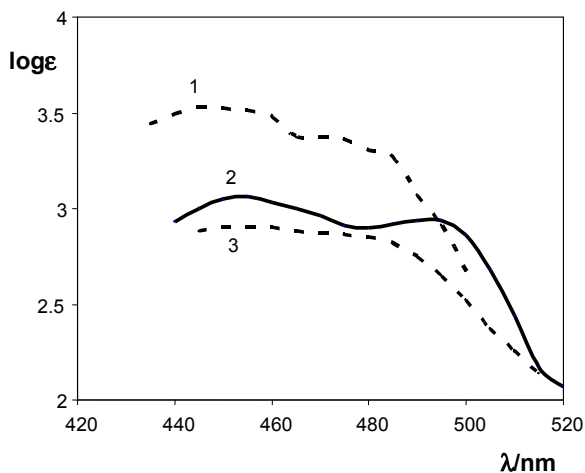


Figure 8. Absorption spectra of molecular form, H_2R , of fluorescein in SDS-based (1), in CTAB-based (2) and in TW 80-based (3) microemulsions; $\varphi = 1.3\%$, $C_{\text{HCl}} = 2\text{--}4\text{ M}$.

Taking ε_{\max} of tautomer (**3a**) equal to that of the ion HR^- (**5a**), one can estimate fractions (‘populations’) of tautomers, α . For instance, in cationic microemulsions, these values are as follows: $\alpha_{3a} = \varepsilon_{\max}(\text{H}_2\text{R})/\varepsilon_{\max}(\text{HR}^-) = 0.033$, $\alpha_{4a} = 1 - \alpha_{3a} = 0.967$, while α_{2a} is supposed to be equal to zero (or, at least, one may assume that $\alpha_{2a} \ll \alpha_{3a}$). For eosin and, even more so, for erythrosin the transfer from water to organic environments does not result in such sharp drops of the fractions of quinonoid tautomers (**3b**) and (**3c**), while zwitter-ionic tautomers are not typical for 2,4,5,7-tetrahalogen derivatives at all, due to the aforementioned high acidity of hydroxyl groups: $K_T' = k_{\pm, \text{COOH}}/k_{0, \text{OH}} = k_{1, \text{COOH}}/k_{1, \text{Z}}$ (Fig. 1).

Figure 9 confirms these regularities for the case of microemulsions.

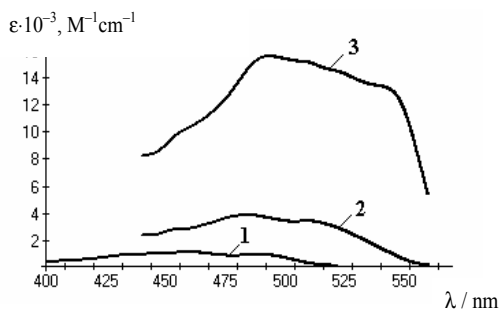


Figure 9. Absorption spectra of molecular forms, H_2R , of fluorescein (1), eosin (2), and erythrosin (3) in CTAB-based microemulsions ($\varphi = 1.3\%$, $C_{\text{HCl}} = 2-4\text{ M}$).

It is clear that the shifts of tautomeric equilibria result from binding of dye molecular species to the nanodroplets. However, such binding may be incomplete. And really, the molar absorptivities of the form H_2R of fluorescein in non-ionic TW 80-based and anionic SDS-based microemulsion at $\varphi = 0.026$ are correspondingly 1.57 and 1.96 times lower than those at $\varphi = 0.013$. Contrary to it, in the case of cationic CTAB-based microemulsions the $\varepsilon_{\text{H}_2\text{R}}$ values stay constant at different φ values. On the one hand, it is reasonable to suppose that only in the last case the binding is practically complete, while in the first two dispersed systems some of molecular species are still present in the bulk (aqueous) phase to certain extent. On the other hand, variations of φ values are known to cause size changes of microdroplets in some cases [14, 20–22].

3.4. Completeness of binding of different dye species to the microdroplets

In the most cases, the pK_a^{app} values differ substantially from the ‘aqueous’ pK_a s (Table 1). This gives evidence for association of the dyes with the organic droplets, though the completeness of the binding of the dye species to the pseudophase may be different. The conclusions concerning the state of the dyes in the colloidal systems may also be made using the comparison of the absorption and emission spectra in water with those at various φ values.

In cationic microemulsion, the anions R^{2-} and HR^- of all the three dyes are bound by positively charged microdroplets thanks to the electrostatic attraction, whereas the neutral species H_2R are solubilized due to their low solubility in the bulk water. Only in the case of the fluorescein cationic form, the electrostatic repulsion probably hinders complete binding. The bathochromic shift of the absorption bands of anions against the position in water is 7 to 22 nm (Table 2). Briefly, all the species of the three dyes studied are practically completely bound to cationic microemulsions, the single exception being the cationic species H_3R^+ (**1**). The last-named are observed at appropriate acidity only for fluorescein (**1a**). For eosin and erythrosin, the species H_3R^+ (**1b**, **1c**) appear at much higher acidity, than that for fluorescein (**1a**), and therefore for these two dyes the equilibrium (1) is not studied here at all.

In anionic microemulsions, the bands of anionic species display but modest shifts, whereas the bathochromic shift for the fluorescein cation reaches 8 nm. In non-ionic dispersions, the band positions of ions coincide with those in CTAB-based ones, with a sole exception of the fluorescein R^{2-} species. The latter is most hydrophilic among the three dianions, and its band with $\lambda_{max} = 490$ nm is like that in water.

Both absorption and emission spectra of R^{2-} dianion of fluorescein in anionic and non-ionic microemulsions, at various φ , stays unchanged as compared with those in water ($\lambda_{max}^m = 515$ nm). Hence, the dianion **7a** stays essentially in the aqueous phase. The pK_{a2}^{app} value of fluorescein in anionic microemulsion (6.62) is very close to that in water at the same I value (6.55), which allows to conclude that the monoanion HR^- (**5a**) is also practically not bound to the pseudophase. The pK_{a2}^{app} value of the dye in non-ionic microemulsion (7.08) is somewhat higher, which allows expecting the binding of a small fraction of (**5a**) ions to nanodroplets.

The emission spectrum of R^{2-} dianion of eosin in water changes negligibly in the presence of anionic nanodroplets, the same is the situation with the absorption spectrum (Table 2). However, absorption spectrum of monoanion HR^- (**6b**) changes markedly in both anionic and non-ionic microemulsions as compared with that in water (Table 2). Hence, the expressed difference of pK_{a2}^{app}

values of eosin in these systems (5.15 and 6.17, correspondingly) and in water at $I = 0.05$ M (3.50) is caused by transfer of (**6b**) species into the pseudophase. Moreover, the dianion (**7b**) is partly bound.

Figure 10 demonstrates the influence of binding by the pseudophase on the dianions R^{2-} fluorescence spectra.

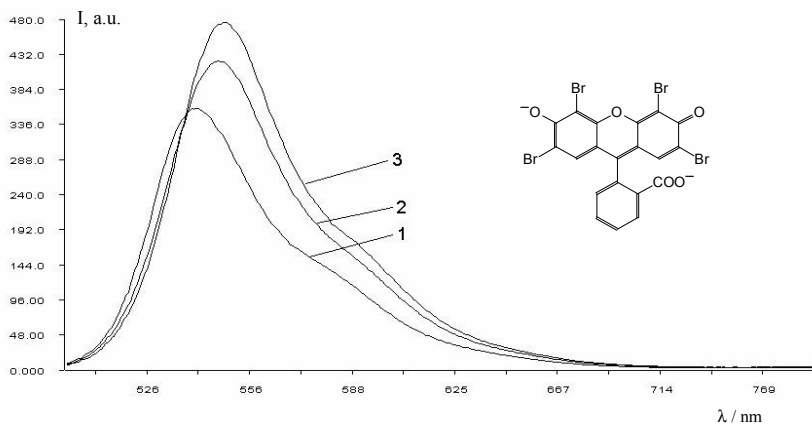


Figure 10. Fluorescence spectra of R^{2-} ion of eosin in water (1) and in non-ionic microemulsions (benzene – $n\text{-C}_5\text{H}_{11}\text{OH}$ – TW 80) at $\varphi = 0.013$ (2) and $\varphi = 0.026$ (3); $C_{\text{dye}} = 3.56 \times 10^{-6}$ M.

It must be noted that further increase in φ values results in such strong changes both in the character of nanodroplets and in the structure of aqueous phase, that alterations in emission spectra may reflect not only the degree of binding.

3.5. The medium effects and the ionization microconstants

The medium effects for the $\text{p}K_a^{\text{app}}$ values of fluorescein and eosin are gathered in Table 3. Some of them were qualitatively discussed above in terms of complete or incomplete binding. In some cases, however, the $\text{p}K_a^{\text{app}}$ s undergo different changes as compared with the corresponding $\text{p}K_a^{\text{w}}$ s even under conditions of practically complete binding of the dye species.

Such differentiating influence of non-aqueous media on the acid-base properties of the dissolved (solubilized) compounds is typical for surfactant micelles and was previously discussed in full [24–29, 71, 74–76].

Table 3. The medium effects on the indices of the ionization constants of fluorescein and eosin in microemulsions; $\varphi = 0.013$, $I = 0.05$ M, 25 °C

Dye/ ΔpK_a^{app}	The values of $\Delta pK_a^{app} = pK_a^{app} - pK_a^w$ in microemulsions:		
	in CTAB-based	in TW 80-based	in SDS-based
Fluorescein, $\Delta pK_{a0}^{app} =$	-2.17	-1.83	+0.47
$\Delta pK_{a1}^{app} =$	+0.04	+2.04	+1.08
$\Delta pK_{a2}^{app} =$	-1.18	+0.28	+0.12
Eosin, $\Delta pK_{a1}^{app} =$	-1.57	+0.83	+0.76
$\Delta pK_{a2}^{app} =$	-0.06	+2.42	+1.40

^a In accord with [Eq. (6)], the thermodynamic pK_a^w values are used in calculations: $pK_{a0}^w = 2.14$, $pK_{a1}^w = 4.45$, and $pK_{a2}^w = 6.80$ for fluorescein and $pK_{a1}^w = 2.81$ and $pK_{a2}^w = 3.75$ for eosin.

This demands a more circumstantial consideration of the protolytic equilibria. From the detailed ionization scheme (Fig. 1), following general equations can be derived:

$$pK_{a0} = pk_{0,OH} - \log(1 + K_T + K_T') = pk_{\pm,COOH} - \log\{1 + K_T'' + (K_T')^{-1}\}; \quad (10)$$

$$\begin{aligned} pK_{a1} &= pk_{1,COOH} + \log(1 + K_T + K_T') - \log(1 + K_{T_x}) \\ &= pk_{1,Z} + \log\{1 + K_T'' + (K_T')^{-1}\} - \log(1 + K_{T_x}) \\ &= pk_{1,OH} + \log(1 + K_T + K_T') - \log(1 + K_{T_x}^{-1}); \end{aligned} \quad (11)$$

$$pK_{a2} = pk_{2,COOH} + \log(1 + K_{T_x}^{-1}) = pk_{2,OH} + \log(1 + K_{T_x}); \quad (12)$$

The equations can be simplified taking into account that the K_{T_x} value is extremely low for fluorescein and high for eosin and erythrosin, and that $(1 + K_T + K_T')$ equals to α_3^{-1} . Namely, for fluorescein it is useful to express the pK_a values as follows:

$$pK_{a0} = pk_{0,OH} + \log \alpha_{3a}; \quad (13)$$

$$pK_{a1} = pk_{1,COOH} - \log \alpha_{3a}; \quad (14)$$

$$pK_{a2} = pk_{2,OH}, \quad (15)$$

whereas for eosin and erythrosin:

$$pK_{a1} = pk_{1,OH} - \log \alpha_{3bc}; \quad (16)$$

$$pK_{a2} = pk_{2,COOH}. \quad (17)$$

Now, the analysis of the medium effects in microemulsions, ΔpK_a^{app} , presented in Table 3, consists in considering the microscopic ionization constants, pk , and the corresponding Δpk values.

Also, it is worthwhile to regard the data obtained in microemulsions for some model compounds with a more simple ionization scheme (Fig. 11).

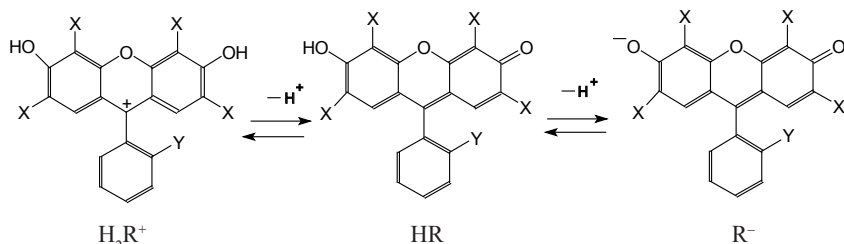


Figure 11. Protolytic conversions of sulfonefluorescein ($X = H$, $Y = SO_3^-$), 6-hydroxy-9-phenyl fluorone ($X = H$, $Y = H$), ethyl fluorescein ($X = H$, $Y = COOC_2H_5$), *n*-decyl fluorescein ($X = H$, $Y = COO-n-C_{10}H_{21}$), ethyl eosin ($X = Br$, $Y = COOC_2H_5$), and *n*-decyl eosin ($X = Br$, $Y = COO-n-C_{10}H_{21}$).

For fluorescein in cationic microemulsions, $K_T = 29$; $pk_{0,OH} = 1.45$; $pk_{1,COOH} = 3.01$; $pk_{2,OH} = 5.62$. The latter value coincides with the $pK_{a2}^{app} = pk_{2,OH} = 5.65$ value of sulfonefluorescein at the same bulk ionic strength in analogous cationic microemulsion [21]. (The sole difference consists in using of CPC instead of CTAB.) The $pK_{a1}^{app} = pk_{1,OH}$ values of 6-hydroxy-9-phenyl fluorone, ethyl fluorescein, and *n*-decyl fluorescein in the same system are lower: 5.04, 5.15, and 5.28 respectively [21]. This should be ascribed to the influence of the additional negative charge of the COO^- or SO_3^- groups in the case of fluorescein and sulfonefluorescein, in line with the Bjerrum–Kirkwood–Westheimer concept [24, 68, 71].

The $pK_{0,OH}$ values of 6-hydroxy-9-phenyl fluorone, ethyl fluorescein, and *n*-decyl fluorescein are equal to 1.70, 1.13, and 0.94 respectively [21]. In the last case, the long hydrophobic hydrocarbon chain ensures complete binding of the dye cation to the positively charged surface, and the decrease in $pK_{0,OH}$ as compared to the ‘aqueous’ value of the three last-named dyes and fluorescein (3.1) is more expressed, in accordance with Eq. (6). The $pK_{0,OH} = 1.45$ and hence $\Delta pK_{0,OH} = -1.65$ values of unsubstituted fluorescein ($Y = COOH$) are in-between those of model compounds with $Y = H$ and $Y = COOC_2H_5$.

The $\Delta pK_{1,COOH} = -0.48$ value of fluorescein markedly differs from $\Delta pK_{2,OH} = -1.18$. This phenomenon is numerously repeated in all the afore-cited papers of our group and should be explained in terms of the γ_j values [Eq. (6)]: the increase in the pK_a values of carboxylic acids on going from water to non-aqueous environments is more pronounced as compared with that of phenols [68]. This effect may in some cases even overcome the negative contribution of the $-\Psi/59$ term in Eq.(6). Another reason for the positive ΔpK_{a1}^{app} value of fluorescein in the cationic microemulsion is the rise in α_{4a} : 0.967 against 0.670 in water.

For eosin in cationic microemulsions, $pK_{1,OH} = -1.65$; this value agrees semi-quantitatively with those for model compounds, ethyl and *n*-decyl eosin, in CPC-based microemulsions: $pK_{1,OH} = -1.2$ to -1.3 [21]. The $\Delta pK_{2,COOH} = -0.06$ value for eosin is much less negative, in accordance with the above-mentioned peculiarity of the behavior of the carboxylic group on going from water to organic environment. Note, that all the ΔpK s are estimated in respect to the thermodynamic values in water. This $\Delta pK_{2,COOH}$ value is also less negative as compared with that of $\Delta pK_{1,COOH}$ (see above), because other things being equal the strength of the anionic acids decreases more noticeably as compared with that of the neutral ones [24, 25].

The increase in the bulk ionic strength results in the rise of the pK_a^{app} s, owing to the shielding of the surface charge of the CTAB-based pseudophase. For fluorescein, the pK_{a1}^{app} and pK_{a2}^{app} are 5.84 and 6.50 respectively at 1 M KCl [26]; the $pK_{a0}^{app} = -0.07$ value [26] is practically the same as at $I = 0.05$ M, because the cationic form H_3R^+ is evidently still located in the bulk, whereas the H_2R form is uncharged. Only in CTAB micellar solutions at 4 M KCl, $pK_{a0}^{app} = 0.60$, $pK_{a1}^{app} = 6.41$, and $pK_{a2}^{app} = 7.17$ [71].

For eosin, the regularities are quite similar. Here, the pK_{a1}^{app} and pK_{a2}^{app} values in cationic microemulsions at 1 M KCl and cationic micelles at 4 M KCl are 1.74 and 5.27 [26] and 1.83 and 5.76 [71] respectively.

Earlier, Kibblewhite *et al.* [54] reported the pK_a^{app} values for lipoidal

derivatives of fluorescein and eosin, fixed in micelles of cationic, anionic, and non-ionic surfactants. The long hydrocarbon chain in the 4'-position of the phthalic acid residue ensures complete binding of all the dyes species by any kind of pseudophase. For cationic micelles both at low and high ionic strength the results are rather close to ours. A detailed comparison is hindered by the difference of the I values.

For anionic micelles some data for completely bound lipoidal dyes markedly differ from ours. So, for fluorescein in SDS-based microemulsions, $pK_{a0}^{app} = 2.61$, $pK_{a1}^{app} = 5.53$, and $pK_{a2}^{app} = 6.62$ (Table 1), while for the lipoidal fluorescein in SDS micelles at low ionic strength $pK_{a0}^{app} = 3.98$, $pK_{a1}^{app} = 5.97$, and $pK_{a2}^{app} = 8.84$ [54]. The last high pK_{a2}^{app} value reflects the binding of the HR^- and R^{2-} species to the negatively charged surface: the $-\Psi/59$ item in Eq. (6) makes a substantial contribution in this case. Correspondingly, the $pK_{a1}^{app} = 8.52$ value of *n*-decyl fluorescein (Fig. 11) in SDS-based microemulsion at $I = 0.05$ M [21] is also high.

5. Conclusions

The present work was devoted to protolytic equilibria of three common hydroxyxanthene luminophores, fluorescein, eosin, and erythrosin, in direct 'benzene-in-water' microemulsions stabilized by pentanol-1 and surfactants: cationic (CTAB), anionic (SDS), and non-ionic (Tween 80). The vis-absorption spectra of dye species and 'apparent' ionization constants (twenty one values) were determined at volume fraction of the dispersed phase $\varphi = 0.013$ and bulk ionic strength $I = 0.05$ M (KCl + buffer). Conclusions concerning tautomerism of the molecular and ionic species were deduced from the spectral data.

The strong differentiating influence of the dispersed phase of microemulsions of different types on the acid-base properties of dyes was explained in terms of shifts of tautomeric equilibrium, specificity of microenvironmental effects, and selective binding of various dye species to the microdroplets.

Concluding, the examined microemulsions affect the complicated protolytic equilibria of the dissolved hydroxyxanthene dyes practically in the same manner as those of simple indicators studied earlier [21, 25].

References

1. *Organized Solutions. Surfactants in Science and Technology*, eds. S.E. Friberg, B. Lindman, Marcel Dekker, Inc.: N. Y., 1992.
2. Berthod, A.; Garcia-Alvarez-Coque, C. *Micellar Liquid Chromatography*. Marcel Dekker, Inc.: N.Y.–Basel, 2000.

3. Shtykov, S.N. *Zh. Anal. Khim.*, **2002**, *57*, 1018–1028.
4. Pallavicini, P.; Diaz-Fernandez, Y.A.; Foti, F.; Mangano, C.; Patroni, S. *Chem. Eur. J.*, **2007**, *13*, 178–187.
5. Holmberg, K. *Eur. J. Org. Chem.*, **2007**, 731–742.
6. Khan, M.N. *Micellar Catalysis*. CRC Press: Boca Raton, 2007.
7. Popov, A. F. *Pure Appl. Chem.*, **2008**, *80*, 1381–1397.
8. Onel, L.; Buurma, N.J. *Annu. Rep. Prog. Chem., Sect. B.*, **2009**, *105*, 363–379.
9. Pallavicini, P.; Diaz-Fernandez, Y.A.; Pasotti, L. *Coord. Chem. Rev.*, **2009**, *253*, 2226–2240.
10. Gainanova, G. A.; Vagapova, G. I.; Syakaev, V. V.; Ibragimova, A. R.; Valeeva, F. G.; Tudriy, E. V.; Galkina, I. V.; Kataeva, O. N.; Zakharova, L. Ya.; Latypov, Sh. K.; Konovalov, A. I. *J. Coll. Int. Sci.* **2012**, *367*, 327–336.
11. Karpichev, Y.; Matondo, H.; Kapitanov, I.; Savsunenko, O.; Vendrenne, M.; Poinot, V.; Rico-Lattes, I.; Lattes, A. *Cent. Eur. J. Chem.*, **2012**, *10*, 1059–1065.
12. Manet, S.; Karpichev, Y.; Dedovets, D.; Oda, R. *Langmuir* **2013**, *29*, 3518–3526.
13. Mchedlov-Petrossyan, N. O.; Vodolazkaya, N. A.; Kamneva, N. N. Acid-base equilibrium in aqueous micellar solutions of surfactants. In: *Micelles: Structural Biochemistry, Formation and Functions & Usage*, N. Y.: Nova Publishers, 2013. Chapter 1.
14. *Microemulsions Structure and Dynamics*, Friberg, S.E. and Bothorel, P., Eds., Boca Raton: CRC, 1987. Translated under the title *Mikroemul'sii: struktura i dinamika*, Moscow: Mir, 1990.
15. Letts, K.; Mackay, R. A. *Inorg. Chem.* **1975**, *14*, 2990–2993.
16. Hermansky, C.; Mackay, R. A. *J. Colloid Int. Sci.* **1980**, *73*, 324–331.
17. Mackay, R. A.; Jacobson, K.; Tourian, J. *J. Colloid Int. Sci.* **1980**, *76*, 515–524.
18. Mackay, R. A. *Adv. Colloid Int. Sci.* **1981**, *15*, 131–156.
19. Berthod, A.; Saliba, C. *Analisis* **1986**, *14*, 414–420.
20. Mchedlov-Petrosyan, N. O.; Isaenko, Yu. V.; Tychina, O. N. *Zh. Obshch. Khim.* **2000**, *70*, 1963–1971.
21. Mchedlov-Petrossyan, N. O.; Isaenko, Yu. V.; Salamanova, N. V.; Alekseeva, V. I.; Savvina, L. P. *Zh. Anal. Khim.* **2003**, *58*, 1140–1154.
22. Mchedlov-Petrossyan, N. O.; Isaenko, Yu. V.; Goga, S. T. *Zh. Obshch. Khim.* **2004**, *74*, 1871–1877.
23. Mchedlov-Petrossyan, N. O.; Vodolazkaya, N. A.; Timiy, A. V.;

- Gluzman, E. M.; Alekseeva, V. I.; Savvina, L. P. <http://preprint.chemweb.com/physchem/0307002>.
24. Mchedlov-Petrosyan, N. O. *Differentiation of the Strength of Organic Acids in True and Organized Solutions*, Kharkov National University Press: Kharkov, 2004.
 25. Mchedlov-Petrosyan, N. O. *Pure Appl. Chem.* **2008**, *80*, 1459–1510.
 26. Vodolazkaya, N. A.; Gurina, Yu. A.; Salamanova, N. V.; Mchedlov-Petrosyan, N. O. *J. Mol. Liquids* **2009**, *145*, 188–196.
 27. Mchedlov-Petrosyan, N. O.; Vodolazkaya, N. A.; Gurina, Yu. A.; Sun, W.-C.; Gee, K. R. *J. Phys. Chem. B* **2010**, *114*, 4551–4564.
 28. Vodolazkaya, N. A.; Mchedlov-Petrosyan, N. O.; Salamanova, N. V.; Surov, Yu. N.; Doroshenko, A. O. *J. Mol. Liquids* **2010**, *157*, 105–112.
 29. Vodolazkaya, N. A.; Kleshchevnikova, Yu. A.; Mchedlov-Petrosyan, N. O. *J. Mol. Liquids* **2013**, *187*, 381–388.
 30. Choi, M. F.; Hawkins, P. *J. Chem. Soc., Faraday Trans.* **1995**, *91*, 881–885.
 31. Choi, M.F.; Hawkins, P. *Sensors and Actuators. B.* **1997**, *39*, 390–394.
 32. Choi, M.M.F. *J. Photochem. Photobiol. A* **1998**, *114*, 235–239.
 33. Chan, M. A.; Lam, S. K.; Lo, D. *J. Fluoresc.* **2003**, *12*, 327–332.
 34. Bailey, R. T.; Cruickshank, F. R.; Deans, G.; Gillanders, R. N.; Tedford, M. C. *Anal. Chim. Acta* **2003**, *487*, 101–108.
 35. Fuh, M. R. S.; Burgess, L. W.; Hirschfeld, T.; Christian, G. D.; Wang, F. *Analyst* **1987**, *112*, 1159–1163.
 36. Pringsheim, E.; Zimin, D.; Wolfbeis, O. S. *Adv. Mater.* **2001**, *13*, 819–822.
 37. Guan, X.; Liu, X.; Su, Z.; Liu, P. *Reactive Funct. Polym.* **2006**, *66*, 1227–1239.
 38. Sjöback, R.; Nygren, J.; Kubista, M. *Biopolymers* **1998**, *46*, 445–453.
 39. Klonis, N.; Clayton, A. H. A.; Voss, E. W.; Sawyer, W. H. *Photochem. Photobiol.* **1998**, *67*, 500–510.
 40. Klonis, N.; Sawyer, W. H. *Photochem. Photobiol.* **2003**, *77*, 502–509.
 41. Yakovleva, J.; Davidsson, R.; Lobanova, A.; Bentsson, M.; Eremin, S.; Laurell, T.; Emneus, J. *Anal. Chem.* **2002**, *74*, 2994–3004.
 42. Kubica, K.; Langner, M.; Gabrielska, J. *Cellular a. Molecular Biol. Lett.* **2003**, *8*, 943–954.
 43. Slyusareva, E. A.; Gerasimov, M. A.; Sizykh, A. G.; Gornostaev, L. M. *Russ. Phys. J.* **2011**, *54*, 485–492.
 44. Yadav, R.; Das, S.; Sen, P. *Austr. J. Chem.* **2012**, *65*, 1305–1313.
 45. Efron, N. *Clin. Exp. Optom.* **2013**, *96*, 400–421.

46. Gerke, K. M.; Sidle, R. C.; Mallants, D. *J. Hydrol. Hydromech.* **2013**, *61*, 313–325.
47. Zhang, F.; Shi, F.; Ma, W.; Gao, F.; Jiao, Y.; Li, H.; Wang, J.; Shan, Z.; Lu, X.; Meng, S. *J. Phys. Chem. C* **2013**, *117*, 14659–14666.
48. Nagarajan, N.; Paramaguru, G.; Vanitha, G.; Renganathan, R. *J. Chem. (Hidwani Publ. Corp.)* **2013**, Article ID 585920, 7 pages.
49. Hahn, U.; Gorka, M.; Vögtle, F.; Vicinelli, V.; Ceroni, P.; Maestri, M.; Balzani, V. *Angew. Chem. Int. Ed.* **2002**, *41*, 3595–3598.
50. Marchioni, F.; Venturi, M.; Credi, A.; Balzani, V.; Belohradsky, M.; Elizarov, A. M.; Tseng, H.-R.; Stoddart, J. F. *J. Amer. Chem. Soc.* **2004**, *126*, 568–573.
51. Li, J. J.; Fang, X.; Tan, W. *Biochem. Biophys. Res. Comm.* **2002**, *292*, 31–40.
52. Kojima, H.; Urano, Y.; Kikuchi, K.; Higuchi, T.; Hirata, Y.; Nagano, T. *Angew. Chem. Int. Ed.* **1999**, *38*, 3209–3212.
53. Nagano, T.; Yoshimura, T. *Chem. Rev.* **2002**, *102*, 1235–1269; and references cited therein.
54. Kibblewhite, J.; Drummond, C. J.; Grieser, F.; Thistlethwaite, P. J. *J. Phys. Chem.* **1989**, *93*, 7464–7473.
55. Song, A.; Zhang, J.; Zhang, M.; Shen, T.; Tang, J. *Coll. Surf. A* **2000**, *167*, 253–262.
56. Pellosi, D. S.; Estevão, B. M.; Semensato, J.; Severino, D.; Baptista, M. S.; Politi, M.J.; Hioka, N.; Caetano, W. *J. Photochem. Photobiol. A* **2012**, *247*, 8–15.
57. Pellosi, D. S.; Estevão, B. M.; Freitas, C. F.; Tsubone, T. M.; Caetano, W.; Hioka, N. *Dyes Pigments* **2013**, *99*, 705–712.
58. Brown, L.; Halling, P. J.; Johnston, G. A.; Suckling, C. J.; Valivety, R. H. *J. Chem. Soc., Perkin Trans. 1* **1990**, 3349–3353.
59. Halling, P. J.; Han, Y.; Johnston, G. A.; Suckling, C. J.; Valivety, R. H. *J. Chem. Soc., Perkin Trans. 2* **1995**, 911–918.
60. Loginova, L. P.; Samokhina, L. V.; Mchedlov-Petrossyan, N. O.; Alekseeva, V. I.; Savvina, L. P. *Colloids Surf. A* **2001**, *193*, 207–219.
61. Schröder, C. R.; Weidgans, B. M.; Klimant, I. *Analyst* **2005**, *130*, 907–916.
62. Zhanga, X.-F.; Liub, Q.; Wang, H.; Fua, Z.; Zhang, F. *J. Photochem. Photobiol. A* **2008**, *200*, 307–313.
63. Hu, J.; Zhang, X.; Wang, D.; Hu, X.; Liu, T.; Zhang, G.; Liu, S. *J. Mater. Chem.* **2011**, *21*, 19030 – 19038.
64. Huang, S. T.; Shi, Y.; Li, N. B.; Luo, H. Q. *Chem. Comm.* **2011**, *48*,

- 747–749.
65. Choi, M. F.; Hawkins, P. *Spectrosc. Lett.* **1994**, *27*, 1049–1063.
 66. Magde, D.; Rojas, G.; Seybold, P. *Photochem. Photobiol.* **1999**, *70*, 737–744.
 67. Mchedlov-Petrosyan, N. O.; Tychina, O. N.; Berezhnaya, T. A.; Alekseeva, V. I.; Savvina, L. P. *Dyes Pigments* **1999**, *43*, 33–46.
 68. Mchedlov-Petrosyan, N. O.; Kukhtik, V. I.; Bezugliy V. D. *J. Phys. Org. Chem.* **2003**, *16*, 380–397.
 69. Mchedlov-Petrosyan, N. O.; Vodolazkaya, N. A.; Surov, Yu. N.; Samoylov, D. V. *Spectrochim. Acta A* **2005**, *61*, 2747–2760.
 70. Mchedlov-Petrosyan, N. O.; Vodolazkaya, N. A.; Salamanova, N. V.; Roshal, A. D.; Filatov, D. Yu. *Chemistry Lett.* **2010**, *39*, 30–31.
 71. Mchedlov-Petrosyan, N. O.; Kleshchevnikova, V. N. *J. Chem. Soc., Faraday Trans.* **1994**, *90*, 629–640.
 72. Mchedlov–Petrosyan, N. O.; Timiy, A. V.; Vodolazkaya, N. A. <http://preprint.chemweb.com/physchem/0203011>.
 73. Mchedlov-Petrosyan, N. O.; Isaenko Y. V.; Vodolazkaya, N. A.; Goga, S. T. <http://preprint.chemweb.com/physchem/0309005>.
 74. Vodolazkaya, N. A.; Shakhova, P. V.; Mchedlov-Petrosyan, N. O. *Zh. Obshch. Khim.* **2009**, *79*, 1081–1089.
 75. Mchedlov-Petrosyan, N. O.; Bryleva, E. Yu.; Vodolazkaya, N. A.; Dissanayake, A. A.; Ford, W.T. *Langmuir* **2008**, *24*, 5689–5699.
 76. Bryleva, E. Yu.; Vodolazkaya, N. A.; Mchedlov-Petrosyan, N. O.; Samokhina, L. V.; Matveevskaya, N. A.; Tolmachev, A. V. *J. Colloid Int. Sci.* **2007**, *316*, 712–722.
 77. Bezkravnaya, O. N.; Mchedlov-Petrosyan, N. O.; Vodolazkaya, N. A.; Alekseeva, V. I.; Savvina, L. P.; Yakubovskaya, A. G. *Zh. Prikl. Khim.* **2008**, *81*, 659–666.
 78. Bogdanova, L. N.; Mchedlov-Petrosyan, N. O.; Vodolazkaya, N. A.; Lebed, A. V. *Carbohydr. Res.* **2010**, *345*, 1882–1890.
 79. Cheipesh, T. A.; Mchedlov-Petrosyan, N. O.; Zagorulko, E. S.; Rodik, R. V.; Kalchenko, V. I. *Dopovidi NAN Ukrainy*, **2013**, no. 12, 131–138.
 80. Cheipesh, T. A.; Zagorulko, E. S.; Mchedlov-Petrosyan, N. O.; Rodik, R. V.; Kalchenko, V. I. *J. Mol. Liquids* **2014**, *193*, 232–238.
 81. Mchedlov-Petrosyan, N. O.; Vodolazkaya, N. A.; Yakubovskaya, A. G.; Grigorovich, A. V.; Alekseeva, V. I.; Savvina, L. P. *J. Phys. Org. Chem.* **2007**, *20*, 332–344.
 82. <http://www-chemo.univer.kharkov.ua/kholin/clinp.html>
 83. Salamanova, N. V.; Vodolazkaya, N. A.; Mchedlov-Petrosyan, N. O.

- Kharkov University Bull.* **2003**, no. 596, Chemistry, issue 10 (33), 137–141.
84. Nikiforova, E. M.; Bryleva, E. Yu.; Mchedlov-Petrossyan, N. O. *Zh. Fiz. Khim.* **2008**, *82*, 1614–1618.
85. Mchedlov-Petrossyan, N. O. *Zh. Anal. Khim.* **1979**, *34*, 1055–1059.
86. Chen, S. C.; Nakamura, H.; Tamura, Z. *Chem. Pharm. Bull.* **1979**, *27*, 475–479.
87. Zhao, Z. G.; Shen, T.; Xu, H.-J. *Spectrochim. Acta.* *1989*, *45 A*, 1113–1116.
88. Amat-Guerri, F.; Lopez-Gonzalez, M. M. C.; Sastre, R.; Martinez-Utrilla, R. *Dyes Pigments* **1990**, *13*, 219–232.
89. Klonis, N.; Sawyer, W. H. *J. Fluoresc.* **1996**, *6*, 147–157.
90. Orte, A.; Crovetto, L.; Talavera, E. M.; Boens, N.; Alvarez-Pez, J. M. J. *Phys. Chem. A.* **2005**, *109*, 734–747.
91. Mchedlov-Petrossyan, N. O.; Salamanova N. V.; Vodolazkaya, N. A.; Gurina, Yu. A.; Borodenko, V. I. *J. Phys. Org. Chem.* **2006**, *19*, 365–375.
92. Mchedlov-Petrossyan, N. O.; Ivanov, V. V. *Zh. Fiz. Khim.* **2007**, *81*, 117–121.

Chapter 9

Functional polymers forming complexes with metal ions

Michał Cegłowski and Grzegorz Schroeder
*Adam Mickiewicz University in Poznań, Faculty of Chemistry,
Umultowska 89b, 61-614 Poznań, Poland*

1. Introduction

Polymer chemistry is among the most important disciplines of material science. Innovative monomer design and a wide range of synthetic strategies allow production of polymers of unique properties. Also over the last two decades, a variety of methods allowing performance of chemical reactions on already polymerized macromolecules have been developed. Many industrially important polymers that possess catalytically active or other functional groups are obtained by the reaction of a polymer chain with an appropriate functionalizing agent [1].

Functional polymers show specific properties such as adhesion, repellence, pH-stability, anti-corrosion etc. Their quality and advanced attributes make them materials with almost unlimited potential of application. The term functional polymer has two meanings:

- a polymer that includes in its structure a functional organic group that is ready to be involved in chemical reactions,
- a polymer showing specific properties and thus be able to be used for a particular purpose for which it has been designed [2].

Coordination compound consists of an central atom or ion that is surrounded by anions or molecules with which it is joined by chemical bonds. The groups that are bonded to the central metal or ion are known as ligands. The chemical bonds that connect central atom or ion with ligands are coordinate or coordinate-covalent in character. The coordination compounds include e.g. biological substances such as vitamin B₁₂ or hemoglobin and synthetic compounds such as dyes, pigments and catalysts [3].

A polymer-metal complex is composed of a polymer and a metal atom or ion, which forms a coordinate bond with a polymer donor site. Such donor sites, which usually contain atoms such as nitrogen, sulfur or oxygen, are introduced by polymerization of appropriate monomer or by chemical functionalization

of a polymer chain with a molecule that is capable of forming coordination compounds. Polymer-metal complexes have found application as heterogeneous catalysts [4, 5], chelating resins for water treatment [6-8] or recovery of trace metal ions [9, 10], hydrometallurgy [11, 12] and polymeric carries of diagnostic agents [13].

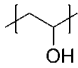
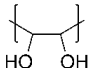
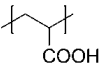
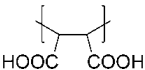
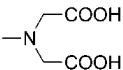
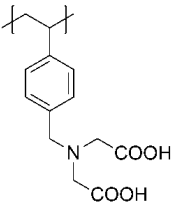
2. Structure and synthesis of polymer-metal complexes

The functional polymers that form complexes with metal ions can be classified in many ways based on method of synthesis, structure or their principal use. The methods of synthesis include making a complex between a polymeric ligand and a metal ion and polymerization of a monomer that already contains a metal ion.

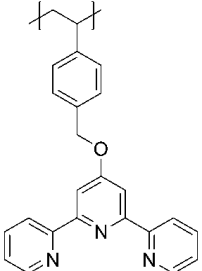
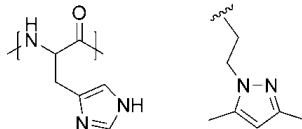
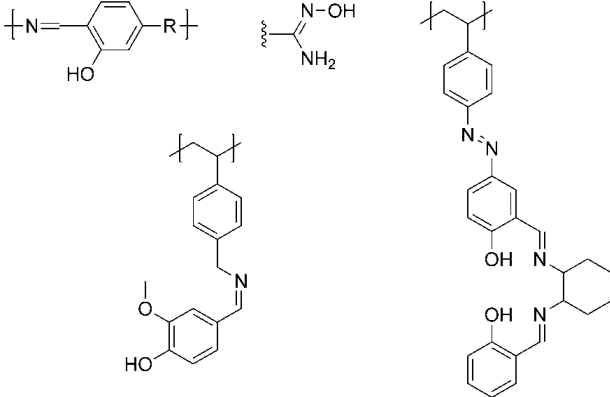
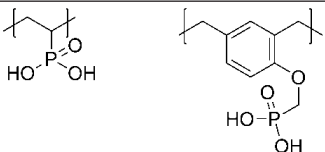
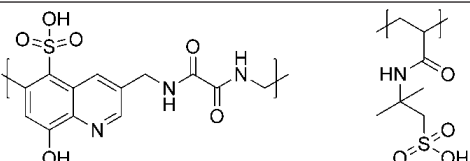
2.1. Reaction of polymeric ligand with metal ion

In water a metal ion forms hydrated ions or complex compounds with different molecules. To bind a metal ion from a solution, a polymer ligand must make more stable complex than the ions or neutral molecules. The nature of the ligand and the strength of bond formed with the metal ion is therefore the fundamental issue in every extraction system. The ligands may be classified according to the characteristic functional groups and/or donor atoms incorporated in their structure. The most commonly used ligands are presented in Table 1. It is worth noticing that some polymers may contain a mixed ligand system to improve their chelating properties or enhance selectivity towards a particular ion.

Table 1. Commonly used polymer ligands.

Coordinating group	Structure of polymer ligand unit			
Alcohols				
Carboxylic acids				

Coordinating group	Structure of polymer ligand unit					
Ketones, ester, amides						
Thiols						
Amines						
Pyridines						
Bipyridines						

Coordinating group	Structure of polymer ligand unit
Terpyridines	
Pyrazoles, imidazoles	
Schiff bases	
Phosphoric acids	
Sulfonic acids	

The reactions between a polymeric ligand and a metal ion can be divided into two groups depending on the structure obtained. The first group are pendant metal complexes, whereas the second groups are inter/intra-molecular complexes [14].

Pendant metal complexes can be classified as monodentate or polydentate complexes depending on the kind of ligand attached to the polymer chain. If the ligand has one donor site it can form monodentate complexes, if it has multiple donor sites it can form polydentate complexes with metal ions.

In the monodentate polymer-metal complexes the ligand donor site occupies one coordinate site of the metal ion, whereas other coordination sites are usually occupied by low-molecular weight anions. If a ligand has several coordination sites it is possible to obtain monodentate complex by appropriate tuning the polymer/metal ratio. If a large excess of metal ion is used, it is highly probable that all donor sites form coordination compounds with only one metal ion, resulting in a monodentate polymer-metal complexes. An example of a monodentate polymer-metal complex is presented in Figure 1.

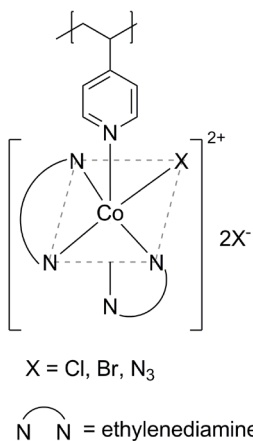


Figure 1. An example of a monodentate polymer-metal complex.

Polydentate ligands are more widespread in polymer-metal complexes. These complexes are usually more stable than those formed by monodentate ligands and have well-defined coordination structure. This is the reason why most of chelating resins possess in their structure a polydentate ligand. An exemplary polydentate polymer-metal complex is presented in Figure 2 [15].

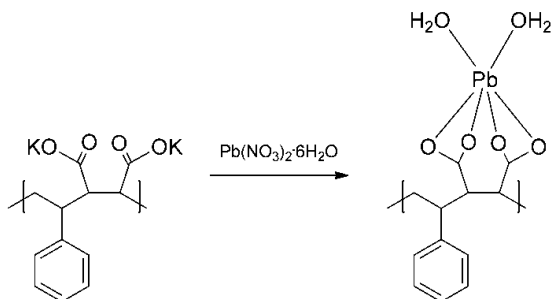


Figure 2. An example of a polydentate polymer-metal complex.

When a metal ion has four or six coordination binding sites, it can create bonds with different ligands that are attached to the main polymer chain or even ligands that are connected to different polymer chains. The first complex type is called intra-polymer chelate, whereas the second one is called inter-polymer chelate. A schematic presentation of these two types of polymer-metal complexes is given in Figure 3.

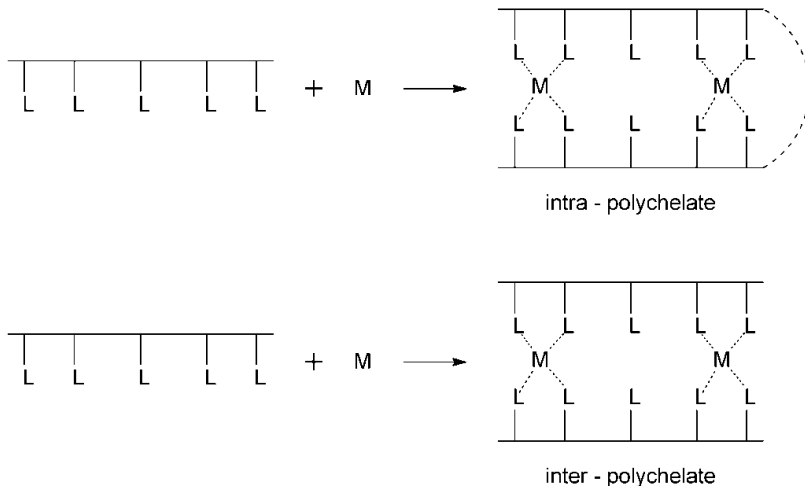


Figure 3. Schematic representation of intra- and inter-polychelates.

From the experimental point of view it is very difficult to distinguish whether a particular polymer-metal complex has an inter- or intra-molecular bridging. In

many examples the product obtained is a mixture of inter and intra-chelates. If the intra-chelate complex, predominates in the overall structure, the product of the reaction is usually insoluble and precipitate from the reaction mixture.

2.2. Polymerization of monomer-metal complexes

This method of synthesis is used to prepare polymer-metal complexes with well-defined coordination structure. The materials obtained are frequently used as heterogeneous catalysts or redox centres. The polymers are usually prepared by radical or ionic polymerization.

Figure 4 presents an exemplary monomer and polymer obtained by the method of polymerization. The polymer was prepared using controlled polymerization by employing the reversible addition–fragmentation chain transfer polymerization (RAFT) with cumyl dithiobenzoate as a chain transfer agent. The obtained side-chain cobaltocenium containing polymer was a metal-containing polyelectrolyte that showed characteristic redox behaviour of cobaltocenium [16].

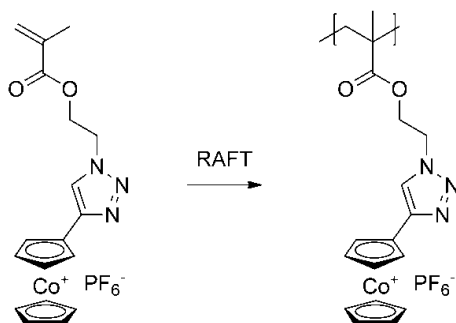


Figure 4. Synthesis of side-chain cobaltocenium-containing polymer.

3. Applications of polymeric ligand systems

3.1. Ion removal

Chelating polymers are used for removal or selective adsorption of heavy metal ions. In many industries, such as mining, hydrometallurgical processes and processes of removal of pollutants it is essential to recover specifically a particular ion. By using appropriate chelating polymer it is possible to reduce overall consumption of energy and materials in this process. Chelating resins are used on a very large scale in water-softening to replace calcium and magnesium ions with monovalent ions.

Removal of Ca, Mg, Pb, Zn metals present as pollutants in Ag-NaCl

solution was conducted on a Lewatit TP-260 ion exchange resin. This resin is an amphoteric aminomethylphosphonic polymer, capable of forming high-affinity complexes with divalent metal ions. Successful separation was achieved in both counter-current and cross-current configurations. Silver was collected in over 99% purity with practically 100% yield. Column efficiency and the liquid to solid flow rate ratio were found to have strong influence on the process performance. It was shown that counter-current simulated moving-bed process can be used for purification of precious metal solutions with overall high yield [17].

Purolite S930 chelating resin, a macroporous polystyrene based chelating resin with iminodiacetic groups, was used for adsorption of copper and nickel, from the pulps being side products of the leaching of low-grade sulfide ores. At the solution pH of around 3, the copper, nickel, and cobalt recovery for a long contact time exceeded 99%. Unfortunately it was established that in the presence of silicic acid in the pulp the rate of recovery of the metals decreased. To ensure high recovery, sorption was carried out at a temperature increased to around 50°C [18].

Uranium mining and hydrometallurgical processes produce a large number of uranium waste water, which can be a serious threat to the environment. Polyamidoamine modified poly(styrene-co-divinylbenzene) adsorbents carrying phosphorus functional groups were prepared and used as adsorbents for adsorption of uranium(VI) from aqueous solution. The maximum adsorption capacity of 99.89 mg/g was observed at pH 5 and the initial uranium concentration of 100 mg/L. The adsorbent obtained has been used repeatedly and adsorption and desorption percentage did not show any noticeable decline after 27 cycles [19].

The adsorption properties of chelating polymer obtained by modification of commercially available ammoniated polystyrene beads with *P,P*-dichlorophenylphosphine oxide toward U(VI) were evaluated using the batch adsorption method. The maximum adsorption rate of U(VI) of 99.72% was noted at 318 K and pH 5. The U(VI) adsorption capacity increased with contact time and attained equilibrium within 4 h [20].

An ion exchange polymer was obtained by immobilization of Kemp's triacid derivatives onto a TentaGel resin. The chelating module was shown to form a 1 : 1 complex with the uranyl ion in solution. The new polymer was completely recyclable with no detectable aging and showed unusual activity for a carboxylate ligand in solutions of high ionic strength. The resins uranyl extraction efficiency was maintained even in the seawater [21].

The concentration of thorium isotopes in seawater is a key parameter in investigation of marine biogeochemical cycles, because they are important tracers for collecting information on the suspended particulate matter dynamics

in the ocean. Their concentration in seawater is extremely low (few fg per kg), therefore co-precipitation methods have been widely used for preconcentration of its radioisotopes. DIAION CR-20 chelating resin, which has a polyamine group as a chelating ligand bonded onto a highly porous crosslinked polystyrene matrix, was used to recover thorium isotopes that co-precipitate with iron hydroxide. Using the proposed method, the time of preconcentration for 5 L seawater samples was markedly reduced from a few days to 3–4 h [22].

The adsorption of Th(IV) and U(VI) was studied on chelating resin synthesized through copolymerization of glycidyl methacrylate in the presence of divinylbenzene followed by further immobilization with 3,4,5-trihydroxybenzoic acid. The novel chelating resin showed a high capacity for Th(IV) and U(VI), maximum adsorption of Th(IV) and U(VI) was 56 and 83.6 mg/g, respectively. The adsorption of Th(IV) and U(VI) was found to proceed according to pseudo second order kinetics, indicating the influence of textural properties of resin on the rate of adsorption [23].

Poly(amido)amine dendron was grown on the surface of styrene divinylbenzene by the divergent polymerization method. This new polymer has been investigated in liquid–solid extraction of thorium. The maximum adsorption capacity of thorium ions was determined to be 36.2 mg/g at 298 K [24].

A chelating ion resin, prepared by functionalization of Merrifield resin with 2,2'-pyridylimidazole, was used to selectively adsorb and separate nickel from other metal ions from their solutions. Even in highly acidic sulfate solution, this adsorbent's efficiency was pretty high with loading capacities in the range 56–79 mg Ni/g resin [25].

Separation of cobalt from mixed-waste mobile phone batteries containing LiCoO₂ cathodic active material was investigated using selective precipitation and chelating resin. Chelating resin was synthesized by polymerization of acrylonitrile followed by amidoximation reaction. Physically cross-linked gel of polyacrylonitrile was obtained by a cooling technique. Cobalt was recovered from the active powder materials containing 47% Co oxide together with Mn, Cu, Li, Al, Fe, and Ni oxides [26].

Poly(1,3-thiazol-2-yl methacrylamide-co-4-vinylpyridine-co-divinylbenzene) was prepared and used as a sorbent for the solid-phase extraction of Cr(VI). The adsorption capacity and binding equilibrium constant were calculated to be 80.0 mg/g and 0.018 L/mg, respectively. The polymer was applied as a sorbent for chromium from stream water and waste water samples [27].

Sorption properties of Presep® PolyChelate resin, which is chelate resin modified with carboxymethylated polyethylenimine were examined. This material showed excellent sorption potential for the solid-phase extraction of the Cd, Co,

Cu, Fe, Mo, Ni, Pb, V and Zn elements. The resin's performance was superior to other commercially available aminocarboxylic acid-type chelating resins [28].

A solid phase preconcentration method has been developed using a new chelating resin prepared by immobilization of 4-(2-thiazolylazo)resorcinol on Chromosorb 106 polymer. The method was optimized for determination of rare earth elements in seawater and estuarine water samples by inductively coupled plasma mass spectrometry. The resin shows large sorption capacity for lanthanides ranging from 81.1 $\mu\text{mol/g}$ for Lu and 108 $\mu\text{mol/g}$ for Nd [29].

Chelating terpolymer resin was synthesized from anthranilic acid, 2-amino pyridine and formaldehyde. The chelating properties of the terpolymer resin were evaluated by the batch equilibrium method for Fe^{3+} , Co^{2+} , Ni^{2+} , Cu^{2+} , Zn^{2+} and Pb^{2+} . It was established that the resin acted as an excellent cation-exchanger. Compared to the commercially available phenolic and polystyrene resins, the resin obtained showed an excellent ion-exchange capacity with the selected metal ions [30].

Polyacrylonitrile fiber with a chelating ligand was obtained by grafting fibers with iminodiacetic acid. The material obtained showed good potential for enrichment of trace amount of Nd(III) from large sample volumes. The sorption capacity of functionalized resin was 8.9 mg/g. The profile of Nd(III) uptake on the sorbent proved good accessibility of the chelating sites in the modified fibers [31].

Polyacrylonitrile-2-aminothiazole resin was synthesized by simple reaction of polyacrylonitrile beads with 2-aminothiazole. The functional group capacity and the percentage conversion of the functional group of the polymeric material prepared under the optimum conditions were 3.94 mmol/g and 41.10%, respectively. The resin shows much better adsorption capacity of 454.9 mg/g towards Hg(II) than towards other metal ions. This chelating polymer could be regenerated through the desorption of Hg(II) anions using nitric acid solution to be reused [32].

3.2. Catalytic properties

The role of catalysts is to increase the rate of chemical reaction without being consumed. Catalyst are divided into homogenous or heterogeneous ones. The former are used as solutions, whereas the latter are usually used in solid state. The advantage of heterogeneous catalysts is the ease of their separation from the products.

Catalytic activity of a heterogeneous catalyst, obtained by adsorption of Cu(II) ions onto a macroporous chelating polymer, functionalized with diethylenetriamine, was examined in decolorization and mineralization of Orange G dye in aqueous solutions with hydrogen peroxide. The catalyst obtained

showed good stability and was efficient for the decolorization and mineralization of Orange G dye under mild reaction conditions. Complete color removal for the dye concentration of 50 mg/L was achieved in 30 min at 24°C and in 15 min at 50°C. The heterogeneous catalyst tested is a cost effective alternative for the treatment of wastewaters containing Orange G dye [33].

A tetradentate Schiff base, obtained from triethylenetetramine and salicylaldehyde, has been covalently bonded to divinylbenzene cross-linked chloromethylated polystyrene. After the reaction with CuCl_2 , CoCl_2 and NiCl_2 , appropriate polymer-bound transition metal complexes have been obtained. The catalytic activities of these polymeric complexes were tested for the liquid-phase oxidation of olefins using hydrogen peroxide as the oxidant. Excellent yield and selectivity of these catalysts toward the oxidation of olefins were observed. The catalysts were found to exhibit higher catalytic activity than those of the corresponding neat complexes. Figure 5 presents the structure of catalysts obtained [34].

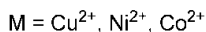
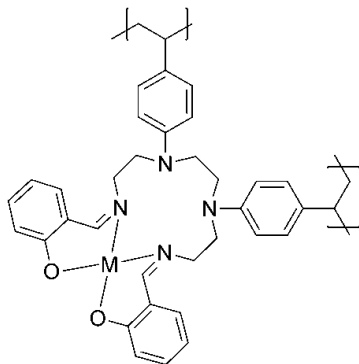


Figure 5. Structure of polymer-anchored Schiff base complex [34].

Catalyst for the Huisgen's [3+2]azide-alkyne cycloaddition have been prepared by immobilization of copper(I) on commercially available polymers functionalized with 1,5,7-triazabicyclo[4.4.0]dec-5-ene. The new catalytic systems enabled development of regioselective, convergent, operationally simple and efficient three-component transformations that allow rapid assembly of 1,2,3-triazoles from simple and readily available starting materials. Figure 6 presents the structure of the functional polymer obtained [35].

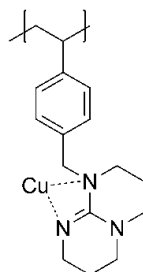


Figure 6. The polymeric catalysts for the Huisgen's [3+2] azide-alkyne cycloaddition [35].

An amphiphilic block copolymer (Figure 7) bearing a chelating *N,N*-dipyrid-2-ylamide-based ligand was prepared via ROMP using a Mo-based Schrock initiator. Functionalization with Rh(I) yielded a polymer catalyst that was used for the hydroformylation of 1-octene under micellar conditions. The use of a micellar catalyst was found to favor the formation of *n*-aldehyde by suppressing the isomerization propensity of a catalyst. The use of the micellar setup allows to reuse the polymeric catalyst and reduce the metal contamination of the products [36].

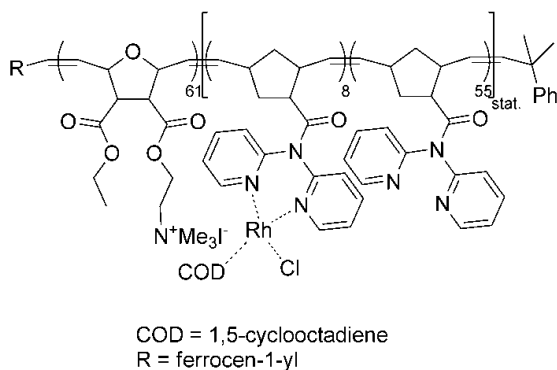


Figure 7. Structure of polymer-rhodium hydroformylation catalyst [36].

Molecularly imprinted polymer beads have been prepared by polymerization of methacryloylhistidine complexes with Co^{2+} , Ni^{2+} or Zn^{2+} (Figure 8) and applied as catalyst in the hydrolysis of paraoxon which is an organophosphate ester that is used as a pesticide. The catalytic performance of polymers having Co^{2+} , Ni^{2+}

or Zn^{2+} ions was evaluated according to the enzyme kinetic model of Michaelis–Menten and their activities were compared to each other. The use of polymers of methacryloylhistidine complexes with Co^{2+} , Ni^{2+} , or Zn^{2+} ions provided an increase in the hydrolysis rate by a factor of 356, 241, and 95, respectively, with respect to that in non-catalyzed media that contained only buffer [37].

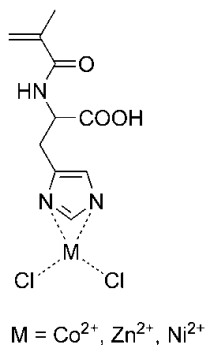


Figure 8. The structure of monomeric methacryloylhistidine complexes with Co^{2+} , Ni^{2+} , or Zn^{2+} [37].

3.3. Biocide properties

The advantages offered by antimicrobial polymers over their low molecular weight analogues include a reduction of agents residual toxicity, increased efficiency and selectivity and prolonged lifetime. Moreover, these materials are non-volatile, chemically stable and do not permeate through skin [1].

Polymer-bound Schiff bases and Cr(III) complexes have been synthesized by the reaction of 4-benzyloxybenzaldehyde, polymer-bound with 2-aminophenol, 2-amino-4-chlorophenol and 2-amino-4-methylphenol. The structures of polymer-metal complexes are presented in Figure 9. All these compounds have also been investigated for antibacterial activity by the well-diffusion method against *Staphylococcus aureus* (RSKK-07035), *Shigella dysenteria* type 10 (RSKK 1036), *Listeria monocytogenes* 4b(ATCC 19115, *Escherichia coli* (ATCC 1230), *Salmonella typhi* H (NCTC 901.8394), *Staphylococcus epidermis* (ATCC 12228), *Brucella abortus* (RSKK-03026), *Micrococcus luteus* (ATCC 93419, *Bacillus cereus* sp., *Pseudomonas putida* sp. and for antifungal activity against *Candida albicans* (Y-1200-NIH). Polymer-bound Schiff bases and their Cr(III) complexes have proven to possess moderate or high activity against examined germs except *S. dysenteria* type 10. According to the results of biological activity, the polymers obtained may be used in various applications as antimicrobial agents [38].

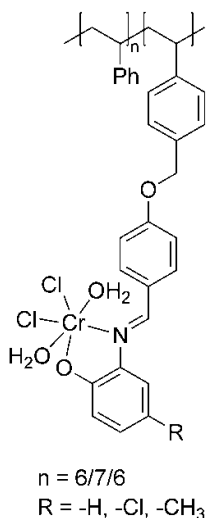


Figure 9. Structure of polymer-bound Schiff bases Cr(III) complexes [38].

A terpolymer involving 2-amino-6-nitrobenzothiazole, melamine, and formaldehyde has been synthesized in the presence of dimethyl formamide medium. The polymer obtained was used to prepare complexes with Cu^{2+} , Ni^{2+} and Zn^{2+} ions, whose structure is presented in Figure 10. The antibacterial activity of the terpolymer and its Cu(II), Ni(II), and Zn(II) complexes was determined by the disc diffusion method with Amoxicillin as the standard antibiotic. The prepared compounds were tested against *S. sonnei*, *E. coli*, *Klebsiella species*, *S. aureus*, *B. subtilis*, and *S. typhimurium* microbes. The studies showed that the ligand and its metal chelates stronger inhibit the growth of *E. coli*, *Klebsiella species*, and *B. subtilis*, whereas the inhibition of the growth of *S. sonnei*, *S. aureus*, and *S. typhimurium* was at a reasonable level [39].

Phenylthiourea–formaldehyde polymer has been synthesized via polycondensation of phenylthiourea and formaldehyde in basic medium. The corresponding metal complexes were prepared with Mn(II), Co(II), Ni(II), Cu(II) and Zn(II) ions (Figure 11). The antibacterial activity of the polymer-metal complexes obtained was tested against *Bacillus subtilis*, *B. megaterium*, *S. aureus*, *E. coli*, *P. aeruginosa* and *S. typhi* using agar well diffusion method, whereas their antifungal activity was examined against *C. albicans*, *T. species*, *A. flavus*, *A. niger*, *F. species*, and *M. species*. All synthesized polymers showed excellent antimicrobial activity against several bacteria and fungi. The polymer-

Cu(II) complex showed the highest antibacterial as well as antifungal activity, interpreted as related to a higher stability constant of Cu(II) ions [40].

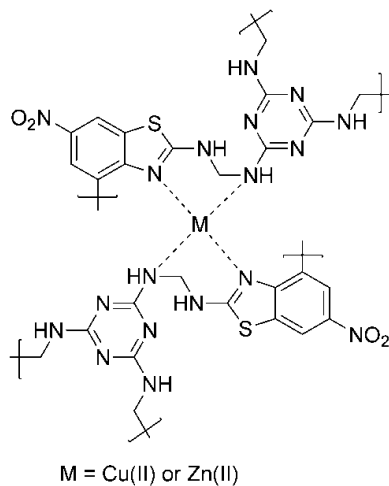


Figure 10. Proposed structure of terpolymer-metal complexes [39].

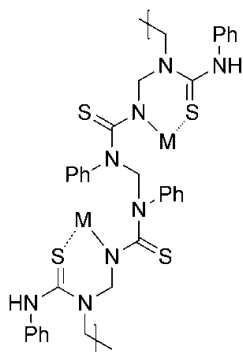


Figure 11. Structure of phenylthiourea-formaldehyde polymer complexes with metal ions [40].

4. Conclusions

Complexes of polymers with metal ions have been widely investigated to understand the relationship between the structure of polymer-metal complex and its chemical properties. The progress in such investigation has been possible thanks to the fact that much information about the structure and properties of polymer-metal complexes can be obtained by analytical methods such as UV-VIS, EPR, NMR, IR or CD spectroscopy and measuring redox potentials. For further development more detailed studies of polymer-metal complexes should be undertaken, including examination of higher-order structure of polymer and dynamic changers in the structure of polymer ligand, determination of configuration within the coordination sphere and stability of the complex formed.

Acknowledgements

This work was supported by the Polish National Science Center (NCN; decision no. DEC-2012/05/N/ST5/01274).

References

1. B.L. Rivas, E. Pereira, A. Maureira, Functional water-soluble polymers: polymer-metal ion removal and biocide properties, *Polym. Int.*, 58 (2009) 1093-1114.
2. K. Horie, M. Barón, R.B. Fox, J. He, M. Hess, J. Kahovec, T. Kitayama, P. Kubisa, E. Maréchal, W. Mormann, R.F.T. Stepto, D. Tabak, J. Vohlidal, E.S. Wilks, W.J. Work, Definitions of terms relating to reactions of polymers and to functional polymeric materials (IUPAC Recommendations 2003), *Pure Appl. Chem.*, 76 (2004) 889-906.
3. T. Kaliyappan, P. Kannan, Co-ordination polymers, *Prog. Polym. Sci.*, 25 (2000) 343-370.
4. S.B. Kim, R.D. Pike, D.A. Sweigart, Multifunctionality of Organometallic Quinonoid Metal Complexes: Surface Chemistry, Coordination Polymers, and Catalysts, *Acc. Chem. Res.*, 46 (2013) 2485-2497.
5. H. Jiang, J. Jiang, H. Wei, C. Cai, Heterogeneous Cyanation Reaction of Aryl Halides Catalyzed by a Reusable Palladium Schiff Base Complex in Water, *Catal. Lett.*, 143 (2013) 1195-1199.
6. X. Ma, Y. Li, Z. Ye, L. Yang, L. Zhou, L. Wang, Novel chelating resin with cyanoguanidine group: Useful recyclable materials for Hg(II) removal in aqueous environment, *J. Hazard. Mater.*, 185 (2011) 1348-1354.

7. P.K. Neghlani, M. Rafizadeh, F.A. Taromi, Preparation of aminated-polyacrylonitrile nanofiber membranes for the adsorption of metal ions: Comparison with microfibers, *J. Hazard. Mater.*, 186 (2011) 182-189.
8. C. Sun, G. Zhang, R. Qu, Y. Yu, Removal of transition metal ions from aqueous solution by crosslinked polystyrene-supported bis-8-oxyquinoline-terminated open-chain crown ethers, *Chem. Eng. J. (Lausanne)*, 170 (2011) 250-257.
9. E. Moazzen, H. Ebrahimzadeh, M.M. Amini, O. Sadeghi, A high selective ion-imprinted polymer grafted on a novel nanoporous material for efficient gold extraction, *J. Sep. Sci.*, 36 (2013) 1826-1833.
10. K.R. Desai, Z.V.P. Murthy, Removal of silver from aqueous solutions by complexation-ultrafiltration using anionic polyacrylamide, *Chem. Eng. J. (Lausanne)*, 185-186 (2012) 187-192.
11. M.J. Hudson, M.J. Shepherd, Selective extraction and separation of metals especially silver (and copper) using poly(2-S-vinyl-1,3,4-thiadiazole-5-thiol), *Hydrometallurgy*, 9 (1983) 223-234.
12. C.O. Giwa, M.J. Hudson, Extraction of metals using poly[N-(dithiocarboxylato)-iminoethenehydrogenoiminoethene], *Hydrometallurgy*, 8 (1982) 65-75.
13. T.K. Bronich, S. Bontha, L.S. Shlyakhtenko, L. Bromberg, T. Alan Hatton, A.V. Kabanov, Template-assisted synthesis of nanogels from Pluronic-modified poly(acrylic acid), *J. Drug Targeting*, 14 (2006) 357-366.
14. E. Tsuchida, H. Nishide, Polymer-metal complexes and their catalytic activity, in: *Molecular Properties*, Springer Berlin Heidelberg, 1977, pp. 1-87.
15. X. Liang, Y. Su, Y. Yang, W. Qin, Separation and recovery of lead from a low concentration solution of lead(II) and zinc(II) using the hydrolysis production of poly styrene-co-maleic anhydride, *J. Hazard. Mater.*, 203-204 (2012) 183-187.
16. Y. Yan, J. Zhang, Y. Qiao, C. Tang, Facile Preparation of Cobaltocenium-Containing Polyelectrolyte via Click Chemistry and RAFT Polymerization, *Macromol. Rapid Commun.*, 35 (2014) 254-259.
17. S. Virolainen, I. Suppula, T. Sainio, Continuous ion exchange for hydrometallurgy: Purification of Ag(I)-NaCl from divalent metals with aminomethylphosphonic resin using counter-current and cross-current operation, *Hydrometallurgy*, 142 (2014) 84-93.
18. V.I. Kuz'min, D.V. Kuz'min, Sorption of nickel and copper from leach pulps of low-grade sulfide ores using Purolite S930 chelating resin,

- Hydrometallurgy, 141 (2014) 76-81.
19. Q. Cao, Y. Liu, C. Wang, J. Cheng, Phosphorus-modified poly(styrene-co-divinylbenzene)-PAMAM chelating resin for the adsorption of uranium(VI) in aqueous, *J. Hazard. Mater.*, 263, Part 2 (2013) 311-321.
 20. Q. Cao, Y. Liu, X. Kong, L. Zhou, H. Guo, Synthesis of phosphorus-modified poly(styrene-co-divinylbenzene) chelating resin and its adsorption properties of uranium(VI), *J. Radioanal. Nucl. Chem.*, 298 (2013) 1137-1147.
 21. A.C. Sather, O.B. Berryman, J. Rebek, Selective recognition and extraction of the uranyl ion from aqueous solutions with a recyclable chelating resin, *Chemical Science*, 4 (2013) 3601-3605.
 22. A. Okubo, H. Obata, M. Magara, T. Kimura, H. Ogawa, Rapid collection of iron hydroxide for determination of Th isotopes in seawater, *Anal. Chim. Acta*, 804 (2013) 120-125.
 23. S. Sadeek, M. El-Sayed, M. Amine, M. Abd El-Magied, A chelating resin containing trihydroxybenzoic acid as the functional group: synthesis and adsorption behavior for Th(IV) and U(VI) ions, *J. Radioanal. Nucl. Chem.*, (2013) 1-8.
 24. [P. Ilaiyaraja, A. Deb, K. Sivasubramanian, D. Ponraju, B. Venkatraman, Removal of thorium from aqueous solution by adsorption using PAMAM dendron-functionalized styrene divinyl benzene, *J. Radioanal. Nucl. Chem.*, 297 (2013) 59-69.
 25. A.I. Okewole, E. Antunes, T. Nyokong, Z.R. Tshentu, The development of novel nickel selective amine extractants: 2,2'-Pyridylimidazole functionalised chelating resin, *Miner. Eng.*, 54 (2013) 88-93.
 26. S. Badawy, A.A. Nayl, R.A. El Khashab, M.A. El-Khateeb, Cobalt separation from waste mobile phone batteries using selective precipitation and chelating resin, *J Mater Cycles Waste Manag.* (2013) 1-8.
 27. [O. Hazer, D. Demir, Speciation of Chromium in Water Samples by Solid-Phase Extraction on a New Synthesized Adsorbent, *Anal. Sci.*, 29 (2013) 729-734.
 28. S. Kagaya, Y. Saeki, D. Morishima, R. Shirota, T. Kajiwara, T. Kato, M. Gemmei-Ide, Potential of Presep® PolyChelate as a Chelating Resin: Comparative Study with Some Aminocarboxylic Acid-type Resins, *Anal. Sci.*, 29 (2013) 1107-1112.
 29. F. Zereen, V. Yilmaz, Z. Arslan, Solid phase extraction of rare earth elements in seawater and estuarine water with 4-(2-thiazolylo)zo resorcinol immobilized Chromosorb 106 for determination by

- inductively coupled plasma mass spectrometry, *Microchem. J.*, 110 (2013) 178-184.
30. R.S. Azarudeen, R. Subha, D. Jeyakumar, A.R. Burkanudeen, Batch separation studies for the removal of heavy metal ions using a chelating terpolymer: Synthesis, characterization and isotherm models, *Sep. Purif. Technol.*, 116 (2013) 366-377.
 31. H.B. Sadeghi, H.A. Panahi, M. Abdouss, B. Esmailpour, M.N. Nezhati, E. Moniri, Z. Azizi, Modification and characterization of polyacrylonitrile fiber by chelating ligand for preconcentration and determination of neodymium ion in biological and environmental samples, *J. Appl. Polym. Sci.*, 128 (2013) 1125-1130.
 32. C. Xiong, Q. Jia, X. Chen, G. Wang, C. Yao, Optimization of Polyacrylonitrile-2-aminothiazole Resin Synthesis, Characterization, and Its Adsorption Performance and Mechanism for Removal of Hg(II) from Aqueous Solutions, *Ind. Eng. Chem. Res.*, 52 (2013) 4978-4986.
 33. V. Dulman, S.M. Cucu-Man, R.I. Olariu, R. Buhaceanu, M. Dumitraş, I. Bunia, A new heterogeneous catalytic system for decolorization and mineralization of Orange G acid dye based on hydrogen peroxide and a macroporous chelating polymer, *Dyes Pigm.*, 95 (2012) 79-88.
 34. S. Islam, M. Mobarok, P. Mondal, A. Roy, N. Salam, D. Hossain, S. Mondal, Use of immobilized transition metal complexes as recyclable catalysts for oxidation reactions with hydrogen peroxide as oxidant, *Transition Met. Chem. (London)*, 37 (2012) 97-107.
 35. A. Coelho, P. Diz, O. Caamaño, E. Sotelo, Polymer-Supported 1,5,7-Triazabicyclo[4.4.0]dec-5-ene as Polyvalent Ligands in the Copper-Catalyzed Huisgen 1,3-Dipolar Cycloaddition, *Adv. Synth. Catal.*, 352 (2010) 1179-1192.
 36. G.M. Pawar, J. Weckesser, S. Blechert, M.R. Buchmeiser, Ring opening metathesis polymerization-derived block copolymers bearing chelating ligands: synthesis, metal immobilization and use in hydroformylation under micellar conditions, *Beilstein J. Org. Chem.*, 6 (2010) 28.
 37. M. Erdem, R. Say, A. Ersöz, A. Denizli, H. Türk, Biomimicking, metal-chelating and surface-imprinted polymers for the degradation of pesticides, *React. Funct. Polym.*, 70 (2010) 238-243.
 38. C. Selvi, D. Nartop, Novel polymer anchored Cr(III) Schiff base complexes: Synthesis, characterization and antimicrobial properties, *Spectrochimica Acta Part A: Molecular and Biomolecular Spectroscopy*, 95 (2012) 165-171.
 39. M.A.R. Ahamed, A.R. Burkanudeen, Thiazole-Based Novel Terpolymer

- Ligand and Its Transition Metal Complexes: Thermal and Biological Studies, *Adv. Polym. Technol.*, 32 (2013) 21376.
40. T. Ahamad, S.M. Alshehri, Physiochemical characterization and antimicrobial evaluation of phenylthiourea–formaldehyde polymer (PTF) based polymeric ligand and its polymer metal complexes, *Spectrochimica Acta Part A: Molecular and Biomolecular Spectroscopy*, 108 (2013) 26-31.

Chapter 10

Application of dilational rheology for analyze the properties of interfacial layers supramolecular systems

Svetlana Khil'ko and Volodymyr Rybachenko

*L.M. Litvinenko Institute of Physical-Organic and Coal Chemistry,
National Academy of Sciences of Ukraine, R. Luxemburg Street 70,
Donetsk 83114, Ukraine*

Introduction

The rheological characteristics of the surface are important for a wide range of systems - from pure liquids unto colloidal systems (emulsions, suspensions, foams). However, these research are particularly important for rheological properties of interfacial layers surfactant, including proteins, surfactants polymers, surfactant mixture, supramolecular systems [1].

Interfacial layers may be organized spontaneously at interfaces as a result of adsorption of the surfactant from solutions. Furthermore, the interfacial layers may be formed artificially by mechanical means - by coating an insoluble film on the surface of the liquid surfactant phase. The thickness of the interfacial layer does not exceed a few tens of nanometers, so they belong to the two-dimensional systems.

Important sources of information on the structure and properties interfacial layers of surfactants are their rheological characteristics. Comparison of the rheological properties of interfacial layers with their composition and internal structure determines the selection and optimization of their composition for various practical applications.

These layers of surfactants are characterized by certain mechanical properties, the most significant of which are the elasticity and viscosity. These properties are caused by the ability of the surfactant molecules to interact with each other and form a structured adsorption layers.

Modern experimental methods for studying the rheological properties of interfacial layers at interfaces belong to the two-dimensional (2D) rheology. There are two groups of methods of two-dimensional 2D rheology. This

rotational viscosity measurement methods modulus at imposing strain shear and dilatational rheology measurement when applied strain tension-compression. Increasingly used methods found dilated rheology. These methods are used in modern laboratory practice and implemented in the form of original and commercial devices [2].

Experimental

The bases of the dilatational rheology measurement of the interfacial layer are dynamic interfacial tension oscillations in the surfactant solution drops.

Principle of the method of a hanging drop consists in the precise determination of the droplet shape and the description of its equation of capillarity Gauss-Laplace (Fig. 1). Principle of the method is described in [3, 4].



Figure 1. Drop (a) and its coordinate (b - points); curves calculated for different values of surface tension.

Measurement scheme of the viscoelastic properties of the interfacial layer by the oscillating drop method is shown in Fig. 2 and 3. The method is based on measuring of the capillary pressure during the oscillations of the drop.

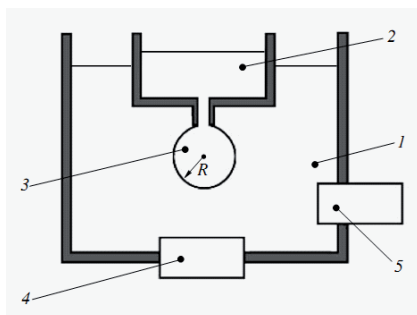


Figure 2. Scheme of the measuring cell:
 1 – aqueous surfactant solution,
 2 – the non-polar liquid / air,
 3 – drop,
 4 – piezo,
 5 – pressure sensor

After reaching adsorption equilibrium area A drop undergoes periodic sinusoidal deformation (oscillation) of small amplitude $\Delta A / A = \pm 7-8\%$, with frequencies in the range $f = 0,005 - 0,2$ Hz. With this action on the droplet surface is continuously recorded and the surface tension is calculated complex modulus of viscoelasticity ($|E|$, mN / m) and phase angle ϕ (angle of lag) (Fig. 4).

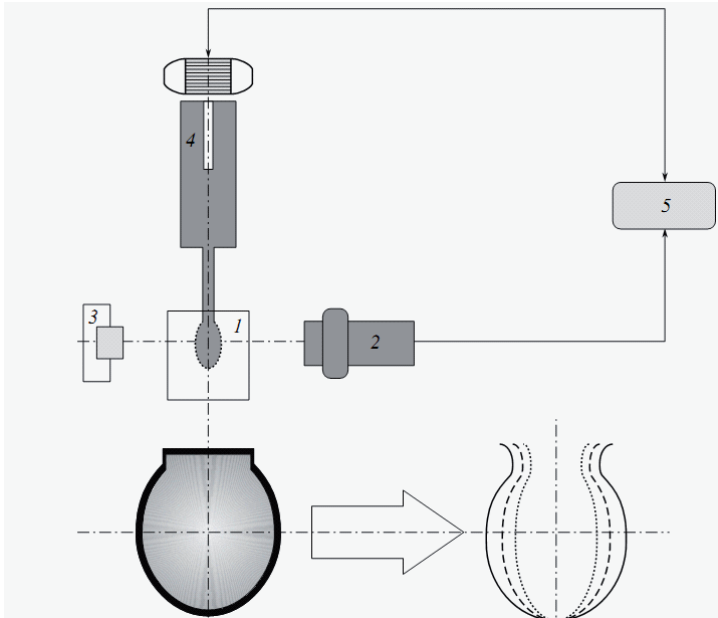


Figure 3. The general scheme of the measurement of the viscoelastic properties of the interfacial layer by the method of oscillating drops: 1 – measuring cell, 2 – a video camera, 3 – light source, 4 – metering device 5 – computer.

Methods shapes of the drop or bubble are demonstrated the dependence of the surface tension from the droplet size or bubble. This dependence can lead to errors in determining the viscoelasticity modulus and the phase angle. In Tensiometer PAT-2P uses a new design procedure described in [4], which significantly reduces the dependence of the surface tension of the drop or bubble from volume. Assessing the impact of this error on the values of the rheological parameters was done in [5]. The error in determining module viscoelasticity using PAT-2P less than 0.4 mN/m.

Dilatational viscous modulus (E_p , mN/m) characterizes the phase lag between

the dependences of the surface tension changes from time to time, $\gamma(t)$, and the droplet surface area change from time to time, $A(t)$. The dilatational elasticity modulus (E_r , mN/m) is proportional to the amplitude dependence of $\gamma(t)$ (Fig. 4) [6, 7]. Dilatational modulus reflects the accumulation of energy and the modulus of viscosity reflects energy loss in the surface layer. These values are associated with the processes of adsorption \leftrightarrow desorption surfactant in the surface layer when applied deformation “expansion \leftrightarrow compression”. A tensile droplet increases the surface area of the interface, wherein a portion of the surfactant molecules from the surface layer reaches the surface (adsorption). When compressing drops part of the surfactant molecules are leaving the surface layer (desorption) – Fig. 5.

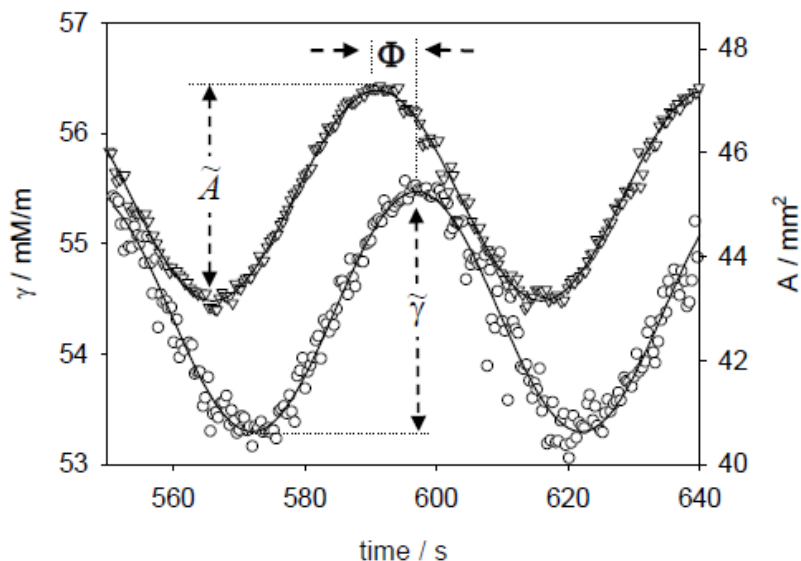


Figure 4. Determination of rheological properties of the surface layers of surfactant with help method of dilatational rheology.

Modules of dilatational elasticity and viscosity can characterize the degree of order in the surface layer, the ability to interactions between the surfactant molecules, and the degree of filling of the surface layer due to adsorption and desorption of surfactants.

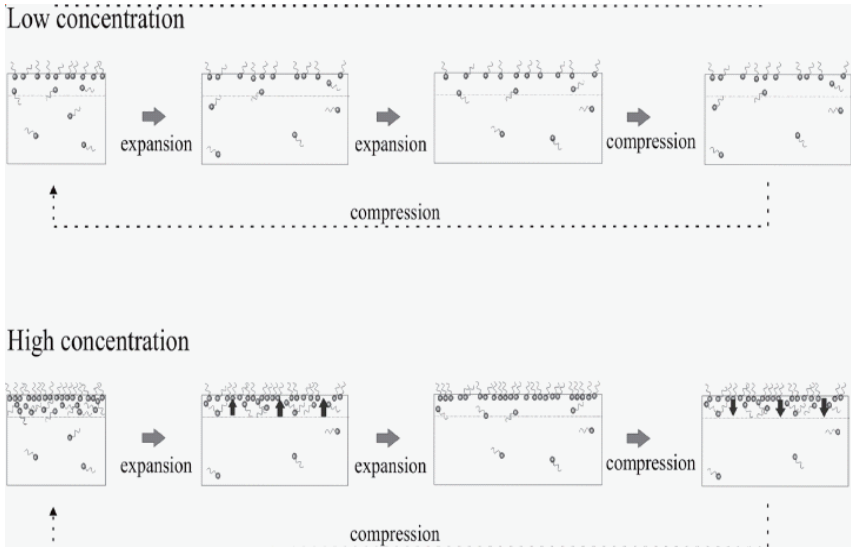


Figure 5. Scheme processes «adsorption↔desorption» of the surfactants at the interface during deformation «expansion ↔ compression.» Image was taken from [8].

Module viscoelasticity (mN/m) characterizes the viscoelastic properties of the surface layers of surfactants and takes into account all the relaxation processes affecting the surface tension γ . At low amplitude harmonic oscillations ΔA surface with an angular frequency $\omega = 2\pi f$, $\Delta A = \Delta \bar{A} \exp(i2\pi f t)$ the expression for the dilatational module viscoelasticity has the form [9]:

$$E = \frac{\Delta\gamma}{\Delta A / A_0} = \frac{d\gamma}{dh A} \quad (1)$$

Modulus E is expressed as complex number, and includes a real and imaginary component:

$$|E| = E_r + E_i, \quad (2)$$

where E_r is the elastic modulus, E_i - viscous modulus.

Real and imaginary parts of the dilatational module determined by the expressions [10]:

$$E_r = |E| \cos \phi, \quad E_i = |E| \sin \phi \quad (3)$$

Expressions for the viscoelastic modulus and phase angle are of the form:

$$|E| = \sqrt{E_i^2 + E_r^2}, \quad \phi = \arctg(E_i / E_r) \quad (4)$$

In the study of the viscoelastic properties at the interface during deformation “expansion↔ compression” of the surface can be obtained value of dilatational 2D viscosity, η_d , from the relations:

$$\eta_d = \frac{\Delta\gamma}{d \ln A / dt}, \quad E_i = 2\pi f \eta_d, \quad \eta_d = \frac{E_i}{\omega}, \quad \omega = 2\pi f - \text{circular frequency} \quad (5)$$

The dilatational viscosity determined phase angle between the change in the surface area and by the change of surface tension [2]:

$$\eta_d = \frac{E_r \operatorname{tg} \phi}{f} \quad (6)$$

The dilatational viscosity may depend on the oscillation frequency of the drop. This indicates the non-Newtonian behavior of the system and reflects the relaxation properties of interfacial layers.

Results of experiments with the harmonic oscillations of the surface of the drop are analyzed using a Fourier transform [11]:

$$E(i\omega) = A_0 \frac{F[\Delta\gamma]}{F[\Delta A]}, \quad (7)$$

where A_0 - initial surface area of the droplet, ω - angular frequency of oscillation.

Application of dilatational rheology

1. Surfactants - non-electrolyte systems

As examples of such systems are considered rheological properties of aqueous solutions of surface layers of sodium dodecylsulfate (SDS) with lower alcohols (ethanol, *n*-propanol). Fig. 6 shows the dependence of the change in the

modulus of viscoelasticity from the oscillation frequency drops for solutions of SDS and its mixtures with alcohols.

Increasing the concentration of alcohol in the system leads to a noticeable decrease in values of the modulus of viscoelasticity, which may be due to the competitive adsorption between molecules the SDS and RON. This helps to reduce the mechanical properties of the surface layers due to substitution of molecules of SDS by molecules of lower alcohols. The magnitudes of viscoelasticity modulus SDS solutions at high alcohol concentrations are close to the magnitudes viscoelasticity modulus of hydro-alcoholic solutions ($E = 2 - 4 \text{ мН/м}$). SDS concentration in the solution and the type of alcohol did not have a noticeable effect on the behavior of the modulus of viscoelasticity from frequency.

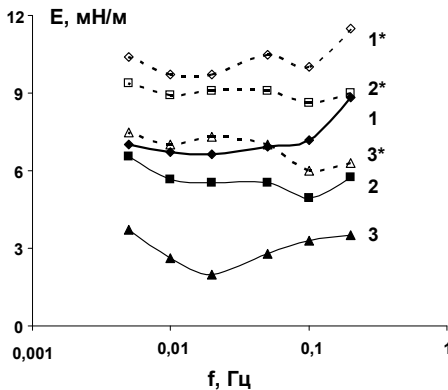


Figure 6. Change modulus viscoelasticity from the oscillation frequency drops of aqueous solutions and water-alcohol solutions of sodium dodecylsulfate: $C_{SDS} = 0.5 \text{ mmol/l}$ (1), $C_{ROH} = 4.0\%$: ethanol (2), *n*-propanol (3);

$C_{SDS} = 1.0 \text{ mmol/l}$ (1*) $C_{ROH} = 4.0\%$: ethanol (2*), *n*-propanol (3*)

The nature of the interfacial layer SDS in the hydroalcoholic solutions may be associated with the formation of complexes between the SDS and alcohol. The possibility of formation of such complexes were shown to Quantum calculations complexes $SDS \cdot (ROH)_m$, which was performed by the PM3 method in the software package MOPAC [12]. Fig. 7 shows the structure of the complex $SDS \cdot (SN3OH)_5$ with optimized geometry [13].

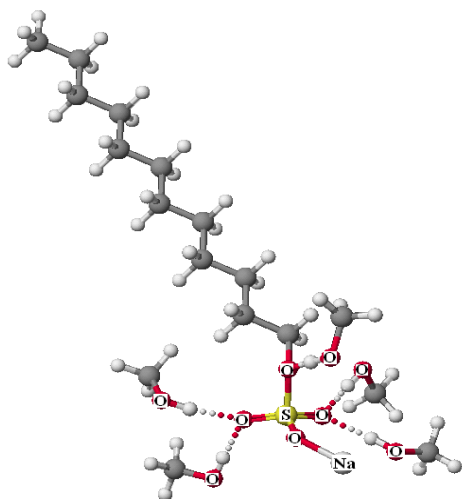


Figure 7. Optimized structure of the complex $(C_{12}H_{23}SO_4Na) \cdot (CH_3OH)_5$.

2. Natural polyelectrolytes

Investigation of the properties of natural polyelectrolytes (humic acid, chitosan, polysaccharides, proteins, nucleic acids, etc.) and polyelectrolyte complexes determined by the needs of both fundamental and applied science. These chemicals are widely used in various fields of chemical engineering, biotechnology, medicine, environmental protection, etc.

In this work were considered the rheological properties of interfacial layers salts of humic acids, proteins, and chitosan.

Experimental dependence of the modulus of viscoelasticity (E) of sodium humate of the surface pressure (Π) at a frequency of 0.1 Hz oscillations are shown in Fig. 8. In this figure also are shows the calculated dependence of the critical elasticity modulus E_0 , for monolayer (curve 1) and bilayer adsorption (curve 2). It is seen that the experimental data best described by the model bilayer adsorption. These dependencies for the nature polyelectrolytes (of the proteins), β -casein and β -lactoglobulin were obtained in [14-16] and are shown in Fig. 8. Experimental values of the modulus of viscoelasticity $|E|$ for sodium humate are comparable to the values for proteins with a molecular weight close to the mass of sodium humate. Furthermore, the dependence $|E|$ on Π for sodium humate occupies an intermediate position between the globular β -lactoglobulin and the linear β -casein. This is probably due to the peculiarities of the molecular structure of sodium humate, which includes both the fused aromatic rings and the fragments with a linear structure.

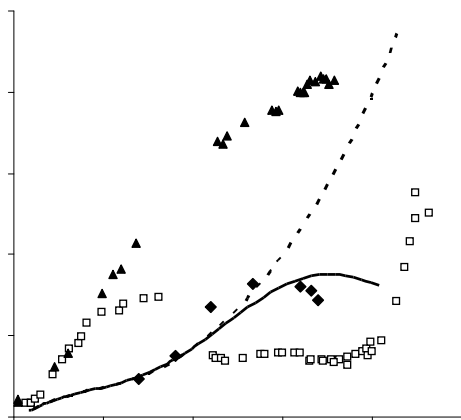


Figure 8. Change module viscoelasticity (E) on the surface pressure (Π) for sodium humate according to this paper (1) and for β -casein (2) and β -lactoglobulin (3) according to [15] for the oscillation frequency drops 0.1 Hz.

Curves 1 and 2 – critical (perfect) elasticity (high-frequency) of the sodium humate solutions:

- 1 – For a monolayer adsorption
2 – For a bilayer adsorption.

According to Table 1, the values of the rheological parameters for sodium humate have intermediate values compared with globular proteins and a linear β -casein, which may also be associated with possible intra-and intermolecular interactions of sodium humate in the surface layer.

Table 1. The rheological characteristics of surface layers of natural polyelectrolytes

Parameters	Albumin [17]	β -Casein [16, 18]	Chitosan [19]	Sodium humate
$ E $, mN/m	70	9.5	20.5-25.5	33
E_r , mN/m	68	9	4-5	32
E_i , mN/m	10	3	20-25	5
ϕ_0	0	0.33	4-6	11

Monomolecular layers of sodium humate can be attributed to the elastic surface films. High modulus of viscoelasticity of surface films of polyelectrolyte characterizes a high degree of order and organization, as well as ability to intermolecular interactions. Monomolecular layers of chitosan are characterized by high values of the phase angle and low values modulus of viscoelasticity. In such surface layers show no signs of structural order.

References

1. A.I. Rusanov, V.A. Prokhorov. *Interfacial Tensiometry* - St. Petersburg: Chemistry, 1994. – 400 p.
2. Derkach, S. R., Kragel J., Miller R. Methods for measuring the rheological properties of interfacial layers (experimental methods 2D rheology) – *Colloid. J.* – 2009. – Vol. 71, № 1. – P. 5 – 21.
3. Loglio G. at all. *Novel Methods to Study Interfacial Layers* – Amsterdam: Elsevier, 2001. – 320 p.
4. S.A. Zhobol at all. Optimization of calculation methods for determination of surface tensions by drop profile analysis tensiometry – *Adv. Colloid Interface Sci.* – 2007. – Vol. 134-135. – P. 322 – 329.
5. V.B. Fainerman at all. Adsorption layer characteristics of Triton surfactants. 4. Adsorption from micellar solutions – *Colloids Surfaces A.* – 2009. – Vol. 334. – P. 22 – 27.
6. Ravera, F., Liggieri L., Loglio G. *Progress in Colloid and Interface Science, Interfacial Rheology.* – Leiden: Brill, 2009. – p. 137 – 143.
7. Kovalchuk V.I. at all. Oscillating bubble pressure experiments for dilational rheology studies – *Adv. Colloid Interface Sci.* – 2005. – Vol. 114 – 115. – P. 303 – 313.
8. Andersen A. *Surfactants Dynamics at Interfaces.* Diss....Dr. rer. nat. 2005.
9. Ravera F., Liggieri L., Loglio G. *Progress in Colloid and Interface Science, Interfacial Rheology.* – Leiden: Brill, 2009. – p. 137 – 143.
10. Kovalchuk V.I. at all. Oscillating bubble pressure experiments for dilational rheology studies – *Adv. Colloid Interface Sci.* – 2005. – Vol. 114 – 115. – P. 303 – 313.
11. Zdziennicka A. at all. The Adsorption of Cetyltrimethylammonium Bromide and Propanol Mixtures with Regard to Wettability of Polytetrafluoroethylene. I. Adsorption at Aqueous Solution-Air Interface – *J. Colloid Interface Sci.* – 2008. – Vol. 317. – P. 44 – 53.
12. Kaplan I.G. *Introduction to the theory of intermolecular interactions.* - Moscow: Nauka, 1982. – 312 p.
13. Макарова Р.А., Хилько С.Л.,
14. Finerman V.B., Miller R. Equilibrium and dynamic characteristics of adsorption layers of proteins at interfaces liquid-gas theory and experiment. - *Colloid. J.* - 2005. - Vol. 67, № 4. - P. 437 - 449.
15. Lucassen-Reynders E.H., Fainerman V.B., Miller R. Surface dilatational modulus and Gibbs' elasticity of protein adsorption layers. - *J. Phys. Chem. B.* – 2004. – Vol. 108. – P. 9173 – 9176.

16. Benjamins J., Lyklema J., Lucassen-Reynders E.H. Compression/expansion rheology of oil/water interfaces with adsorbed proteins. Comparison with the air/water surface - *Langmuir*. – 2006. – Vol. 22. – P. 6181 - 6188.
17. Miller R., Fainerman V.B., Makievski A.V., Krägel J., Grigoriev D.O., Kazakov V.N., Sinyachenko O.V. Dynamics of protein and mixed protein/surfactant adsorption layers at the water/fluid interface - *Advances in Colloid and Interface Science*. 2000. V. 86. P. 39-82.
18. Miller R., Fainerman V.B., Makievski A.V., Krägel J., Wütsneck R. - *Colloids and Surfaces A: Physicochemical and Engineering Aspects*. 2000. V. 161. P. 151.
19. Babak V.G. Dynamic Surface Tension and Dilational Viscoelasticity of Adsorption Layers of Alkylated Chitosans and Surfactant-Chitosan Complexes - *Colloid. Polym. Sci.* 2006. V. 284. P. 745-751.

Chapter 11

Oligomerization thermodynamics of fatty alcohols and carboxylic acids at the air/water interface. Quantum chemical approach

E. S. Fomina, E. A. Belyaeva and Yu. B. Vysotsky
*Donetsk National Technical University, Artema Str. 58,
83000 Donetsk, Ukraine*

The modern instrumental methods for investigations of Langmuir monolayers are capable of detailed investigation of their condensed phase structure. Generally, the structural peculiarities of amphiphilic monolayers depend on the conformational flexibility, length and structure of the alkyl chain, type and location of the functional group with respect the alkyl chain, as well [1]. The analysis of numerous experimental data [2-7] have shown that amphiphiles with small head group (such as alcohols and carboxylic acids) tend to form condensed phases with hexagonal unit cell, whereas amphiphiles with more bulky functional groups show phase diagrams with orthorhombic and oblique unit cells. The first studies using quantum chemical methods to characterize condensed phases of Langmuir monolayers on the basis of clusterization processes started with aliphatic alcohols [8-10]. This type of compounds along with carboxylic acids has been frequently used as standard model for experimental studies of monolayer properties.

The existing experimental data show that condensed Langmuir monolayers of aliphatic alcohols with alkyl chains of 10-12 carbon atoms are formed at 4-25°C [11-15]. Present phase diagrams of saturated carboxylic acid monolayers reveal that at the higher pressure and normal temperature liquid-condensed and solid phases exist. Both phases possess the hexagonal crystal lattice [16-20]. The geometric parameters of alcohol and acid hexagonal unit cell are close to the relation $b = a\sqrt{3}$ and vary within the range of $a = 4.75\text{-}5.0 \text{ \AA}$, $b = 7.5\text{-}8.5 \text{ \AA}$, $t = 0\text{-}9^\circ$ [17, 21-28]. The molecules arrange parallel to each other and are in linear conformation when all hydrogen atoms of methylene groups are in *trans*-configuration [29]. It should be noted that behavior of the surfactant monolayers

were also investigated in the framework of MD simulations, although not so extensively [21, 30-32]. The study of ref. [30] shows that alcohols with alkyl chain lengths of 29-31 carbon atoms at temperatures below zero tend to form hexagonal aggregates with the next geometrical parameters: $a = 5.1-5.3 \text{ \AA}$, $b = 7.7-7.8 \text{ \AA}$. It is apparent that the temperature conditions accepted for simulations are far from standard.

In this connection it seems interesting to define how adequately it is possible to describe the structural parameters of hexagonal monolayers of nonionic amphiphiles in the framework of the quantum chemical model, which was successfully applied for the study of the thermodynamic clusterization parameters [8-10, 33-42]. The aim of the present work is to investigate the thermodynamic parameters of oligomers that form hexagonal lattice structures of aliphatic alcohols and carboxylic acids with unbranched alkyl chain at the air/water interface using the quantum chemical semiempirical PM3 method. The calculations were done for molecules with the general formula $C_nH_{2n+1}OH$ ($n = 6-16$) and $C_nH_{2n+1}COOH$ ($n = 7-16$) under standard conditions.

1. Model and Method

The calculation of the thermodynamic (enthalpy, entropy and Gibbs' energy) and structural parameters of clusterization for the hexagonal lattice structure of alcohol monolayers is carried out using quantum chemical semiempirical method PM3 according to the model described in detail elsewhere [35] in compliance with the next procedure:

1. Conformational analysis, which includes the construction of the potential energy surface of the monomer depending on the values of torsion angles of the functional groups in the hydrophilic part of amphiphile with respect to the hydrophobic alkyl chain; and calculation of the thermodynamic parameters of the formation for the found conformers;
2. Determination of the tilt angle of the alkyl chains of the amphiphiles in the monolayer with respect to the interface, according to the scheme described in detail elsewhere [42, 44]; and search of the geometric parameters of the unit cell of the 2D lattice;
3. Calculation in supermolecular approximation of the thermodynamic parameters of clusterization of small aggregates (dimers, tetramers, hexamers) constructed on the basis of the found conformers which orient with a tilt angle to the interface found previously;
4. Construction of the additive scheme on the basis of the results of direct calculations. This scheme defines the values of enthalpy, entropy and Gibbs' energy of clusterization as the total contribution of the

intermolecular CH \cdots HC interactions and interactions of the hydrophilic parts of the amphiphiles realized in the cluster and calculation of the thermodynamic clusterization parameters per one monomer molecule of the 2D film.

This paper describes first three stages of the procedure and provides regarded thermodynamic parameters only for oligomers that underlie the additive scheme for calculation of the thermodynamic clusterization parameters per one monomer molecule of the untilted hexagonal monolayers.

2. Results and Discussion

2.1 Aliphatic alcohols

Monomers. The ref. [9] contains the conformational analysis for aliphatic alcohol monomers. Two stable conformations were found as a result. They are the mirror reflections with the dihedral angles of the OH-group $\angle\alpha=C_2-C_1-O-H=60^\circ$ and 300° (-60°), respectively (cf. Fig. 1). An additional optimization confirmed the isoenergetic formation of these two structures. Thus, the alcohol monomer structure with the dihedral angle $\angle\alpha=60^\circ$ was used in all further calculations. The optimized structure of the alcohol monomer is shown in Fig. 2 on the example of a molecule with 10 carbon atoms in the alkyl chain.

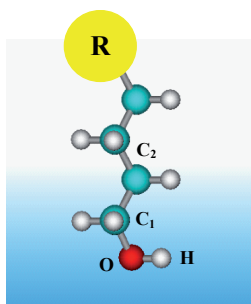


Figure 1. Torsion angle of the functional group of alcohol (R – hydrophobic chain)

For the described monomer structures the thermodynamic parameters (enthalpy, absolute entropy and Gibbs' energy) of the monomer formation were calculated previously in ref. [45]. So, here we list only the correlation dependencies of the thermodynamic formation parameters on the alcohol alkyl chain length (n):

$$\Delta H_{298, \text{mon}}^0 = -(22.68 \pm 0.00) \cdot n - (30.84 \pm 0.01) \text{ [S} = 0.02 \text{ kJ/mol; N} = 15\text{]}, \quad (1)$$

$$S_{298, \text{mon}}^0 = (32.22 \pm 0.04) \cdot n + (181.65 \pm 0.42) \text{ [S} = 0.61 \text{ J/(mol} \cdot \text{K); N} = 15], \quad (2)$$

$$\Delta G_{298, \text{mon}}^0 = (8.32 \pm 0.01) \cdot n - (46.08 \pm 0.13) \text{ [S} = 0.19 \text{ kJ/mol; N} = 15]. \quad (3)$$

Here and further S is the standard deviation, N is a sample size. The corresponding correlation coefficients exceed 0.9999. Note, that calculated parameters of absolute entropy of formation for the alcohol monomers are smaller than the experimental values because PM3 method does not take into account the increment of the free rotation of the methylene groups in the alkyl chain to the entropy. Therefore, we considered these increments in the calculation of the absolute entropy of formation using corresponding corrections. This correction is found on the basis of experimental data for the absolute entropy of formation and is $(6.12 \pm 0.22) \text{ J/(mol} \cdot \text{K)}$ per one methylene group [45].

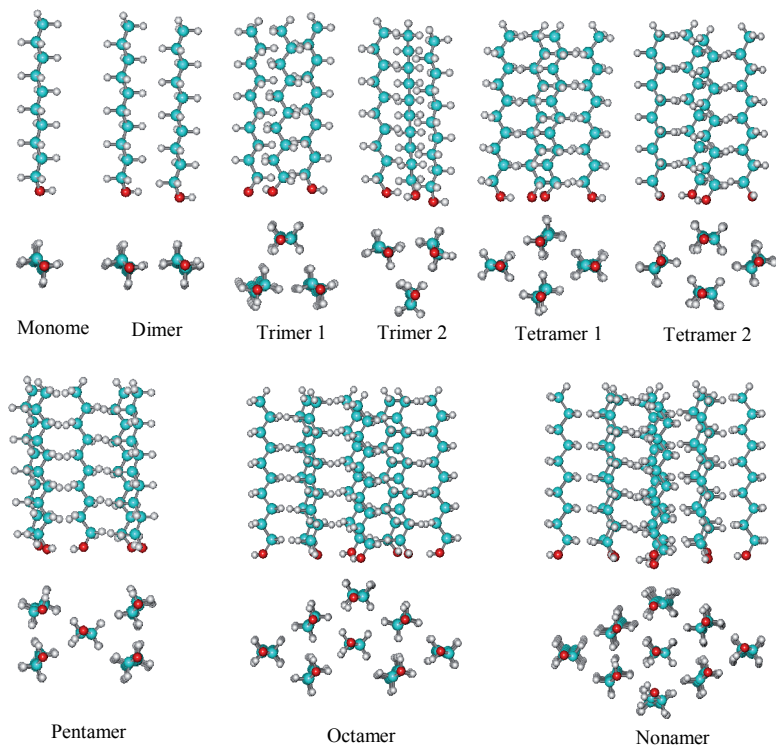


Figure 2. Optimized structures of the small aggregates of fatty alcohols for the hexagonal monolayer phase

Table 1. Thermodynamic parameters of formation and alcohol monomers

Molecule	$\Delta H^0_{298, \text{mon}}$, kJ/mol		$S^0_{298, \text{mon}}$, J/(mol·K)		$\Delta G^0_{298, \text{mon}}$, kJ/mol	
	Calculation	Experiment [46]	Calculation	Experiment [46]	Calculation	Experiment [46]
C ₃ H ₇ OH	-257.53	-255.2	304.63 (324.80)	322.47	-167.53 (-162.43)	-159.9
C ₄ H ₉ OH	-274.43	-274.6	337.08 (363.17)	361.48	-159.20 (-152.41)	-150.3
C ₅ H ₁₁ OH	-302.38	-298.74	369.86 (402.54)	402.5	-151.02 (-142.53)	-146.02
C ₆ H ₁₃ OH	-319.62	-316.5	402.22 (441.50)	440.1	-142.72 (-132.53)	-134.4
C ₇ H ₁₅ OH	-334.85	-336.4	435.09 (480.45)	479.19	-134.58 (-122.48)	-125.3
C ₈ H ₁₇ OH	-357.06	-355.5	467.75 (520.49)	518.5	-126.38 (-112.62)	-115.5
C ₉ H ₁₉ OH	-386.89	-381.2	501.33 (558.35)	557.7	-118.46 (-102.48)	-112.2
C ₁₀ H ₂₁ OH	-403.25	-396.7	533.57 (597.31)	597.0	-110.14 (-92.55)	-98.79
C ₁₁ H ₂₃ OH	-422.21	-418.4	568.57 (636.26)	636.2	-102.65 (-82.35)	-91.53
C ₁₂ H ₂₅ OH	-442.83	-436.7	603.18 (675.21)	675.21	-95.04 (-73.75)	-80.82
C ₁₃ H ₂₇ OH	-463.46	-460.4	638.63 (712.83)	714.7	-87.68 (-62.03)	-75.66
C ₁₄ H ₂₉ OH	-484.09	-475.9	672.19 (751.78)	753.9	-79.75 (-52.60)	-62.2
C ₁₅ H ₃₁ OH	-504.67	-501.8	706.39 (790.73)	793.2	-72.02 (-42.03)	-59.18
C ₁₆ H ₃₃ OH	-525.26	-522.5	737.03 (829.69)	832.4	-63.22 (-32.30)	-50.93

Structural parameters. Previously in refs. [8-10, 45] we considered the alcohol monolayers with an oblique unit cell. In the present work the monomer molecules described above are organized in such a way that the formed monolayer has a hexagonal lattice structure. The numbers of molecules in both directions of the spread monolayer are defined as p and q (see Fig. 3). Small one-edged arrows in Figure 3 define the direction from carbon atom to hydrogen atom of the methylene fragment. They show the herringbone arrangement of the molecules in the monolayer in agreement with the existing experimental data [2]. For the determination of the molecular tilt angle with respect to the normal to the interface we use the procedure, which became standard in the studies of the regarded issue and is described in detail elsewhere [42]. It should only be mentioned that in the dimers (which are the sides of the monolayer unit cell in both p and q directions), a parallel shift of one molecule with respect to another one is applied. In the obtained dependencies of the dimerization Gibbs energy on the δ and φ angles the minima were found. These minima correspond to optimum δ and φ values, which define the value of the general tilt angle t of the alkyl chain of the amphiphile with respect to the normal to the interface. Thereby the values of angles are found: $\delta=3^\circ$ and $\varphi=3^\circ$, $t=4^\circ$, agreeing well with the existing experiment data [17, 22-25].

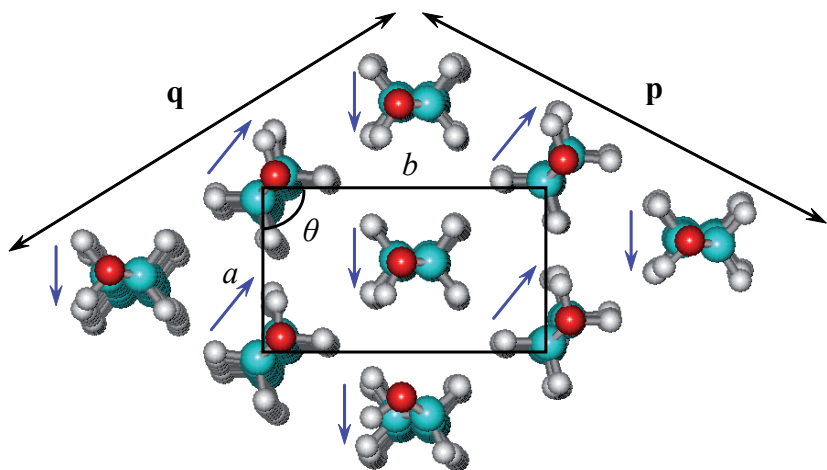


Figure 3. Structure of the unit cell of the hexagonal 2D cluster of alcohols: view along the molecular chain axis.

In order to determine the geometric parameters of the unit cell the nonamer is constructed. On the basis of its optimized structure the unit cell with the geometric parameters $a = 4.3 \text{ \AA}$; $b = 7.4 \text{ \AA}$, $\theta=87^\circ$ is singled out. The obtained values are in reasonable correspondence with GIXD results: $a = 5.0 \text{ \AA}$; $b = 7.5 \text{ \AA}$, $\theta=90^\circ$. Therefore, we consider only such aggregates, which form the monolayer of the structure regarded above, in further calculations of the thermodynamic parameters (enthalpy, entropy and Gibbs' energy) of the alcohol clusterization.

Oligomers. Figure 3 illustrates the fragment of the aliphatic alcohol monolayer (bottom view), in which two types of intermolecular $\text{CH}\cdots\text{HC}$ interactions formed between hydrocarbon chains are marked. These types of interactions are designated as K_a and K_f (see Figure 4a) in analogy with those in refs. [9, 10]. It should be noted, that the K_f interactions structurally differ from the interactions found previously. In formation of one $\text{CH}\cdots\text{HC}$ interaction of 'a'-type between two alkyl chains only one hydrogen atom participates from every second methylene fragment of each interacting chain whereas for the $\text{CH}\cdots\text{HC}$ interaction of 'f'-type every second methylene fragment of one molecule form an interaction with analogous methylene fragments of two other molecules at the same time. The interactions of 'f'-type resembles to some extent the structure of the interactions of 'c'-type. The only difference is that the interactions of 'f'-type involve only two molecules out of three, whereas the interactions of 'c'-type involve all three molecules (see Figure 5). However, it will be further proved that the interactions of both 'a' and 'f'-types are virtually isoenergetic.

Six possible types of interactions between the hydroxylic groups of the alcohol molecules can be singled out. They are represented in Figure 3b. The increments from these interactions differ from each other because of the different mutual orientation of alcohol hydrophilic parts with respect to one another. In order to describe the 2D monolayer phase one should define the increment of each $\text{CH}\cdots\text{HC}$ interaction and the interaction between the functional groups in the clusterization enthalpy and entropy. To accomplish this requirement the structures of small aggregates (dimers, trimers, tetramers, pentamers, octamers and nonamers) are marked in the cluster (see Figure 4). These aggregates involve all the considered interactions in their structure. Figure 2 illustrates the optimized structures of alcohol small aggregates, which are used for the correlation analysis of the increments of the intermolecular interactions to the values of the thermodynamic clusterization parameters depending on the number of these interactions realized in the cluster.

Consider now the structure of regarded aggregates in detail. It is possible to single out six types of dimers by the number of interaction types between the

hydroxylic groups of alcohols for the hexagonal 2D cluster given in Figure 4. However, it is possible to get the optimized structure without any edge effects [42] only for a dimer with n_1 interaction of hydrophilic parts (see Figure 4b). The structure of this dimer is illustrated in Figure 2 on the example of the aggregate with the alkyl chain length of 10 carbon atoms. Note, that the $\text{CH}\cdots\text{HC}$ interactions between the alkyl chains of alcohols are not realized in the fragment possessing n_2 interaction (see Figure 4a). Therefore, the regarded dimer is out of consideration while the optimization procedure. The considered fragment of the monolayer has also two types of trimers and tetramers. There are the next interactions between the monomers in these trimers: n_1 , n_3 and n_5 for trimer 1 and n_2 , n_4 and n_6 for trimer 2. However, only trimer 2 has the hydrogen interaction n_4 . It should be noted that there are only $\text{CH}\cdots\text{HC}$ interactions of 'a'-type in the described structures of dimers and trimers whereas in tetramers the alcohol molecules orientate in such way that tetramer 1 has $\text{CH}\cdots\text{HC}$ interactions of 'a'-type, and tetramer 2 has $\text{CH}\cdots\text{HC}$ interactions of 'f'-type as well. But during the optimization of the tetramer 2 another 'b'-type of $\text{CH}\cdots\text{HC}$ interactions appears between the middle monomers, whereas these interactions are not realized in larger clusters and 2D monolayer phases. That is why it would be unreasonable to calculate the thermodynamic parameters of clusterization for such aggregates and include them in the further construction of the additive scheme. Larger clusters, such as, octamers and nonamers were built to obtain the energetic increments of the interactions n_2 , because in dimers, trimers and tetramers they are not realize or distorted by edge effects. The chosen clusters are presented in Figure 2 on the example of structures with 10 carbon atoms in the alkyl chains. Octamers and nonamers have one or two interactions n_2 correspondingly. In addition these clusters possess the considered two types of intermolecular $\text{CH}\cdots\text{HC}$ interactions. Note, that for nonamers only several structures are built with alkyl chains of 11-14 carbon atoms. It is given rise by the fact that the clusters with shorter alkyl chains has edge effects, and for clusters with longer chains it is impossible to calculate the thermodynamical properties of formation because of atom number restriction.

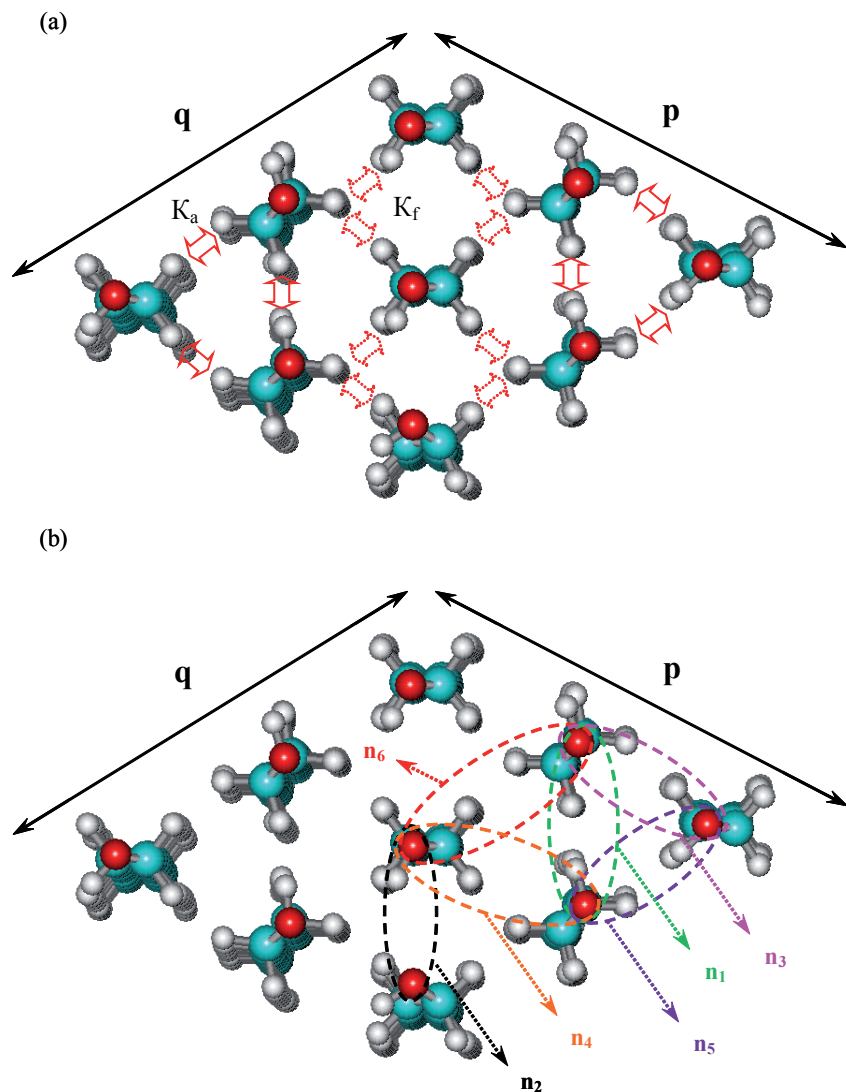


Figure 4. Types of pair intermolecular a) $\text{CH}\cdots\text{HC}$ interactions and b) interactions between the hydroxylic groups

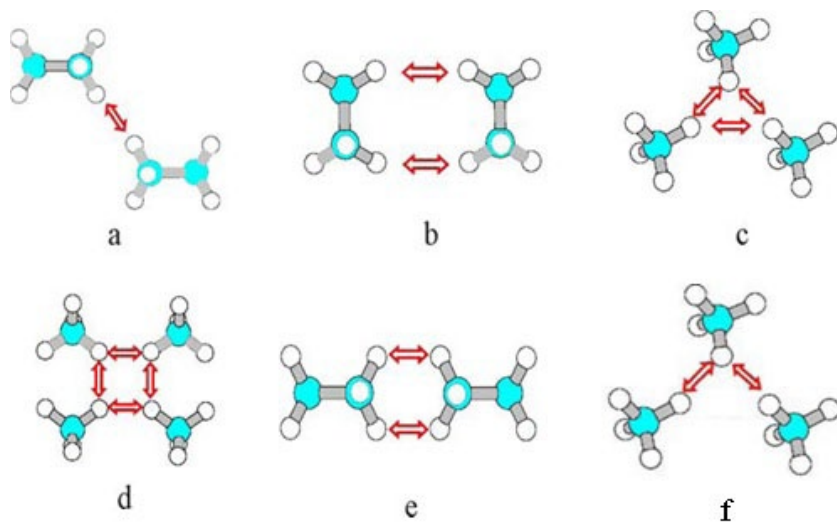


Figure 5. Intermolecular $CH\cdots HC$ interactions of different types

For all the small aggregates described above the thermodynamic parameters of their formation and clusterization are calculated. Enthalpy, entropy and Gibbs' energy of clusterization are calculated as previously [8-10, 33-42] according to the formulas:

$$\Delta H_{T,m}^{Cl} = \Delta H_T^0 - m \cdot H_{T,mon}^0 ; \Delta S_{T,m}^{Cl} = S_T^0 - m \cdot S_{T,mon}^0 ; \Delta G_{T,m}^{Cl} = \Delta H_{T,m}^{Cl} - T \cdot \Delta S_{T,m}^{Cl} ,$$

where ΔH_T^0 and S_T^0 are enthalpy and entropy of the aggregates at a certain temperature T , $H_{T,mon}^0$ and $S_{T,mon}^0$ are enthalpy and entropy of the corresponding monomers at the same temperature T , and m is the number of monomers in the cluster.

The corresponding values of enthalpy, entropy and Gibbs energy of clusterization are listed in Table 2. Here, we do not give the values of the thermodynamic clusterization parameters for tetramers 2 and nonamers (except the structures possessing 11-14 carbon atoms in the alkyl chains). These clusters have edge effects, so they are excluded from the further construction of the additive scheme for hexagonal monolayers of alcohols.

Table 2. Thermodynamic parameters of fatty alcohol aggregates

molecule	$\Delta H_{298,m}^{Cl}$, kJ/mol	$\Delta S_{298,m}^{Cl}$, J/(mol·K)	$\Delta G_{298,m}^{Cl}$, kJ/mol	$\Delta H_{298,m}^{Cl}$, kJ/mol	$\Delta S_{298,m}^{Cl}$, J/(mol·K)	$\Delta G_{298,m}^{Cl}$, kJ/mol
Dimer			Trimer 1			
C ₆ H ₁₃ OH	-29.93	-154.53	16.12	-84.79	-369.80	25.41
C ₇ H ₁₅ OH	-37.96	-165.11	11.24	-110.62	-420.52	14.69
C ₈ H ₁₇ OH	-40.44	-173.61	11.30	-114.33	-427.83	13.17
C ₉ H ₁₉ OH	-48.34	-173.42	3.34	-140.08	-476.41	1.89
C ₁₀ H ₂₁ OH	-50.86	-191.52	6.22	-143.85	-478.24	-1.33
C ₁₁ H ₂₃ OH	-58.73	-205.34	2.46	-169.58	-528.49	-12.09
C ₁₂ H ₂₅ OH	-61.25	-217.91	3.68	-173.35	-546.22	-10.57
C ₁₃ H ₂₇ OH	-69.12	-237.98	1.79	-199.09	-576.48	-27.30
C ₁₄ H ₂₉ OH	-71.66	-251.97	3.42	-202.87	-589.71	-27.13
C ₁₅ H ₃₁ OH	-79.53	-266.50	-0.12	-228.63	-635.49	-39.25
C ₁₆ H ₃₃ OH	-82.07	-264.68	-3.20	-232.40	-643.92	-40.51
Trimer 2			Tetramer 1			
C ₆ H ₁₃ OH	-86.88	-376.52	25.33	-129.86	-602.56	49.70
C ₇ H ₁₅ OH	-96.15	-395.00	21.56	-154.04	-659.61	42.52
C ₈ H ₁₇ OH	-116.42	-436.12	13.54	-173.93	-695.47	33.32
C ₉ H ₁₉ OH	-125.61	-451.46	8.92	-198.32	-752.55	25.94
C ₁₀ H ₂₁ OH	-146.00	-490.11	0.05	-218.24	-785.10	15.72
C ₁₁ H ₂₃ OH	-155.13	-506.60	-4.16	-242.66	-838.31	7.16
C ₁₂ H ₂₅ OH	-175.56	-562.19	-8.02	-262.62	-899.69	5.49
C ₁₃ H ₂₇ OH	-184.68	-559.75	-17.87	-287.07	-936.00	-8.14
C ₁₄ H ₂₉ OH	-205.13	-607.65	-24.05	-307.07	-982.68	-14.23
C ₁₅ H ₃₁ OH	-214.23	-619.08	-29.74	-331.45	-1031.30	-24.12
C ₁₆ H ₃₃ OH	-234.68	-664.81	-36.56	-351.44	-1069.99	-32.58

molecule	$\Delta H_{298,m}^{Cl}$, kJ/mol	$\Delta S_{298,m}^{Cl}$, J/(mol·K)	$\Delta G_{298,m}^{Cl}$, kJ/mol	$\Delta H_{298,m}^{Cl}$, kJ/mol	$\Delta S_{298,m}^{Cl}$, J/(mol·K)	$\Delta G_{298,m}^{Cl}$, kJ/mol
Pentamer						
C ₆ H ₁₃ OH	-171.31	-757.85	54.53	-320.28	-1441.59	109.31
C ₇ H ₁₅ OH	-206.44	-830.10	40.93	-379.29	-1570.30	88.66
C ₈ H ₁₇ OH	-230.50	-875.97	30.54	-429.04	-1667.58	67.90
C ₉ H ₁₉ OH	-265.47	-943.27	15.62	-488.24	-1796.68	47.17
C ₁₀ H ₂₁ OH	-289.71	-987.74	4.63	-538.08	-1898.65	27.71
C ₁₁ H ₂₃ OH	-324.59	-1057.39	-9.49	-597.34	-2076.03	21.32
C ₁₂ H ₂₅ OH	-348.90	-1123.70	-14.04	-647.31	-2212.05	11.88
C ₁₃ H ₂₇ OH	-383.79	-1167.71	-35.82	-706.62	-2362.18	-2.69
C ₁₄ H ₂₉ OH	-408.13	-1218.81	-44.93	-756.68	-2410.92	-38.23
C ₁₅ H ₃₁ OH	-442.98	-1286.90	-59.48	-815.99	-2532.51	-61.30
C ₁₆ H ₃₃ OH	-467.27	-1332.86	-70.08	-866.06	-2628.24	-82.84
Nonamer						
C ₁₁ H ₂₃ OH	-695.15	-2377.45	13.33			
C ₁₂ H ₂₅ OH	-754.36	-2519.44	-3.56			
C ₁₃ H ₂₇ OH	-822.64	-2629.85	-38.94			
C ₁₄ H ₂₉ OH	-882.02	-2758.36	-60.03			

The correlation dependencies on the number of intermolecular CH \cdots HC interactions and interactions between the functional groups are built on the basis of calculated thermodynamic clusterization parameters (see Table 1):

$$\Delta H_{298,m}^{Cl} = -(9.15 \pm 0.07) \cdot (K_a + K_p) - (18.42 \pm 1.22) \cdot n_1 + (11.11 \pm 1.53) \cdot n_4$$

[R = 0.9998; S = 7.00 kJ/mol; N = 70], (4)

$$\Delta S_{298,m}^{Cl} = -(19.79 \pm 0.19) \cdot (K_a + K_f + n_4) - (117.24 \pm 3.59) \cdot n_1 - (80.44 \pm 5.19) \cdot n_5 - (95.08 \pm 4.85) \cdot n_6 \quad [R = 0.9999; S = 15.47 \text{ J}/(\text{mol}\cdot\text{K}); N = 70], \quad (5)$$

where K_a and K_f are the number of $\text{CH}\cdots\text{HC}$ interactions of both 'a' and 'f' type realized in the regarded cluster.

They can be obtained (see Figure 4) as follows:

$$K_a = \left\{ \frac{n-1}{2} \right\}, \quad K_f = \left\{ \frac{n}{2} \right\} \quad \text{for the dimers with the interactions } n_1 \text{ and } n_3, n_5 \quad (6)$$

$$\text{and } K_f = \left\{ \frac{n+1}{2} \right\} \quad \text{for the dimers with } n_4 \text{ and } n_6, \text{ respectively} \quad (7)$$

where n is the number of methylene groups in the alkyl chain of the alcohols; the braces denote the integer part of the number; n_i are the descriptors of interactions of the monomer functional groups in the structures of the regarded clusters.

In the case that interactions between the functional groups of the hydrophilic part exist in the aggregate structure then the value of the corresponding descriptor n_i is equal to the number of such interactions. If the considered interaction is absent, this descriptor is zero.

Using equation $\Delta G_{298,m}^{Cl} = \Delta H_{298,m}^{Cl} - T \cdot \Delta S_{298,m}^{Cl}$ the correlation dependency for clusterization Gibbs' energy is obtained:

$$\Delta G_{298,m}^{Cl} = -(3.26 \pm 0.13) \cdot (K_a + K_f) + (16.52 \pm 2.29) \cdot n_1 + (17.01 \pm 1.59) \cdot n_4 + (23.97 \pm 1.55) \cdot n_5 + (28.34 \pm 1.44) \cdot n_6. \quad (8)$$

It is plain to see from the correlation dependencies (4), (5) and (8), that the energetic increments of the intermolecular $\text{CH}\cdots\text{HC}$ interactions of both types are identical. This allows one not to distinguish these interactions in further calculations according to the additive scheme for larger clusters up to 2D films and assuming them as one 'a' type. It should be mentioned that the values of the standard deviations of clusterization enthalpy and entropy for small aggregates of alcohols formed hexagonal monolayer are commensurable with ones formed a monolayer with oblique unit cell [9].

The dependencies of the clusterization parameters per one monomer

molecule on the alkyl chain length of alcohol at 298 K are shown in Figures 6-8. Here, the lines correspond to the dependencies calculated according to the correlation equations (6)-(8), whereas the points define the results of the direct calculations using the PM3 method. Note that the parameters for all small aggregates calculated according to the correlation expressions (4), (5), (8) are divided by the number of the monomers in the regarded cluster (by $m=2$ for dimers, by $m=3$ for trimers etc.). The presented graphs show that the results obtained according to the correlation equations agree well with the results of the direct calculation.

Analysis of given dependencies of the clusterization Gibbs' energy allows assumptions about the possible way of the formation of the hexagonal lattice structure. Figure 8 indicates that the smallest values of clusterization Gibbs' energy belong to the structures of trimers 1 and 2 among all the aggregates of alcohols. The formation of trimer 1 is slightly more favorable. This suggests that the alcohol hexagonal structures are formed from these two trimer structures. In what follows the aggregation of mentioned trimers will go on via formation of hexamers and larger clusters up to 2D condensed phases.

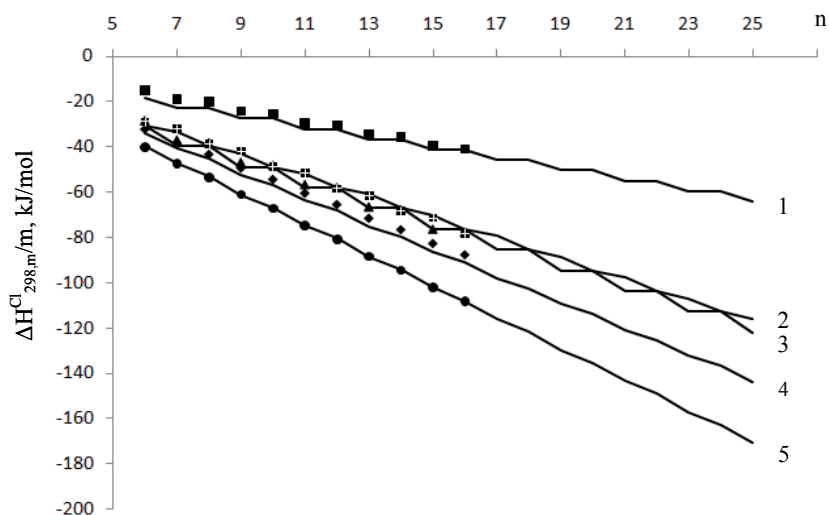


Figure 6. Dependence of the variation of the oligomerization enthalpy of aliphatic alcohols on the alkyl chain length: 1 – dimer; 2 – trimer 2; 3 – trimer 1; 4 – tetramer 1; 5 – octamer

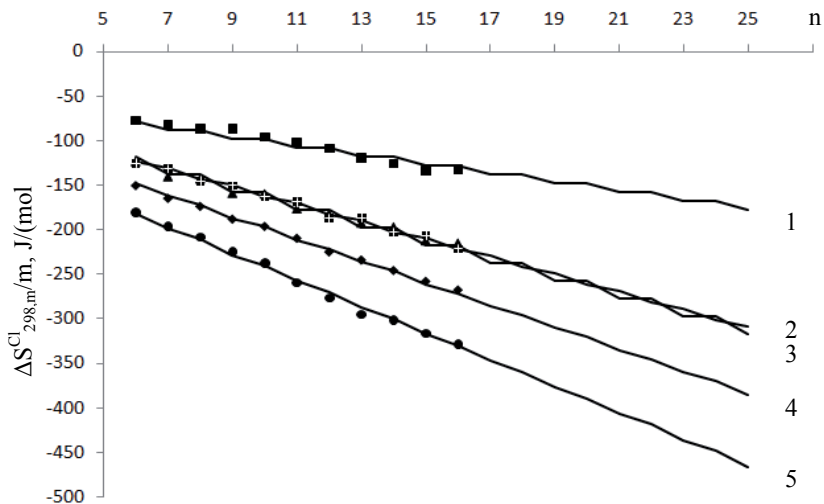


Figure 7. Dependence of the variation of the oligomerization entropy for aliphatic alcohols on the alkyl chain length (definitions 1-6 have the same meaning as in Figure 6)

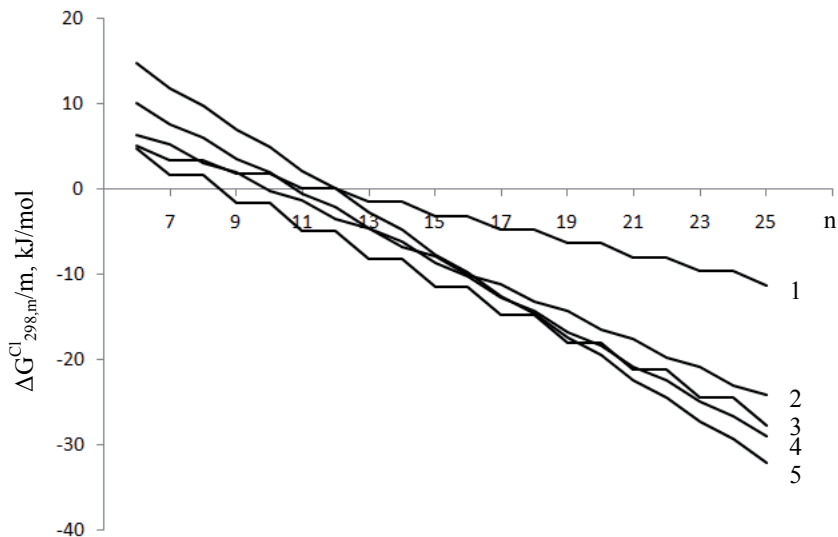


Figure 8. Dependence of the variation of the oligomerization Gibbs' energy for aliphatic alcohols on the alkyl chain length (definitions 1-6 have the same meaning as in Fig. 6)

The foregoing assumption about the possible way of formation of alcohol hexagonal films conforms to the results of the simulation of the experimental $\Pi - A$ isotherms for alcohol homologues series with 12-14 and 16 carbon atoms in the alkyl chain [8-10]. The thermodynamic model exploited in these studies is capable of the theoretical description of adsorption monolayer behavior at the air/water interface, including the thermodynamic clusterization parameters and aggregation number m for small clusters, which are the basic structures during the clusterization process. These studies reveal that LE-LC phase transition in alcohol monolayers takes place between aggregates with $m=2.3$ for dodecanol (at 15°C), $m=2.75$ for tridecanol (at 25°C), $m=3.0$ for tetradecanol (at 25°C) [8-10, 15]. Consequently, it is reasonable to conclude that the hexagonal phase of alcohol monolayers is formed on the basis of the trimer formation and their subsequent aggregation.

2.2. Carboxylic acids

Monomers.

Structural parameters. After carrying out the conformational analysis (varying the values of the torsion angles $\angle\beta=C_2-C_1-O_1-H$ and $\angle\gamma=C_3-C_2-C_1-O_2$ (see Fig. 9) from 0° to 360° with the step 15°) for the monomers of carboxylic acid it was demonstrated that there is one energetic minima for the angle $\angle\beta=C_2-C_1-O_1-H$ equal to 180°, while for the angle $\angle\gamma=C_3-C_2-C_1-O_2$ there two minima: one from -75° to -112°, and another from -35° to -40°. It should be mentioned that the value of the first minima is the same with corresponding parameter obtained earlier for molecules of the fatty carboxylic acids in the cluster with oblique unit cell [34].

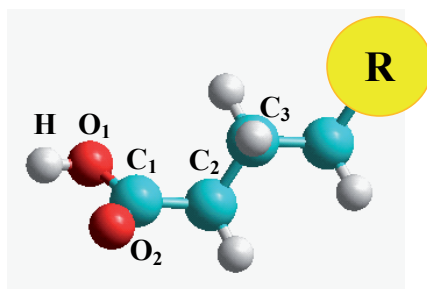


Figure 9. Structural fragment of the carboxylic acid molecular in the monolayer (R is hydrocarbon radical)

To obtain a tilt angle between the molecules and the normal to the interface one should use the procedure described in details in [42]. Analysis shows that this angle varies in range from -15° to 25° . So there are two minima on the dependence of the Gibbs' energy of formation on this angle: $15^\circ-16^\circ$ and $1^\circ-2^\circ$ to the normal to the air/water interface. These data corresponds to the experimental parameters for the tilted and untilted monolayer [47-49]. In this work structural and thermodynamic parameters of the clusterization were calculated for dimers, trimers and tetramers of untilted structure.

Thermodynamic parameters. Quantum chemical calculations of the thermodynamic parameters of formation and clusterization were carried out within semiempiric program complex Mopac 2012 (PM3 method).

Earlier in [34] enthalpy and Gibbs' energy of formation of the carboxylic acid monomers and their absolute enthalpy were calculated (such monomers were indicated as Monomers 1 in [34] and in this paper). In [34] calculations of the thermodynamic parameters were carried out in the frameworks of the program complex Mopac 2000 [43], as calculations in this work were made with the help of Mopac 2012, the necessity to compare corresponding parameters appeared. Also all results of the calculations were compared with the corresponding experimental parameters. Also the same parameters were carried out for the monomers with value of the torsion angle $\angle \gamma=C_3-C_2-C_1-O_2$ equal to -35° ; these monomers were indicated as Monomers 2. All results are listed in Table 3.

From the Table 3 one can see that parameters of the Monomers 1 and Monomers 2 coincide. So, in the further calculations only parameters of the Monomers 1 were used. Besides that results obtained in the frameworks of the Mopac 2012 good reproduce not only parameters calculated earlier in Mopac 2000, but also what is more important present experimental data. Standard derivation for the enthalpy of formation for the Monomers 1 and Monomers 2 calculated in Mopac 2012 from the parameters calculated within Mopac 2000 are 0.10 and 0.11 kJ/mol correspondingly and from the experimental parameters 4.74 kJ/mol. Standard derivation for the enthalpy calculated in Mopac 2000 from the experimental data are 5.9 kJ/mol for carboxylic acids [34], 23.0 kJ/mol for alcohols [50, 51], 15.6 and 10.8 kJ/mol for amines [36], 5.7 and 3.9 kJ/mol for thioalcohols [37].

As earlier, the Mopac 2012 does not include increment of the free rotation of the methylene fragments into the values of the absolute entropy calculations. That is why as previously (e.g. refs. [10, 35-37]), values of this correction for the free rotation was obtained with the least-squares method. For the Monomers 1 it

is 7.84 J/(mol·K) per methylene group, for Monomers 2 – 7.71 J/(mol·K), while analogous correction obtained earlier within Mopac 2000 for carboxylic acids was 6.1 J/(mol·K) [34]. Similar corrections for the alcohols, thioalcohols and amines were 6.6, 7.03 and 7.08 J/(mol·K) correspondingly [10, 35-37]. So, the values of the all corrections are quite close to each other. There are values of the absolute entropy and Gibbs' energy of monomers formation with the accounting of this correction in the Table 3. These results are in the good agreement with corresponding experimental data. Standard derivation of the absolute entropy from the experimental values are 5.48 and 5.51 J/(mol·K).

Table 3. Thermodynamic parameters of monomers of carboxylic acids

Molecule	Mopac 2000	Mopac 2012		Experiment [50, 51]
	Monomer 1	Monomer 1	Monomer 2	
	$\Delta H_{298, \text{mon}}^{\circ}$, kJ/mol			
C ₇ H ₁₅ COOH	-535.52	-558.66	-558.64	-556.00
C ₈ H ₁₇ COOH	-558.20	-581.38	-581.35	-577.30
C ₉ H ₁₉ COOH	-580.86	-604.10	-604.14	-594.30
C ₁₀ H ₂₁ COOH	-603.54	-626.83	-626.83	-614.60
C ₁₁ H ₂₃ COOH	-626.22	-649.56	-649.60	-640.00
C ₁₂ H ₂₅ COOH	-648.90	-672.30	-672.31	-660.20
C ₁₃ H ₂₇ COOH	-671.58	-695.03	-695.07	-683.00
C ₁₄ H ₂₉ COOH	-694.26	-717.77	-717.77	-699.00
C ₁₅ H ₃₁ COOH	-716.94	-740.49	-740.49	-723.00
C ₁₆ H ₃₃ COOH		-763.25	-763.25	-743.00
	$S_{298, \text{mon}}^{\circ}$, J/(mol·K)			
C ₇ H ₁₅ COOH	535.30	528.29	527.81	520.00
C ₈ H ₁₇ COOH	573.36	566.43	565.60	559.00
C ₉ H ₁₉ COOH	612.20	604.52	604.40	599.00
C ₁₀ H ₂₁ COOH	651.25	641.63	641.61	638.00
C ₁₁ H ₂₃ COOH	688.88	679.88	680.59	677.40

Molecule	Mopac 2000		Mopac 2012		Experiment [50, 51]
	Monomer 1	Monomer 1	Monomer 1	Monomer 2	
C ₁₂ H ₂₅ COOH	727.75	717.21	716.62	716.62	717.00
C ₁₃ H ₂₇ COOH	765.40	754.79	756.88	756.88	754.00
C ₁₄ H ₂₉ COOH	802.55	792.33	791.41	791.41	796.00
C ₁₅ H ₃₁ COOH	841.22	829.43	829.21	829.21	833.00
C ₁₆ H ₃₃ COOH		865.52	865.37	865.37	874.00
$\Delta G_{298, \text{mon}}^{\circ}$, kJ/mol					
C ₇ H ₁₅ COOH	-331.58	-331.85	-331.69	-331.69	-325.00
C ₈ H ₁₇ COOH	-324.96	-325.33	-325.06	-325.06	-317.00
C ₉ H ₁₉ COOH	-318.58	-318.80	-318.81	-318.81	-305.00
C ₁₀ H ₂₁ COOH	-312.27	-311.99	-311.98	-311.98	-296.63
C ₁₁ H ₂₃ COOH	-305.54	-305.51	-305.75	-305.75	-293.10
C ₁₂ H ₂₅ COOH	-299.17	-298.77	-298.60	-298.60	-284.50
C ₁₃ H ₂₇ COOH	-292.44	-292.09	-292.75	-292.75	-278.00
C ₁₄ H ₂₉ COOH	-285.57	-285.41	-285.14	-285.14	-266.00
C ₁₅ H ₃₁ COOH	-279.14	-278.58	-278.52	-278.52	-260.00
C ₁₆ H ₃₃ COOH		-271.49	-271.45	-271.45	-252.00

On the basis of these calculated data dependencies of the enthalpy of monomers formation and absolute entropy on the number of carbon atoms in the chain (n) were obtained:

$$\Delta H_{298, \text{mon}}^{\circ} = -(22.68 \pm 0.00) \cdot n - (339.51 \pm 0.01), \text{ kJ/mol},$$

$$[R = 1, S = 0.0016 \text{ J}/(\text{mol} \cdot \text{K}), N = 20]; \quad (9)$$

$$S_{298, \text{mon}}^{\circ} = (29.78 \pm 0.10) \cdot n + (266.13 \pm 1.17), \text{ J}/(\text{mol} \cdot \text{K}),$$

$$[R = 0.9999, S = 1.27 \text{ J}/(\text{mol} \cdot \text{K}), N = 20]. \quad (10)$$

Slopes of the correlation dependencies (9) and (10) characterize the increment of the one methylene group to the corresponding parameter coincide with the corresponding parameters which were calculated earlier within Mopac 2000 or very close to them. So values of the slopes of correlation dependencies of enthalpy and entropy calculated earlier in Mopac 2000 for the carboxylic acids, are $-(22.68 \pm 0.00)$ kJ/mol and (38.23 ± 0.05) J/(mol·K) [34] correspondingly; for the *cis*-unsaturated carboxylic acids they are $-(22.68 \pm 0.00)$ kJ/mol and (30.55 ± 0.17) J/(mol·K) [37], for *trans*-unsaturated $-(22.68 \pm 0.00)$ kJ/mol and (30.53 ± 0.05) J/(mol·K) [41]. Increments of the carboxylic groups characterized by the free term of the dependencies (9) and (10) are equal to $-(399.47 \pm 0.01)$ kJ/mol and (268.19 ± 0.57) J/(mol·K) (within Mopac 2000) for the enthalpy and entropy correspondingly [34]. So these parameters are also in good agreement with the corresponding parameters calculated in the frameworks of Mopac 2012.

Oligomers. There is the fragment of the carboxylic acids monolayer is shown in the Fig. 10 (bottom view). There are three types of the pair intermolecular $\text{CH}\cdots\text{HC}$ interactions between neighbor hydrocarbon chains. These types of interactions were indicated as “a”-, “b”- and “c”-type and there numbers – as K_a , K_b and K_c (see Fig. 10) correspondingly. These types of interactions are discussed in details in [9, 10, 52]. There are also six types of the pair intermolecular interactions between carboxylic groups (see Fig. 11). Symbolically direction from the carbon atom to the ketonic oxygen atom in the carboxylic group is indicated by arrows. Increments from these interactions in the thermodynamic parameters differ because of the different mutual orientation of the interacting groups. To describe infinite cluster of the carboxylic acids (monolayer) one need to obtain increments in the enthalpy and entropy of clusterization from the each pair intermolecular $\text{CH}\cdots\text{HC}$ interaction and each pair interaction between carboxylic groups. For this purpose the structures of dimers, trimers and tetramers were investigated. They are the parts of the investigated cluster and comprise all these types of the interactions.

From the Figs. 10 and 12 one can see that interactions of the “a”-type form as a result of the interaction between each second methylene group, interactions of the “b”-type as a result of the interaction between each methylene group, so with the same chain length there are twice more interactions of the “b”-type than “a”-type. There are one pair intermolecular interaction of the “a”-type, two – of the “b”-type and three – of the “c”-type in the Fig. 10 which are indicated by the arrows.

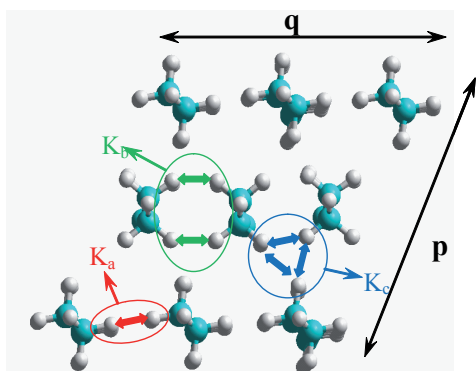


Figure10. Types of intermolecular $CH\cdots HC$ interactions

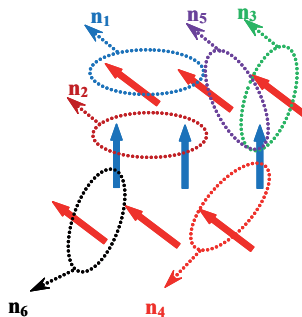


Figure11. Types of pair intermolecular interactions between carboxylic groups

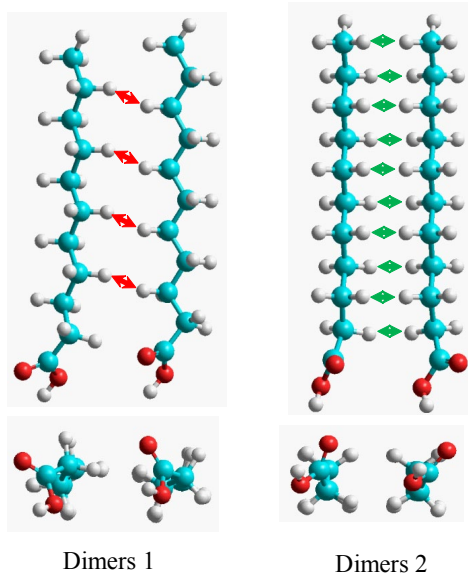


Figure 12. Optimized structures of the dimers of fatty carboxylic acids of untilted monolayer

For the dimers structures presented in Fig. 11 thermodynamic parameters of formation and clusterization were calculated. Pair intermolecular $CH\cdots HC$

interactions are indicated by the arrows. Thermodynamic parameters of formation ($\Delta H_{298,m}^0$, $\Delta S_{298,m}^0$) and clusterization ($\Delta H_{298,m}^{Cl}$, $\Delta S_{298,m}^{Cl}$, $\Delta G_{298,m}^{Cl}$) calculated within Mopac 2012 were compared with the corresponding parameters calculated earlier within (see Table 4).

Table 4. Thermodynamic parameters of dimers 1 of carboxylic acids

Molecule	$\Delta H_{298,m}^0$	$\Delta S_{298,m}^0$	$\Delta H_{298,m}^{Cl}$	$\Delta S_{298,m}^{Cl}$	$\Delta G_{298,m}^{Cl}$
	kJ/mol	J/(mol·K)	kJ/mol	J/(mol·K)	kJ/mol
Mopac 2000					
C ₇ H ₁₅ COOH	-1149.19	792.45	-32.89	-183.43	21.78
C ₈ H ₁₇ COOH	-1202.01	851.46	-40.38	-188.56	15.81
C ₉ H ₁₉ COOH	-1249.92	901.92	-42.94	-200.36	16.76
C ₁₀ H ₂₁ COOH	-1303.00	952.03	-50.68	-215.86	13.65
C ₁₁ H ₂₃ COOH	-1350.91	1002.77	-53.46	-224.26	13.37
C ₁₂ H ₂₅ COOH	-1404.04	1052.24	-61.04	-242.08	11.10
C ₁₃ H ₂₇ COOH	-1451.90	1103.82	-63.53	-249.93	10.95
C ₁₄ H ₂₉ COOH	-1505.09	1153.16	-71.43	-267.15	8.18
C ₁₅ H ₃₁ COOH	-1552.98	1206.51	-73.99	-273.99	7.66
Mopac 2012					
C ₇ H ₁₅ COOH	-1150.22	765.79	-32.90	-181.03	21.04
C ₈ H ₁₇ COOH	-1203.14	820.47	-40.38	-186.95	15.33
C ₉ H ₁₉ COOH	-1251.25	866.38	-43.05	-201.54	17.01
C ₁₀ H ₂₁ COOH	-1304.34	916.29	-50.68	-210.17	11.95
C ₁₁ H ₂₃ COOH	-1352.41	967.24	-53.29	-220.04	12.28
C ₁₂ H ₂₅ COOH	-1405.62	1012.66	-61.02	-233.6	8.59
C ₁₃ H ₂₇ COOH	-1453.67	1062.94	-63.61	-242.8	8.74
C ₁₄ H ₂₉ COOH	-1506.93	1107.31	-71.39	-257.83	5.45
C ₁₅ H ₃₁ COOH	-1554.98	1157.53	-74.00	-266.13	5.31
C ₁₆ H ₃₃ COOH	-1608.25	1202.01	-81.75	-282.01	2.29

As one can see values of the corresponding characteristics are in the good agreement. The standard derivation for the enthalpy and entropy of dimerization calculated in the frameworks of the program complex Mopac 2012 from the

previously calculated parameters (Mopac 2000) are correspondingly the next: 0.08 kJ/mol, 3.0 J/mol·K. For the row of the Dimers 1 ($n = 7 - 16$) correlation dependencies of the calculated parameters of clusterization on the number of the pair intermolecular $\text{CH}\cdots\text{HC}$ interactions (only “a”-type of interactions is realized in Dimers 1 (see Fig. 12) and one type of the pair interactions between carboxylic acids n_1 (see Fig. 11)):

$$\Delta H_{298,m}^{Cl} = - (10.02 \pm 0.03) \cdot K_a - (2.11 \pm 1.67) \text{ kJ/mol},$$

$$[R = 0.997, S = 1.39 \text{ J/(mol}\cdot\text{K)}, N = 10]; \quad (11)$$

$$\Delta S_{298,m}^{Cl} = - (21.27 \pm 1.28) \cdot K_a - (111.18 \pm 7.32), \text{ J/(mol}\cdot\text{K)},$$

$$[R = 0.99, S = 6.09 \text{ J/(mol}\cdot\text{K)}, N = 10], \quad (12)$$

hereinafter K_a is the number of the “a”-type of the pair intermolecular $\text{CH}\cdots\text{HC}$ interactions.

Increments in the enthalpy and entropy of dimerization from the one $\text{CH}\cdots\text{HC}$ intermolecular interaction of “a”-type are characterized by the slopes from the expressions (11) and (12) and increment from the pair intermolecular interactions between carboxylic groups by the free terms. Values of slopes calculated for the carboxylic acids within Mopac 2000 were $-(10.29 \pm 0.33)$ kJ/mol and $-(24.76 \pm 1.59)$ J/(mol·K) for the enthalpy and entropy correspondingly. Values of the free term of the expressions (11) and (12) obtained in the frameworks of the program Mopac 2000 were $-(0.57 \pm 1.71)$ kJ/mol and $-(96.91 \pm 8.28)$ J/(mol·K) for the enthalpy and entropy correspondingly.

Besides dimers structures of the five trimers (see Fig. 13) and two tetramers (see Fig. 14) of the carboxylic acids were considered. For all regarded clusters thermodynamic parameters of their formation and clusterization were calculated (see Table 5).

Series of our previous works about thermodynamic parameters of the calculations of the substituted alkanes at air/water interface demonstrated that the values of the parameters calculated within quantum chemical semiempiric PM3 method (Mopac 2000) reproduce corresponding experimental parameters with the good level of accuracy [9, 10, 34-37, 39, 41, 52].

As thermodynamic parameters of monomer and dimer formation and clusterization (in terms of the Dimers 1) are very close to the parameters calculated earlier in Mopac 2000 [34], it allows us to make conclusion that thermodynamic parameters of monomers and clusters of the substituted alkanes (in particular

carboxylic acids) calculated within Mopac 2012 will describe experimental parameters with the same accuracy. So such comparison did not take place for the other types of the clusters considered in this paper (see Figs. 12 – 14).

On the base of the calculated thermodynamic parameters (see Table 3 and table 5) correlation dependencies of the enthalpy and entropy of clusterization on the number of the pair $\text{CH}\cdots\text{HC}$ and interactions between functional groups of the different types were obtained

$$\begin{aligned} \Delta H_{298,m}^{Cl} = & - (9.34 \pm 0.08) \cdot K_a - (6.10 \pm 0.05) \cdot K_b - (7.19 \pm 0.053) \cdot K_c \\ & - (5.19 \pm 0.99) \cdot n_1 + (1.09 \pm 0.49) \cdot (n_2 + n_4 + n_5) - (1.58 \pm 0.69) \cdot n_3 - \\ & - (6.09 \pm 0.81) \cdot n_5 - (3.50 \pm 0.80) \cdot n_6 - (3.30 \pm 0.61) \cdot n_7, \text{ kJ/mol} \\ [R = 0.9999; S = 2.89 \text{ kJ/mol}; N = 120]; \end{aligned} \quad (13)$$

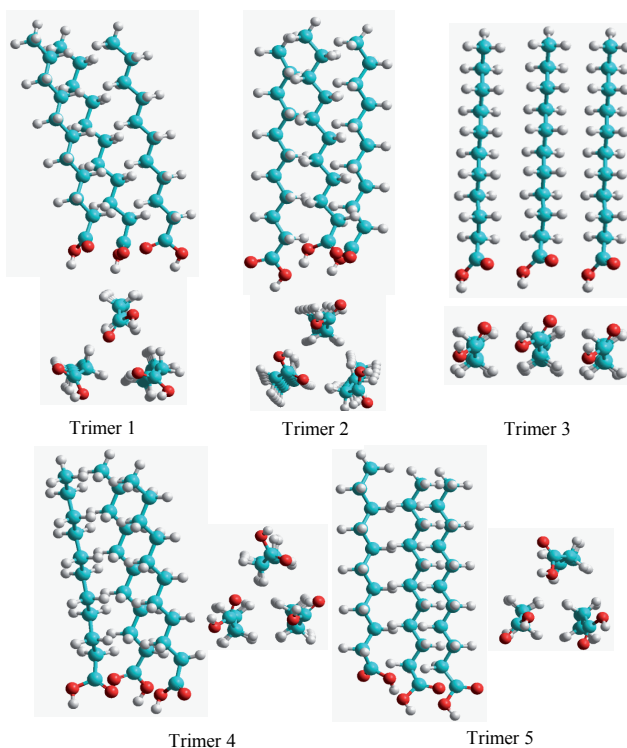


Figure 13. Optimized structures of the trimers of fatty carboxylic acids

Table 5. Thermodynamic parameters of dimers, trimers and tetramers of carboxylic acids

molecule	$\Delta H_{298,m}^0$ kJ/mol	$\Delta S_{298,m}^0$ J/(mol·K)	$\Delta H_{298,m}^{Cl}$ kJ/mol	$\Delta S_{298,m}^{Cl}$ J/(mol·K)	$\Delta G_{298,m}^{Cl}$ kJ/mol	$\Delta H_{298,m}^0$ kJ/mol	$\Delta S_{298,m}^0$ J/(mol·K)	$\Delta H_{298,m}^{Cl}$ kJ/mol	$\Delta S_{298,m}^{Cl}$ J/(mol·K)	$\Delta G_{298,m}^{Cl}$ kJ/mol
Dimers 2										
C ₇ H ₁₅ COOH	-1160.45	708.39	-43.13	-238.43	27.92	-1765.93	1005.57	-89.95	-414.66	33.61
C ₈ H ₁₇ COOH	-1212.05	749.55	-49.29	-257.87	27.55	-1857.50	1059.36	-113.36	-451.77	21.26
C ₉ H ₁₉ COOH	-1263.68	792.77	-55.48	-275.15	26.52	-1931.63	1133.45	-119.33	-468.43	20.26
C ₁₀ H ₂₁ COOH	-1315.30	832.62	-61.64	-293.84	25.93	-2023.29	1185.73	-142.80	-503.96	7.38
C ₁₁ H ₂₃ COOH	-1366.93	874.34	-67.81	-312.94	25.44	-2097.43	1261.85	-148.75	-519.07	5.93
C ₁₂ H ₂₅ COOH	-1418.56	915.94	-73.96	-330.32	24.47	-2189.14	1313.26	-172.24	-556.13	-6.52
C ₁₃ H ₂₇ COOH	-1470.20	957.81	-80.14	-347.93	23.54	-2263.27	1389.09	-178.18	-569.52	-8.46
C ₁₄ H ₂₉ COOH	-1521.84	999.40	-86.30	-365.74	22.69	-2355.01	1438.51	-201.70	-609.20	-20.16
C ₁₅ H ₃₁ COOH	-1573.49	1040.19	-92.51	-383.47	21.77	-2429.13	1514.42	-207.66	-621.07	-22.58
C ₁₆ H ₃₃ COOH	-1625.13	1080.32	-98.63	-403.70	21.67	-2520.90	1564.41	-231.15	-661.62	-33.99
Trimers 3										
C ₇ H ₁₅ COOH	-1764.71	1008.17	-88.73	-412.06	34.06	-1757.96	941.86	-81.98	-478.37	60.58
C ₈ H ₁₇ COOH	-1844.72	1072.27	-100.58	-438.86	30.20	-1838.42	996.65	-94.28	-514.48	59.03
C ₉ H ₁₉ COOH	-1930.54	1135.81	-118.24	-466.07	20.64	-1918.72	1054.05	-106.42	-547.83	56.83
C ₁₀ H ₂₁ COOH	-2010.38	1199.00	-129.89	-490.69	16.34	-1999.21	1107.07	-118.72	-582.62	54.90
C ₁₁ H ₂₃ COOH	-2096.42	1260.71	-147.74	-520.21	7.28	-2079.59	1162.29	-130.91	-618.63	53.44
C ₁₂ H ₂₅ COOH	-2176.17	1322.45	-159.27	-546.94	3.71	-2160.06	1218.11	-143.16	-651.28	50.92
C ₁₃ H ₂₇ COOH	-2262.32	1386.25	-177.23	-572.36	-6.66	-2240.49	1272.87	-155.40	-685.74	48.95

molecule	$\Delta H_{298,m}^0$, kJ/mol	$\Delta S_{298,m}^0$, J/(mol·K)	$\Delta H_{298,m}^{Cl}$, kJ/mol	$\Delta S_{298,m}^{Cl}$, J/(mol·K)	$\Delta G_{298,m}^{Cl}$, kJ/mol	$\Delta H_{298,m}^0$, kJ/mol	$\Delta S_{298,m}^0$, J/(mol·K)	$\Delta H_{298,m}^{Cl}$, kJ/mol	$\Delta S_{298,m}^{Cl}$, J/(mol·K)	$\Delta G_{298,m}^{Cl}$, kJ/mol
Trimers 4										
C ₁₄ H ₂₉ COOH	-2342.01	1446.00	-188.70	-601.71	-9.39	-2320.96	1327.83	-167.65	-719.88	46.88
C ₁₅ H ₃₁ COOH	-2428.23	1510.72	-206.76	-624.77	-20.58	-2401.42	1383.71	-179.95	-751.78	44.09
C ₁₆ H ₃₃ COOH	-2507.87	1568.83	-218.12	-657.20	-22.27	-2481.87	1438.03	-192.12	-788.00	42.70
Trimers 5										
C ₇ H ₁₅ COOH	-1765.27	963.39	-89.29	-456.84	46.85	-1764.52	990.38	-88.54	-429.85	39.56
C ₈ H ₁₇ COOH	-1851.01	1010.73	-106.87	-500.40	42.24	-1841.94	1066.87	-97.80	-444.26	34.59
C ₉ H ₁₉ COOH	-1928.71	1081.28	-116.41	-520.60	38.73	-1928.14	1115.08	-115.84	-486.80	29.22
C ₁₀ H ₂₁ COOH	-2014.74	1124.32	-134.25	-565.37	34.23	-2005.57	1190.92	-125.08	-498.77	23.56
C ₁₁ H ₂₃ COOH	-2092.31	1193.63	-143.63	-587.29	31.38	-2091.87	1239.13	-143.19	-541.79	18.26
C ₁₂ H ₂₅ COOH	-2178.51	1238.42	-161.61	-630.97	26.42	-2169.27	1315.69	-152.37	-553.70	12.63
C ₁₃ H ₂₇ COOH	-2256.02	1308.90	-170.93	-649.71	22.68	-2255.64	1360.51	-170.55	-598.10	7.68
C ₁₄ H ₂₉ COOH	-2342.30	1350.37	-188.99	-697.34	18.81	-2333.02	1441.24	-179.71	-606.47	1.02
C ₁₅ H ₃₁ COOH	-2419.77	1420.70	-198.30	-714.79	14.70	-2419.44	1484.60	-197.97	-650.89	-4.00
C ₁₆ H ₃₃ COOH	-2506.11	1461.88	-216.36	-764.15	11.36	-2496.80	1561.95	-207.05	-664.08	-9.16
Tetramers 1										
C ₇ H ₁₅ COOH	-2380.50	1217.24	-145.86	-676.40	55.71	-2379.60	1203.79	-144.96	-689.85	60.61
C ₈ H ₁₇ COOH	-2504.61	1271.78	-179.09	-743.06	42.34	-2489.55	1288.46	-164.03	-726.38	52.43
C ₉ H ₁₉ COOH	-2608.67	1369.72	-192.27	-766.12	36.03	-2607.99	1348.15	-191.59	-787.69	43.15
C ₁₀ H ₂₁ COOH	-2732.91	1422.40	-225.59	-830.52	21.90	-2717.82	1434.91	-210.50	-818.01	33.27

molecule	$\Delta H_{298,m}^0$ kJ/mol	$\Delta S_{298,m}^0$ J/(mol·K)	$\Delta H_{298,m}^{Cl}$ kJ/mol	$\Delta S_{298,m}^{Cl}$ J/(mol·K)	$\Delta G_{298,m}^{Cl}$ kJ/mol	$\Delta H_{298,m}^0$ kJ/mol	$\Delta S_{298,m}^0$ J/(mol·K)	$\Delta H_{298,m}^{Cl}$ kJ/mol	$\Delta S_{298,m}^{Cl}$ J/(mol·K)	$\Delta G_{298,m}^{Cl}$ kJ/mol
C ₁₁ H ₂₃ COOH	-2837.04	15116.06	-238.80	-858.50	17.03	-2836.45	1495.40	-238.21	-879.16	23.77
C ₁₂ H ₂₅ COOH	-2961.34	1569.64	-272.14	-922.88	2.88	-2946.23	1579.55	-257.03	-912.97	15.03
C ₁₃ H ₂₇ COOH	-3065.50	1663.02	-285.38	-948.46	-2.74	-3064.95	1641.70	-284.83	-969.78	4.16
C ₁₄ H ₂₉ COOH	-3189.83	1714.66	-318.75	-1015.62	-16.09	-3174.69	1724.98	-303.61	-1005.30	-4.03
C ₁₅ H ₃₁ COOH	-3293.98	1809.15	-332.02	-1038.17	-22.65	-3293.47	1786.17	-331.51	-1061.15	-15.29
C ₁₆ H ₃₃ COOH	-3418.35	1860.81	-365.35	-1107.23	-35.39	-3403.19	1870.18	-350.19	-1097.86	-23.02

$$\begin{aligned}
 \Delta S_{298,m}^{Cl} = & -(18.40 \pm 0.34) \cdot K_a - (17.05 \pm 0.40) \cdot K_b - (13.91 \pm 0.30) \cdot K_c - \\
 & -(122.29 \pm 4.29) \cdot (n_1 + n_2) - (80.76 \pm 3.25) \cdot (n_3 + n_4) - (66.51 \pm 4.90) \cdot n_4 - \\
 & -(49.19 \pm 4.60) \cdot n_6 - (56.00 \pm 5.11) \cdot n_7 - (112.27 \pm 4.62) \cdot n_8, \text{ J/(mol}\cdot\text{K)} \\
 (\text{R} = 0.9998; \text{S} = 16.50 \text{ kJ/mol}; \text{N} = 120)
 \end{aligned} \tag{14}$$

$$\begin{aligned}
 \Delta G_{298,m}^{Cl} = & -(3.86 \pm 0.18) \cdot K_a - (1.02 \pm 0.17) \cdot K_b - (3.06 \pm 0.14) \cdot K_c + \\
 & + (31.25 \pm 2.27) \cdot n_1 + (37.53 \pm 1.77) \cdot n_2 + (22.49 \pm 1.66) \cdot n_3 \\
 & + (20.91 \pm 1.95) \cdot n_4 + (17.98 \pm 1.78) \cdot n_5 + (11.16 \pm 2.17) \cdot n_6 \\
 & + (13.39 \pm 2.13) \cdot n_7 + (34.55 \pm 1.87) \cdot n_8, \text{ kJ/mol}
 \end{aligned} \tag{15}$$

where K_a , K_b , and K_c are the numbers of the pair intermolecular CH...HC interactions of 'a', 'b', and 'c'-types respectively; $n_1 - n_6$ are the numbers of the pair intermolecular interactions between carboxylic groups with the different mutual orientation (see Fig. 11).

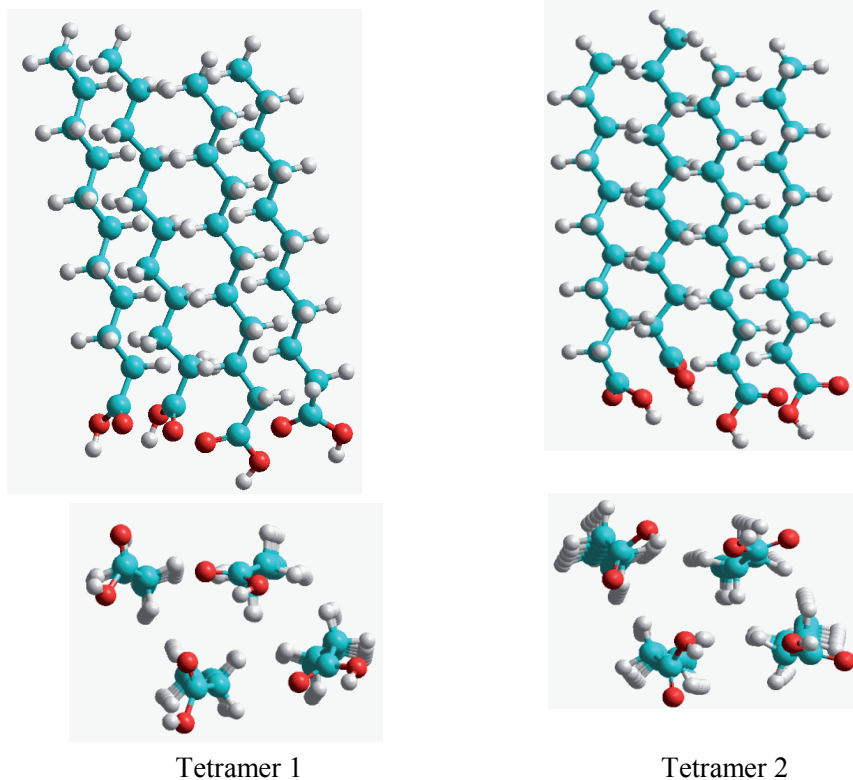


Figure 14. Optimized structures of the tetramers of fatty carboxylic acids of tilted monolayer

Values of the slopes in the expressions (13) and (14) coincide with the calculated earlier analogical parameters for the carboxylic acids and other classes of the substituted alkanes calculated in the frameworks of the Mopac 2000. These values are equal to $-(9.20 - 10.40)$ kJ/mol and $-(18.28 - 24.49)$ J/(mol·K) for the enthalpy and entropy correspondingly [9, 10, 35-37, 41, 51, 52].

Increment from the one intermolecular interaction in Gibbs' energy of clusterization is equal to -3.86 kJ/mol for 'a'-type interactions, -0.51 kJ/mol for 'b'-type, and -3.06 kJ/mol for 'c'-type. So 'a'-type of the pair $\text{CH}\cdots\text{HC}$ interactions is the most preferable. This fact is in the correspondence with our previous results [9, 10, 34-37, 41, 51, 52].

Using expression (15) graphic dependencies of Gibbs' energy of clusterization per one monomer on the number of the carbon atom in the chain (n) were plotted (see Fig. 15). As in the previous section for all considered clusters (from dimers to tetramers) parameters calculated using the expression (15) were referred to the number of the monomers in the cluster (thermodynamic parameters of dimerization were divided by two, of trimerization by three, of tetramerization by four).

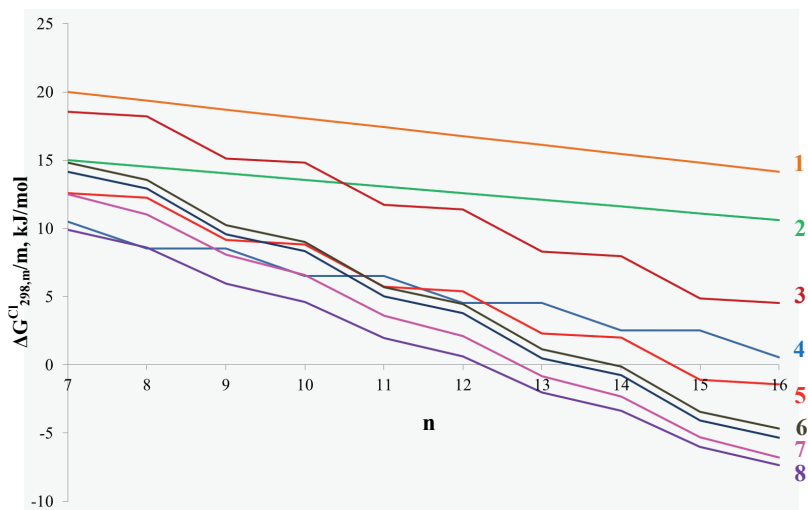


Figure 15. Dependences of the clusterization Gibbs' energy per monomer on the number of carbon atoms: 1 – trimers 3; 2 – dimers 2; 3 – trimers 4; 4 – dimers 1; 5 – trimers 5; 6 – tetramers 1, 2; 7 – trimers 1; 8 – trimers 2.

All obtained results are necessary to calculate thermodynamic parameters of the monolayer formation of hexagonal structure with untitled molecules of carboxylic acid and make an assumption about possible way of aggregation process.

Conclusion

The thermodynamic parameters of oligomerization clusterization are calculated for molecules with the general formula $C_nH_{2n+1}OH$ ($n=6-16$) and $C_nH_{2n+1}COOH$ ($n=7-16$). Calculated parameters of the monomer formation for regarded surfactants reproduce corresponding experimental parameters with

the high level of accuracy. Deviations of the calculated enthalpy of formation and absolute entropy from the experimental data are 4.25 kJ/mol and 1.64 J/(mol·K) for alcohols and 4.74 kJ/mol and 5.51 J/(mol·K) for carboxylic acids correspondingly.

The analysis of the calculated dependencies of the thermodynamic clusterization parameters per one monomer for small alcohol aggregates suggest the possible way of the formation of the hexagonal monolayer phase via formation of alcohol trimers and their further aggregation up to the infinite monolayer structure. This assumption corresponds well with the small aggregation numbers $m=2.3-3.0$ for the LE phase obtained by thermodynamic analysis of experimental $\Pi - A$ isotherms of homologues $C_{12}-C_{14}$ alcohols [8-10].

Spontaneous oligomerization of carboxylic acids is the most advantageous for structures of Trimers 1 and 2. Formation of these oligomers takes place for acids with alkyl chain length of 12-13 carbon atoms. Experimental data also indicates that at 298 K highly-ordered monolayers can be formed for the tetradecanoic (myristic) acid and the next members of the homologous series [53]. Scheme of the possible clusterization process was proposed: spontaneous clusterization probably starts from the formation of the trimers of two types which further form hexamers, larger clusters up to monolayers with the hexagonal unit cell.

References

1. Kuzmenko, I., Rapaport, H., Als-Nielsen, J., Als-Nielsen, J., Weissbuch, I., Lahav, M., Leiserowitz, L. *Chem. Rev.*, **2001**, *101*, 1659-1696.
2. Wang, J.-L., Leveiller, F., Jacquemain, D., Kjaer, K., Als-Nielsen, J., Lahav, M., Leiserowitz, L. *J. Am. Chem. Soc.*, **1994**, *116*, 1192-1204.
3. Weissbuch, I., Berfeld, M., Bouwman, W., Kjaer, K., Als-Nielsen, J., Lahav, M., Leiserowitz, L. *J. Am. Chem. Soc.*, **1997**, *119*, 933-942.
4. Nandi, N., Vollhardt, D. *Chem. Rev.*, **2003**, *103*, 4033-4075.
5. Vollhardt, D., Siegel, S., Cadenhead, D. A. *J. Phys. Chem. B*, **2004**, *108*, 17448-17456.
6. Weinbach, S. P., Jacquemain, D., Leveiller, F., Kjaer, K., Als-Nielsen, J., Leiserowitz, L. *J. Am. Chem. Soc.*, **1993**, *115*, 11110.
7. Kaganer, V. M., Möhwald, H., Dutta, P. *Rev. Modern Phys.*, **1999**, *71*, 779-819.
8. Vysotsky, Yu. B., Bryantsev, V. S., Fainerman, V. B., Vollhardt, D., Mille, R. *J. Phys. Chem. B*, **2002**, *106*, 121-131.
9. Vysotsky, Yu. B., Bryantsev, V. S., Fainerman, V. B., Vollhardt, D. *J. Phys. Chem. B*, **2002**, *106*, 11285-11294.
10. Vysotsky, Yu. B., Bryantsev, V. S., Fainerman, V. B., Vollhardt, D., Miller,

- R. *Coll. & Surf. A: Physicochem. Eng. Asp.*, **2002**, *209*, 1-14
11. Aveyard, R., Carr, N., Slezok, H. *Can. J. Chem.*, **1985**, *63*, 2742.
 12. Tsay, R.-Y., Wu, T.-F., Lin, S.-Y. *J. Phys. Chem. B*, **2004**, *108*, 18623-18629.
 13. Braun, R.; Casson, B. D.; Bain, C. D. *Chem. Phys. Lett.*, **1995**, *245*, 326.
 14. Melzer, V.; Vollhardt, D.; Weidemann, G.; Brezesinski, G.; Wagner, R.; Mohwald, H. *Phys. Rev. E*, **1998**, *57*, 901.
 15. Vollhardt, D.; Fainerman, V. B.; Emrich, G. *J. Phys. Chem.*, 2000, *104*, 8536.
 16. Kenn, R. M.; Biihm, C.; Bib, A. M.; Peterson, I. R.; Möhwald, H. *J. Phys. Chem.*, **1991**, *95*, 2092-2097.
 17. Friedenber, M. C.; Fuller, G. G.; Frank, C. W.; Robertson C. R. *Langmuir*, **1996**, *12*, 1594-1599.
 18. Maruyama, T. Lauger, J.; Fuller, G. G.; Frank, C. W.; Robertson, C. R. *Langmuir*, **1998**, *14*, 1836-1845.
 19. Riviere, S.; Henon, S.; Meunier, J., Schwartz, D. K., Tsao, M.-W., Knobler, C. M. *J. Chem. Phys.* **1994**, *101*, 10045-1051.
 20. Overbeck, G. A.; Mobius D. *J. Phys. Chem.*, **1993**, *97*, 7999-8004.
 21. Shin, M. C., Bohanon, T. M., Mikrut, J. M., Zschack, P., Dutta, P. *J. Chem. Phys.*, **1992**, *97*, 4485-4488.
 22. Kraack, H., Ocko, B. M., Pershan, P. S., Sloutskin, E., Tamam, L., Deutsch, M. *Langmuir*, **2004**, *20*, 5386-5395.
 23. Weinbach, S. P., Weissbuch, I., Kjaer, K., Bouman, W. G., Als-Nielsen, J., Lahav, M., Leiserowitz, L. *Adv. Mater.*, **1995**, *7*, 857-862.
 24. Majewski, J., Popovitz-Biro, R., Bouwman, W. G., Kjaer, K., Als-Nielsen, J., Lahav, M., Leiserowitz, L. *Chem. Eur. J.*, **1995**, *1*, 304-311.
 25. Vollhardt, D., Fainerman, V. B. *Adv. Coll. Int. Sci.*, **2010**, *154*, 1-19.
 26. Bohanon, T. M., Lin, B., Shih, M. C., Ice, G. E., Dutta, P. *Phys. Rev. B*, **1990**, *41*, 4846-4849.
 27. Kaganer, V., Möhwald, H., Dutta, P. *Rev. Mod. Phys.*, **1999**, *71*, 779-819.
 28. Kaganer, V. M., Loginov, E. B. *Phys. Rev. E*, **1995**, *51*, 2237-2249.
 29. Can, S. Z., Mago, D. D., Walker, R. A. *Langmuir*, **2006**, *22*, 8043-8049.
 30. Dai, J., Evans, J. S. *J. Phys. Chem. B*, **2001**, *105*, 10831-10837.
 31. Siepmann, J. I., McDonald, I. R. *Langmuir*, **1993**, *9*, 2351-2355.
 32. Bareman, J. P., Klein, M. L. *J. Phys. Chem.*, **1990**, *94*, 5202-5205.
 33. Vysotsky Yu. B., Bryantsev V. S., Boldyreva F. L., Fainerman V. B., Vollhardt D. *J. Phys. Chem. B*, **2005**, *109*, 454-462.

34. Vysotsky Yu. B., Muratov D. V., Boldyreva F. L., Fainerman V. B., Vollhardt D., Miller R. *J. Phys. Chem. B*, **2006**, *110*, 4717-4730.
35. Vysotsky Yu. B., Belyaeva E. A., Fainerman V. B., Vollhardt D., Miller R. *J. Phys. Chem. C*, **2007**, *111*, 5374-5381.
36. Vysotsky Yu. B., Belyaeva E. A., Fainerman V. B., Aksenenko E. V., Vollhardt D., Miller R. *J. Phys. Chem. C*, **2007**, *111*, 15342 – 15349.
37. Vysotsky Yu. B., Belyaeva E. A., Fainerman V. B., Aksenenko E. V., Vollhardt D., Miller R. *J. Phys. Chem. B*, **2009**, *113*, 4347–4359.
38. Vysotsky Yu. B., Shved A. A., Belyaeva E. A., Aksenenko E. V., Fainerman V. B., Vollhardt D., Miller R. *J. Phys. Chem. B*, **2009**, *113*, 13235–13248.
39. Vysotsky Yu. B., Fomina E. S., Belyaeva E. A., Fainerman V. B., Aksenenko E. V., Vollhardt D., Miller R. *J. Phys. Chem. B*, **2009**, *113*, 16557–16567.
40. Vysotsky Yu. B., Fomina E. S., Belyaeva E. A., Fainerman V. B., Aksenenko E. V., Vollhardt D., Miller R. *J. Phys. Chem. B*, **2011**, *115*, 2264–228.
41. Vysotsky Yu. B., Belyaeva E. A., Fomina E. S., Vollhardt D., Fainerman V. B., Miller R. *J. Phys. Chem. B*, **2012**, *116*, 2173–2282.
42. Vysotsky Yu. B., Fomina E. S., Belyaeva E. A., Vollhardt D., Fainerman V. B., Miller R. *J. Phys. Chem. C*, **2012**, *116*, **26358-26376**.
43. Stewart J. J. *MOPAC 2000.00 Manual*; Tokyo, Fujitsu Limited, **1999**.
44. Fomina, E. S., Vysotsky, Yu. B., Vollhardt, D., Fainerman, V. B., Miller, R. *Soft Matter*, **2013**, *9*, **7601-7616**.
45. Vysotsky, Yu. B., Fomina, E. S., Belyaeva, E. A., Fainerman, V. B., Vollhardt, D. *Phys. Chem. Chem. Phys.*, **2013**, *15*, 2159-2176.
46. Stull, D. R.; Westrum, E. F., Jr.; Sinke, G. C. *The Chemical Thermodynamics of Organic Compounds*; John Wiley & Sons: New-York, **1969**.
47. Johann, R; Brezesinski, G; Vollhardt, D; Möhwald, H. The effect of headgroup interactions on structure and morphology of arachidic acid monolayers. *J. Phys. Chem. B*, **2001**, *105*, 2957-2965.
48. Weidemann, G.; Brezesinski, G.; Vollhardt, D.; Bringezu, F.; de Meijere, K.; Möhwald, H. *J. Phys. Chem. B*, **1998**, *102*, 148-153.
49. Peterson, I. R.; Brezesinski, G.; Struth, B.; Scalas E. *J. Phys. Chem. B*, **1998**, *102*, 9437.
50. Daubert, T. E.; Dannerm R. P.; Sibul, H. M.; Stebbins, C. C. *Physical and thermodynamic properties of pure chemicals: Data Compilation, Part 1 – Part 5*; Taylor & Francis: Pennsylvania, **1998**. – 9860 p.

51. Zwolinski, B.J; Wilhoit, R. *Heats of formation and heats of combustion in "American Institute of physics handbook"* 3-rd edition by D.E. Gray. Mc. Graw-Hill. New-York, **1972** – P. 4-342.
52. Vysotsky, Yu.B.; Belyaeva, E.A.; Vollhardt, D.; Aksenenko, E.V.; Miller, R. *J. Coll. & Int. Sci.*, **2008**, *326*, 339–346.
53. Dynarowicz-Latka, P.; Dhanabalanb, A.; Oliveira, O. N. Jr. *Adv. Coll. & Int Sci.*, **2001**, *91*, 221-293.

Chapter 12

Inverse phase transfer catalysis in organic synthesis

Viktor Anishchenko¹, Volodymyr Rybachenko¹, Grzegorz Schroeder²,
Konstantine Chotiy¹ and Andrey Redko¹

¹*L.M. Litvinenko Institute of physical-Organic and Coal Chemistry,
National Academy of Science of Ukraine, Department of Spectrochemical
Researches, R. Luxemburg 70, 81-134 Donetsk, Ukraine*

²*Adam Mickiewicz University in Poznań, Faculty of Chemistry,
Umultowska 89b, 61-614 Poznań, Poland*

The works of Mąkosza and Starks formed the base of the theory of phase-transfer catalysis (PTC). This powerful technique allows performing the reaction between substances located in two immiscible phases. In 1986 Mathias and Vaidya presented a new PTC methodology, namely inverse phase-transfer catalysis (IPTC) [1]. In contrast to the classic PTC in case of IPTC system, the hydrophobic reactant reacts with the catalyst in organic phase to form a water soluble intermediate. Commonly, this intermediate is highly reactive and rapidly reacts with the hydrophilic substrate to produce the desired product. The catalysis is regenerated in the aqueous-phase reaction.

The problem of environmental protection is very significant, because many reactions still involve the use of toxic organic solvents, which are partly discharged into the atmosphere with a host of negative environmental effects. Replacement of these solvents with environmental benign reaction media such as water brings about potential advantages, such as the opportunity for environmentally benign processing, lower costs, and easy separation of the catalysts from the reaction medium. And IPTC method allows decreasing quantity of toxic organic solvents thanks to using water as a main solvent.

Today, significant number of compounds was found to be capable of acting as the IPT catalyst. Among them are transition metal complexes, quaternary ammonium salts, surfactants, cyclodextrins, calyx[n]arenes and heterocyclic amines. Further, the different IPTC catalysts and their applications will be considered.

1. Surfactants

Boyer and coworkers explored a general method dealing with the IPTC [2-5]. It is based upon the fact that any lipophilic substrate could be transferred into the aqueous phase by means of hydrosoluble surfactants. The fact, that micelles formed in the aqueous phase, above the CMC, are able to solubilize a fraction of the hydrophobic substrate in equilibrium with the organic phase, allow to investigate the following IPTC reactions using surfactants as the IPTC catalysts: the epoxidation of α,β -unsaturated ketones by H_2O_2 in heptane – 0.5 M NaOH(aq) system [2-4] and the reduction of ketones by sodium borohydride [5]. Dodecyltrimethylammonium bromide was used as a catalyst.

According to the mechanism of IPTC, reaction takes place at the surface of the micelles in the water phase. The reaction product, normally lipophilic, is transferred into the organic phase (Fig. 1). However, in presence of surfactant micelles two catalytic processes are involved: an inverse phase transfer – the surfactant allows the transfer of the lipophilic substrate into the water phase and the micellar catalysis – the charged transition state formed at the micelle surface can be stabilized by the surfactant ionic head groups only in the situation where the charges are opposite.

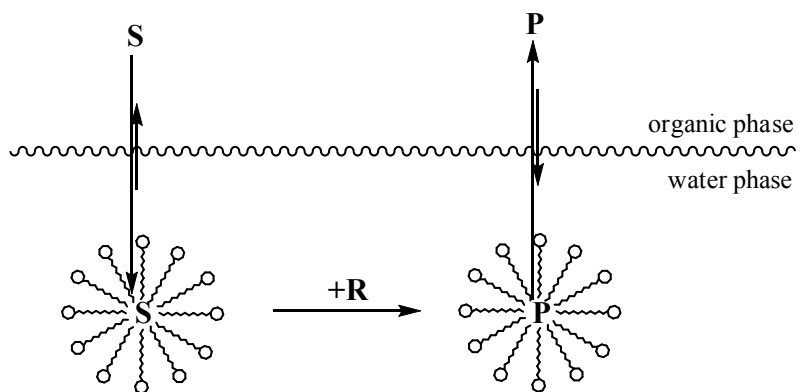
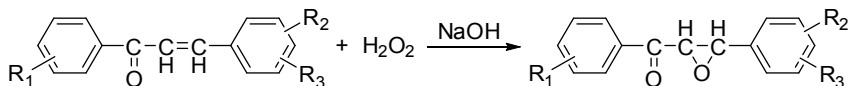


Figure 1. IPTC principle involving a surfactant as catalyst

The results indicated that the reaction was catalyzed by water-soluble micellar aggregates of the surfactant and the catalytic effects depended strongly on the hydrophobicity of the substrate. Interesting results were observed in the study of the effect of surfactant concentration on the epoxidation of chalcone by H_2O_2 .



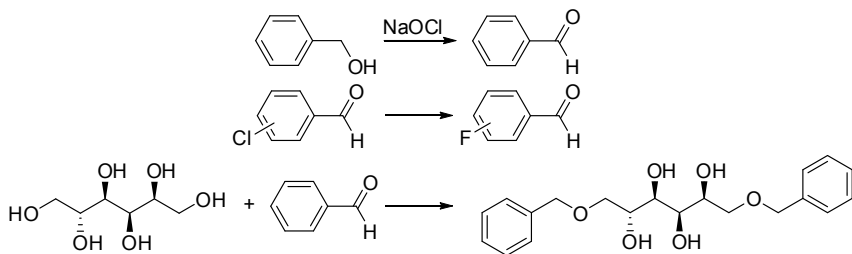
It appeared that under slow agitation (100 rpm), the reaction occurred mainly via IPTC, while under vigorous agitation (1200 rpm) it took place mainly at the interface due to the formation of an emulsion.

This type of IPTC is of interest especially in the reduction of highly hydrophobic ketones by sodium borohydride and in the epoxidation of α,β -unsaturated ketones by hydrogen peroxide.

2. Tetramethylammonium Salts

Due to low lipophilicity of low molecular weight quaternary salts, such as tetramethyl or tetraethylammonium salts are normally poor PTC catalysts for transferring reactant anions into the organic phase.

However, these salts could act as the IPTC catalyst, e.g., tetramethylammonium bromide have been employed as IPTC catalysts to carry out highly selective carbohydrate reactions in the aqueous phase. Trimethylammonium groups attached to ion-exchange resins also act as IPT catalysts in the oxidation of benzyl alcohol by NaOCl to yield benzaldehyde, the fluorination of chlorobenzaldehydes [6], the acetalization of sorbitol with benzaldehyde to produce dibenzalsorbitol [7]. Commonly, there are other methods for obtaining these substances, but all of them have disadvantages. The most popular disadvantage is formation of by-product resulting from hydrolysis one of reactant.



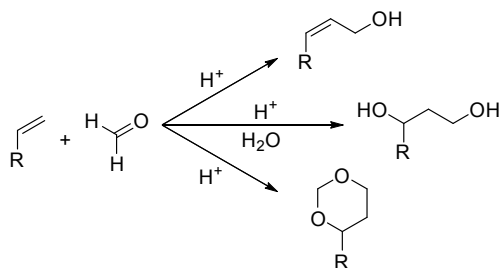
In case of synthesis of 2,4-dichlorophenoxyacetic acid in presents tetramethylammonium bromide, authors have analyzed several effects[8]. The dependents of conversations from speed of agitation have a maximum point.

The effect of phase volume ratio was studied for 1:1, 1:2 and 2:1 ratios of organic phase to aqueous phase volumes under otherwise similar experimental conditions. When the phase ratio of organic to aqueous phase is 1:2, the best conversion values are obtained. Suggested, that the organic phase as a dispersed phase leads to higher interfacial values that in turn enhance the mass transfer rates.

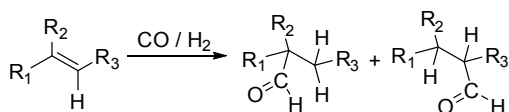
Thus, for certain systems where the reaction in the organic phase was not possible, the quaternary salts could react as IPTC catalysts.

3. Transition Metal Complexes

Cuprous chloride, water-soluble rhodium- and palladium-based catalysts are used as an IPTC catalyst. Ability of cuprous chloride to form water-soluble complexes with the lowest olefins has been used for catalyze by IPTC method in the two-phase hydrolysis and the Prins reactions [9, 10].



Analogously, water-soluble rhodium-based catalysts were used as IPTC catalysts for the hydroformylation of olefins to produce aldehydes for the fine chemicals market [11]. Various catalysts on the basis of palladium complexes with organic ligands have been used for dehalogenation reactions of allyl and benzyl halides, and as for alkylation of allylic substrates and nucleophiles such as ethyl acetoacetate [12]. As a result of alkylation have been received regio- and stereospecific products in quantitative yields. Ito *et al.* used a self-national assembled nanocage, based on chelate palladium complex, as an IPTC catalyst for Walker oxidation of styrene [13].



4. Calix[n]arenes

Another class of supramolecules which was successfully used as IPTC catalysts are calix[n]arenes (Fig. 2). In contrast to mentioned above cyclodextrins, water-soluble calix[n]arenes ($n = 4, 6, 8$) were proposed as IPTC catalysts only a few years ago [14].

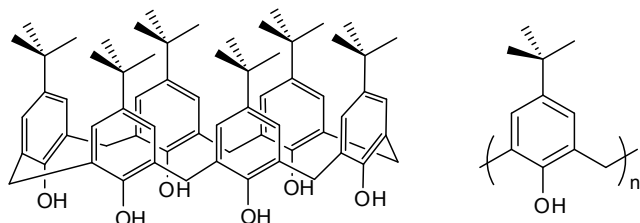


Figure 2. Calix[n]arenes.

Shimizu and coworkers found that nucleophilic displacement of arylalkyl and alkyl halides with NaCN, KI, KSCN in water can be catalyzed by substituted calix[n]arenes with trimethylammoniomethyl groups (Fig. 3). The catalytic activity of such compounds exceeded that of various cyclodextrin, whereas monomeric unit of the calix[n]arene (4-methoxybenzyltrimethylammonium chloride) did not catalyze reaction. It was also noted that the efficiency of the calix[n]arenes strongly depends on the geometry of the substrates, because of that it was proposed that they behave similarly to cyclodextrins.

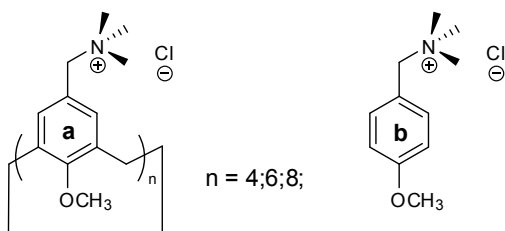
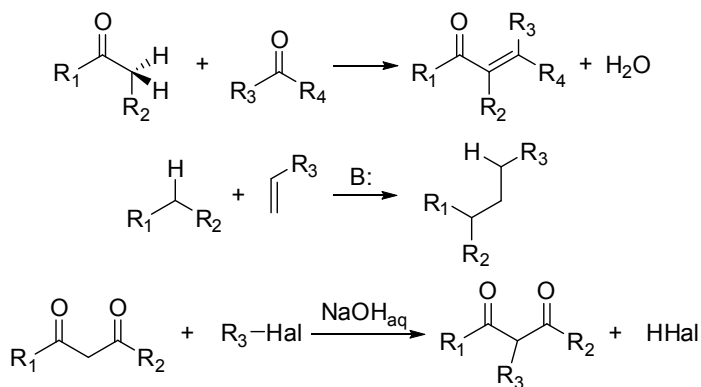


Figure 3. Water-soluble calix[n]arenes (a) and their monomeric unit (b).

Calix[n]arenes were used as IPTC catalysts in the aldol-type condensation and Michael addition reactions [15], and in alkylation of active methylene compounds by alkyl halides in aqueous NaOH solutions [16].



The aldol-type condensation of indene or acetophenone with benzaldehyde in aqueous NaOH under IPTC condition were compared with those conducted in aqueous micelles in the presence of cetyltrimethylammonium bromide as the surfactant. It was shown that in both cases selectivity's and yields were similar. On the other hand the IPTC procedure avoided the formation of emulsions, thus facilitating product separation and catalyst recovery. The alkylation under IPTC of phenylacetone with octyl bromide allows intensifying alkylation versus hydrolysis and selectivities of reaction (C versus O alkylation) in comparison to the classical PTC reaction (with tetrabutylammonium bromide or hexadecyltributylammonium bromide as catalysis). Furthermore, the aqueous layer containing catalyst solution can be easily separated from the organic phase, where products contain, and no organic solvent was required.

Further, water-soluble calyx[n]arenes were integrated into catalytic systems, where organometallic catalysis are combined with calyx[n]arenes in a single molecule. Phosphacalix[4]arenes (Fig. 4) were synthesized and used as polydentate ligands in the rhodium-catalyzed hydroformylation of 1-octene and 1-decene [17].

Recently, stability of the complexes formed in result of the inclusion of aromatic guests in the hydrophobic pocket of the water-soluble calixarenes **I-IV** was studied. For that reason ¹H-NMR titration experiments in aqueous buffered solutions were conducted. Additionally, molecular modeling studies in combination with ab initio NMR shift calculations were performed [18].

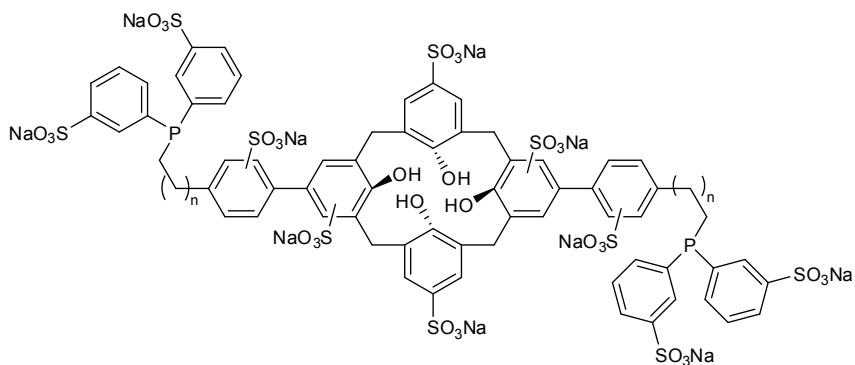
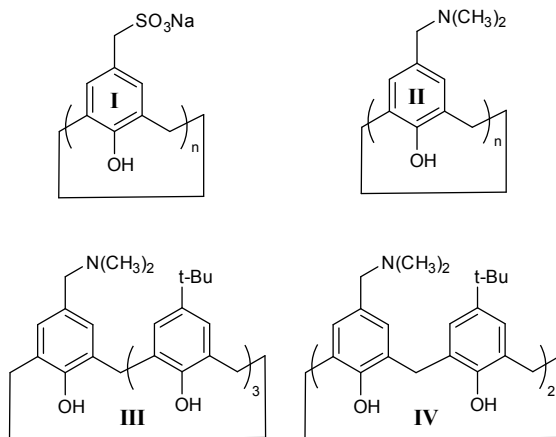


Figure 4. Water-soluble phosphacalix[4]arenes.



Association constants of various aromatic compounds with **I** were found to be close to those observed with β -cyclodextrin. But, it should be noted that iodobenzene, showed a higher affinity to β -cyclodextrin in contrast to the calixarenes. The association constants with the amino methyl-substituted calixarene **II** under acidic conditions were also higher than those measured with **I** at pH 7.4. Calix[n]arenes **I-IV** were used for catalyzing the Suzuki coupling of phenylboronic acid and iodobenzene in water under IPTC, yielding diphenyl as a product. In order to avoid the effect of inhibiting by product and to compare initial reaction rates the effect of **I-IV** was studied at low levels of conversions (10-15%). Better results were achieved with using amino-substituted calix[4]arenes **II-IV**.

5. Cyclodextrins

Cyclodextrins are cyclic oligosaccharide/polyalcohols of α -D-glucose with six to eight monomeric units terms are commercially available under the names of α -, β -, and γ -cyclodextrin, respectively. These compounds are characterized by cylindrical-like structures in aqueous solution (Fig. 5). The inner cavity is essentially hydrophobic and can host organic guests via the various intermolecular forces between host and guest molecules [19], whereas hydrophilic-OH groups span from the upper and the lower rim, ensuring water solubility to the molecule.

Before the concept of IPTC was created, unmodified α - and β -cyclodextrins were used as carriers of organic molecules into water. For example, Trifonov and Nikiforov showed that β -cyclodextrin accelerate the reaction of the nucleophilic displacement of neat octyl bromide with aqueous cyanide, iodide, and thiocyanate anions [20]. Also, it was shown that α -cyclodextrin can catalyzed reaction too, but β -cyclodextrin are preferable.

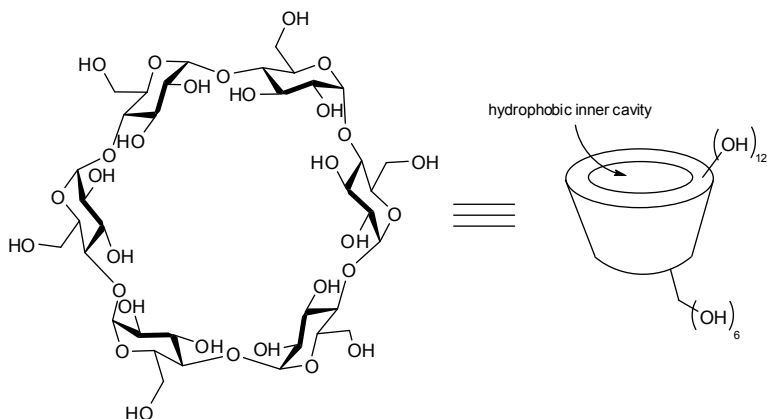


Figure 5. α -cyclodextrin structure.

After establishing of the IPTC concept, cyclodextrins found applications as IPTC catalysis in several important organic reactions catalyzed by transition metals. For instance, isomerization of 4-allylanisole catalyzed by IrCl_3 [21], oxidation CuCl_2 of olefins to ketones in water under aerobic condition and in presence of PdCl_2 and CuCl_2 (Wacker process) [22], the $\text{HCo}(\text{CN})_5^-$ catalyzed hydrogenation of conjugated dienes to monoolefins [23].

Further, the influence of chemically modification hydroxyls group of cyclodextrins on catalytic activity was studied. In 1994 by Mortreux and

coworkers were found that the Wacker process of oxidation of 1-decene to 2-decanone with excellent yield (98%) in water, using $O_2/PdSO_4/CuSO_4/H_9PV_6-Mo_6O_{40}$ as the redox system. The lipophilic substrate was transferred into the aqueous phase by an amphiphilic β -cyclodextrin, in which about 60% of the free-OH groups were methylated [24]. Testing of other cyclodextrins (native α -, β -, γ -, fully acetylated β -cyclodextrin or 2-hydroxypropyl- β -cyclodextrins with different degrees of substitution) shows limited success. The optimal ratio of lipophilic and hydrophilic properties had a great importance, but obtained results shows a significant role of molecular recognition based on reversible interactions between the cyclodextrins' host cavity and 1-decene. The methylated β -cyclodextrin was used as IPTC catalysts for the rhodium-catalyzed hydroformylation of water-insoluble olefins with high yield in an aqueous two-phase system free of organic solvent [25]. In contrast to terminal olefins, less-reactive internal olefins were found to be almost inert [26].

A general scheme obtained from these research studies: the amphiphilic cyclodextrin wraps the hydrophobic substrate (guest-molecule), acting as a host-molecule and transferring it into the aqueous phase, where the reaction occurs. The stability constant of the new host-guest complex is lower, and the product is then released into the organic phase (Fig. 6).

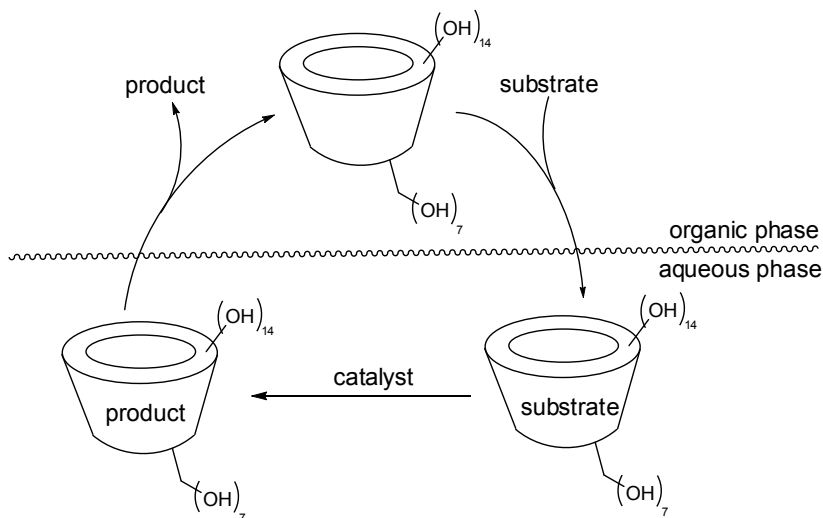


Figure 6. Catalytic cycle of cyclodextrin.

This scheme was confirmed by other catalytic organometallic reactions. Interesting results were obtained in the cleavage of allylic substrates in the presence of $\text{Pd}(\text{OAc})_2/\text{P}(\text{C}_6\text{H}_4\text{SO}_3\text{Na})_3$ [27, 28], the hydrocarboxylation of olefins catalyzed by $\text{PdCl}_2/\text{P}(\text{C}_6\text{H}_4\text{SO}_3\text{Na})_3$ to give carboxylic acids [29], and the biphasic hydrogenation of water-insoluble aldehydes to alcohols catalyzed by $\text{RuCl}_3/\text{P}(\text{C}_6\text{H}_4\text{SO}_3\text{Na})_3$ [30].

The effect of partly methylated β -cyclodextrins on the other component of the catalytic system was studied in the case of the hydroformylation of alkenes. Monflier and coworkers reviewed their previous model, considering formation of complexes between the cyclodextrin and some components of the catalytic system (e.g., $\text{P}(\text{C}_6\text{H}_4\text{-SO}_3\text{Na})_3$) [31]. Independently, Kalck and coworkers proposed that the catalytically active rhodium complex include at least two cyclodextrin molecules [32]. From these results was concluded that chemically cyclodextrins influence the biphasic reaction not only as IPTC catalyst but also by modifying the equilibria between the components of the catalytic system [33].

More complicated catalytic systems based on β -cyclodextrin with combination of different functions in the same molecule were also conceived. Such complexes of modified β -cyclodextrin (Fig. 7) with rhodium were used as IPTC catalysts for the hydrogenation and the hydroformylation of alkenes in water-organic two-phase systems [34].

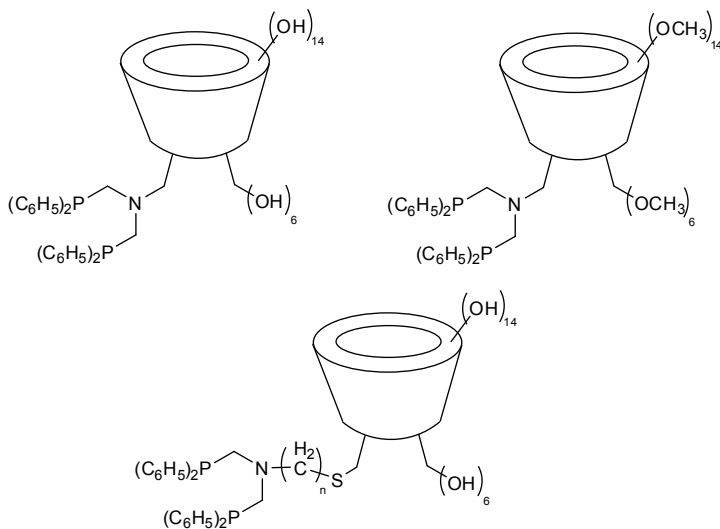


Figure 7. Multicomponent ligands for organometallic catalysis.

Such supramolecular catalysts showed high catalytic activity in the hydroformylation reactions and substrate selectivity in competition hydrogenation experiments. In contrast to the simple methylated β -cyclodextrin mentioned above, internal and cyclic olefins were oxidation into aldehydes. These improvements were explained with the formation of an inclusion complex at the phase boundary, with the cyclodextrin host fixing the substrate in the proximity of the catalytically active metal center (Fig. 8) [35].

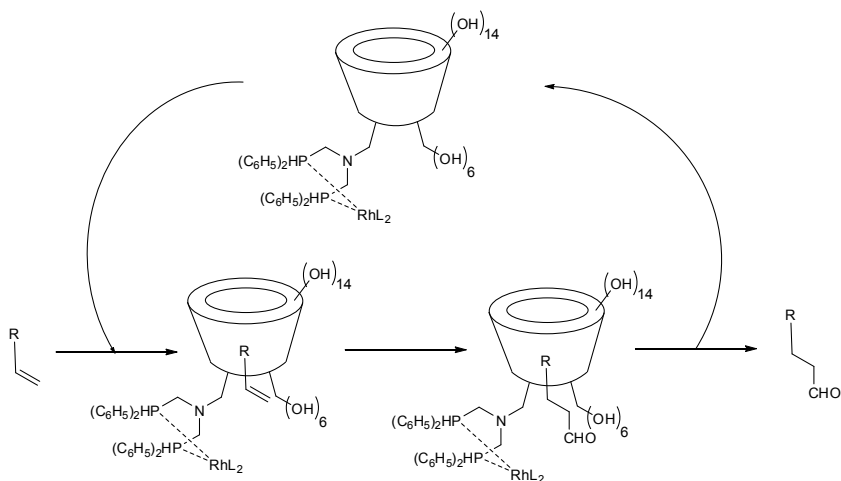


Figure 8. Proposed scheme of olefins oxidation by rhodium complexes of chelating phosphines tethered to β -cyclodextrins.

The effect of guest-molecule structure and type of cyclodextrin on binding constant was investigated using NMR and UV/VIS spectroscopy [36]. Chlorinated phenols were used as guest-molecules. α - and β -cyclodextrin form inclusion complexes with several chlorophenols with modest to low equilibrium constants. Results of studies are consistent with a simple 1 : 1 stoichiometry and the stability of the complexes is dependent on the structure of the chlorophenol and the cyclodextrin used. In general, the most stable complexes are formed between β -cyclodextrin and the 4-substituted chlorophenols. This suggests that the stability of the complexes is strongly influenced by the sizes and shapes of the guest and the cavity of the host. The polarity of the host chlorophenol plays an important role on the stability of the complex but is far less important than geometric fitting.

Recently, the Markovnikov enantioselective hydration of double bonds by an oxymercuration-demercuration reaction with cyclodextrins as catalysts was investigated [37]. Moderate ee (up to 32%) and yields (14–60%) were obtained for allylic amines and protected allylic alcohols as starting materials. It was found that an aromatic ring must be present in the substrate to achieve enantioselectivity. The best results are always obtained with α - or β -cyclodextrin. Modified cyclodextrins (2,6-di-O-methyl and random methyl cyclodextrins) neither improve yield nor enantioselectivity. N-allyl- N-benzylmethylamine is an interesting example as the benzyl group may be removed by catalytic hydrogenation.

Kunishima and co-workers reported about a novel system for substrate-specific activation of carboxylic acids leading to the formation of carboxamides [38]. A combination of a water-soluble dehydrocondensing agent, 4-(4,6-dimethoxy-1,3,5-triazin-2-yl)-4-methylmorpholinium chloride (DMT-MM), and (hydroxypropyl)cyclodextrin (HP- β -CD), in a water/ether biphasic solvent system was found to be most effective. A lipophilic carboxylic acid with a strong affinity for the cavity of HP- β -CD can be selectively transferred to the aqueous phase and predominantly reacts with DMT-MM, dissolving in the aqueous phase. The substrate specificity was similar to that observed with a complex artificial enzyme based on CD. In result was found that substrate specificity similar to that obtained with a complex artificial enzyme can be achieved by using DMT-MM and a CD. This is the first example of a dehydrocondensation involving a step of carboxylic acid activation under IPTC conditions. It can be expected that this concept to be applicable to various solvent systems composed of fluoruous solvents or ionic liquids, and such applications are now under investigation.

A novel and efficient procedure has been developed by Li *et al.* for the preparation of Urapidil, from 6-[(3-chloropropyl)amino]-1,3-dimethyluracil and 1-(2-methoxyphenyl) piperazine hydrochloride under IPTC conditions [39]. To optimize the reaction conditions, the alkylation reaction was carried out with a range of IPTC catalysts, agitation speeds, reaction times, reaction temperatures, mole ratios and catalyst loadings. The experimental results demonstrate that the alkylation of 1-(2-methoxy- phenyl) piperazine hydrochloride with 6-[(3-chloropropyl)amino]-1,3-dimethyl-2,4(1H,3H)-pyrimidinedione is very rapid in the presence of cyclodextrins in aqueous media. β -cyclodextrin is the best catalyst owing to its excellent catalytic activity and eco-friendly nature. Urapidil was obtained as a white crystalline powder in 82.6% isolated yield with 99.6% purity after 2-3 h reaction in alkaline aqueous media at 95°C with an agitation rate of 1500 rpm. Compared to the N-alkylation under the same

conditions without catalyst, the proposed method is suitable for the industrial scale synthesis of Urapidil.

6. Pyridine derivatives

Pyridine derivatives are of interest as IPTC catalysts, because of their low cost and availabilities in comparison with cyclodextrins and calix[n]arenes. Pyridines relate to an important class of IPTC catalyst, which can react with hydrophobic substrate in organic phase with formation of intermediate. These compounds have an ionic structure that's why it passes into aqua phase and here take place main reaction between ionic intermediate and hydrophilic substrate. In result of that reaction form products and regenerate catalyst. This class of IPTC catalysts includes 4-(dimethylamino)pyridine (DMAP), 4-pyrrolidinopyridine, pyridine-1-oxide (PNO), 4-methoxypyridine-1-oxide, 4-methylpyridine-1-oxide, etc.

Mathias and Vaidya were first who studied the acylation reaction of alanine with decanoyl- or 4-chlorobenzoyl chloride catalyzed by DMAP in $H_2O - CH_2Cl_2$ system (Fig. 9) [1]. DMAP was also used as IPTC catalyst to improve the tosylation of alcohols and amines with tosyl chloride [40].

The IPTC reaction of acid chloride with carboxylate ions [41] and with phenols [42] catalyzed by PNO in $H_2O - CH_2Cl_2$ system to produce accordingly acid anhydride and aromatic ester were reported. In the latter case was observed that the IPTC reaction was more efficient than the normal PTC reaction catalyzed by quaternary ammonium salts. Further, DMAP- and PNO-catalyzed IPTC reactions will be considered more detail.

DMAP as a catalysts in IPTC system

Two independent investigations of the DMAP-catalyzed IPTC reaction of benzoyl chloride with glycine were made. The main different was in the pH of water phase.

Wang and coworkers investigated this reaction in $H_2O - CH_2Cl_2$ system and pH of water phase was between 7 and 11 [43]. It was observed that the rates of both the uncatalyzed and DMAP-catalyzed reactions were fast and the yields of hippuric acid were very high (up to 100%). Also was founded that the reaction rate depended on the shape of the reaction vessel and on agitation rate below 1200 rpm.

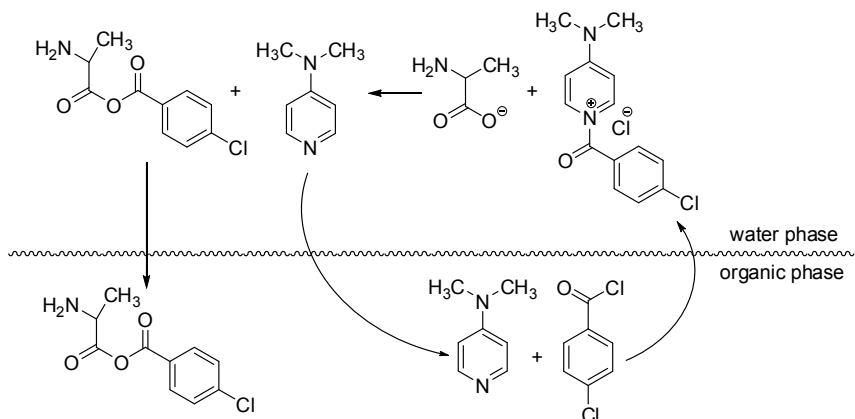
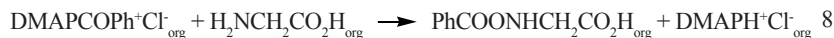
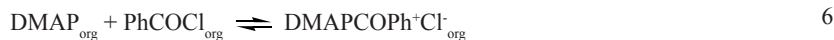


Figure 9. Scheme of reaction between 4-chlorobenzoyl chloride and alanine catalyzed by DMAP in $H_2O - CH_2Cl_2$ system.

The mechanism of the DMAP-catalyzed reaction can be described as follows:



The DMAPCOPh⁺Cl⁻ is the active ionic intermediate, formed by the reaction of benzoyl chloride and DMAP in the organic phase. The reactions 1-4 described the uncatalyzed reaction between benzoyl chloride and glycine in H₂O – CH₂Cl₂ system. The hippuric acid can be generated via Eq. 3 in the organic phase (org) and Eq. 4 in the interfacial region (if). In case of DMAP-catalyzed reaction the hippuric acid mainly generated via reactions 9-10 in water phase (aq).

The reaction has taken place in the kinetic region. It was confirmed by parallel experiments in which DMAP was presented initially in organic and in the aqueous phase, respectively. In all cases the reaction rates were similar, which implied that the mass transfer of DMAP between the two phases was extremely rapid. Both the uncatalyzed and DMAP-catalyzed reactions followed pseudo-first-order kinetics in the initial presence of excess amount of the sodium salt of glycine.

The effective pseudo-first-order rate constants increased with the initial concentrations of sodium salt of glycine and DMAP in the aqueous phase in cases of uncatalyzed and DMAP-catalyzed reaction, respectively. These facts confirm that in the uncatalyzed reaction, the reaction rate determines by reactions 3 and 4 and in the DMAP-catalyzed reaction it control by reactions 6, 8 and 10.

The nucleophilicity of RNH₂ is considerably higher than that of the RCOO⁻ ion, because the pK_a values relative to water are pK_a(RNH₃⁺) = 10-11, pK_a(RCOOH) = 4-5, and pK_a(H₂O) = -1.74. Therefore, the reaction of PhCOCl with H₂NCH₂CO₂⁻ to yield PhCOOCOCH₂NH₂ is negligible, as observed [44]. The hydrolysis of PhCOCl was also negligible, because no benzoic acid was detected.

Also, analogous experiments with sodium salts of other α-amino acids were realized and similar results were obtained. These reactions proceeded rapidly to produce PhCONRCHR'COOH with high yields (85 - 100%). In the follow row the reactivity's of amino acids increased 2-methylalanine < DL-alanine « glycine « N-methylglycine ≈ L-prolinene [45]. There are three facts, which determined reactivity's of these amino acids: nucleophilicities, organophilicities (solubility's in CH₂Cl₂) and the steric hindrance, e.g., the low reactivity of 2-methylalanine was due to both the low solubility in CH₂Cl₂ and the steric hindrance of the methyl group.

In contrast Asai and coworkers studied that reaction in H₂O – CH₂Cl₂ system in the absence of alkali [46]. They obtained high yields (up to 94%) of hippuric acid. It was observed that the overall reaction rates were proportional to the interfacial concentration of ionic intermediate in the aqueous phase. In the absence of DMAP, the reaction was about three to four orders slower than that of the DMAP-catalyzed reaction. The yield of hippuric acid decreased with

increasing amounts of NaOH added, due to the hydrolysis of benzoyl chloride. In that case the mechanism of the DMAP-catalyzed reaction can be described by reactions 2, 3 and 5-9.

An attractive application of the IPTC technique was demonstrated in the protection of the amino group of DL-serine with carbobenzoxy chloride (benzyl chloroformate) in $H_2O - C_2H_4Cl_2$ system catalyzed by DMAP [41, 47]. This method is useful for preparing the precursor for synthesizing the peptide containing the serine moiety, since the protection of amino acids by the carbobenzoxy group is generally made in the alkaline solution, which is not applicable to DL-serine due to its decomposition in the alkaline solution to produce byproducts such as glycine.

PNO as a catalysts in IPTC system

Acid anhydrides are very important precursors for the synthesis of esters, amides, and peptides and they being less reactive than acyl chlorides. An attractive application of the IPTC technique was demonstrated in produce of acid anhydride from acid chlorides and carboxylate ions by Fife and coworkers [41, 48]. They have proposed the next scheme of catalytic process (Fig. 10):

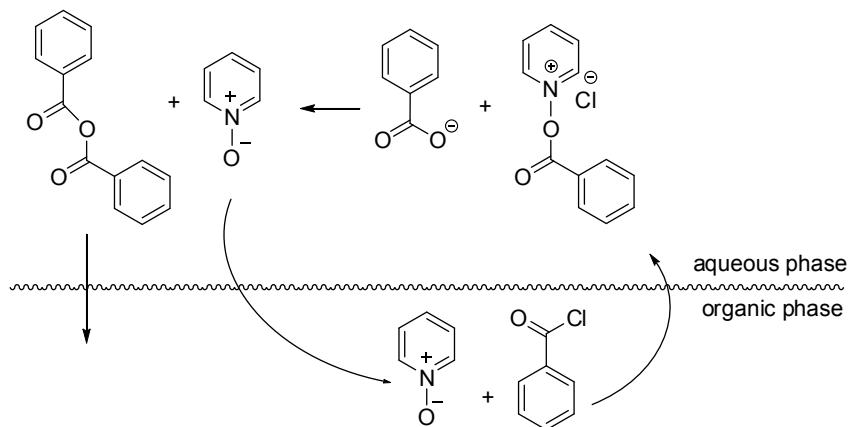
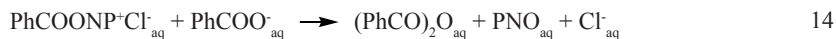


Figure 10. Inverse phase transfer catalysis: the PNO-catalyzed reaction of benzoyl chloride and benzoate ion.

Jwo and coworkers [49-59] have investigated the kinetics and mechanism of the reactions of benzoyl chlorides and carboxylate ions using PNO as the IPTC catalyst in $H_2O - CH_2Cl_2$ system. Based on the kinetic results, a detailed

mechanism was proposed for the PNO-catalyzed substitution reaction of benzoyl chloride and benzoate ion in this system [49]. The main elementary acts are shown as follows:



Reaction 16 can take place in both the organic and aqueous phases and in the interfacial region.

It was generally observed that the reaction rate was independent of the agitation speed beyond 1100 rpm in $\text{H}_2\text{O} - \text{CH}_2\text{Cl}_2$ system, but with agitation speed below 1100 rpm the reaction rate decreased with decreasing of agitation speed. The PNO-catalyzed IPTC reactions of benzoyl chloride and benzoate ion produced a prime product (benzoic anhydride) and by product of a hydrolysis (benzoic acid). Under suitable reaction conditions, the reaction followed pseudo-first-order kinetics as shown in Eq. 17:

$$-\frac{d[\text{PhCOCl}]_{\text{org}}}{dt} = k_{ef}[\text{PhCOCl}]_{\text{org}} \quad 17$$

The effective pseudo-first-order rate constant (k_{ef}) depended linearly on the initial concentration of PNO in the aqueous phase ($[\text{PNO}]_{\text{aq},0}$) and could be expressed as:

$$k_{ef} = k_h + k_c[\text{PNO}]_{\text{aq},0} \quad 18$$

In Eq. 18, k_h and k_c were the uncatalyzed (or hydrolysis) rate constant and catalyzed rate constant, respectively. Since, in general $k_h \gg k_c$, then reaction of PhCOCl with PNO in the organic phase are the rate-determining act in the reaction of production as prime product the benzoic anhydride catalyzed

by PNO. For obtaining the value of k_h were measured k_{ef} for reactions with various initial concentration of catalyst. From this data were obtained equation of linear regression, which represented dependence of k_{ef} from $[PNO]_{aq,0}$. Free factor in obtained equation were numerically equal k_h . The value of k_h obtained from the dependence of k_{ef} from $[PNO]_{aq,0}$ was generally consistent with that obtained in the uncatalyzed reaction. Therefore, reaction 16 was the main act in the uncatalyzed (hydrolysis) path, which led to the production of benzoic acid.

Effects of the substrates structure

Generally, in the IPTC system the rate-determining elementary act is the reaction of hydrophobic substrate and catalyst in which produce ionic intermediate. In case of the PNO-catalyzed reaction of benzoyl chloride with benzoate ion in $H_2O - CH_2Cl_2$ medium, the reaction of benzoyl chloride and PNO in the CH_2Cl_2 phase was the rate-determining act. Therefore, it was worthwhile investigating the effects of the substrates structure on this system. The substrates structure was varied by means of substituent's, which included H_3C- , $(CH_3)_3C-$, CH_3O- , F-, Cl-, Br-, and I- groups. Similar to the $PhCOCl/PhCOONa$ system, these reactions followed pseudo-first-order kinetics with the effective pseudo-first-order rate constant, which submit to Eq. 18. The values of the catalyzed rate constant (k_c) for different $X_nC_6H_{5-n}COCl$ and $Y_kC_6H_{5-k}COONa$ are summarized in Table 1.

Table 1. Effects of substituent's on catalyzed rate constant (k_c) for PNO-catalyzed reaction of benzoyl chloride ($X_nC_6H_{5-n}COCl$) and benzoate ion ($Y_kC_6H_{5-k}COONa$) in $H_2O - CH_2Cl_2$ system

X	Y	k_c , $M^{-1}\cdot s^{-1}$	T, °C	X	Y	k_c , $M^{-1}\cdot s^{-1}$	T, °C
H	H	3.60	22	4-Cl	4-Cl	5.37	22
2-CH ₃	2-CH ₃	1.49	10	4-Cl	H	5.43	22
3-CH ₃	3-CH ₃	2.53	20	2-Br	2-Br	7.10	15
4-CH ₃	4-CH ₃	1.53	20	2-Br	H	7.37	15
3-CH ₃ O	3-CH ₃ O	3.40	20	3-Br	3-Br	6.10	15
3-CH ₃ O	H	1.83	20	3-Br	H	6.21	15
4-CH ₃ O	4-CH ₃ O	0.71	20	4-Br	4-Br	5.80	15
4-CH ₃ O	H	0.64	20	4-Br	H	5.61	15

X	Y	k_c^o $M^{-1}\cdot s^{-1}$	T, °C	X	Y	k_c^o $M^{-1}\cdot s^{-1}$	T, °C
4-C(CH ₃) ₃	H	1.87	20	2-I	2-I	17.5	20
2-F	2-F	9.10	20	2-I	H	10.9	20
2-F	H	10.4	20	4-I	H	6.83	20
3-F	3-F	6.10	20	2,3-Cl ₂	2,3-Cl ₂	15.6	22
3-F	H	6.80	20	2,3-Cl ₂	H	11.6	22
4-F	4-F	3.40	20	2,4-Cl ₂	2,4-Cl ₂	11.1	22
4-F	H	3.93	20	2,4-Cl ₂	H	12.4	20
2-Cl	2-Cl	8.10	22	3,4-Cl ₂	3,4-Cl ₂	15.4	22
2-Cl	H	10.1	22	3,4-Cl ₂	H	7.98	20
3-Cl	3-Cl	6.43	22	3,5-Cl ₂	3,5-Cl ₂	57.3	22
3-Cl	H	6.37	22	3,5-Cl ₂	H	10.5	22

For more detail analysis, the Hammett correlations were constructed. Good correlations were obtained for the meta- and para- substituent's in the coordinate of $\log(k_c/k_{cH})$ in the X-direction and σ in the Y-direction, where σ was the substituent constant and k_{cH} was the catalyzed rate constant of the benzoyl chloride (Fig. 10) [59]. The reaction constant (ρ) as slope were obtained from with correlation. The value of ρ was +1,3. Therefore this reaction is a nucleophilic substitution reaction and it can be accelerated by the electron-withdrawing substituent and retarded by the electron-donating substituent. This completely agrees with data which were observed in these reactions. It is well known that the application of the Hammett equation to the ortho-substituent is usually poor, because of the steric effect. However, the inductive and resonance effects, the electron-withdrawing ortho-substituent (F-, Cl-, Br-, or I-) also facilitates the reaction considerably by complexing with the positively charged nitrogen atom of the pyridinium moiety. In contrast, the electron-donating ortho-substituent (H₃C- or CH₃O-) also retards the reaction via the steric effect.

Also in the course of investigations of the substrates structure effects, the effects of carboxylate ions were examined. Various mono- and dicarboxylate were taken for exploration. The effects of carboxylate [RCOONa] ions on the PNO-catalyzed IPTC reactions of PhCOCl and sodium carboxylates in H₂O – CH₂Cl₂ system were investigated for selected carboxylate ions (Table 2) [52].

These results were rationalized by the good correlations of the distribution of PNO in the CH_2Cl_2 phase and the carboxylate ions in the aqueous phase [52, 56].

Table 2. Effects of carboxylate ions on PNO-catalyzed reaction of benzoyl chloride with sodium carboxylates in $\text{H}_2\text{O} - \text{CH}_2\text{Cl}_2$ system

Carboxylate ion	$k_c, \text{M}^{-1}\cdot\text{s}^{-1}$	Carboxylate ion	$k_c, \text{M}^{-1}\cdot\text{s}^{-1}$
HCOO^-	3.50	$n\text{-C}_4\text{H}_9\text{COO}^-$	3.83
CH_3COO^-	3.55	$n\text{-C}_5\text{H}_{11}\text{COO}^-$	3.75
$\text{C}_2\text{H}_5\text{COO}^-$	3.52	$n\text{-C}_6\text{H}_{13}\text{COO}^-$	3.83
$(\text{CH}_3)_2\text{CHCOO}^-$	3.77	$n\text{-C}_7\text{H}_{15}\text{COO}^-$	3.35

$[\text{PhCOCl}]_{\text{org},0} = 0,0100\text{M}$, $[\text{RCOONa}]_{\text{aq},0} = 0,500\text{ M}$, at 18°C .

Also, the effects of dicarboxylate $[\text{R}(\text{COONa})_2]$ ions on the composition of products of the PNO-catalyzed IPTC reactions of PhCOCl and sodium dicarboxylates in $\text{H}_2\text{O} - \text{CH}_2\text{Cl}_2$ system were analyzed on several dicarboxylate ions. There are oxalate, malonate, maleate, fumarate, succinate, adipate, nonanedioate, phthalate, isophthalate, and terephthalate among them [53]. The compositions of the obtained products depended on the molecular structure of the dicarboxylate ion. The reaction rates depended significantly on the type of dicarboxylates analogously to the effects of monocarboxylates (Table 3).

Table 3. Effects of dicarboxylate ions on PNO-catalyzed reaction of benzoyl chloride with sodium dicarboxylates in $\text{H}_2\text{O} - \text{CH}_2\text{Cl}_2$ system

Dicarboxylate ion	$k_c, \text{M}^{-1}\cdot\text{s}^{-1}$	Dicarboxylate ion	$k_c, \text{M}^{-1}\cdot\text{s}^{-1}$
malonate	4.10	nonanedioate	4.08
succinate	4.02	phthalate	3.80
maleate	3.83	isophthalate	2.73
fumarate	3.03	terephthalate	2.72
adipate	4.27		

$[\text{PhCOCl}]_{\text{org},0} = 0,0100\text{M}$, $[\text{R}(\text{COONa})_2]_{\text{aq},0} = 0,500\text{ M}$, at 18°C .

These results were also rationalized by the good correlations of the distribution of PNO in CH_2Cl_2 and the dicarboxylate ions, with the exception of the nonanedioate ion, due to interference by the emulsion phenomenon [52]. Generally, products included mono- and bis-(benzoyloxycarbonyl) compounds, benzoic anhydride, and benzoic acid. Accordingly to distribution of products the four types of dicarboxylate ions were classified (Table 4).

Elementary acts for the generation of mono- and bis-(benzoyloxycarbonyl) were proposed as follows:

Aqueous phase reaction:



Organic phase reaction:



Interfacial reaction:



Table 4. Types of dicarboxylate ions

Type	Main products	Minor product	Dicarboxylate
I	PhCOOH, (70-80%)	(PhCO) ₂ O	oxalate, malonate, maleate, and succinate
II	PhCOOCORCOOH	(PhCO) ₂ O, PhCOOH	phthalate
III	R(COOCOPh) ₂ , (70-88%)	(PhCO) ₂ O, PhCOOH, PhCOOCORCOOH	fumarate, isophthalate, terephthalate, and nonanedioate
IV	PhCOOH R(COOCOPh) ₂	(PhCO) ₂ O, PhCOOCORCOOH	adipate

Type I dicarboxylates ion tend to exist in the aqueous phase due to their low organophilicities. The steric difficulties because of the nearby second carboxylate group, reduce to inhibition of the reactions 19 and 20 or 23 and 24. That is the reason that the reaction was dominated by the hydrolysis path (reactions 15 and 16) to produce PhCOOH.

Type II dicarboxylates ion includes the conjugate acids such as phthalate. The PhCOOCORCOOH is the main product for this type of dicarboxylates, because of they had higher organophilicities than those of the Type I dicarboxylates. The observed main product could be generated by reactions 19, 21, and 23. However, reactions 20, 22, and 24 were inhibited by the steric effect of the second carboxylate group at the ortho-position, that explain why no $C_6H_4(COOCOPh)_2$ was detected.

In type III dicarboxylates ion the steric hindrance of the second carboxylate group is absence. That is why, the main products were the bis(benzoyloxycarbonyl) compounds $[R(COOCOPh)_2]$ for this type of dicarboxylates. The main product generated in the various reactions, against of dicarboxylate, e.g. for isophthalate and terephthalate systems, reactions 19-24 were involved in the generation of $C_6H_4(COOCOPh)_2$, for the fumarate system, trans- $C_2H_4(COOCOPh)_2$ was generated mainly via reactions 19 and 20, 23 and 24, for the nonanedioate system, $(CH_2)_7(COOCOPh)_2$ was produced mainly by reactions 23 and 24 due to its surfactant property.

For type IV dicarboxylates ion, such as succinate, a wide distribution of products was observed, because of their properties seemed to occur at an intermediate position.

Solvent effects

PNO is polar substance and so, thermodynamically, the distribution of PNO in the organic phase is favored by the polarity of the organic solvent. Kinetically, the reaction is also more favorable to take place in polar organic solvent, since the transition state formed by PhCOCl and PNO (Eq. 12) is more ionic than both PhCOCl and PNO. The order of relative reaction rates with respect to the polarity of organic solvents was cyclohexanone > CH_2Cl_2 » $CHCl_3$ > CCl_4 , which was consistent with the order of polarities. In case of non-polar solvent such as benzene the benzoic acid was obtained, instead of anhydride. Similar results were generally observed for other benzoyl chlorides and carboxylate ions [54, 55, 57-59].

Table 5. Effect of organic phase composition on PNO-catalyzed reaction of benzoyl chloride with sodium benzoate in H_2O – organic solvent system

Organic solvent	$k_{ef} \cdot 10^4, s^{-1}$	Organic solvent	$k_{ef} \cdot 10^4, s^{-1}$
Cyclohexanone	17.7	CH_2Cl_2 (0.5 M PhCN)	10.1
$CHCl_3$	3.25	CH_2Cl_2 (0.5 M $PhNO_2$)	9.50
CCl_4	2.70	CH_2Cl_2 (1.5 M $PhNO_2$)	10.1
CH_2Cl_2	8.08	CH_2Cl_2 (0.5 M CCl_4)	7.08
CH_2Cl_2 (0,5 M $PhCH_2CN$)	10.2	CH_2Cl_2 (1.5 M CCl_4)	4.75
CH_2Cl_2 (1,5 M $PhCH_2CN$)	12.0		

$[PhCOCl]_{org,0} = 0,0100M$, $[PhCOONa]_{aq,0} = 0,500 M$, and $[PNO]_{aq,0} = 2,00 \cdot 10^{-4} M$, at $18^\circ C$.

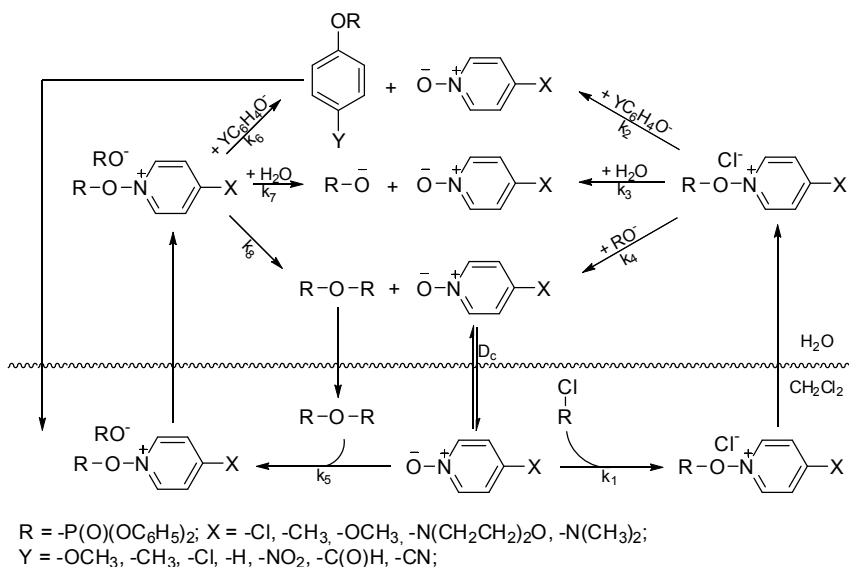
Apparently from the Table 5, addition of an inert organic substance, which have larger polarity than solvent reduce to increasing of the reaction rate and vice versa, addition of an inert organic substance, which have smaller polarity than solvent reduce to decreasing of the reaction rate. That was obtained in the $H_2O - CH_2Cl_2$ system with, keeping the volume of organic phase constant.

Phosphorylation

The IPTC methodology was successfully used for performing phosphorylation of different mono- and bisphenols [60-64]

The phosphorylation of para- substituted monophenols by diphenyl chlorophosphate under IPTC was studied [60]. Potassium carbonate was used as acid acceptor, thereby the optimal value of pH was provided and as a consequence the side reaction of hydrolysis was minimized. Pyridine-1-oxide derivatives (4-chloropyridine-1-oxide (ClPNO), 4-methylpyridine-1-oxide (MePNO), 4-methoxy-pyridine-1-oxide (MeOPNO), 4-morpholinopyridine-1-oxide (MorphPNO), 4-dimethylaminopyridine-1-oxide (DMAPNO)) were chosen as catalysts, because they demonstrated high efficiency in the case of reaction between acyl halides with benzoate anions [50-53].

The advanced scheme of phosphorylation of phenols under IPTC shown in Figure 11.



Kinetic studies were carried out for reaction of diphenyl chlorophosphate with sodium p-nitrophenolate. The result of experiments showed that reaction rate and product yield increase in the series of catalysts: CIPNO < MePNO < MOPNO < MorphPNO < DMAPNO (Table 6).

$$k_{obs} = \frac{v_0}{(1 + D_c) \cdot [PNO]_{aq,0} \cdot [R - Cl]_{org,0}} \quad (25)$$

Table 6. Results of IPTC reaction of diphenyl chlorophosphate with sodium 4-nitrophenolate

Catalyst	pK _{BH} ⁺	lgk _{obs}	Yield, %
CIPNO	0.33	-2.45	35
MePNO	1.29	-1.62	50
MeOPNO	2.05	-1.00	60
MorphPNO	3.25	-0.164	81
DMAPNO	3.88	0.290	86

IPTC polycondensation of various phosphonic(phosphoric) dichloride's (PD) with bisphenols (B) was described by Iliescu et. al. [61-64] (Table 7). Methyl dichlorophosphate (MOP), phenyl dichlorophosphate (POP), p-chlorophenyl dichlorophosphate (p-ClPOP), phenyl dichlorophosphate (PPD) were used as phosphorus monomers. 4,4'-methylenediphenol (BHF), bisphenol A (BPA), 4,4'-(propane-2,2-diyl) bis(2,6-dibromophenol) (BrBPA), 4,4'-(cyclohexane-1,1-diyl)diphenol (BPZ), 4,4'-(diazene-1,2-diyl)diphenol (DHB) were used as phenol monomers.

Table 7. Results of IPTC polycondensation of various phosphonic(phosphoric) dichlorides with bisphenols

PD	B	Catalyst	Base	T, °C	Yield, %	η_{inh} , dl·g ⁻¹
PPD	BPA	DMAP	NaOH	15	86.5	0.40 ^a
PPD	BPA	DMAP	NaOH	-12	93.1	0.63 ^a
PPD	BPA	DMAP	NaOH	-12	92.9	0.64 ^a
PPD	BPA	DMAP	NaOH	-12	92.9	0.64 ^a
PPD	BPA	DMAP	NaOH	-12	93.0	0.64 ^a
PPD	BrBPA	DMAP	NaOH	15	65.5	0.32 ^a
PPD	DHB	DMAP	NaOH	15	80.8	0.45 ^a
PPD	HPM	DMAP	NaOH	15	60.0	0.25 ^a
PPD	BPZ	PNO	NaOH	0	60.0	0.36 ^b
PPD	BPZ	PNO	Ba(OH) ₂	0	75.2	0.52 ^b
p-ClPOP	HPM	DMAP	NaOH	15	68.5	0.28 ^a
POP	BPA	DMAP	NaOH	15	78.5	0.35 ^a
POP	BrBPA	DMAP	NaOH	15	63.5	0.30 ^a
POP	DHB	DMAP	NaOH	15	80.2	0.42 ^a
MOP	BPA	DMAP	NaOH	15	92.0	0.65 ^a

^a The inherent viscosities η_{inh} were determined for solutions of 0.5 g/100 ml, in tetrachloroethane, at 30°C

^b The inherent viscosities η_{inh} were determined for solutions of 0.25 g/100 ml, in dichloroethane, at 25°C

The results of experiments with different pyridine derivatives showed that yield and polymer inherent viscosity increase in the series of catalysts: pyridine (Py) < pyridine-1-oxide (PNO) < 4-dimethylaminopyridine (DMAP).

In addition, influence of reaction conditions on yield and polymer inherent viscosity was investigated [62]. The MINITAB statistical software was used for obtaining the mathematical model of the synthesis process. Using this model the main effect of the control factors and their interactions were evaluated. Optimal values of the control factors for obtaining polymer with long chain and high yield were found:

- monomer molar ratio PD:B = 1:1;
- base concentration = 1.1M;
- reaction temperature = -12°C;

Furthermore, the advantage of using barium hydroxide compared to sodium alkali was shown [63]. Using of bases with limited solubility prevents the polymer degradation and phosphorus monomer hydrolysis. However, such bases can provide sufficient concentration of hydroxyl ions to neutralize released acid during polycondensation. Thus, IPTC method can be exploited for the synthesis different polyphosphates and polyphosphonates with high inherent viscosity and good yield. In contrast to PTC there is no need for vigorous stirring (500-1000 rpm instead of 10000 rpm) but as opposed to PTC process, where a small amount of catalyst is enough to produce a polymer, IPTC polycondensation can take place only at much higher catalyst concentration.

References

1. Mathias L.J., Vaidya R.A. *J. Am. Chem. Soc.* 1986; 108: 1093-1094.
2. Boyer B., Betzer J.F., Lamaty G., Leydet A., Roque J.P. *New J. Chem.* 1995; 19: 807-811.
3. Boyer B., Hambardzoumian A., Lamaty G., Leydet A., Roque J.P., Bouchet P. *New J. Chem.* 1996; 20: 985-988.
4. Boyer B., Hambardzoumian A., Roque J.P. *Tetrahedron.* 1999; 55: 6147-6152.
5. Boyer B., Hambardzoumian A., Roque J.P., Beylerian N. *Tetrahedron.* 2000; 56: 303-307.
6. Wild J., Goetz N. *Ger Offen DE 3,820,979*, 1989; *Chem. Abstr.* 113: 40150.
7. Fleche G. *Starch/Staerke* 42: 31-35, 1990; *Chem. Abstr.* 112: 120970.
8. Yadav G.D., Yogeeta B., Jadhav B. *J. Molec. Cat. A.* 2002; 184: 151-160.
9. Starks C.M., Liotta C. *Phase Transfer Catalysis, Principles and*

- Techniques. London, New York: Academic Press, 1978.
10. Suzuki A., Nakata T., Tanaka W. *Jap. Pat.* 70/10/26; *Chem. Abstr.* 73: 44885.
 11. Russell M.J.H. *Platinum Met. Rev.* 1988; 32: 179-186.
 12. Paetzold E., Oehme G., Costisella B. *Z. Chem.* 1989; 29: 447-448.
 13. Ito H., Kusukawa T., Fujita M. *Chem. Lett.* 2000; 598-599.
 14. Shimizu S., Kito K., Sasaki Y., Hirai C. *Chem. Commun.* 1997; 1629-1630.
 15. Shimizu S., Shirakawa S., Suzuki T., Sasaki Y. *Tetrahedron.* 2001; 57: 6169- 6173.
 16. Shimizu S., Suzuki T., Sasaki Y., Hirai C. *Synlett.* 2000; 1664-1666.
 17. Shimizu S., Shirakawa S., Sasaki Y., Hirai C. *Angew. Chem., Int. Ed.* 2000; 39: 1256-1259.
 18. Baur M., Frank M., Schatz J., Schildbach F. *Tetrahedron.* 2001; 57: 6985-6991.
 19. Bender M.L., Komiyama M. Berlin: Springer. 1978.
 20. Trifonov A., Nikiforov T. *J. Mol. Catal.* 1984; 24: 15-18.
 21. Barak G., Sasson Y. *Bull. Soc. Chim. Fr.* 1988; 584.
 22. Zahalka H.A., Januszkiewicz K., Alper H. *J. Mol. Catal.* 1986; 35: 249-253.
 23. Lee J.T., Alper H. *J. Org. Chem.* **1990**; 55: 1854-1856.
 24. Monflier E., Blouet E., Barbaux Y., Mortreux A. *Angew. Chem., Int. Ed.* 1994; 33: 2100-2102.
 25. Monflier E., Fremy G., Castanet Y., Mortreux A. *Angew. Chem., Int. Ed.* 1995; 34: 2269-2271.
 26. Monflier E., Tilloy S., Fremy G., Castanet Y., Mortreux A. *Tetrahedron Lett.* 1995; 56: 9481-9484.
 27. Lacroix T., Bricout H., Tilloy S., Monflier E. *Eur. J. Org. Chem.* 1999; 3127-3129.
 28. Widehem R., Lacroix T., Bricout H., Monflier E. *Synlett.* 2000; 722-724.
 29. Tilloy S., Bertoux F., Mortreux A., Monflier E. *Catal. Today.* 1999; 48: 245-253.
 30. Monflier E., Tilloy S., Castanet Y., Mortreux A. *Tetrahedron Lett.* 1998; 39: 2959-2960.
 31. Dessoudeix M., Urrutigoity M., Kalck P. *Eur. J. Inorg. Chem.* 2001; 1797-1800.
 32. Tilloy S., Bertoux F., Mortreux A., Monflier E. *Catal. Today.* 1999; 48: 245-253.

33. Mathivet T., Meliet C., Castanet Y., Mortreux A., Caron L., Tilloy S., Monflier E. *J. Mol. Catal., A Chem.* 2001; 176: 105-116.
34. Reetz M.T., Waldvogel S.R. *Angew. Chem., Int. Ed.* 1997; 36: 865-867.
35. Reetz M.T. *Catal. Today.* 1998; 42: 399-411.
36. Leyva E., Moctezuma E., Strouse J., Garcia-Garibay M.A. *J. Incl. Phenom. Macrocyclic Chem.* 2001; 39: 41-46.
37. Abreu A.R., Costa I., Rosa C., Ferreira L.M., Lourenc A., Santos P.P. *Tetrahedron.* 2005; 61: 11986-11990.
38. Kunishima M., Watanabe Y., Terao K., Tani S. *Eur. J. Org. Chem.* 2004; 4535-4540.
39. Wen L., Wenya Z., Xiaoqing M., Panpan W., Menghong D. *Appl. Catal. A.* 2012; 210-214.
40. Du J., Huaxue. *Shiji.* 1993; 15: 183-189.
41. Fife W.K., Xin Y. *J. Am. Chem. Soc.* 1987; 109: 1278-1279.
42. Wen Y.L., Yeh M.Y., Lee Y.S., Shih Y.P. *J. Chin. Inst. Chem. Eng.* 1996; 27: 427-436.
43. Wang M.L., Ou C.C., Jwo J.J. *Chem. Eng. Commun.* 2000; 179: 233-252.
44. March J. *Advanced Organic Chemistry*, 2nd ed. New York: McGraw-Hill 1977, pp 227.
45. Wang M.L., Ou C.C., Jwo J.J. *J. Chin. Chem. Inst. Eng.* 2000; 23: 171-178.
46. Asai S., Nakamura H., Okada W., Yamada M. *Chem. Eng. Sci.* 1995; 50: 943-949.
47. Nakamura H., Asai S., Yamada M. *Chem. Eng. Sci.* 1996; 51: 1343-1346.
48. Fife W.F., Zhang Z. *J. Org. Chem.* 1986; 51: 3746-3748.
49. Kuo C.S., Jwo J.J. *J. Org. Chem.* 1992; 57: 1991-1995.
50. Wang M.L., Ou C.C., Jwo J.J. *Ind. Eng. Chem. Res.* 1994; 33: 2034-2039.
51. Wang M.L., Ou C.C., Jwo J.J. *Bull. Chem. Soc. Jpn.* 1994; 67: 2949-2955.
52. Wang M.L., Ou C.C., Jwo J.J. *J. Mol. Catal. A.* 1995; 99: 153-160.
53. Wang M.L., Ou C.C., Jwo J.J. *Bull. Chem. Soc. Jpn.* 1995; 68: 2165-2174.
54. Ou J.S., Chen R.H., Jwo J.J. *J. Mol. Catal. A.* 1996; 110: 95-103.
55. Liou Y.M., Jwo J.J. *J. Chin. Inst. Chem. Eng.* 1996; 27: 405-410.
56. Wang M.L., Ou C.C., Jwo J.J. *Chem. Eng. Commun.* 1998; 165: 151-165.

57. Hung M.L., Jwo J.J. *J. Mol. Catal. A.* 2000; 154: 55-63.
58. Chang Y.S., Jwo J.J. *J. Mol. Catal. A.* 2000; 160: 357-366.
59. Lu Y.L., Jwo J.J. *J. Mol. Catal. A.* 2001; 170: 57-65.
60. Anishchenko V.N., Rybachenko V.I., Chotii K.Y., Redko A.N. *Theor. Exp. Chem.* 2012; 48: 172-175.
61. Iliescu S., Ilia G., Pascariu A., Popa A., Plesu N. *Polymer.* 2006; 47: 6509-6512.
62. Iliescu S., Grozav I., Plesu N., Pascariu A., Ilia G. *Polym. Eng. Sci.* 2008; 48: 1304-1311.
63. Pascariu A., Iliescu S. *Annals of West University of Timisoara Series of Chemistry.* 2007; 16: 67-72.
64. Iliescu S., Pascariu A., Macarie L., Plesu N., Ilia G. *Polym. Bull.* 2009; 63: 485-495.

Chapter 13

Solubilization of carbon nanotubes in water and in organic solvents

Grażyna Bartkowiak and Grzegorz Schroeder

Adam Mickiewicz University in Poznań,

Faculty of Chemistry, Umultowska 89b, 61-614 Poznań, Poland

NanoBioMedical Centre, Umultowska 85, 61-614 Poznań, Poland

Introduction

Carbon nanotubes (CNTs), new molecular form of carbon, were discovered by Iijima [1] and soon focused great attention of scientist from many fields because of their unique properties. CNTs reveal high thermal and electrical conductivity [2], as well as excellent mechanical properties [3, 4] they are also chemically inert and resistant to acids and bases. Rapidly they found application in catalysis [5], as materials for gas-sensors production [6] and for the fabrication of composites [7].

Carbon nanotubes belong to the great family of graphitic filaments, which may have diameters from 0.4 to 500 nm and length from hundreds of nanometers to about micro- or even centimeters [8]. These filaments are classified into three main structural categories, depending on the angle of the graphene layers with respect to the filament axis [9]: *stacked* (where graphene layers are perpendicular to the fiber axis), *herringbone* or *cup-stacked* (where layers are placed at an angle to the axis) and *nanotubular* (where cylindric walls are parallel to the axis of the tube). The category “carbon nanotubes” is currently used mainly for tubular structures, which are of a cylinder shape, but in broader meaning it is applied also to other graphitic nanofibers.

There are two main types of “classical”, i. e. cylindric carbon nanotubes: SWCNTs, single-walled carbon nanotubes and MWCNTs, multi-walled carbon nanotubes. The building of nanotubes depends on the preparation method and selection of synthesis parameters. The main preparation methods are basing on the chemical vapor deposition (CVD) process or on the arc discharge technique, supported by various metallic catalysts. Modifications of vapor deposition

methods are: thermal chemical vapor deposition, catalytic chemical vapor deposition (CCVD) and plasma enhanced chemical vapor deposition (PEVCD) [10]. As can be seen later in the text, iron, cobalt and nickel are most frequently used as metallic catalysts in carbon nanotubes fabrication.

Four major SWNT synthetic methods used for commercial purposes are:

1. Ni/Y-catalyzed arc discharge;
2. Fe/Mo catalyzed CVD;
3. Fe-catalyzed CVD;
4. Co/Mo-catalyzed CVD.

The obtained single-walled carbon nanotube powders are further classified as raw (as-produced soot directly from the reactor), purified (refined single-walled nanotubes with low degree of chemical functionalization) and carboxylated (refined with higher degree of introduced carboxyl group on the sidewalls and at the tube ends) [11].

Many characterization methods are used for description and explanation of CNTs properties. Among them the most important are:

- X-ray photoelectron spectroscopy (XPS) – for surface characterization [12];
- Fourier-transformed infrared spectroscopy (FTIR) – for functional groups identification [13, 14];
- Brunauer, Emmett, Teller (BET) analysis – i.e. to measure BET surface area of pristine and functionalized CNTs – enables determination if the ends of nanotubes opened and/or if defects are generated on the sidewalls [10];
- temperature-programmed desorption with gas chromatography; TPD (in He) with GC – registers ion current vs. temperature, enables evaluation of oxygen containing groups, which evolve CO_2 and CO [10, 15, 16] – quantitative analysis of functional groups;
- thermogravimetric analysis (TGA) – to determine weight loss with temperature; time and temperature of thermal oxidation could be estimated from the curves of TGA [10];
- scanning electron microscope, SEM [10] – for imaging of fine structures of materials obtained and their morphological analysis;
- transmission electron microscope, TEM – for characterization of interior structure of CNTs, for example measuring nanotube diameter and bundle diameter and calculating the number of nanotubes in the bundle [10];
- TEM with EDX (Energy-Dispersive X-ray spectroscopy) – enables judging of elemental composition of the sample and detection of

- metallic catalyst residues;
- ultraviolet/visible spectroscopy and near-infrared spectroscopy; UV-Vis NIR;
- Raman spectroscopy [17];
- AFM – Atomic Force Microscopy –information about the length of nanotubes and the approximate diameter of the nanotubes bundles; indirect method of morphological analysis [10];
- fluorescence – inspecting of extensive conjugated electronic structures in CNTs [18];
- EPR – detection of carbon radicals presence [18];
- XRD – crystallinity of nanotubes and degree of their graphitization [18].

Pristine nanotubes (as-prepared) are inert and highly hydrophobic [11], they reveal also low solubility in water and organic solvents. The main reason for this behavior is van der Waals attraction between tubes, which are joined in bundles [19] or ropes, containing hundreds of close-packed, tightly bound and often entangled nanotubes. Van der Waals attraction energy is $500\text{eV}/\mu\text{m}$ of tube-tube contact [20]. All carbon atoms in carbon nanotubes have sp^2 hybridization and possess delocalized π -electrons, which enable π - π stacking interactions.

For biological, biotechnological and medical applications, low water-solubility of carbon nanotubes is a crucial limitation [21]. In order to obtain solubilization of carbon nanotubes in water or improve their interactions with other molecules (for example molecules of organic solvents), modification of their surface is necessary. This modification may consist in the chemical functionalization of the open ends or exterior walls (convex face) or interior walls (concave face) of the nanotubes as well as wrapping the nanotubes in hydrophilic material. The most widespread approaches involve: wrapping of CNTs in biocompatible organic substance, i. e. starch [22], or poly(vinylpyrrolidone) [23] PVP, attachment of glucosamine [24], crown ether [25], poly(ethylene oxide) with terminal $-\text{NH}_2$ groups [26] to the nanotube sidewalls, possessing carboxylic groups, functionalization with amino acids [27]. The $-\text{COOH}$ groups are commonly generated through the strong acid treatment.

Chemical modifications

Solubilization of carbon nanotubes in organic solvents was reported in literature since 1998 [21, 28, 29]. First attempts of obtaining soluble carbon nanotubes were made by Haddon *et al.*, when aqueous suspension of purified SWNTs (100 to 300 nm in length) were submitted to the action of HCl, which resulted in attaching of carboxyl groups ($-\text{COOH}$, IR frequency $\nu_{\text{C=O}} = 1719\text{ cm}^{-1}$), rather than carboxylate

groups ($-\text{COO}^-$; $\nu_{\text{C=O}} = 1620 \text{ cm}^{-1}$) to the tubes ends and walls.

To ensure the solubilization of SWNTs in organic solvents, carboxylated nanotubes (SWNT-COOH) were reacted with thionyl chloride SOCl_2 to yield carbon nanotubes with acyl chloride function (SWNT-COCl) and subsequently acyl chloride groups obtained were modified with octadecylamine (ODA, $\text{CH}_3(\text{CH}_2)_{17}\text{NH}_2$) via amide formation.

Protocol of solubilization of shortened single-walled carbon nanotubes reported by Haddon [19] is described. The SWNTs, obtained by modified electric arc technique [30], were purified and shortened by the method developed by Smalley and co-workers [31].

100 mg of shortened SWNTs were stirred in 20 ml SOCl_2 with 1 ml of dimethylformamide (DMF) at 70°C for 24 hours, centrifuged and a solid remained after decantation of supernatant was washed with anhydrous tetrahydrofuran (THF). After second centrifugation and decantation, the remaining solid was dried at room temperature under vacuum. Resulting SWNTs were mixed with octadecylamine (ODA, melting point $55\text{-}57^\circ\text{C}$, 2 g) and heated at $90\text{-}100^\circ\text{C}$ for 96 hours, cooled to the room temperature and the excess of amine was washed out with ethanol (by sonication with EtOH for 5-10 minutes at 40 kHz for four times). The obtained solid was dissolved in dichloromethane, filtered and the black-coloured filtrate was evaporated to dryness on a rotary evaporator. The resulting black solid was dried at room temperature under vacuum.

The material obtained in such a way, in sharp contrast to as-prepared shortened SWNTs, shows substantial solubility in chloroform, dichloromethane, benzene, toluene, chlorobenzene, 1,2-dichlorobenzene and CS_2 . The solution was stable upon prolonged standing and no precipitation was observed. These modified carbon nanotubes are however insoluble in water, ethanol and acetone.

There are many methods and protocols of chemical functionalization of carbon nanotubes reported in literature, however the first step of chemical modification is commonly the surface oxidation to obtain active functional groups.

Chemical oxidation

Chemical oxidation of carbon nanotubes proceeds similarly as graphite or graphene oxidation, i.e. it generates different oxygen-containing groups like $-\text{OH}$, $-\text{O}-$, $\text{C}=\text{O}$ or $-\text{COOH}$ on the surface [32]. First of all these groups are formed in defect sites on the nanotube end, however, when strong enough oxidizers are applied, the modified defects are formed on the sidewalls of nanotubes as well. The amount and type of functional groups created depends on the treatment method. Upon the action of nitric acid mainly phenol, lactol and carboxyl groups

are formed [33, 34], whereas using the oxygen plasma carbonyl and lactone groups formation is observed [19].

Extensive oxidation methods and other vigorous treatments often result in opening the ends of tubes [35] or deeper destruction of nanotubes, like shortening [41] and breaking them into pieces, defect formation on the surface of CNTs [36, 37] accumulation of carbonaceous impurities [38] or formation of carbon nanoflakes [39]. Strong acids, acting on nanotubes during a long period of time finally oxidize carbon to CO_2 , however many protocols are applied, which exploit mineral acids to purify CNTs and make them more soluble in polar solvents. Carboxylic groups created on the surface of nanotubes by oxidation enable further chemical modification through the reactions with many compounds possessing other functionalities as well as polymer grafting to CNTs [40].

The most common agent used to oxidize of carbon nanotubes is nitric acid. There are two main approaches to perform the oxidation with use of HNO_3 :

1. Boiling of carbon nanotubes in diluted nitric acid (2-3 M) for prolonged time (16-48 h);
2. Treatment of CNTs in ultrasonic bath for 3-5 hours with a mixture of concentrated sulfuric and nitric acids (ordinarily 3:2 v/v)

Rinzler *et al.* [41] reported dilute nitric acid (2.6 M) washing treatment to remove metal catalyst and amorphous carbon from single-walled carbon nanotubes. This method was subsequently adopted by many other researcher using different time and temperatures [38, 42]. Liu *et al.* [43] used concentrated nitric acid for modification of insoluble part of CNTs with surficial carboxylic acid groups. Water-soluble carbon nanotubes were obtained by Rao and co-workers [44] by refluxing multi-walled CNTs with H_2SO_4 - HNO_3 mixture, 3:2 ratio by volume. Naseh *et al.* [13] reported oxidation of CNTs using nitric acid (refluxing in HNO_3 for 4 hours) and by dry treatment using dielectric-barrier discharge plasma under air atmosphere. Treatment with piranha solution (a mixture of 96% H_2SO_4 and 30% H_2O_2) or with a mixture $\text{HNO}_3/\text{H}_2\text{SO}_4$ were used to the shortening of nanotubes [45]. The same solutions or concentrated mineral acids (HNO_3 , H_2SO_4) as well as H_2O_2 were applied to remove the nanotubes of smaller diameter from the whole material [46]. Less frequently used oxidizers were ozone [47] and KMnO_4 [48], water as a weak oxidizer is also reported [49]. There are report about electrochemical oxidation or thermal annealing [50] as methods of carbon nanotubes purifying and resulting in the surface oxidation. Ramanathan *et al.* [51] stated that a treatment of carbon nanotubes with deuterated acid mixture (3:1 ratio of D_2SO_4 : DNO_3) results in apparent enhancement in solubility when compared with *H-acid mixture* (3:1 mixture of

common concentrated sulfuric and nitric acids). The solubility improvement is attributed to the strong affinity of deuterium to the nanotube surface.

In the procedure given by Boskovic and co-workers [52], the raw carbon nanotubes, obtained by CCVD method using ethylene as carbon source and bimetallic Fe-Ni catalyst on Al_2O_3 , were purified by means of boiling the carbon material for 6 hours with reflux in 3M NaOH solution and subsequently 3M HNO_3 solution with intermediate washing with water. This treatment efficiently removed catalyst particles embedded in the nanotubes top, but was non-efficient towards the metal particles, encapsulated inside the thicker nanotube bodies. The method of liquid oxidation applied therein has gone up population of tiniest nanotubes, that prove destructive character of this technique.

Refluxing of carbon nanotubes in 55% HNO_3 is regarded as most harsh purification method, since it generates the most rough carbon surface and decreases the outer diameter of the tubes [53], thermal stability and crystallinity of the material, but increases its catalytic activity and the total amount of surface oxygen groups [53].

From many experiments with carbon nanotubes oxidation the general conclusions can be drawn about the relation of CNTs solubility to their length, diameter and oxidation conditions. The common observation is that oxidation of SWNTs with nitric acid improves their dispersability in water, methanol and dimethylformamide (DMF). The commercially available single-walled nanotubes have average diameters 0.8 nm (company CoMoCat) [54], 1.0 nm (company HiPco) [55] or 1.3 nm (company PLV) [56] and only minor number of the tubes are individual, most of them appear to be in bundles. Oxidizers like HNO_3 penetrate between tubes in bundles, react with defects on the sidewalls and break bundles into smaller packs or into individual tubes.

Oxidizing agents primarily attack the ends of nanotubes and the defects on their sidewalls [31, 57, 59]. The capped ends of nanotubes are more strained and therefore more susceptible to opening. Oxidation at the ends of CNTs causes opening of the tubes and further leads to the removal of carbon atoms, whereas oxidation at the defects in sidewalls may lead to cutting nanotubes into pieces i.e. to shorten their length. The more severe oxidation leads to the larger number of functional groups introduced and the further shortening of tubes. The smaller diameter of nanotubes, the more readily and easily they are oxidized [55, 61, 59, 60].

There are two main procedures of chemical oxidation of carbon nanotubes: the method involving a sonication or a reflux of nanotubes with oxidizing agent. Tchoul and co-workers [59] recommend following procedures of SWNTs oxidation (based on AFM and Raman spectroscopy measurements):

1. For the tiniest nanotubes (CoMoCat SWNTs, 0.8 nm diameter) – sonication in 8M HNO₃ for 1.5 h and avoiding of reflux which is harmful for this material.
2. For nanotubes of average diameter about 1 nm (HiPco SWNTs) – reflux in 2.6 M HNO₃ for no longer than 4 h, which ensures higher degree of functionalization and at the same time minimizes tube shortening and loss of carbon material.
3. For nanotubes of average diameter about 1.3 nm (PLV SWNTs) – sonication in 8 M for 1-4 hours, because a longer period of sonication time produces in this case longer and more soluble single-walled nanotubes without material loss.

Generally, the sonication method is less destructive to nanotubes and results in catalyst metal residues removal almost without a loss of carbon. The reflux method results in better functionalization of sidewalls and increased number of polar groups on the nanotubes surface, so in consequence better solubility, but also in deeper destruction of tube's structure. The optimal reflux time seems to be 4 hours, when the functionalization is good enough. The prolongation of reflux time to 12 hours yields the tube breaking and carbon loss. The nitric acid oxidation produces mainly carboxylic functional groups on the nanotubes surface [62, 63]. Functionalization of nanotubes with use of nitric acid is more destructive than with use of oxygen plasma [13].

Commonly, the oxidized nanotubes with carboxylic and carbonyl groups are further modified through covalent attachment of specific molecules, which enable better dispersion or dissolution in water. There are however many other methods to attach polar molecules to the external walls of carbon nanotubes. The strategy described by Georgakilas *et al.* [27] engaged 1,3-dipolar addition of N-protected amino acid to the carbon surface. Amino acid molecules, which were attached to the walls, were subsequently deprotected at the chain-end through removal of the N-*tert*-butoxycarbonyl (BOC) protecting group by acid (HCl) treatment. The free amino groups of amino acid were at that time converted to ammonium chloride salt and therefore the ionic groups formed made the NTs remarkably soluble in water.

Surfactant-coating

Main challenge in operating with nanotubes is to obtain a uniform homogenous dispersion of CNTs, which would be stable for a long time. This can be achieved with aid of surface active agents, i.e. surfactants and specific block copolymers. The stabilization of suspension can be affected by the surfactant used, adsorption mechanism and surface charge. The main reason of

low solubility/dispersability of carbon nanotubes is their tendency to join into bundles, so the challenging task is to “debundle” the aggregates and isolate the single nanotubes from a bundle. A mechanism of debundling of nanotubes using ultrasonication and surfactant absorption was proposed by Strano *et al.* [64] and involves: a) high local shear, basically at the bundle ends, through the ultrasonication; b) forming spaces and gaps at the bundle ends, generated by the adsorption of surfactant; c) separating of nanotubes from the bundle. During this process, called also “unzipping”, surfactant molecules get into the spaces between the tubes in a bundle and prevent them from re-aggregating.

Surfactant reveal two important features, which find their application in stabilization of colloidal dispersion: they adsorb at interface and tend to self-accumulate into supramolecular structures. The adsorption of surfactant on the surface of water, organic solvent or inorganic material depends on chemical character of all components, i.e. surfactant, solvent and inorganic particles. The adsorption driving force may be the electrostatic attraction between the oppositely charged surface and surfactant head group (for ionic surfactants) or hydrophobic attraction between the surface and non-polar surfactant tail groups (for non-ionic surfactants). The knowledge about the carbon nanotubes surface charge is crucial for understanding the interaction mechanism between CNT and surfactant and for the proper choice of surfactant type to stabilize CNT dispersion. Generally for water solutions of nanotubes ionic surfactant are preferred, whereas for dispersions in organic solvents nonionic surfactants are recommended [65].

The commonly used ionic surfactants to improve carbon nanotubes dispersability in water are sodium dodecyl sulfate (SDS) [66-71] and dodecyl-benzene sodium sulfonate (NaDDBS) [72-75], Dowfax surfactant (anionic alkyldiphenyl-oxide disulfonate) [73], Aerosol OS (sodium diisopropyl-naphthalene sulfonate) [73], Tween-60 and Tween-80 (polyethylene oxide) sorbitan monostearate and monooleate, respectively) [76]. Carbon nanotubes have been reported to be soluble in micellar solutions of some other detergents, for example aqueous 1 wt % lithium dodecyl sulfate (LDS) solution [77]. To disperse carbon nanotubes in organic solvent, nonionic surfactant are needed. Generally, hydrophobic CNTs are expected to be better soluble in organic solvents than in water and physiological aqueous fluids. In fact, however, only limited number of organic solvents show sufficient dispersability properties for carbon nanotubes. Among them dimethylformamide (DMF), dimethyl acetamide (DMAc) and dimethylpyrrolidone (NMP) play important role [78]. It appeared also that immersing single-walled carbon nanotubes in DMF causes a damage of CNT structure [79].

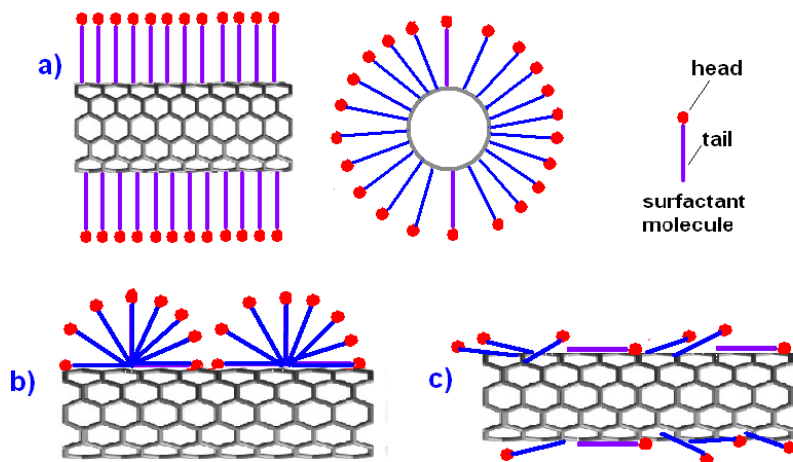


Figure 1. Proposed schematic mechanism by which surfactants help to disperse SWNT. (a) SWNT encapsulated in a surfactant micelle (both cross section and side-view); (b) hemimicellar adsorption of surfactant molecules on a SWNT; (c) random adsorption of surfactant molecules on a SWNT (according to [80]).

Surfactant-coated carbon nanotubes find also various applications, i. e. industrial, for the fabrication of CNT-polymer composites (CNTs with cetyltrimethylammonium bromide, CTAB [81] and O π -10 (polyethylene oxide(10) nonylphenyl ether) [82], as well as biological (SWNT wetted with Triton X-100 [83]).

Many attempts were made to find general regularities ruling the solubility of carbon nanotubes. Ham *et al.* [85] studied the solubility of CNTs at various organic solvents, such as acetone, chloroform, toluene, benzene, dimethylformamide (DMF) and others, in terms of Hansen solubility parameters:

$$\delta_t^2 = \delta_d^2 + \delta_p^2 + \delta_h^2$$

where δ_d stand for the energy from dispersion force between molecules, δ_p for the energy from dipolar intermolecular forces, and δ_h for the energy from hydrogen bonds.

The authors concluded that the tubes are suspended well in solvents with dispersive component in boundaries of certain values (between 17 and 18 MPa^{1/2}), but they precipitate in solvents with high polar and hydrogen-bonding

components (δ_p and δ_h). They found however no specific dependency between the dispersion state and the total solubility parameter δ_t . Preferred surfactants for carbon nanotubes coating are these that have relatively high HLB (Hydrophyle-Hydrophyle Balance).

Surfactant-coating is regarded as simplest straightforward method of improving CNTs solubility in many solvent, but a disadvantage is that the surface-active species used are often able to denaturize biological molecules. The other limitation of surfactant-approach is the accessible concentration [85].

Polymer wrapping

Another method of improving solubility of carbon nanotubes is their functionalization with polymers, often containing hydrophilic groups. This solubility can be achieved by reversible non-covalent attachment of linear polymers to the sidewalls of CNTs. The dispersion of CNTs associated with polymers may be enhanced in water [24, 86] and in organic solvents [87]. Joining nanotubes with polymer is used also to enable better separation of CNTs from metal and carbonaceous impurities [88, 89].

Two mechanisms of polymer action towards nanotubes are proposed: (a) thermodynamically driven “wrapping” with following damage of a hydrophobic interface between the tubes and water [24] as well as (b) kinetically driven long-ranged entropic repulsion among polymer-coated nanotubes [88].

Water-soluble polymers play a role in preparing stable aqueous dispersions of carbon materials through wrapping. The most successfully used polymers to result water solubility of nanotubes are polyvinylpyrrolidone (PVP) [90] and polystyrene sulfonate (PSS). This physical association may be reversed by changing the solvent system.



The AFM images and field-flow fractionalization (FFF) technique show that the PVP-polymer and carbon nanotubes are tightly connected and form a single entity, which can be operated and manipulated as a whole and also easier purified,

fractionalized and functionalized. The PVP-SWNTs exhibit monolayer covering of the nanotubes with the polymer. The surface of nanotubes is uniformly covered by the polymer. The mechanism of polymer “wrapping” is discussed since the tight interaction of polymer molecules with carbon nanotubes sidewalls would disturb the strong van der Waals forces between the nanotubes in bundles and separate them to individual tubes. Among the biopolymers used for wrapping nanotubes bovine serum albumin (BSA) and dextran are notably important.

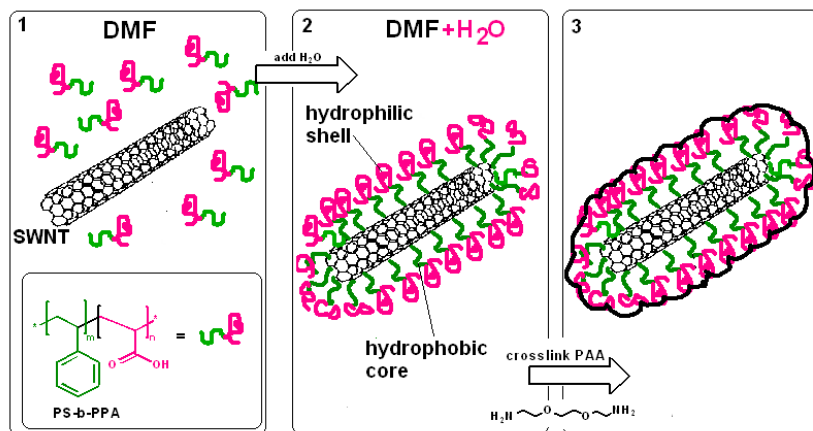
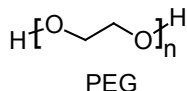


Figure 2. The general strategy for encapsulating SWNT within shells of amphiphilic block copolymer PS-*b*-PAA (according to [87] and [65])

Recently, Gerstel and co-workers [91] investigated several polymers towards their wrapping ability and enhance the solubility of carbon nanotubes. They checked fourteen different conjugated polymers, which were derivatives of 9,9-dioctylfluorene, containing various lateral groups like biphenyle, stilbene, azomethine or azobenzene units. Specifically, four polymers of azomethine type have been found to be very effective in highly selective solubilization of SWCNTs. The results were supported by molecular dynamics simulations.

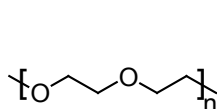
An alternative approach to wrapping nanotubes in hydrophilic polymer is to prepare CNT-polymer composites, where water-soluble (or organic solvent-soluble) polymers are used. The assumption is that if a polymer is soluble in particular solvent, its CNT composites could also be soluble. Indeed, such a simple polymer as poly(vinyl alcohol, PVA) in a composite with amorphous carbon nanotubes (a-CNTs) exhibits a much enhanced solubility in water [92].

For stepwise synthesis of composites different supplementary polymers can be used, for example PEG [poly(ethylene glycol)] was applied to obtain PEG-ylated MWNTs for the further fabrication of PVA/MWNT nanocomposite [93].

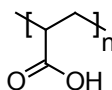


In general, poly(ethylene glycol) (PEG) is very commonly used in carbon nanotube functionalization, for water-soluble CNT-polyethylene grafted copolymers [94] synthesis, for MWNTs dedicated to drug delivery [95], as a stabilizer for pyrene-functionalized multi-walled carbon nanotubes [96] and for many other applications, including straightforward wrapping. The CNT modified with PEG and PEG-composites induced only low acute toxicity, [95]⁹⁵ so this polymer can be regarded as biocompatible to mammals.

Other frequently used polymers, capable of dispersing CNTs, are polyethylene oxide, (PEO) [97] and poly(acrylic acid), (PAA) [98].



poly(ethylene oxide), PEO



poly(acrylic acid), PAA

The functionalized carbon nanotubes of better solubility can be obtained with use of classical polymers, popular in nanotechnology, like polyaniline, polyurethane, siloxanes, poly(N-isopropylacrylamide) PNiPAM, weak polyelectrolites, like poly(methacrylic acid) PMAA, poly(allylamine) PAAM, branched polyethyleneimine (BPEI) and many others [99].

Conclusions

Different approaches are suggested to decrease the carbon nanotube agglomeration and increase their solubility, namely ultrasonication and high-shear mixing as well as methods, which alter the surface chemistry of nanotubes either covalently (through functionalization) or non-covalently (through adsorption). Worth of mentioning are: plasma method of oxidation with O₂ or

Ar/O₂/C₂H₆, ozonolysis by UV/ozone treatment, mineral acids action, surface modification with aromatic compounds, polymers, biomolecules, natural products, surfactants, DNA etc. The solubilization of carbon nanotubes offers exciting opportunities for their widespread applications and development of high property materials.

Acknowledgements

Financial support from the National Centre for Research and Development under research grant “Nanomaterials and their application to biomedicine”, contract number PBS1/A9/13/2012, is gratefully acknowledged.

References

1. S. Iijima; Helical microtubules of graphitic carbon; *Nature*, **354**, 56, (1991).
2. Y. J. Noh, H. S. Kim, S. Y. Kim; Improved electrical conductivity of a carbon nanotube mat composite prepared by in-situ polymerization and compression molding with compression pressure, *Carbon Letters*, **13**, 243–247, (2012).
3. S. Chen, W. She, G. Wu, D. Chen, M. Jiang; A new approach to the functionalization of single-walled carbon nanotubes with both alkyl and carboxyl groups; *Chem. Phys. Lett.*, **402**, 312–317, (2005).
4. L. J. Cui, H. Z. Geng, W. Y. Wang, L. T. Chen, J. Gao; Functionalization of multi-wall carbon nanotubes to reduce the coefficient of the friction and improve the wear resistance of multi-wall carbon nanotube/epoxy composites, *Carbon*, **54**, 277–282, (2013).
5. P. Serp, M. Corrias, P. Kalck; Carbon nanotubes and nanofibers in catalysis; *Applied Catalysis A: General*, **253**, 337–358, (2003).
6. M. Fleischer, H. Meixner; Selectivity in high-temperature operated semiconductor gas-sensors; *Sensors and Actuators B*, **52**, 179–187, (1998).
7. A. M. Shanmugaraj, J. H. Bae, K. Y. Lee; Physical and chemical characteristics of multiwalled carbon nanotubes functionalized with aminosilane and its influence on the properties of natural rubber composites; *Composites Science Technology*, **67**, 1813–1822, (2007).
8. Wang, X.; Li, Qunqing; Xie, Jing; Jin, Zhong; Wang, Jinyong; Li, Yan; Jiang, Kaili; Fan, Shoushan; Fabrication of Ultralong and Electrically Uniform Single-Walled Carbon Nanotubes on Clean Substrates. *Nano Letters*, **9**, 3137–3141, (2009).

9. C. A. Bessel, K. Laubernds, N. M. Rodriques, R. T. K. Baker; Graphite nanofibers as an electrode for fuel cell applications; *J. Phys. Chem.B*, **105**, 1115, (2001).
10. K. Safarova, A. Dvorak, R. Kubinek, M. Vujtek, A. Rek; Usage of AFM, SEM and TEM for the research of carbon nanotubes; *Modern Research and Educational Topics in Microscopy*, eds. A. Mendez-Vilas and J. Diaz; Formatex, 513-519, (2007).
11. R. Wang, C. Mikoryak, S. Li, D. Bushdiecker II, I. H. Musselman, P. Pantano, R. K. Draper; Cytotoxicity screening of single-walled carbon nanotubes: Detection and removal of cytotoxic contaminants from carboxylated carbon nanotubes; *Mol. Pharmaceutics*, **8**, 1351-1361, (2011).
12. W. Xia, Y. Wang, R. Bergstra, S. Kundu, M. Muhler; Surface characterization of oxygen-functionalized multi-walled carbon nanotubes by high-resolution X-ray photoelectron spectroscopy and temperature-programmed desorption; *Applied Surface Science*, **254**, 247-250, (2007).
13. M. V. Naseh, A. A. Khodadadi, Y. Mortazawi, O. A. Sahraei, F. Pourfayaz, S. M. Sedghi; Functionalization of carbon nanotubes using nitric acid oxidation and DBD plasma; *Int. J. Chem. Biol. Eng.*, **2**, 66-68, (2009).
14. D. B. Mawhinney, V. Naumenko, A. Kuznetsova, J. T. Yates, J. Liu, R. E. Smalley; Infrared spectra evidence for the etching of carbon nanotubes: Ozone oxidation at 298K; *J. Am. Chem. Soc.*, **122**, 2383-2384, (2000).
15. T. Kyotani, S. Nakazaki, W. Xu, A. Tomita; Chemical modification of the inner walls of carbon nanotubes by HNO₃ oxidation, *Carbon*, **39**, 771-785, (2001).
16. H. P. Boehm, Surface oxides on carbon and their analysis: A critical assesment; *Carbon* **40**, 145-149, (2002).
17. Y. C. Choi, K.-I. Min, M. S. Jeong, Novel Method of Evaluating the Purity of Multiwall Carbon Nanotubes Using Raman Spectroscopy; *Journal of Nanomaterials*; (2013), Article ID 615915, 6 pages.
18. P. Dubey, D. Muthukumar, S. Dash, R. Mukhopadhyay, S. Sarkar; Synthesis and characterization of water-soluble carbon nanotubes from mustard soot; *Pramana – Journal of Physics*, **65**, 681-697, (2005).
19. B. Ruelle, S. Peeterbroeck, R. Gouttebaron, T. Godfroid, F. Monteverde, J. Dauchot, M. Alexandre, M. Hecq, P. Dubois; Functionalization of carbon nanotubes by atomic nitrogen formed in a microvawe plasma Ar+N₂ and subsequent poly (ϵ -caprolactone)grafting; *J. Mater. Chem.*,

- 17**, 157-159, (2007).
20. L. A. Girifalco, M. Hodak, R. S. Lee; Carbon nanotubes, buckyballs, ropes, and a universal graphitic potential; *Phys. Rev. B.*; **62**, 13104, (2000).
 21. J. Chen, M. A. Hamon, H. Hu, Y. Chen, A. M. Rao, P. C. Eklund, R. C. Haddon; Solution properties of single-walled carbon nanotubes; *Science*, **282**, 95, (1998).
 22. A. Star, D. Steuerman, J. R. Heath, J. F. Stoddart; Starched carbon nanotubes, *Angew. Chem. Int. Ed.*, **41**, 2508, (2002).
 23. M. J. O'Connell, P. Boul, L. Erickson, C. Huffman, Y. Wang, E. Haroz, C. Kuper, J. Tour, K. D. Ausman, R. E. Smalley; Reversible water-solubilization of single-walled carbon nanotubes by polymer wrapping; *Chem. Phys. Lett.*, **342**, 265, (2001).
 24. F. Pompeo, D. E. Resasco; Water solubilization of single-walled carbon nanotubes by functionalization with glucosamine; *Nano Lett.*, **2**, 369, (2002).
 25. G. M. C. Kahn, S. Banerjee, S. S. Wong; Solubilization of oxidized single-walled carbon nanotubes in organic and aqueous solvents through organic derivatization; *Nano Lett.*, **2**, 1215–1218, (2002).
 26. M. Sano, A. Kamino, J. Okamura, S. Shinkai; Self-Organization of PEO-graft-Single-Walled Carbon Nanotubes in Solutions and Langmuir–Blodgett Films; *Langmuir*, **17**, 5125, (2001).
 27. V. Georgakilas, N. Tagmatarchis, D. Pantarotto, A. Bianco, J.-P. Briand, M. Prato; Amino acid functionalisation of water soluble carbon nanotubes; *Chem. Commun.*, 3050-3051, (2002).
 28. Y. Chen, G. Chen, H. Hu, M. A. Hamon, M. E. Itkis, R. C. Haddon; Solution-phase EPR studies of single-walled carbon nanotubes; *Chem. Phys. Lett.*, **299**, 532-535, (1999).
 29. S. Niyogi, M. A. Hamon, H. Hu, B. Zhao, P. Bhowmik, R. Sen, M. E. Itkis, R. C. Haddon; Chemistry of single-walled carbon nanotubes; *Acc. Chem. Res.*, **35**, 1105-13, (2002).
 30. C. Journet, W. K. Maser, P. Bernier, A. Loiseau, M. Lamy de la Chapelle, S. Lefrant, P. Deniard, R. Lee, J. E. Fischer, Large-scale production of single-walled carbon nanotubes by the electric-arc technique; *Nature*, **388**, 756-758, (1997).
 31. J. Liu, A. G. Rinzler, H. J. Dai, J. H. Hafner, R. K. Bradley, P. J. Boul, A. Lu, T. Iverson, K. Shelimov, C. B. Huffman, F. Rodriguez-Macias, Y.-S. Shon, T. R. Lee, D. T. Colbert, R. E. Smalley; Fullerene pipes; *Science*, **280**, 1253-1256, (1998).

32. Y. Si, E. T. Samulski; Synthesis of water-soluble graphene; *Nano Lett.* **8** (6), 1679-1682, (2008).
33. M. A. Montes-Moran, D. Suarez, J. A. Mendez, E. Fuente; On the nature of basic sites on carbon surfaces: An overview; *Carbon*, **42**, 1219-1225, (2004).
34. Y. Li, S. Wang, Z. Luan, J. Ding, C. Xu, D. Wu; Adsorption of cadmium(II) from aqueous solution by surface oxidized carbon nanotubes; *Carbon*, **41**, 1057-1062, (2003).
35. S. Tsang, Y. Chen, P. Harris, M. Green, A simple chemical method of opening and filling carbon nanotubes; *Nature*, **372**, 159, (1994).
36. S. Banerjee, T. Hemraj, S. Wong; Covalent surface chemistry of single-walled carbon nanotubes; *Adv. Mater.*, **1**, 17, (2005).
37. M. Chen, H. W. Yu, J. H. Chen, H. S. Koo; Effect of purification treatment on adsorption characteristics of carbon nanotubes, *Diamond Relat. Mater.*, **16**, 1110-1115, (2007).
38. H. Hu, B. Zhao, M. E. Itkis, R. C. Haddon; Nitric acid purification of single-walled carbon nanotubes; *J. Phys. Chem. B*, **107**, 13838-13842, (2003).
39. C. G. Salzmann, V. Nicolosi, M. L. H. Green; Edge-carboxylated carbon nanoflakes from nitric acid oxidized arc discharge material; *J. Mater. Chem.*, **20**, 314-319, (2010).
40. D. Tasis, N. Tagmatarchis, A. Bianco, M. Prato; Chemistry of carbon nanotubes; *Chem. Rev.*, **106**, 1105-1135, (2006).
41. A.G. Rinzler, J. Liu, H. Dai, P. Nikolaev, C. B. Huffman, F. J. Rodríguez-Macias, P. J. Boul, A. H. Lu, D. Heymann, D. T. Colbert, R. S. Lee, J. E. Fischer, A. M. Rao, P. C. Eklund, R. E. Smalley, Large-scale purification of single-wall carbon nanotubes: process, product, and characterization; *Appl. Phys. A*, **67**, 29-37, (1998).
42. A. A. Mamedov, N. A. Kotov, M. Prato, D. M. Guldi, J. P. Wicksted, A. Hirsch; Molecular design of strong single-wall carbon nanotube/polyelectrolyte multilayer composites; *Natur. Mater.*, **1**, 190-194, (2002).
43. L. Liu, S. Zhang, T. Hu, Z.-X. Guo, C. Ye, L. Dai, D. Zhu; Solubilized multi-walled carbon nanotubes with broadband optical limiting effect, *Chem. Phys. Lett.*, **359**, 191-195, (2002).
44. C. N. R. Rao, A. Govindaraj, B. C. Satishkumar; Functionalised carbon nanotubes from solutions, *Chem. Commun.*, 1525-1526, (1996).
45. J. J. Liu, A. G. Rinzler, H. Dai, J. H. Hafner, R. K. Bradley, P. J. Boul, A. Lu, T. Iverson, K. Shelimov, C. B. Huffman, F. Rodríguez-Macias,

- D. T. Colbert, R. E. Smalley, Fullerene pipes; *Science*, **280**(5367),1253-1256, (1998).
46. Y. Miyata, Y. Maniwa, H. Kataura; Selective oxidation of semiconducting single-wall carbon nanotubes by hydrogen peroxide; *J. Phys. Chem. B.*, **110**, 25-29, (2006).
 47. L. Cai, J. L. Bahr, Y. Yao, J. M. Tour; Ozonation of single-walled carbon nanotubes and their assemblies on rigid self-assembled monolayers, *Chem. Mater.*, **14**, 4235-4241, (2002).
 48. J. Zhang, H. Zou, Q. Qing, Y. Yang, Q. Li, Z. Liu, X. Guo, Z. Du; Effect of chemical oxidation on the structure of single-walled carbon nanotubes *J. Phys. Chem. B.*, **107**, 3712-3718, (2003).
 49. K. Hata. D. N. Futaba, K. Mizuno, T. Namai, M. Yumura, S. Iijima; Water-assisted highly efficient synthesis of impurity-free single-walled carbon nanotubes; *Science* **306**, 1362-1364, (2004).
 50. P. X. Hou, C. Liu, H. M. Cheng; Purification of carbon nanotubes; *Carbon*, **46**, 2003, (2008).
 51. T. Ramanathan, F. T. Fischer, R. S. Ruoff, L. C. Brinson; Apparent enhanced solubility of single-wall carbon nanotubes in a deuterated acid mixture; *Research Letters in Nanotechnology*, Article ID 296928, (2008).
 52. G. Boskovic, S. Ratkovic, E. Kiss, O. Geszti; Carbon nanotubes purification constrains due to large Fe-Ni/Al₂O₃ catalyst particles encapsulation; *Bull. Mater. Sci.*, **36**, 1-7, (2013).
 53. M. A. M. Motchelaho, H. Xiong, M. Moyo, L. L. Jewell, N. J. Coville; Effect of acid treatment on the surface of multiwalled carbon nanotubes prepared from Fe-Co supported on CaCO₃; Correlation with Fischer-Tropsch catalyst activity; *J. Mol. Catal. A*, **335**, 189-198, (2011).
 54. S. M. Bachillo, L. Balzano, J. E. Herrera, F. Pompeo, D. E. Resasco, R. B. Wiesman; Narrow (n, m)-distribution of single-walled carbon nanotubes grown using a solid supported catalyst; *J. Am. Chem. Soc.*, **125**, 11186, (2003).
 55. W. Zhou, Y. H. Ooi, R. Russo, P. Papanek, D. E. Luzzi, J. E. Fischer, M. J. Bronikowski, P. A. Willis, R. E. Smalley; Structural characterization and diameter-dependent oxidative stability of single wall carbon nanotubes synthesized by the catalytic decomposition of CO; *Chem. Phys. Lett.*, **350**, 6-14, (2001).
 56. M. Yudasaka, N. Sensui, M. Takizawa, S. Bandow, T. Ichihashi, S. Iijima; Formation of single wall carbon nanotubes catalyzed by Ni separation from Y in laser ablation or in arc discharge using a C target

- containing a NiY catalyst; *Chem. Phys. Lett.*, **312**, 155-160, (1999).
57. J. Zhang, H. Zou, Q. Qing, Y. Yang, Q. Li, Z. Liu, X. Guo, Z. Du; Effect of chemical oxidation on the structure of single-walled carbon nanotubes; *J. Phys. Chem. B.*, **1**, 834, (1999).
 58. D. B. Mawhinney, V. Naumenko, A. Kuznetsova, J. T. Yates, J. Liu, R. E. Smalley; Surface defect site density on single walled carbon nanotubes by titration; *Chem. Phys. Lett.*, **324**, 213-216, (2000).
 59. M. N. Tchoul, W. F. Ford, G. Lolli, D. E. Resasco, S. Arepalli; Effect of mild nitric acid oxidation on dispersability, size, and structure of single-walled carbon nanotubes, *Chem. Matter.*, **19**, 5765-5772, (2007).
 60. Y. Yang, H. Zou, B. Wu, Q. Li, J. Zhang, Z. Liu, X. Guo, Z. Du; Enrichment of large-diameter single-walled carbon nanotubes by oxidative acid treatment; *J. Phys. Chem. B.*, **106**, 7160-7162, (2002).
 61. M. Zhang, M. Yudasaka, S. Iijima; Diameter enlargement of single-wall carbon nanotubes by oxidation; *J. Phys. Chem. B.*, **108**, 149-153, (2004).
 62. Y. Lin, M. J. Meziani, Y.-P. Sun, Functionalized carbon nanotubes for polymeric nanocomposites, *J. Mater. Chem.*, **17**, 1143, (2007).
 63. J. Chen, A. M. Rao, S. Lyuksyutov, M. E. Itkis, Y. Chen, M. A. Hamon, H. Hu, R. W. Cohn, P. C. Eklund, D. T. Colbert, R. E. Smalley, R. C. Haddon; Dissolution of Full-Length Single-Walled Carbon Nanotubes; *J. Phys. Chem. B*, **105**, 2525-2528, (2001).
 64. M. S. Strano, V. C. Moore, M. K. Miller, M. J. Allen, E. H. Haroz, C. Kittrell, R. H. Hauge, R. E. Smalley; The role of surfactant adsorption during ultrasonication in the dispersion of single-walled carbon nanotubes. *J. Nanosci. Nanotech.*, **3**, 81-86, (2003).
 65. L. Vaisman, H. D. Wagner, G. Marom; The role of surfactants in dispersion of carbon nanotubes; *Adv. Coll. Interface Sci.*, **128-130**, 37-46, (2006).
 66. M. J. O'Connell, S. M. Bachilo, C. B. Huffman, V. C. Moore, M. S. Strano, E. H. Haroz, K. L. Rialon, P. J. Bout, W. H. Noon, C. Kittrell, M. Jianpeng, R. H. Hauge, R. B. Weisma, R. E. Smalley; Band gap fluorescence from individual single-walled carbon nanotubes; *Science*, **297**, 593, (2002).
 67. J. Steimetz, M. Glerup, M. Paillet, P. Bernier, M. Holzinger; Production of pure nanotube fibers using a modified wet-spinning method, *Carbon*, **43**, 2397-2400, (2005).
 68. P. Poulin, B. Vigolo, P. Launois; Films and fibers of oriented single wall nanotubes, *Carbon*, **40**, 1741-1749, (2002).

69. K. Fugami, M. Sano; Role of polymers in fabrication of carbon nanotube fibers using flow-induced condensation method; *New Diam. Front Carbon Technol.*, **15**, 53-58, (2005).
70. C. A. Dyke, J. M. Tour; Overcoming the insolubility of carbon nanotubes through high degrees of sidewall functionalization; *Chem. Eur. J.*, **10**, 812-817, (2004).
71. L. Jiang, L. Gao, J. Sun; Production of aqueous colloidal dispersions of carbon nanotubes; *J. Colloid Interface Sci.*, **260**, 89-94, (2003).
72. D. Tasis, N. Tagmatarchis, V. Georgakilas, M. Prato; Introducing functional groups onto the surface of carbon nanotubes helps to solubilize these useful molecules and facilitates their study; *Chem. Eur. J.*, **9**, 4001-4008, (2003).
73. Y. Tan, D. E. Resasco; Dispersion of single-walled carbon nanotubes of narrow diameter distribution; *J. Phys. Chem. B*, **109**, 14454, (2005).
74. E. Camponeschi, B. Florkowski, R. Vance, G. Garrett, H. Garmestani, R. Tannenbaum; Uniform directional alignment of single-walled carbon nanotubes in viscous polymer flow; *Langmuir*, **22**, 1858-1862, (2006).
75. O. Matarredona, H. Rhoads, Z. Li, J. H. Harwell, L. Balzano, D. E. Resasco, Dispersion of single-walled carbon nanotubes in aqueous solutions of the anionic surfactant NaDDBS; *J. Phys. Chem. B*, **107**, 133357, (2003).
76. L. Vaisman, G. Marom, H. D. Wagner; Dispersions of surface-modified carbon nanotubes in water-soluble and water-insoluble polymers; *Adv. Funct. Mater.*, **16**, 357-363, (2006).
77. V. Krstic, G. S. Duesberg, J. Muster, M. Burghard, S. Roth; Langmuir-Blodgett Films of Matrix-Diluted Single-Walled Carbon Nanotubes; *Chem. Mater.*, **10**, 2338-2340, (1998).
78. B. Kim, Y.-H. Lee, J.-H. Ryu, K.-D. Suh, Enhanced colloidal properties of single-wall carbon nanotubes in α -terpineol and Texanol; *Colloid Surf. A Physicochem. Eng. Appl.*, **273**, 161-164, (2006).
79. M. Monthieux, B. W. Smith, B. Burtiaux, A. Claye, J. E. Fischer, D. E. Luzzi; Sensitivity of single-wall carbon nanotubes to chemical processing: an electron microscopy investigation; *Carbon*, **39**, 1251-1272, (2001).
80. K. Yurekli, C. A. Mitchell, R. Krishnamoorti; Small-angle neutron scattering from surfactant-assisted aqueous dispersions of carbon nanotubes; *J. Am. Chem. Soc.*, **126**, 9902-9903, (2004).
81. H. J. Barazza, F. Pompeo, E. A. O' Rear, D. E. Resasco; SWNT-filled thermoplastic and elastomeric composites prepared by miniemulsion

- polymerization; *Nano Lett.*, **2**, 797, (2002).
82. X. Zhang, J. Zhang, R. Wang, T. Zhu, Z. Liu; Surfactant-directed polypyrrole/CNT nanocables: synthesis, characterization, and enhanced electrical properties; *ChemPhysChem.*, **5**, 998-1002, (2004).
 83. M. Shim, N. Wong Shi Kam, R. J. Chen, Y. Li, H. Dai; Functionalization of carbon nanotubes for biocompatibility and biomolecular recognition; *Nano Lett.*, **2**, 285-288, (2002).
 84. H. T. Ham, Y. S. Choi, I. J. Chung, An explanation of dispersion states of single-walled carbon nanotubes in solvents and aqueous surfactant solutions using solubility parameters; *J. Colloid Interface Sci.*, **286**, 216-223, (2005).
 85. Vigolo, A. Penicaud, C. Coulon, C. Sauder, R. Pailier, C. Journet, P. Bernier, P. Poulin; Macroscopic fibers and ribbons of oriented carbon nanotubes, *Science*, **290**, 1331-1334, (2000).
 86. R. Bandhyopadhyaya, E. Nativ-Roth, O. Regev, R. Yerushalmi-Rozen; *Nano Lett.*, **2**, 25, (2002).
 87. Y. Kang, T. A. Taton, Micelle encapsulated carbon nanotubes: A route to nanotube composites.; *J. Am. Chem. Soc.*, **125**, 5650-5651, (2003).
 88. R. Shvartzman-Cohen, E. Nativ-Roth, E. Baskaran, Y. Levi-Kalishman, Y. Szleifer, R. Yerushalmi-Rozen, Selective dispersion of single-walled carbon nanotubes in the presence of polymers: the role of molecular and colloidal length scales; *J. Am. Chem. Soc.*, **126**, 14850-14857, (2004).
 89. M. Yudasaka, M. Zhang, C. Jabs, S. Iijima, Effect of an organic polymer in purification and cutting of single-wall carbon nanotubes; *Appl. Phys. A*, **71**, 449-451, (2000).
 90. S. H. Kim, D. Debnath, W. S. Lee, K. E. Geckeler; Polyvinylpyrrolidone (PVP) as a tool; *Polymer Int.*, **61**, 1228-1233, (2012).
 91. P. Gerstel, S. Klumpp, F. Hennrich, A. Poschlad, V. Meded, E. Blasco, W. Wenzel, M. Kappes, C. Barner-Kowollik, Highly Selective Dispersion of Single-Walled Carbon Nanotubes via Polymer Wrapping: A Combinatorial Study via Modular Conjugation; *ACS Macro Lett.*, **3**, 10-15, (2014).
 92. D. Banerjee, A. Jha, K. K. Chattopadhyay; Synthesis and characterization of water functionalized amorphous carbon nanotube-poly(vinyl alcohol) composite; *Macromol. Res.*, **20**, 1021-1028, (2012).
 93. M. J. Kim, J. Lee, D. Jung, S. E. Shim, Surface modification of carbon nanotube by poly(ethylene glycol) for the preparation of poly(vinyl alcohol) nanocomposite, *J. Macromol. Sci., Part A: Pure Appl. Chem.*, **47**, 588-594, (2010).

94. I. Kalinina, K. Worsley, C. Lugo, S. Mandal, E. Bekyarova, R. C. Haddon; Synthesis, dispersion, and viscosity of poly(ethylene glycol)-functionalized water-soluble singlewalled carbon nanotubes, *Chem. Mater.*, **23**, 1246–1253, (2011).
95. H. Li, T. Zhang, G. Liang, Y. Zhang and X. Wang, In vivo evaluation of acute toxicity of water-soluble carbon nanotubes, *Toxicol. Environ. Chem.*, **93**, 603–615, (2011).
96. H. Luetzen, M. Wirts-Ruetters, A. Hartwig, Structural studies of aromatic surfactants for dispergation of multiwall carbon nanotubes, *Soft Mater.*, **10**(4), 462–471, 2012.
97. N. M. Uddin, F. M. Capaldi and B. Farouk, Molecular dynamics simulations of the interactions and dispersion of carbon nanotubes in polyethylene oxide/water systems, *Polymer*, **52**, 288-296, (2011).
98. J. Li, F. Yang, G. Guo, D. Yang, J. Long, D. Fu, J. Lu; C. Wang, Preparation of biocompatible multi-walled carbon nanotubes as potential tracers for sentinel lymph nodes, *Polym. Int.*, **59**, 169–174, (2010).
99. O. V. Kharissova, B.I. Kharisov, E. G. de Casas Ortiz; Dispersion of carbon nanotubes in water and non-aqueous solvents; *RSC Adv.*, **3**, 24812, (2013).

Chapter 14

Thin CVD diamond films – synthesis, properties, applications

Robert Bogdanowicz
*Gdansk University of Technology, Faculty of Electronics,
Telecommunications and Informatics
Gabriela Narutowicza 11/12, 80-233 Gdańsk, Poland*

Diamonds are valuable not only as the most expensive jewellery material, but most of all as material, which optic, dielectric, mechanical and thermal properties aren't replaceable by other materials. The potential use of diamonds, which indicates from its properties are presented in Table 1 [1].

Table 1. Physico-chemical diamond properties [1].

high hardness (<i>ok.</i> 90 GPa)
high bulk modulus ($1.2 \times 10^{12} \text{ N m}^{-2}$)
low compressibility ($8.3 \times 10^{-13} \text{ m}^2 \text{ N}^{-1}$)
high heat conductivity ($2 \times 10^3 \text{ W m}^{-1} \text{ K}^{-1}$)
low thermal expansion ($1 \times 10^{-6} \text{ K}$)
wide range of high optical transmittance [0.2 - 6 μm [2, 1)]
the highest speed of sound propagation (17.5 km s^{-1})
good insulator (surface resistivity $\sim 10^{16} \Omega \text{ cm}$ @ 20°) [1]
semiconductor with a wide energy gap $\sim 5.4 \text{ eV}$ -after doping [3]
resistance to chemicals and corrosion
biocompatibility
low coefficient of friction

Natural, monocrystalline diamond is an allotropic carbon C form with the

highest packing coefficient. Natural condition of diamond synthesis is pressure above 60 GPa and temperature around 1000K. These conditions make possible the orbital hybridisation of sp^3 electronic carbon C and also are creating strong covalent bonds. Natural conditions of synthesizing diamonds are 160 km beneath the earth surface. Nowadays, diamond material can be made due to the process of:

- High-pressure HPHT (High Pressure High Temperature),
- Low-pressure CVD (Chemical Vapour Deposition).

In the HPHT process, which imitates condition of natural diamond synthesis, small defected crystal is received. These crystals are used mostly as emery/sand material. Although process is conducted in stabilized conditions for diamonds.

In the low-pressure CVD process, additionally contributed by Plasma Assisted or Hot Filament there is possible to create thin, polycrystalline diamond films, which are polluted with graphite and/or amorphous phase, caused by conditions of pressure and temperature in CVD chamber. These conditions are stabile for graphite and glassy carbon, but for diamonds are metastable. Despite of defects, these films show natural diamonds properties. They have also found many applications in technology and medicine. The average growth rate for these films is 1 $\mu\text{m/h}$.

When we compare the results of several science groups, we can discover that the diamond films from HF CVD process have higher non-diamond content, but it is possible to cover relatively large surfaces (700 cm^2) due to this process. In the PA CVD process, the diamond films have clearly higher diamonds phase, but the process is much slower. The surface covered using the PA CVD is smaller, which results from difficulties in making properly big technological microwave plasma chambers.

Polycrystalline diamond films with high diamond phase content find use in important aspects of our life such as: microelectronics, IR optics, and optoelectronics. For this reason improving the PA CVD process, which currently isn't controlled enough, is research and development problem. Many leading laboratories are still conducted by research groups to improve growth rate of thin diamonds films and to reduce non-diamond phase content.

Low pressure methods of thin diamond film synthesis

In room conditions (288 K, 1 kPa) graphite is stable, diamond is metastable. In nature, the process of diamond synthesis proceeds in balanced conditions with 60 GPa pressure and 1250°C temperature [4]. These conditions normally occur on earth around 160 km under the surface. The phase graph of carbon with diamond, graphite areas and liquid phase appearances is presented in the Figure 1.

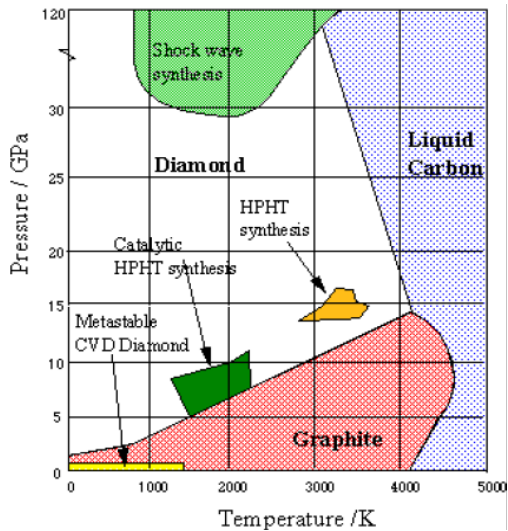


Figure 1. Carbon phase diagram [4].

The dark green field on the Figure 1 is zone of diamond synthesis in stable conditions. In this range diamond is synthesized with high pressure HPHT. This technique is based directly on simulation of natural conditions and crossing via energetic barrier. Between graphite and diamond there is a small difference of around 2.9 KJ/mol of free energy amount, but the conversion from one to another state requires a vast crossing of energetic barrier of around 717 KJ/mol, which is illustrated in the Figure 2.

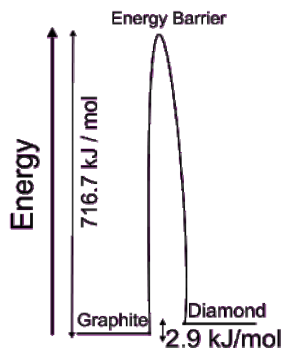


Figure 2. Energy levels diagram during graphite to diamond transformation [5].

This work concentrates around diamond synthesis with low pressure ($P < 500$ bar) and temperature under 1000°C . The phase graph indicates that those are the stable conditions for graphite. Therefore the films will be synthesized in CVD process in the area of potentially metastable conditions for diamond.

Diamond films growth and nucleation

The basic model of diamond films growth, in the low pressure synthesis, deposition from the CVD gas phase, is the mixture of hydrocarbon gas in presence with activated hydrogen and its nucleation on the substrate as a result of pyrolysis reaction. It allows to cross the great energetic barrier between graphite and diamond. High pressure and temperature are replaced by change of electronic structure of atoms into gas precursors of carbon.

First CVD experiments were conducted by Eversole [6], and then independent results of Derjaguin *et al.* [7] confirmed it. These teams were successful in creating diamond mono-layer from hydrocarbon on the surface of natural diamond. During the further process, the layer was graphitized. Angus *et al.* [8] had observed, that the presence of atomic hydrogen allows to digest, defecting the crystalline non diamond phase structure and allows to cyclical deposition of diamond. The atomic hydrogen was achieved by stimulating it on hot wolfram's filament, which means local generation of hydrogen plasma. Continuation of Anguse's research by Derjaguin confirmed this fact. Derjaguin also claimed that the atomic hydrogen allows to deposit the films on the surfaces different than diamond [9].

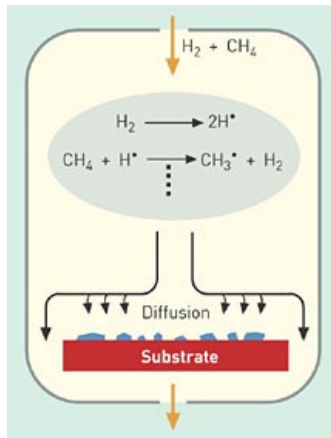


Figure 3. Basic schema of reaction in gas phase during CVD diamond growth [9].

In the beginning of the 80's Japanese scientists from NIRIM Institute published the results of comparison the growth of diamond films on the silicon substrate (temperature around 900°C) in plasma with hot filament HF [10] with Microwave Plasma Assisted (MPA) with use of gas mixture of methane and hydrogen (1% : 99%). These results were an impulse for many other groups to conduct the research in this direction. These results made common the technology of CVD diamond films synthesis. Since then, many teams are handling the low pressure CVD synthesis and studying the properties of created samples.

During the process of diamond films synthesis with use of hydrocarbon and hydrogen mixture, there is strong reduction atmosphere due to presence of an atomic hydrogen, which is highly reactive. It is used to activate the carbon precursors and to digest a non-diamond phase on the substrate.

Atomic hydrogen can be manufactured by the dissociation of H₂ molecules process with use of thermal process like HF (Hot Filament) (1.1). It can be also created by exchange of energy during the collision of particles with stimulated free electrons (1.2). in microwave plasma [6].



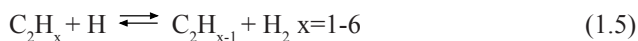
Dynamic reactions between mono atomic hydrogen and hydrocarbon are dominating in conditions of hydrocarbon radicals (1.3) [3]:



Further reactions between radicals (1.3) lead to C₂H₅ creation and higher M order hydrocarbons. Reaction 1.4 is an example of this. This effect results from the slower generation of atomic hydrogen in areas, where it exists in lower concentrations.



The dissociation of hydrogen in reaction with C₂H_x [6] molecules was also observed. The course of this process is described by reaction (1.5).



The modelling research made by Mankelevich *et al.* [7, 8] in the HF reactor showed that decomposing of acetylene to methane was highly possible only in the low temperature of plasma (T < 1000 °C). On the other hand, in the high temperature of plasma, comparable with those achieved in the CVD synthesis,

there is a domination of an opposite reaction.

The fundamental works of diamond synthesis theory, in microwave plasma were made by Frenkelach M., Spear K.E. [9] and Tsuda *et al.* [10, 11]. Frenkelach and Spear proposed a radical growth mechanism which depended on creating of the acetylene C_2H_2 molecule in place of C_d -H bounding on the surface of a growing diamond phase, after creating this bounding by atomic hydrogen. The acetylene molecule creates on the growing surface vinyl radicals, which allows to create another bounding between vinyl radical and other atom of carbon.

Tsuda *et al.* proposed, instead of radical Frenklach mechanism, two degree ion mechanism, claiming that only radicals which possess charge and ions can participate in reactions of bonding the carbon atoms to the diamond growth surface.

From the conducted research works, it could indicate that the advantageous parts of low temperature synthesis are the atomic hydrogen H [12] and methyl radical the CH_3 [13]. The results of researches and analysis of nucleation processes of diamond films confirm the relevant part of hydrogen in radicals creation and radical bounds saturation on the growth surface [6, 14]. Equally, the CH_3 particles role, as the most important precursors leading to build the structure with sp^3 hybridisation, was confirmed by independent research conducted by Garrison *et al.* [15] and Harris *et al.* [16].

Thin diamond layer synthesis process modelling with molecular dynamics methods, conducted in our group, in consider with in-between atomic influence, which is described by quantum mechanics (AM1 hamiltonian or ab initio) allows to theoretic description of a role of H_2 , H^+ , CH_3^+ , CH_3 particles in the growth mechanism. The results of synthetic modelling are presented in Table 2 [17].

Performed research indicate that the higher growth dynamic can be achieved by effecting on the diamond growth surface with stream of H^+ and CH_3^+ ions than with neutral particles like H_2 , H, CH_3 .

Table 2. The particles role in undergoing growth surface reactions.(particles on the growth surface were mark with "s" index) [17]

H_2	takes part mostly in momentum transport and energy exchange,
	saturates carbon values on the growing layer surface
H	Reacts with hydrogen on the layer surface creating neutral values:
	$H + C_{(s)} \rightarrow CH_{(s)}$ $H + CH_{(s)} \rightarrow C_{(s)} + H_2$

H^+	<p>exchanges the charge with growing layer, activates the layer:</p> $H + CH_{(s)} \rightarrow C H_{(s)}^+ + H$ <p>activates the layer with hydrogen removing:</p> $H^+ + CH_{(s)} \rightarrow C_{(s)}^+ + H_2$
CH_3^+	<p>takes part in growth reaction:</p> $CH_3^+ + CH_{(s)} \rightarrow CCH_3^+_{(s)} + H$ <p>takes part in momentum transport with hydrogen removing:</p> $CH_3^+ + CH_{(s)} \rightarrow C_{(s)}^+ + CH_4$
CH_3	<p>takes part in growth process, but slower than CH_3^+:</p> $CH_3 + C_{(s)} \rightarrow CCH_3_{(s)}$ <p>removes surface hydrogen:</p> $CH_3 + CH_{(s)} \rightarrow C_{(s)} + CH_4$

Hydrogen H^+ ions during the collision with methane molecules cause ionization of CH_4 , according to the following (1.6) reaction.



This reaction, which occurs in gas phase, allows to conclude that for diamond synthesis process it would be righteous to stimulate methane beyond the charge zone, by mixing the ionized hydrogen stream with neutral carbon precursor. It would allow the plasma generator to work in optimal regime to produce hydrogen ions.

One of the most relevant parameter of diamond films synthesis is the weight relation of hydrocarbon to hydrogen, which influences a lot on nucleation processes on the substrate. For example, <2% methane content makes better quality of the films, but it also slows its growth (Figure 4). On the other hand, more content of a methane >4% accelerates nucleation dynamic, but unfortunately it leads to reducing of the grains growth (more amount of defects) [6].

The influence of gas environment, which favours diamond growth, isn't exactly researched. It is certain that the carbon precursor and atomic hydrogen are needed for synthesis [14, 6]. In some researches argon [18] and oxygen [19] were added, which allows the synthesis possible in lower temperatures of plasma and substrate. Silva *et al.* [20] suggested that the argon acts like some kind of an "extender", and it reduces amount of carbon/ hydrocarbon relations and activates particles by the Penning effect. The influence of gases with oxygen content causes increasing of particles mobility on the growth surface, which also allows to reduce required substrate temperature [21].

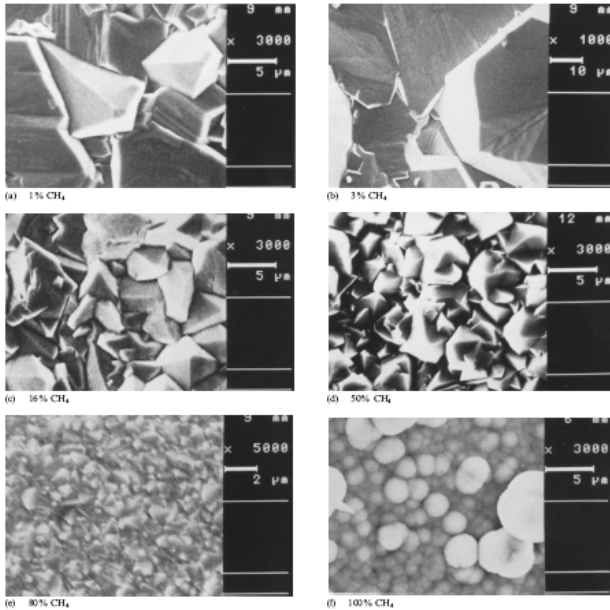


Figure 4. Diamond films surface microscopic pictures with different CH₄ percentage (a-1 %, b-3 %, c-16 %, d-50%, e-80 %, f-100%) [22].

Dependence diagram (Figure 5) between gas precursors and made CVD synthesis products is a sum up of a C/O/H particles role in the known Bachman paper [23].

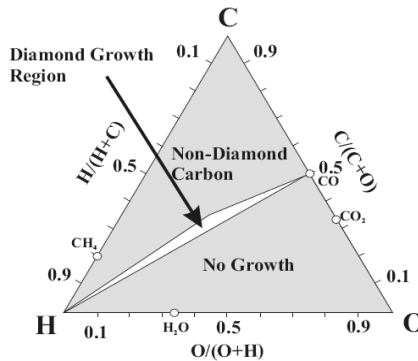


Figure 5. Bachman's C/O/H phase diagram [23].

Bachman also claimed that the work gas method stimulation doesn't have the influence on raising layer type, with the assumption, that the stimulation is efficient enough.

The substrate temperature, in which layer is set, is next critical parameter of low pressure processes. Substrate temperature for the diamond growth films concludes in range of 500°C to 1000°C [14]. Lower temperature causes deposition of amorphous carbon. On the other hand, higher temperatures cause graphitisation. The substrate temperature activates pyrolysis reaction on the substrate and influence on particles mobility on its surface [6]. Robertson proposed a growth process model based on three different phenomena's: layer penetration, relaxation in the layer and impacting the particle into the layer. This schematic phenomena is presented on the Figure 6 [24].

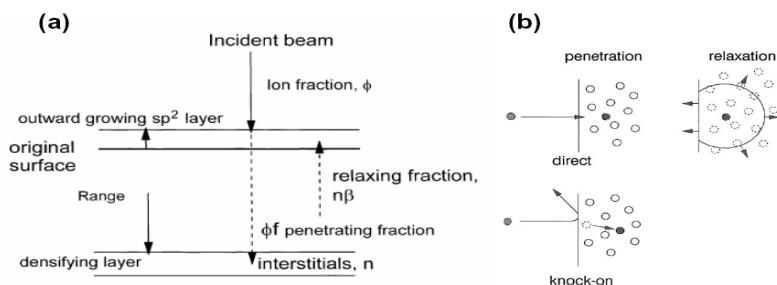


Figure 6. Surface processes- a – the course of growth process, b- possibilities of the course of growth process [24].

The substrate material is important for the nucleation process. It should have size of a crystalline lattice, closed to a diamond and should be resisted to high temperatures influence. Based on literature, most of CVD processes were realized on monocrystalline silicon, molybdenum and diamond radicals achieved by HPHT method [14]. Introductory cover of the silicon substrate with radicals allows to achieve the growth with lesser films defect level [25]. The trials were made with GaN films realisation used to manufacture high power diodes [26].

To activate gas precursors many different techniques are used. Each one of them allow to achieve certain parameters of diamond films which indicates from used plasma stimulation state.

Table 3. Processes used for diamond films synthesis.

Process	Method properties
Hot filament HF CVD	Low cost of the system, large substrate [33] High growth dynamic (~ 10 μ m/h) [34] Filament pollution with material Films low optic quality [35] Used by the industry [33]
Microwave plasma assisted	Clean and useful plasma Films high optical quality Relatively low growth dynamic (~1-5 μ m/h) [30]
Torch combustion	Atmospheric pressure High growth dynamic (~50 μ m/h) High defects level [3]
Magnetron sputtering	Large substrate [37] Vast problem with ion beam deposition control High growth dynamic ~40 μ m/h
Arc plasma jet	High growth dynamic ~80 μ m/h [38] Used in industry [39] Low arc heads lifetime
Ion beam deposition	Focused ion beam allows to control the growth precisely [40] High cost of the system Very slow growth < 1 μ m/h High films quality [41]
Pulsed laser deposition	Allows to control the growth precisely [42] Very slow growth and small substrate surfaces [43]

Table 3 presents currently dominative technological method used in the diamond synthesis. The most important and the most used are closely presented in the next chapters. The focus is on the synthesis aided by the microwave plasma and it was compared with hot filament method, which is the most competitive technology in the diamond films synthesis [24].

Hot filament plasma

Thermal activation of the gas particles is the oldest and least complicated method of chemical vapor deposition (CVD). This method was worked out in 1982 by Matsuo *et al.* [38] and its configuration still remains the same. To activate this method metallic, tantalum or wolfram filament, heated to 2200°C

is used. The process is conducted in the hydrogen- methane mixture with 1% of methane, at the pressure lowered to around 20 Torr. In the synthesis process the monocrystalline silicon substrate heated to temperature in range to 900°C, which is placed relatively close to the filament (5-20 mm), is used. Typical HF reactor topography is presented in the Figure 7.

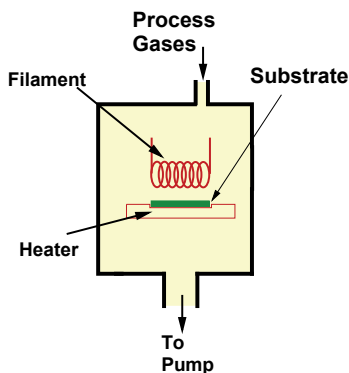


Figure 7. HF reactor scheme [30].

In the CVD conditions the filament reacts with gas precursors creating carbide, which cause the partial hydrogen adsorption from the gas phase. Thermal energy of carbide is used for hydrogen dissociation, which diffuses to the gas phase. The atomic hydrogen amount depends strictly from the filament size and its mechanical stability (carbide layer stability) [28]. Atomic hydrogen mediates in methane radicals creation reactions and in the nucleation processes on the substrate.

The quality of diamond films synthesized with HF depends mostly from the contamination coming from the filament material [29] and from the precursors stimulated state spatial disperse in the area between filament and the substrate.

Standard growth rate level are in 1-10 $\mu\text{m/h}$ range with the 150 W heat power made on the filament [39]. From the research point, the impossibility of oxygenized gases use because of potential oxygen process with filament material, it is a great method limitation.

HF method is used on the industrial scale. It offers relatively high films quality with equally large surfaces with different shapes [27].

Microwave plasma processes

The microwave frequency activation of plasma (2.45 GHz) is based on

the free electron acceleration phenomena through electric and magnetic field compound feedback. Electron energy growth is proportional to the microwave radiation intensity [6]. Additionally electrons energy can be upgraded by forcing the electron cyclotron resonance ECR conditions. In these conditions the particles ionization level is higher for about 100 times than in the classic microwave system [40]. In the cyclotron procedure the oscillating electrons achieve high energy and through collision with gas molecules they cause its stimulation, dissociation and ionization. The higher electron energy, more particles achieve demanded electronic structure. This system is defined as unbalanced plasma [41], because the electrons have energy, which is a couple levels higher than the stimulated ions. In the case of diamond films synthesis, the stimulated atomic hydrogen initiates radical reactions in the gas phase [42, 43] and then it catalyses reactions on the substrate.

As first, Kamo *et al.* [44] used microwave plasma to contribute diamond films synthesis process. In their works they used the silicon tube, through which hydrogen and 1-3% methane mixture under 10-60 Torr pressure flew. The 1000°C substrate temperature was placed on the crossing with waveguide which popularized radiation on frequency. These approach allows to generate automatic non electrode plasma inside the reactor, which significantly decreases metallic pollutions level in the layer.

Currently reactors are built from stainless steel and the radiation is introduced to the reactor by the antenna through the quartz viewport. This configuration is less tense to aggressive plasma environments (strongly reduction atomic hydrogen) and it minimizes silicon pollution from the reactor's tube. It was proposed by the Bachman team in cooperation with Astex company in 1988 [30]. The reactor schemes made by Kamo (NIRIM) and Bachman systems are presented in the Figure 8.

The Bachman group first used ECR to increase the electron energy and the particles ionization level [30]. In their research works they used high power (around 6 kV) microwave reactors. This allows to synthesize significantly less defected films and more precise growth control in comparison with HF technology [45]. Unfortunately these advantages fades with much higher system realisation cost and lesser films dynamic growth [24].

Microwave plasma processes are currently the most used and researched method of precursors activation in diamond films CVD synthesis. Microwave method allows to selectively produce particles with different stimulation level, which allows high quality diamond films synthesis. It has potential of industry use, because it allows to cover large surfaces with complicated shapes.

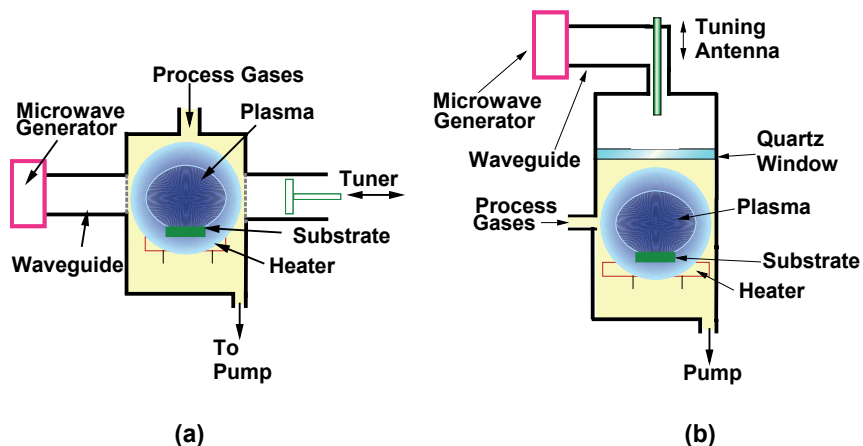


Figure 8. CVD reactors with microwave plasma (a)-NIRIM system, (b)- Bachman system Astex-like [30].

The research works from microwave plasma diamond synthesis area are focused on problems connected with growth process [46], with optical [47] and mass analysis of the plasma species [48]. The results of these researches were compared with theoretical models [49, 50], but full description of the course of the synthesis process and synthesis control are the object of intense research works [51, 52].

Thin diamond films

Over the years, many scientists have tried to know the diamond structure and properties. In 1976 Smithson Tennant researched its molecular structure and determined it as allotropic form of a carbon [53]. In 1954 General Electric team was successful in creating first artificial diamond over the world [54]. Group that built the apparatuses tried to improvise natural conditions of diamond creation. This diamond was synthesized from graphite in high pressure (150 kbar) and high temperature 3000 °C conditions (HPHT) [55].

Group VIII metals usages catalyse the high temperature processes and allow to lower the technological parameters accordingly to ~90 bar and 2000°C [56]. HPHT result synthesis is only diamond dust- small, little crystals [57]. This fact decreases the usage possibilities with limitation of optical and microelectronic applications [45].

In the same time there were conducted researches on diamond layers from

the gas phase low temperature synthesis. First results in these area were achieved by Eversole [58], who synthesized the layer on diamond radicals heated to around 900°C and placed in surrounding of carbon-hydrogen at the <1 atm pressure. This technology is developing until today and it is defined as low pressure synthesis in the CVD process [45]. This method has many advantages in comparison with HF technique. The synthesis is realized with low temperature and pressure and it allows to cover the substrate thin diamond film [27].

Diamond films – physical- chemical properties

Atomic carbon exists in several allotrophic forms: graphite cages, (such as fullerenes, nano tubes, grapheme) amorphous carbon and diamond. Each of them has its own properties which indicate from different atomic carbon valent orbit hybridisation.

Carbon atoms with sp^2 hybridisation electron structure create hexagonal form with unhybridized p orbital perpendicular to the structure. There are three electrons on the valent level. Above structure is described by graphite, where hexagonal forms creates layer structure (Figure 9). Atoms composition creates three equally strong covalent bonds and one weaker bound (van der Waals forces). These properties make graphite a fine grease material and a good electronic conductor. Three dimensional cage forms have also sp^2 hybridisation, which arise from sixty or more carbon atoms and create hexagonal or pentagonal structures [2].

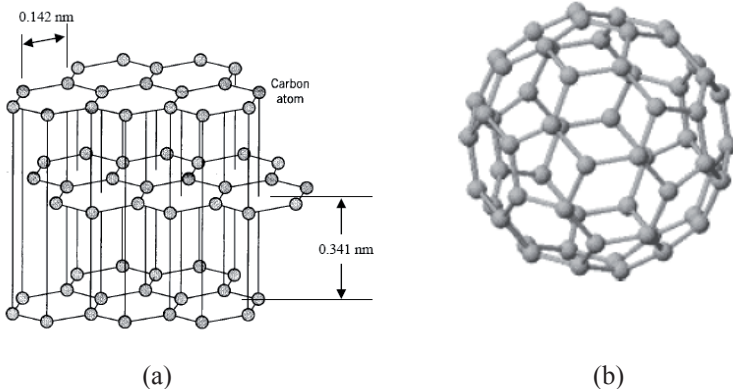


Figure 9. Allotropic carbon form crystalline structure with sp^2 hybridisation a- graphite, b- C_{60} molecule sp^2 .

Carbon atoms in diamond lattice create tetrahedral structure with covalent bounds with sp^3 hybridisation with 1.5445 Å length placed under 109° [2]. Four electrons with the same energy amount are placed on last the carbon orbital. Basic diamond crystal structure is presented in the Figure 10.

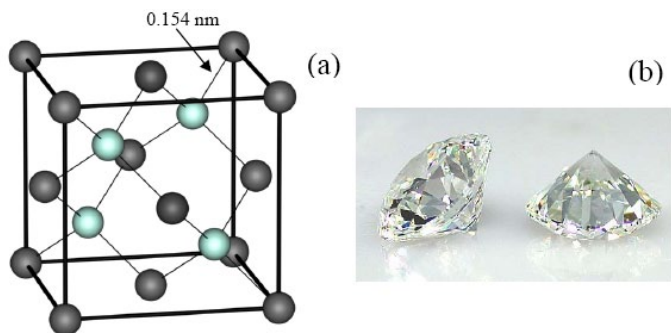


Figure 10. Diamond crystalline structure (a) and polished natural crystal (b).

The connection of very strong covalent bounds and perfect symmetry leads to physico-chemical parameters, which aren't achieved in other known materials. These parameters are only achievable however only for single-crystal diamond. In most of the described experiments in the literature, polycrystalline diamond layers are created (heteroepitaxial growth) [59] and only in a limited areas of the surface monocrystalline regions appeared (epitaxial growth) [60]. Monocrystalline diamond comparison with currently achieved diamond layers are presented in Table 4 [24].

Table 4. Parameters of natural and artificial synthesized diamonds [24].

Material	sp^3 (atomic %)	H (atomic %)	density (g/cm^3)	energy band gap (eV)	thickness (GPa)
Diamond	100	0	3.515	5.5	100
ta-C	80-88	0	3.1	2.5	80
a-C:H (thick)	40	30-40	1.6-2.2	1.1-1.7	10-20
a-C:H (soft)	60	40-50	1.2-1.6	1.7-4	<10
ta-C:H	70	30	2.4	2-2.5	50

For the classification needs Robertson [24, 61] defined three main achieved structures type of synthesized diamond layers.

- ta - C - tetrahedral amorphous carbon,
- ta - C:H - hydrogenated tetrahedral amorphous carbon,
- a - C:H – hydrogenated amorphous carbon.

Each of defined form has different hydrogen amount and different sp^3 and sp^2 hybridisation percentage content. Figure 11 present Robertson's diagram which allows to classify achieved diamond samples.

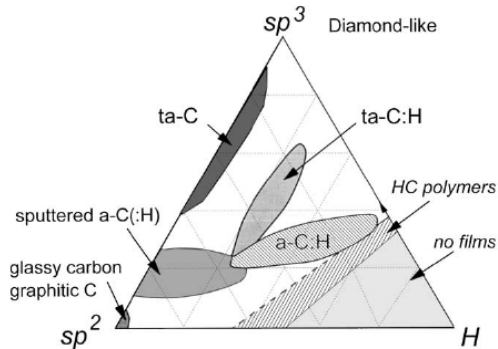


Figure 11. Diamond layers classification diagram [51, 24].

Larger sp^3 content means larger thickness of the layer with equally increased grain size, which increases the layers roughness [62]. On the other hand ultrananocrystalline layers with grains of less than 10 nm size [63, 64] are very smooth layers with optical usage. The thickness of these layers is lower than the diamond thickness. The thickness is on 50 GPa level [62]. This achieved structure diversity results from used process conditions and from gas precursors [65].

Diamond films applications

Depending on its parameters, the diamond layers applications, which were described in previous chapter, can be divided to the following groups:

- Mechanical
- Optical
- Microelectronic
- Medical

The diamond layers applications in the thick hardening layer are mostly

desired. Moreover in their case there is no need of high surface smoothness and transmission range (optical quality). This type of application has use in: magnetic disc heads covers [66], shaving blades [67], tools and sport equipment [68]. The possibility of diamond layers usage in tubes coverage, which work with highly reactive liquids, because of its corrosive resistance and hydrophobic properties, were researched [69].

Layers biocompatibility was used in trials to secure implants such as heart valve [68] and knee [70]. Despite of having much better parameters than TiN or SiN, the layers high production cost is a stopping barrier for these applications [71].

The optical uses are relatively new products, because the high quality and basis different than silicon are needed. For example: diamond layers working in infrared zone for the rocket launchers direction systems and high power CO₂ lasers [72]. First, serve to secure germanium lenses in the infrared cameras optic [73].

Second, because of its high thermal conductivity and low temperature light refractive index dependence minimizes thermal effects in laser system lenses [74].



Figure 12. Optical elements high power CO₂ laser covered by diamond films [75].

Electronic products are wide group of diamond layers applications. Because of increasing of the computer performance, exhaling thermal power increases as well. High thermal diamond layers conductivity is a solution for this problem. There are conducted researches on heat spreaders [76, 77]. The substrate high

temperature for diamond synthesis is a relevant barrier to commercialize them. The use of CH_4/CO_2 gases (halogens and oxygen) decreases the temperature below 500°C [78, 21]. It allows to use aluminium, gallium arsenide, nickel or steel substrate.

In the active electronic elements diamond layer must be doped to achieve semiconductor properties. The ta-C layer variant is type p semiconductor. This fact is a result of high layers defect density, which creates vacants [79].

P doping with boron technology was worked out by Derjaguin *et al.* [80] and confirmed by Fujimori *et al.* [81]. Boron is the perfect acceptor and it relatively easy compose to the diamond structures and it achieves 0.37 eV level [79]. For doping, B_2H_6 was used, realizing the synthesis process with standard CH_4/H_2 mixture in both hot filament and microwave activation processes [82]. Hartman *et al.* and Wag *et al.* researched precisely the boron dope influence to diamond layers properties [83, 84]. Small boron addition in the gas mixture (< 500 ppm B/C) enhances the layers quality and increases the growth dynamic. On the other hand more than 4000 ppm boron contribution causes defects in diamond structure and layer graphitization [84].

Type n doping is arguable in the diamond layers case, because widely used electron donors such as phosphorus, oxygen or arsenic atoms are larger than the carbon atom, which makes difficulties in doping it into the diamond structure. Donor energetic level shouldn't be too low, because the diamond layers have significantly narrower energetic break than the diamond (ta-C – 2.2 eV). First research works in this area were focused on the nitrogen doping [85, 86, 87], which relatively easy is doped in the diamond structure. Unfortunately donor resultative energetic level is ~ 1.9 eV, below the conductivity zone and it block the flow of thermally stimulated electrons [85, 88]. Nitrogen creates CN_x compounds which defect diamond structure and it is an additional problem [89].

In 1993 Veerasamy *et al.* [90] achieved 1% type n doping of ta- C layers with phosphorus contribution. For this purpose he used arc charge with carbon cathode doped with phosphorus. Helmhold [91] achieved 11% dope with capacity conjugated RF plasma contribution. Unfortunately this type films achieve five rows higher conductivity and quite high activation barrier (~ 0.6 eV) [92, 39]. Golzam *et al.* examined, that the 3% phosphorus donor doping destabilizes tetrahedral structure and it prefers sp^2 hybridisation phase nucleation [93].

Publications speak of sulphur use as a type n donor. Barber and Yarbrough published the results of doping with several CS_2 percent in HF plasma use [94] but they didn't discuss application parameters in semiconductors. Experiments with 1% H_2S doping were conducted by Sakaguchi *et al.* [95]. He achieved type n doping with 0.038 eV level of activation in microwave plasma. Unfortunately

significant growth dynamic drop and larger layer defects were simultaneously observed [96]. From the other researches it is known that H_2S implementation decreases CH_3 radicals concentration and, as a result of this fact, slows layer growth dynamic [97].

In the result of type n doping problems, currently there are practically realized only elements with type p doping. Unipolar elements [98, 99, 100], UV sources [101], X- ray [102] and UV detectors [103] can be listed to these elements and they can work in extremely difficult environmental conditions. Another applications are elements with acoustic surfacial wave in wireless telecommunication [104] and micro switches used for high powered microwave amplifiers [105]. Diamond layers can be used as cold cathodes in Field Emission Display [106], because they allow the electron emission with very low stimulated field valves [107].

Latest publications inform of an experimental biosensors realisations in base on DNA chains attached to diamond surface [108]. This structure is sensitive to bio molecules which are attaching to it. This solution can be used in genetic sensor or to monitor diabetics [52].

Diamond films are also researched with increasing optical fibre sensors capability as a cover material of multi home PCS (Polymer Clas Silica) fibre cores [109]. Because of diamond biocompatibility these sensors can be put into the living organism as probes to examine chemical compound concentration in physiological fluids. Śmietana and Szmidi *et al* researches results indicate 6-8 times improvement of these type sensors after diamond films use [110].

References

1. J. E. Field, Properties of Natural and Synthetic Diamond (Academic Press Limited), (1992).
2. H.O. Pierson, Handbook of Carbon, Graphite, Diamond and Fullerenes (Noyes Publications, New Jersey, (1993).
3. P. W. May, Philosophical Transactions of the Royal Society of London Series a-Mathematical Physical and Engineering Sciences, vol. 358, 473 (2000).
4. F. P. Bundy, J. Geophys. Res. 85, 6930 (1980).
5. D. R. Lide i H. P. R. Frederikse, CRC Handbook of Chemistry and Physics, 14 ed., CRC Press, New York, USA (1992).
6. D.G. Goodwin, J.E. Butler, Handbook of Industrial Diamonds and Diamond Films, Marcel Dekker, New York (1998).
7. Yu. A. Mankelevich, A. T. Rakhimov, N. V. Suetin, Diamond Relat. Mater. 7, 1133 (1998).

8. Yu. A. Mankelevich, N. V. Suetin, M. N. R. Ashfold, J. A. Smith, E. Cameron, *Diamond Relat. Mater.* 10, 364 (2001).
9. M. Frenklach, K. E. Spear, *J. Matter Res.*, 3, 133, (1988).
10. M. Tsuda, M. Nakajima, S. Oikawa, *J. Am. Chem. Soc.*, 108, 5780, (1986).
11. M. Tsuda, M. Nakajima, S. Oikawa, *Jpn. J. Appl. Phys.*, 26, 527, (1987).
12. F. G. Celii, P. E. Pehrsson, H. t. Wang, and J. E. Butler, *Appl. Phys. Letts.* 52, 2043 (1988).
13. D. M. Gruen, C. D. Zuiker, A. R. Krauss, and X. Pan, *J. Vac. Sci. Tech. A.* 13, 1628 (1995).
14. J. E. Butler and D. G. Goodwin, *Properties, Growth and Applications of Diamond*, ed. M. H. Nazar, A. J. Neves, Institution of Electrical Engineers, Stevenage (2001).
15. B. J. Garrison, E. J. Dawnkaski, D. Srivastava, and D. W. Brenner, *Science* 255, 835 (1992).
16. S. J. Harris, A. M. Weiner, and T. A. Perry, *J. Appl. Phys.* 53, 1605 (1988).
17. Herman A., Wroczyński P., *Advances in Science and Technology*, 6, 141 (1994).
18. A. Gicquel, M. Chenevier, K. Hassouni, A. Tserepi, and M. Dubus, *J. Appl. Phys.*, 83, 7504 (1998).
19. E.J. Corat, R.C. Mendes de Barros, V.J. Traba-Airoldi, N.G. Ferreira, N.F. Leite, K. Iha, *Diam. Relat. Mater.* 6, 1172 (1997).
20. F. Silva, A. Gicquel, A. Tardieu, P. Cledat, and T. Chauveau, *Diamond Relat. Mater.*, vol. 5, 338 (1996).
21. Y. Muranaka, H. Yamashita, H. Miyadera, *Diamond Relat. Mater.* 3, 313 (1994).
22. T.H. Chein, *Diamond and Related Materials*, 8, 1686–1696 (1999).
23. P. K. Bachmann, D. Leers, H. Lydtin and D.U. Wiechert, *Diamond Relat. Mater.* 1, 267 (1991).
24. J. Robertson, *Materials Science & Engineering R-Reports* 37, 129-281 (2002).
25. H. Liu, D.S. Dandy, *Diamond Chemical Vapour Deposition, Nucleation and Early Growth Stages*, Noyes Publications, New Jersey, (1995).
26. P. W. May, H. Y. Tsaib, W. Wang i J. A. Smith, *Diamond and Related Materials*, vol. 15,4-8, s. 526-530 (2006).
27. D. M. Li, T. Mantyla, R. Hernberg, and J. Levoska, *Diamond Relat. Mater.*, 5, 350 (1995).
28. S. Zhou, Z. Zhihao, X. Ning, and Z. Xiaofeng, *Mat. Sci. Eng. B.* 25, 47

- (1994).
29. M. Griesser, G. Stinger, M. Grasserbauer, H. Baumann, F. Link, P. Wurzinger, H. Lux, R. Haubner, B. Lux, *Diamond Relat. Mater.* 3, 638 (1994).
 30. P.K. Bachmann, W. Drawl, D. Knight, R. Weimer, R. Messier, *Diamond and diamond-like materials. Mater. Res. Soc. Symp. Proc. EA-15 99* (1988).
 31. M. Rubin, C. B. Hopper, N. H. Cho, and B. Bhushan, *Journal of Materials Research* 5, 2538-2542 (1990).
 32. K. Kurihara, K. Sasaki, M. Kawarada, and N. Koshino, *Appl. Phys. Lett.* 52 437 (1988).
 33. I. G. Brown, *Annual Review of Materials Science* 28, 243-269 (1998).
 34. S. Aisenberg and R. Chabot, *Journal of Applied Physics*, 2953 (1971).
 35. P. J. Fallon, V. S. Veerasamy, C. A. Davis, J. Robertson, G. A. Amaratunga, W. I. Milne, J. Koskinen, *Phys. Rev. B* 49, 2287 (1994).
 36. R. J. Lade, D. J. Munns, S. E. Johnson, P. W. May, K. N. Rosser, M. N. R. Ashfold, *Diamond and Related Materials* 7, 699-703 (1998).
 37. Y. F. Lu, S. M. Huang, C. H. A. Huan, and X. F. Luo, *Applied Physics a-Materials Science & Processing* 68, 647-651 (1999).
 38. S. Matsumoto, Y. Sato, M. Kamo, N. Setaka, *Jap. J. Appl. Phys.* 21, L183 (1982).
 39. Y. Koide, S. Koizumi, H. Kanda, M. Suzuki, H. Yoshida, N. Sakuma, T. Ono, T. Sakai, *Appl. Phys. Lett* 86, 232105 (2005).
 40. M. Ohring, *The Materials Science of Thin Films*, Academic Press, San Diego, CA (2002).
 41. V.M. Lelevkin, D.K. Otorbaev, D.C. Schram, *Physics of Non-equilibrium Plasmas*, North-Holland, Amsterdam (1992).
 42. K. Hassouni, O. Leroy, S. Farhat, and A. Gicquel, *Plasma Chem. Plasma P.* 18, 325 (1998).
 43. W. L. Hsu, *J. Appl. Phys* 72, 3102 (1992).
 44. M. Kamo, U. Sato, S. Matsumoto, N. Setaka, *J. Cryst. Growth*, 62, 642 (1983).
 45. P. K. Bachmann, *Adv. Mater.*, 5, 137 (1993).
 46. J. Achard, A. Tallaire, R. Sussmann, F. Silva, and A. Gicquel, *J. Cryst. Growth.* 284, 396 (2005).
 47. V. Mortet, Z. Hubicka, V. Vorliceck, K. Jurek, and M. V. J. Rosa, *Phys. Stat. Sol. (a)* 201, 2425 (2004).
 48. J. R. Petherbridge, P. W. May, S. R. J. Pearce, K. N. Rosser, M. N. R. Ashfold, *J. Appl. Phys* 89, 1484 (2001).

49. K. Hassouni, T. A. Grotjohn, and A. Gicquel, *J. Appl. Phys* 86, 134 (1999).
50. G. Lombardi, K. Hassouni, G.-D. Stancu, L. Mechold, J. Ropcke, A. Gicquel, *J. Appl. Phys.* 98, 53 303 (2005).
51. J. Robertson, *Semicond. Sci. Technol.* 18 No 3, S12-S19, (2003).
52. P. W. May, tom 319, p. 490, *Science*, 319, 490 (2008).
53. S. Tennant, *Philosophical Transactions of the Royal Society of London*, vol. 87, 123 (1797).
54. F. P. Bundy, H. T. Hall, H. M. Strong i R. H. Wentorf, *Nature*, 176, 51 (1955).
55. J. Martin, *Ind. Diamond Rev.* 59, 291 (1990).
56. M. Wakatsuki, *Jpn. J. Appl. Phys.* 5, 337 (1966).
57. D. Choudhary and J. Bellare, *Ceramics International* 26, 73 (2000).
58. C. P. Eversole, "U.S. Patents". Patent 3,030,187, 3,030,188, 1962.
59. S. K. Han, M. T. McClure, C. A. Wolden, B. Vlahovic, A. Soldi, and S. Sitar, *Diamond Relat. Mater.* 9, 1008 (2000).
60. W. Chunlei, I. Masatake, I. Toshimichi, *Jap.J. Appl. Phys.*, vol. 40, 3A, s. L212-L214, (2001).
61. J. Robertson, *Thin Solid Films*, 383, 81, (1999).
62. A. R. Krauss, O. Auciello i D. M. Gruen, *Diamond Related Materials*, 10(11), 1952 (2001).
63. D. M. Gruen, S. Liu, A. R. Krauss, and X. Pan, *J. Appl. Phys.*, 75(3):1758,(1994).
64. D. Zhou, D. Gruen, L. Qin i T. McCauley, *J. Appl. Phys.*, 84(4), 1981–1989 (1997).
65. D. M. Gruen. *Nanocrystalline diamond films. Annu. Rev. Mater. Sci.*, 29:211–259, (1999).
66. M. Schlatter, *Diamond and Related Materials*, vol.1(10), 1781-1787 (2002).
67. C. J. Clipstone, „Razor blade technology”. Patent US 6684513, (2004).
68. Hauer R., *Tribol. Internat.* 37, 991-1003 (2004).
69. Miyagawa S., Nakao S., Ikeyama M., Miyagawa Y., *Surf. Coat. Technol.* 156, 322-327 (2002).
70. R. J. Narayan, *Mat. Sci.Eng. C* 25, 405-416 (2005).
71. S. A. Klaffke D., *Surface and Coatings Technology*, vol. 98(1), s. 953-961 (1998).
72. S. F. Rusli, Q. F. Huang i S. R. P. Silva, *INSPEC, The Institution of Electrical Engineers, London*, (2003).
73. De Beers Industrial Diamond publicity announcement for DIAFILM

- OP CVD diamond for Optical Applications, De Beers (1999).
74. V. Konov, S. Kononenko, A. Pimenov, V. Prokhorov, V. Paveleyev i V. Soifer, SPIE Proc., vol. 3822, 2-5 (1999).
 75. „www.iiviiinfrared.com,” II-VI INFRARED. [Online].
 76. „http://www.sp3inc.com/spreader.htm,” SP3. [Online].
 77. P. H. Chen, C. L. Lin, Y. Liu, T. Y. Chung i L. Cheng-Yi, IEEE Photonics Technology Letters, vol. 20(10), 845-847 (2008).
 78. I. Schmidt, C. Benndoeft. Diamond. Relat. Mater. ,8 231 (1999).
 79. A. T. Collins, A. W. S. Williams, J. Phys. C: Solid State Phys 4, 1789 (1971).
 80. B.V. Spitsyn, L.L. Bouilov, B.V. Derjaguin, J. Cryst. Growth, 52, 219,2 (1981) .
 81. H. Shiomi, K. Tanabe, Y. Nishibayashi, N. Fujimori, Jpn. J. Appl. Phys. 29, 34 (1990) .
 82. R. Kalish, Carbon,37, 781 (1999).
 83. M.N. Gamo, E. Yasu, C. Xiao, Y. Kikuchi, K. Ushizawa, I. Sakaguchi, T. Suzuki, T. Ando, Diamond Relat. Mater. 9, 941 (2000).
 84. R. Kalish, A Reznik, C. Uzan-Saguy, C. Cytermann, Appl. Phys. Lett. 76, 757 (2000) .
 85. R. G. Farrer, Solid State Commun. 7, 685 (1969).
 86. R. Locher, C.Wild, N. Herres, D. Behr, and P. Koidl, Applied Physics Letters 65, 34 (1994).
 87. J. Birrell, J. E. Gerbi, O. Auciello, J. M. Gibson, D. M. Gruen, and J. A. Carlisle, Journal of Applied Physics 93, 5606-5612 (2003).
 88. S. Bohr, R. Haubner, and B. Lux, Applied Physic Letters 68, 1075 (1996).
 89. Y.-Y. Chang, D.-Y. Wang i W. Wu, Diamond and Related Materials, vol. 12(10-11), 2077 (2003).
 90. V. S. Veerasamy, G. A. J. Amaratunga, C. A. Davis, A. E. Timbs, W. I. Milne, D. R. McKenzie, Journal of Physics-Condensed Matter 5, L169-L174 (1993).
 91. P. Helmbold, U. Hammer, J. K. Thiele, D. Rohwer i A. Meissner, Philosophical Magazine B-Physics of Condensed Matter Statistical Mechanics Electronic Optical and Magnetic Properties, vol. 72, 335 (1995).
 92. O. Gaudin, D. K. Troupis, R. B. Jackman, C. E. Nebel, S. Koizumi, E. Gheeraert, J. Appl. Phys. 94, 5832 (2003).
 93. M. M. Golzan, D. R. McKenzie, D. J. Miller, S. J. Collocott, and G. A. J. Amaratunga, Diamond and Related Materials 4, 912-916 (1995).

94. G.D. Barber, W.A. Yarbrough, *J. Am. Ceram. Soc.* 80, 1560 (1997).
95. I. Sakaguchi, M.N. Gamo, Y. Kikuchi, E. Yasu, H. Haneda, *Phys. Rev. B* 60, R2139 (1999).
96. M.N. Gamo, C. Xiao, Y. Zhang, E. Yasu, Y. Kikuchi, I. Sakaguchi, T. Suzuki, Y. Sato, T. Ando, *Thin Solid Films*, 382, 113 (2001).
97. H. Sternschulte, M. Schreck, B. Strizker, *Diamond Relat. Mater.* 11,296 (2002).
98. J. Isberg, J. Hammersberg, E. Johansson, T. Wikstrom, D. J. Twitchen, A. J. Whitehead, S. E. Coe, G. A. Scarsbrook, *Science* 297, 1670 (2002).
99. A. Gicquel, K. Hassouni, F. Silva i J. Achard, *Curr. Appl. Phys.*, vol. 1, 479 (2001).
100. T. Guzdek, J. Szmidt, M.Dudek, P.Niedzielski, *Diamond and Related Materials*, 13,1059-1061 (2004).
101. S. Koizumi, K. Watanabe, F. Hasegawa, and H. Kanda, *Science* 292, 1899 (2001).
102. P. Bergonzo, R. Barrett, O. Hainaut, D. Tromson, C. Mer, B. Guizard, *Diamond Relat. Mater.* 11, 418 (2002).
103. V.I. Polyakov, A.I. Rukovishnikov, N.M. Rossukanyi, A.I. Krikunov, V.G. Ralchenko, A. A. Smolin, V. I. Konov, V. P. Varnin, I. G. Teremetskaya, *Diamond Relat. Mater.* 7, 821 (1998).
104. H. Nakahata, K. Higaki, A. Hachigo, S. Shikata, N. Fujimori, Y. Takahashi, T. Kajihara, Y. Yamamoto, *Jpn. J. Appl. Phys.* 33, 324 (1994).
105. M. Adamschik, J. Kusterer, P. Schmid, K.B. Schad, D. Grobe, A. Floter, E. Kohn. *Diamond Relat Mater.* 11,672 (2002) .
106. R.L Fink, Z.L Tolt, Z Yaniv, *Surface Coat. Tech.* 109, 570 (1998).
107. H. Kawamura, M. Tetsuro i T. Kobayashi, *Jpn. J. Appl. Phys.* 38, 2622-2625 (1999).
108. C. E. Nebel, *J. R. Soc. Interface* 4, 439 (2007).
109. M. Smietana, J. Szmidt, M. Dudek, *Diam. Rel. Mat.*,13:954 -957 (2004).
110. M. Smietana, j. Szmidt, M.L. Korwin-Pawlowski, W.J. Bock, *Proc. SPIE* 6189, 186-195, (2006).

Chapter 15

Design and reactivity of alpha nucleophiles for decontamination reactions: relevance to functionalized surfactants

Namrata Singh¹, Yevgen Karpichev², Kamil Kuca³
and Kallol K. Ghosh¹

¹ *School of Studies in Chemistry, Pt. Ravishankar Shukla University,
Raipur (C.G), 492010, India*

² *L.M. Litvinenko Institute of Physical Organic and Coal Chemistry,
Donetsk, 83114, Ukraine*

³ *University of Hradec Kralove, Faculty of Science,
Department of Chemistry, Rokitanskeho 62, 50003 Hradec Kralove,
Czech Republic*

Organophosphate (OP) includes a large variety of compounds with different physical, chemical and biological properties including toxicity. Intentional, accidental and occupational OP poisoning is a major health problem and the use of organophosphorus nerve agents by terrorist groups in recent years is posing a great threat.^{1,2} The broadest spectrum of these compounds is used as pesticides, insecticides and chemical warfare agents. Exposure to even small amount of these organophosphorus compounds (OPCs) is fatal and may result into death due to respiratory failure. In developing countries, the number of cases of exposures and poisonings is much greater because of lack of protective measures and regulatory restrictions.³ The main toxic mechanism of OPCs is the irreversible inhibition of the cholinesterases such as acetylcholinesterase (AChE) or butyrylcholinesterase (BChE) and other related esterases at the muscarinic and nicotinic synapses. Human exposure to OPCs results in acute poisoning manifested by salivation, tremors, respiratory paralysis, hypotension, and with more extreme exposure to death.^{4,6} The general structure of OP compounds that act as AChE inhibitors is shown in Fig. 1.

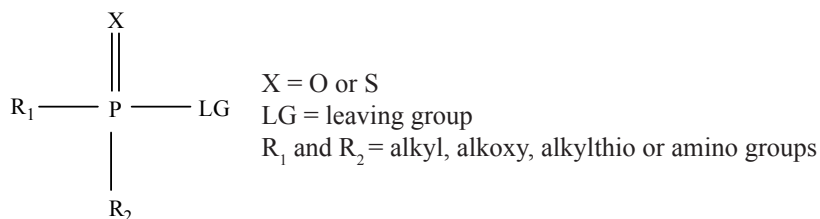


Figure 1. General structure of organophosphorus compounds

OPCs exhibit marked variation of action depending on the substituents R_1 , R_2 and X . The extreme toxicity is associated with those compounds in which X is a strong electronegative group such as halide, cyanide or thiocyanate. Due to the day-to-day applications of these OPCs as pesticides and insecticides their facile hydrolysis is of theoretical and practical interest. Chemical decontamination of these toxic esters require systems that may ensure:

- commercial availability and high reactivity of the reagents and cost effective
- universal applicability of the system against all kinds of chemical warfare agents
- ecofriendly reactions between the system and toxic substrates
- chemical stability of the system
- efficiency of the decontamination system under mild conditions

Destruction of carboxylate, phosphate and sulfonate based esters is of prime significance and several remedies including reactions of various toxic esters with oximes, hydroxamic acids, oximates in micellar solutions, surface active oximes, peroxides etc. have been suggested. Since rate of nucleophile aided hydrolysis of esters is enhanced by cationic micelles, a variety of surfactant based reagents incorporating peroxides, iodosylcarboxylates and oxime functionality have been developed.⁷⁻⁸ Oximate ions ($-\text{CH}=\text{NO}^-$) are important tools in kinetic, mechanistic and biochemical studies. By virtue of their high affinity for enzyme acetylcholinesterase (AChE) and their inherent nucleophilicity, these have drawn attention of many researchers.⁹⁻¹¹ Study of oximes as AChE reactivators is vital against organophosphate (OP) poisoning. Oximes are particularly appealing class of α -nucleophiles with $\text{p}K_a$ values falling in the range of 7-10 which makes them ideal candidates for decontamination reactions. As α -nucleophile, these have been widely used for cleavage of several toxic organophosphorus compounds (OP) and their stimulants.¹²⁻¹³

The main objective of the present article is to study the micellar catalyzed reactions of OP simulants using α -nucleophilic systems especially functionalized

aggregates. Hence, information based on toxic chemical warfare agents and their simulants along with their detoxification chemistry is of paramount importance to have intimate understanding of mechanisms involved.

Organophosphates and nerve agent poisoning

OPCs comprise of a diverse group of chemicals and majority of them have been shown to result in high levels of acute neurotoxicity and carcinogenicity. OPCs may be broadly categorized into four groups (Fig. 2).

Typical representatives of group I are sarin, soman, and cyclosarin; group II is represented by VX and different V-compounds; for group III, tabun is typical while group IV is represented by GV compounds (Fig. 3).

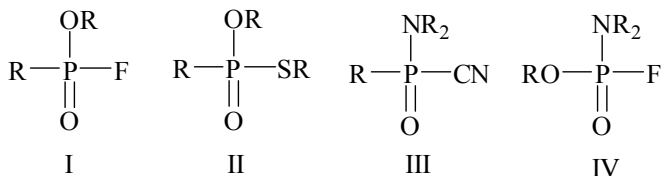


Figure 2. Groups of organophosphorous compounds

Chemical warfare agents (CWAs) and organophosphorus pesticides

The first organophosphorus (OP) nerve agents, tabun (GA) and sarin (GB) were developed in 1930s by Gerhard Schrader. These, and the more toxic soman (GD) developed in 1944, are members of the so-called G-agents.¹⁴⁻¹⁶ These compounds have emerged as the major nerve agents known to have been produced and weaponized. The frequent terrorist attacks reveal the ease with which these weapons can be utilized.¹⁷⁻¹⁸ The nerve agents are alkylphosphonic acid esters. Tabun contains a cyanide group. Sarin and soman, which contain a fluorine substituent, are methylphosphonofluoridate esters. These nerve agents contain a C–P bond that is almost unique and is not found in other pesticides. This C–P bond is very resistant to hydrolysis. VX contains a sulfur atom and is an alkylphosphonothiolate. Considerable efforts are being made to devise methods and materials that may neutralize the hazardous effects of these agents.¹⁹⁻²² The OP pesticides are one of the most abundant environmental and food chain pollutants, which drew global attention with respect to human, animal and insect health.

For protective measures it is important to know the sources of pollutants and the magnitude of the threat. Hence, the detection methods for OP pesticides

are a prime concern.²³ Structures of some highly toxic CWAs and pesticides that have been widely used for decades in agriculture, medicine and industries due to their high efficiency as insecticides or for typical enzyme inhibition²⁴⁻²⁵ are shown in Fig. 3.

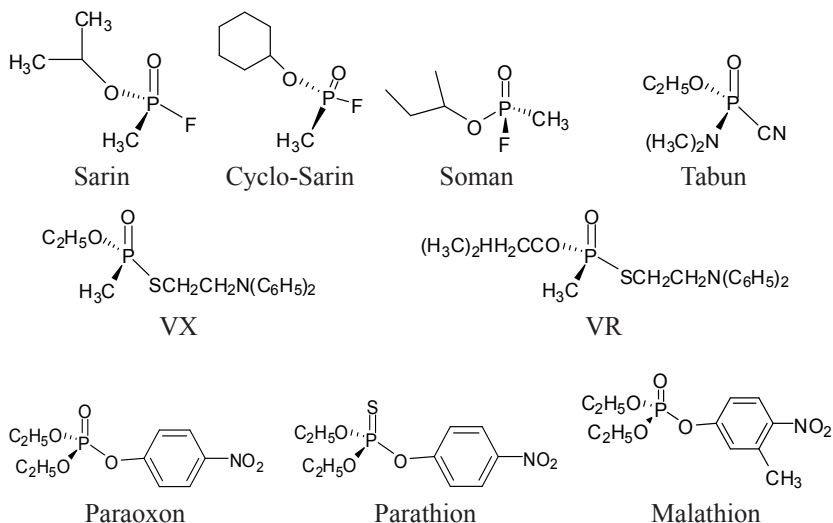
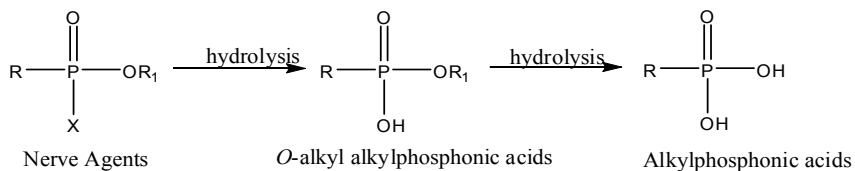


Figure 3. Chemical warfare agents and organophosphorus pesticides

The hydrolysis of phosphate esters is an important chemical reaction since, these are hydrophobic phosphorus substrates, and their decontamination involves dephosphorylation or hydrolysis²⁵ as shown in Fig. 4.



R = CH₃, C₂H₅, *i*-C₃H₇, *n*-C₃H₇
 R₁ = C₁-C₁₀ alkyl and cycloalkyl
 Sarin: R = CH₃, R₁ = *i*-C₃H₇, X = F
 VX: R = CH₃, R₁ = C₂H₅, X = SCH₂CH₂N(R)₂

Figure 4. Hydrolytic pathway of nerve agents

Detoxification systems

The toxicity and long term environmental hazards of OPCs require detailed studies on detoxification mechanisms and development of efficient, readily available and inexpensive systems for their decontamination. A simple and straightforward method for the detoxification of OPCs involves their reactions with α -nucleophiles. Different α -nucleophiles like hydroxamic acid,²⁶⁻²⁷ *o*-iodosyl carboxylates,²⁸⁻²⁹ hydroxyl benzotriazoles,³⁰⁻³¹ hydroxylamine,³²⁻³³ hydrazine,³⁴ and hypochlorite³⁵ etc. have been used to detoxify nerve agents.

Oximes reduce the effects of such hazardous compounds and have attracted attention of various scientists and researchers worldwide.³⁶⁻³⁷ Of these, pyridinium oximes have emerged to be effective antidotes against OP and nerve agent intoxications. There are extensive evidences to support the ability of pyridinium oximes to reactivate phosphorylated acetylcholinesterases.⁴⁴⁻⁴⁶ Most of the oximes investigated so far, can be classified into uncharged tertiary and charged quaternary oximes. Those having clinical applications can be divided in two groups: quaternary monopyridinium and bispyridinium oximes. Tertiary oximes viz. monoisonitroso acetone (MINA) and butane-2,3-dione monoxime (BDMO) are strong α -nucleophiles capable of hydrolyzing phosphate ester bonds.^{24,49} Oximes such as pralidoxime, HI-6, and obidoxime have been used in the clinic to treat intoxication by certain OPs for decades, but little is known about their reactivation mechanisms at the structural level.⁵¹⁻⁵² The current standard treatment of OP poisoning with reactivators includes different types of quaternary oximes with a similar basic structure differing by the number of pyridinium rings and by the position of the oxime group in the pyridinium ring. The more electron withdrawing effect of quaternary nitrogens in pyridinium oxime increases the acidity of the hydroxyimino group which is relatively low in non-substituted aromatic or aliphatic oximes ($pK_a \approx 12-13$). The increased acidity of pyridinium aldoximes and ketoximes ($pK_a \approx 8-10$) provides sufficient concentration of the nucleophilic oximate anion even in neutral solutions. It has also been proved that oximes are actively involved as potent α -nucleophiles in various hydrolytic reactions (Fig. 5) of phosphate diesters and triesters.³⁸⁻³⁹ Use of α -nucleophiles as the basis for such systems makes it possible to provide anomalously high rates of nucleophilic cleavage of organophosphorus compounds.

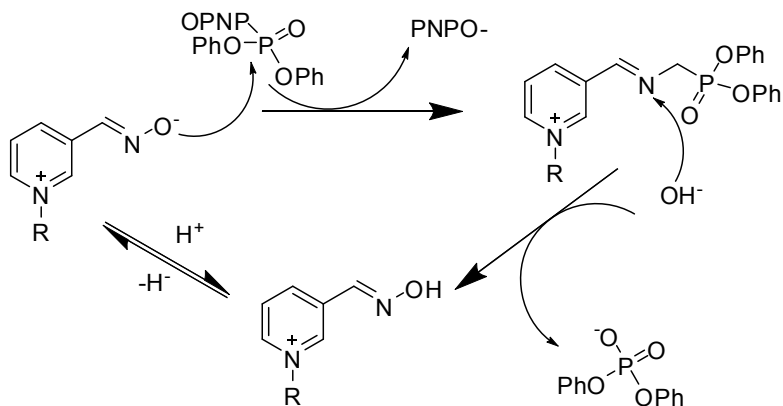


Figure 5 Mechanism of hydrolysis of a *p*-nitrophenyl phosphate using pyridinium 3-aldoxime

Catalysis in micellar media

Chemical warfare agents and pesticides are organic compounds of low polarity and their chemical decontamination is less effective in aqueous medium due to solubility problem with water soluble reactants and organic solvent imposes some operational problems in field conditions. Effects of organized assemblies e.g. micelles,⁴⁰⁻⁴² microemulsions⁴³ and vesicles on chemical reactivity and the positions of chemical equilibrium have been rationalized in terms of differences between the properties of interfacial and bulk water. In such medium, organic reactants are portioned into the surfactant aggregates by electrostatic and hydrophobic interactions, and the observed rate accelerations are largely due to the increased localization of the reactants.

Quantitative treatments of reactivity in association colloids frequently use the pseudophase model. One of its primary assumptions is that such an aggregate constitutes a pseudophase, separated from the bulk solution where it is dispersed, so that reagents partition between the bulk phase and the aggregate pseudophase. Thus, bimolecular nucleophilic reactions can be described as illustrated in Fig. 6, where S and Nu are the substrate and the nucleophile in water (subscript w) or in the micellar pseudophase (subscript m), k_w and k_m are the second-order rate constants for substrate/nucleophile reactions in the aqueous phase and in the micellar pseudophase, respectively, and K_s is the binding constant of the substrate to the micelles based on the concentration of micellized surfactant, defined as the difference in the total concentration of surfactant and the critical micelle concentration (cmc), i.e., $[M] = [\text{surfactant}]_{\text{total}} - \text{cmc}$.

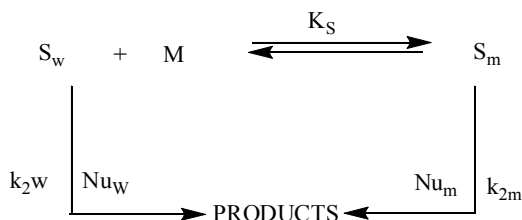
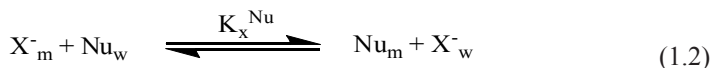


Figure 6. Partitioning of the reactants between water and micelle.

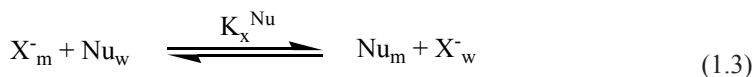
According to the pseudophase partitioning model (PPM), the second-order rate constant k_{2m} is written in terms of the local concentration of the nucleophile in units of moles per liter of reaction volume within the micellar pseudophase (Nu_m), which cannot be measured directly. The concentration of the nucleophile can also be taken as a mole fraction of the bound reactive anion to the micellized surfactant, defined as $\text{Nu}_m = [\text{Nu}_m] / [M]V_m = \beta/V_m$, where β is the degree of counterion binding to the micelle and V_m is the molar volume of the reactive region in the aggregate. V_m also relates the apparent measurable micellar rate constant, k_m to k_{2m} (i.e., $k_m = k_{2m}/V_m$). Thus, formulation of the kinetics of bimolecular reactions under pseudo-first-order conditions ($[\text{Nu}] \gg [S]$) gives eq. (1.1). The value of V_m is unknown, so that in order to estimate k_{2m} from k_m , one assumes a value for V_m ; typical estimates range from 0.14 M^{-1} (the volume of the micellar Stern layer) to $0.37 - 0.5 \text{ M}^{-1}$ (estimated volume of the micelles).⁴⁴

$$k_{\psi} = \frac{k'_w[\text{Nu}] + k_m K_s [\text{M}]}{1 + K_s [\text{M}]} = \frac{k'_w + (k_{2m}/V_m) \beta K_s [\text{M}]}{1 + K_s [\text{M}]} \quad (1.1)$$

Berezin approach allows us to rewrite eq. (1.2) using values of the binding constants of both nucleophile and substrate in the following form:



The micellar surface also behaves as a selective ion exchanger, and competition between reactive (Nu) and inert (X) counterions can be expressed as in eq. (1.3), in which an empirical ion exchange constant, K_x^{Nu} , accounts both for ionic and hydrophobic contributions to the binding.



This extension of the pseudophase model has been called the pseudophase ion exchange model or PIE and successfully fits the kinetics of many bimolecular reactions in micellar solutions. In the PIE model, β (the degree of counterion association to the micellar surface) is assumed to be constant and insensitive to surfactant and salt concentrations.

α -Nucleophilicity of oximate ions

Efforts are being made by scientists in order to design more potent reagents for the environmentally benign detoxification of organophosphorus pollutants.⁴⁵⁻⁴⁶ Nucleophilic reactivity of oximate ions has long attracted specific interest since 1950s because some potent efficient cholinesterase reactivators (antidotes) for some representatives of this unique class of nucleophiles have been found. The antidotal activity of oximes are seem to be directly originates from their anomalously high reactivity. Therefore, an important problem was to elucidate factors governing the α -effect of oximate ions. It's worth noting that Bronsted plot for oximate ions undergoes leveling-off at pK_a ca. 9.0, irrespectively of the acyl substrate, whereas alkoxides ions demonstrate similar behavior at pK_a ca. 12.5 – 13.5. Thus, oximate ions with $pK_a > 9.0$ (β_N is ca. 0.1) have some negative from the Bronsted plot for oximates having low basicity (β_N is ca. 0.5 – 0.6) and are of the same reactivity as alkoxides if have $pK_a > 12.5$). Comprehensive analysis of their reactivcities make them promising precursors for functionalized surfactants.

Recently, Churchill *et al.*⁴⁷ have published an excellent review on the destruction and detection of chemical warfare agents, along with the history of pesticides, molecular structures and their toxicology. There has been great interest in the studies of quaternary and tertiary pyridinium oximes as α -nucleophiles for the hydrolysis of organophosphorus nerve agents and their application to the reactivation of phosphorylated acetylcholinesterase.¹⁷

Significant studies on nucleophilicity of oximate ions in cationic micelles have been carried out. Bunton *et al.*⁴⁸ demonstrated oximate ion mediated dephosphorylation and deacylation reactions in cationic micelles of cetyltrimethylammonium bromide (CTAB). Contributions of Buncl and co-workers⁴⁹⁻⁵⁰ deserve special mention in this context as they have studied degradation of pesticide Fenitrothion using an oxime α -nucleophile i.e. antipyrvaldehyde-1-oxime (monoisonitrosoacetone: MINA) in the presence

of cationic surfactants. Substrate orientation within the micelle was clearly manifested in their work. Changes in reactivity and mechanistic pathways under micellar influence have been discussed in detail. Similar approach was made by Vanloon and coworkers⁵¹ to study micellar accelerated degradation of Fenitrothion in solutions and soils. Tolluec *et al.*⁵² examined phosphate triester hydrolysis catalyzed by micelles of hexadecyltrimethylammonium *anti*-Pyruvaldehyde-1-Oximate. Phosphorolytic reactivity of *o*-Iodosylcarboxylates and related nucleophiles was reviewed by Moss *et al.*⁵³

Functionalized surfactants: an overview

One of the most promising ways of modification of cationic surfactant molecules include the introduction of functional groups into the head part capable of forming highly reactive anionic species, e.g., fragments of α -nucleophiles.⁵⁴⁻⁵⁶ Bound substrate molecules can be brought into close proximity with micellar functions, each surfactant molecule being functionalized with predictable kinetic advantages. Pyridinium based functionalized surfactants are used for detoxification of organophosphorus compounds and nerve agents. In addition, pyridinium oximes also show direct pharmacological effects.⁵⁷⁻⁵⁸ Fig. 7 shows orientation of functionalized surfactants at micellar/water interface.

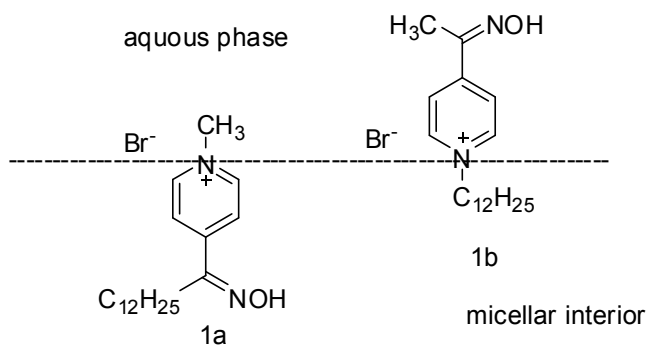


Figure 7. Orientation of surfactants 1a and 1b at micelle/water interface

Modern approaches include the design of active components for fast and irreversible decomposition of ecotoxicants. For instance, the micellar effects of surfactants in the reactions of anionic nucleophiles may be applied to design organized molecular systems which would cleave highly toxic organophosphorus compounds, esters and acid halides of phosphorus acids. The most efficient

micellar systems would be and are those combining the advantages of micro-heterogenic environment characterized by a high solubilizing ability with respect to the substrate and of inorganic anionic α -nucleophile characterized by an abnormally high reactivity with respect to the electron-deficient sites (phosphorus, sulfur, and carbon atoms). The immediate advantage of functional surfactants is the maximum possible local concentration of α -nucleophile fragment which is reached at any micelle concentration and the highest rates are observed for the most hydrophobic esters. Due to this, many laboratories in the world are interested in synthesis of oxime functionalized surfactants for the development of effective decontamination systems.⁵⁹⁻⁶⁰ Functionalized surfactants are the most common catalysts in the functional micellar catalysis. Special attention has been directed to the development of novel functionalized surfactants.⁶¹⁻⁶²

Applications of functionalized surfactants

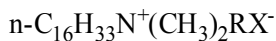
- (i) Pyridinium based surfactants are employed in cosmetics, gene delivery, polymerization and many other industrial applications.
- (ii) Entry of oximate moiety into the head group cationic surfactants is potentially significant for dermatological applications.
- (iii) Such formulations, increase oxime reactivity, solubilize the insoluble phosphates and insecticides and enhance the degradation reactions of the toxic esters and nerve agents. These are also effective phase transfer agents catalysts and acylating agents

A large variety of functionalized surfactants based on pyridinium and imidazolium rings have been synthesized and their catalytic properties have been explored⁶³⁻⁶⁵. Sufficient efforts have been made worldwide to study the mechanisms involved with functionalized surfactant-aided hydrolysis of various carboxylate, phosphate and sulfonate esters.

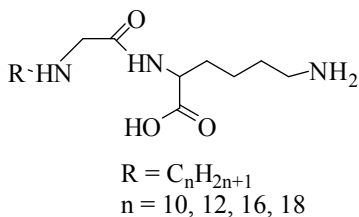
Burczyk *et al.*⁶⁶ studied the solution properties of selected quaternary ammonium based functionalized surfactants (I) viz. hexadecyl(2-hydroxyethyl)dimethylammonium, hexadecyl(2-hydroxypropyl)dimethyl-ammonium, hexadecyl(2-hydroxybutyl)dimethylammonium, and 2-hydrohexadecyl-trimethylammonium bromides. They have synthesized and studied the surface properties of these functional amphiphiles. It was concluded that the surface properties of studied compounds depend on the nature and position of hydroxyl group. This study formed the basis of development of novel and more effective functional aggregates.

Similar alkoxide compounds (II) were synthesized by Bunton and Biresaw⁶⁷ to study the size versus reactivity of functionalized assemblies for deacylation

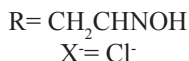
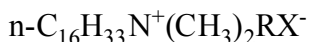
and dephosphorylation reactions. In order to obtain more reactive systems, functionalized aggregates (**III-IV**) were investigated by Tonellato⁶⁸ and coworkers. They observed large rate enhancements for nucleophilic substitution reactions using these functionalized assemblies and concluded that the rate acceleration was mainly due to concentration effects.



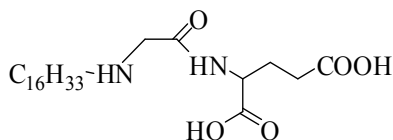
I



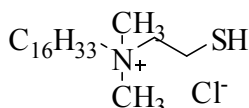
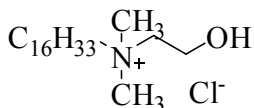
IIIa



II



IIIb



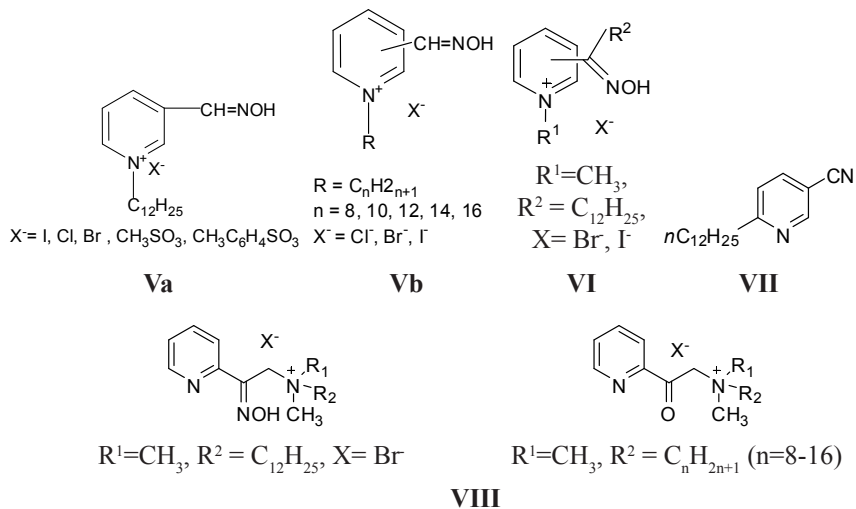
IV

Critical micelle concentrations of **IIIa** functionalized ligands have been reported as 2.5×10^{-3} M ($\text{C}_{10}\text{H}_{21}$), 1.5×10^{-3} M ($\text{C}_{12}\text{H}_{25}$), 3.3×10^{-5} M ($\text{C}_{16}\text{H}_{33}$), 4.9×10^{-5} M ($\text{C}_{18}\text{H}_{37}$) and for **IIIb** functional amphiphiles the cmc has been documented as 1.7×10^{-4} M.⁵⁶

Pyridinium based functionalized surfactants

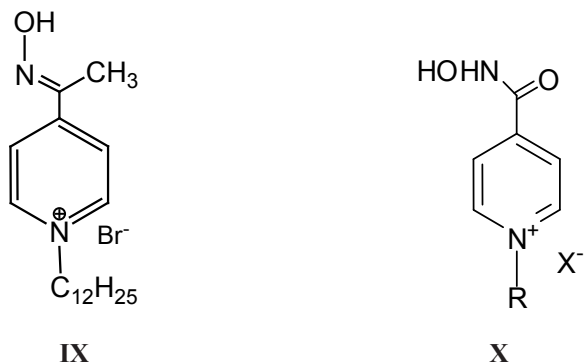
Epstein *et al.*⁶⁹ have systematically studied the micellar behaviour of 1-n-dodecyl-3-(hydroxyiminomethyl) pyridinium salts **Va** against two neutral organophosphates, diethyl *p*-nitrophenyl phosphate and *O*-ethyl S-2- diisopropyl

aminoethyl methyl phosphonothiolate. Reactivity of these functionalized surfactants depends on the solubility of the substrate in the micelle. Hampel and co-workers⁷⁰⁻⁷¹ have synthesized several amphiphilic quaternary pyridinium ketoximes (**Vb**) comicellized with CTAB and have examined their efficiency for hydrolysis of *p*-nitrophenyldiphenyl phosphate and other simulants of organophosphates.



They found that the nucleophilicity of the deprotonated hydroxyimino group in these functional surfactants depends on its position relative to micellar surface. Series of micellar hydrolytic pyridine ketoximes (**VI**) were prepared and 2- and 4-[(hydroxyimino)tridecyl]-1-methylpyridinium bromides were surprisingly the most effective.

Besides good yields of pyridinium ketoximes, 6-dodecylpyridine-3-carbonitrile (**VII**) has been obtained. An efficient method for the synthesis of *N*-[2-hydroxyimino-2-(pyridin-2-yl-ethyl)]-dialkylmethylammonium and *N*-[2-oxo-2-(pyridin-2-yl-ethyl)]-dialkylmethylammonium lipophilic salts (**VIII**) was reported and these compounds were used for metal ion extraction from aqueous solutions into organic solvents.⁷²



The research team of Simanenkov⁷³ have studied head group modification by preparing pyridine functional detergents with aldoximes (V), ketoxime (IX) and hydroxamate (X) functional groups. Comparative study of their reactivity in cationic surfactants (as comicelles) for cleavage of PNPDP and PNPTS was carried. Hydroxamate functional detergents showed lowest basicity ($pK_a = 4.0$) and highest basicity was observed for ketoxime group ($pK_a = 8.51$) whereas aldoxime functionalized surfactant showed moderate basicity ($pK_a = 7.92$) (Fig. 8).

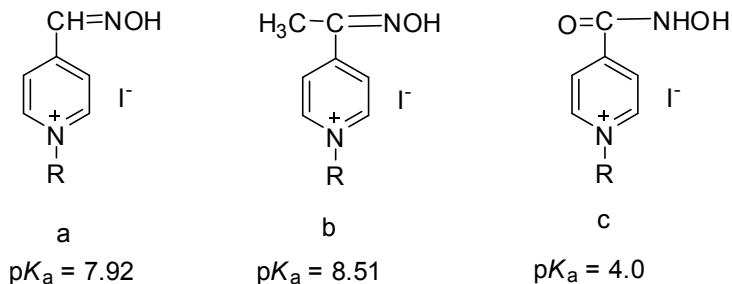
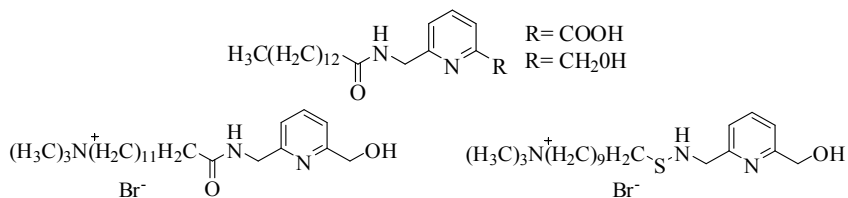


Figure 8. Functionalized surfactants with different α -nucleophilic functional groups

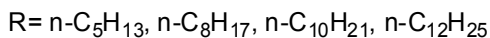
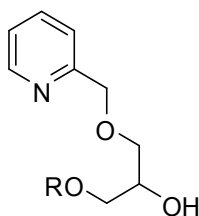
Micellar ligands (XI) were analyzed by Scrimin, Tecilla and Tonellato *et al.*⁷⁴⁻⁷⁵ by monitoring their catalytic activity towards hydrolysis of *p*-nitrophenyl hexanoate (PNPH), *p*-nitrophenyl acetate (PNPA) and *p*-nitrophenyl picolinate (PNPP). They have also studied incorporation of metal ions into these ligands to produce metallomicellar catalysts. The (deprotonated) hydroxyl bound to the pyridine moiety of the catalyst in the ternary complex acts as a nucleophile

leading to a transacylation intermediate that undergoes a rapid metal ion assisted hydrolysis “turning over” the catalyst.



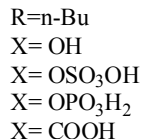
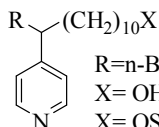
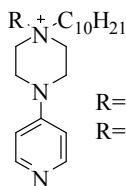
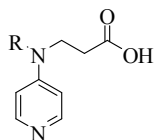
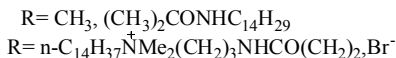
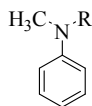
XI

Cheng *et al.*⁷⁶ have investigated the effect of introducing a long chain and metal ions in the pyridine ligands (**XII**). The nucleophilic rate enhancements were dependent on the type of metal ion and ligand and pH, which clearly indicated the formation of metal complexes. Interestingly, the effect of long chain was different for various metal ion complexes. Among the metal ions Cu^{2+} , Zn^{2+} , and Ni^{2+} metal-ligand association constant is lower for Cu (II) than Ni (II) and Zn (II).

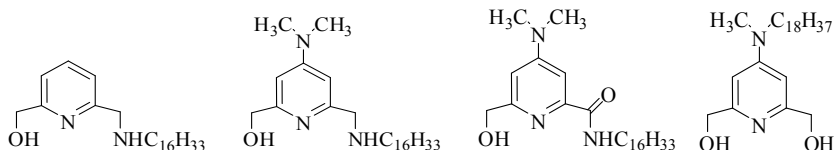


XII

Bhattacharya *et al.*⁷⁷⁻⁷⁸ have studied the structure and reactivity of some pyridine functionalized micellar and metallomicellar aggregates. Dialkylaminolpyridine-functionalized surfactants (**XIII**) have been synthesized and micelles were generated either from the surfactant alone in aqueous buffer (pH 8.5 or 9.0) or by comicellization with CTAB solution at pH 8.5 or 9.0. Such aggregates were used to cleave *p*-nitrophenyl alkanoates or *p*-nitrophenyl diphenylphosphate (PNPDPP).



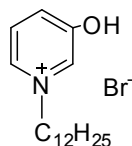
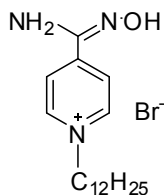
XIII



XIV

The second-order „catalytic” rate constants for esterolysis of the substrate *p*-nitrophenyl octanoate with nucleophilic reagents were determined. Similarly, some copper chelating dialkylaminopyridine amphiphiles (**XIV**) were also synthesized for the cleavage of PNPP and PNPDP.

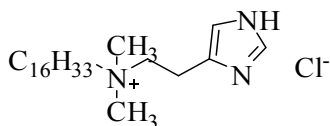
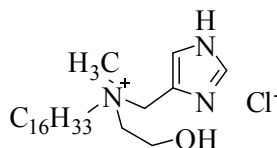
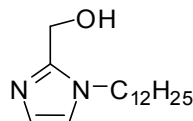
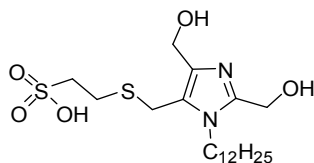
Since last few years, our research group has been engaged in physicochemical and kinetic studies of various oximes and oxime based functionalized surfactants (**Vb**) (discussed earlier) and (**XV**) for the hydrolysis of carboxylate, phosphate and sulfonate esters (PNPA, PNPB, PNPDP and PNPTS).⁷⁹⁻⁸²



XV

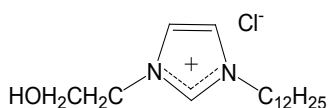
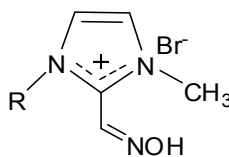
Imidazolium based functionalized surfactants

Research groups of Tecilla⁵⁶, Tonellato⁸³ and Tagaki⁸⁴⁻⁸⁵ have not only contributed towards the study and development of pyridinium based amphiphiles and metalloligands but have also studied imidazole based functionalized surfactants with hydroxyl group as nucleophilic moiety (**XVI**, **XVII**).

**XVI****XVII**

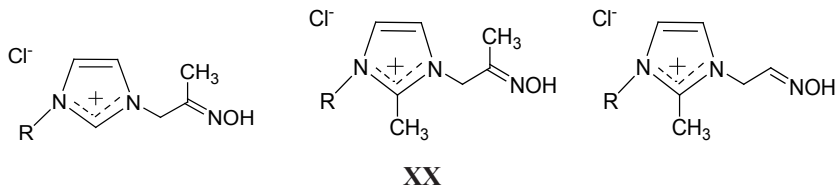
Liu *et al.*⁸⁶ synthesized hydroxyl functionalized imidazolium based ionic liquid surfactants (**XVIII**), studied their micellar properties and for the first time reported their second cmc.

Recently, Kapitanov⁸⁷ synthesized some new functionalized gemini surfactants to study the decomposition of 4-nitrophenyl esters derived from phosphorus and sulfur acids. The nucleophilicity of oximate fragment from amphiphilic derivatives of 2-(oximinomethyl)imidazole micellar systems (**XIX**) were used to examine cleavage of 4-nitrophenyl diethyl phosphate (PNPDPP).⁸⁸ Peroxyhydrolysis of PNPDP with imidazolium based monomeric surfactants was also studied.⁸⁹

**XVIII****XIX**

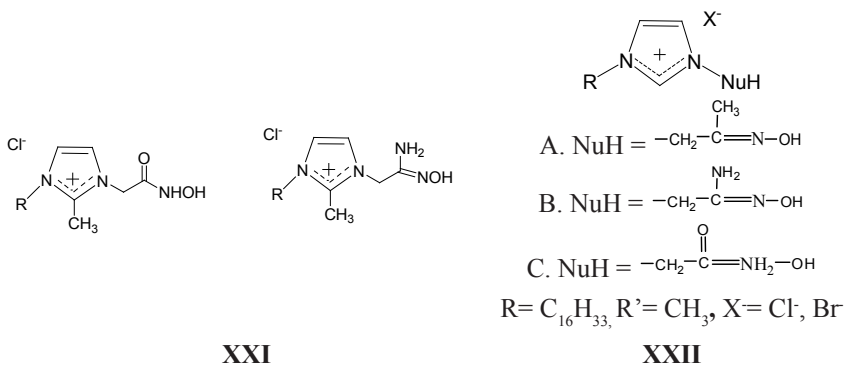
Hydrophobic properties of imidazolium functional detergents of the

type 1-alkyl-3-(2-oximinopropyl) imidazolium chloride **XX** for cleavage of environmental toxicants were also documented by this team.⁹⁰



The reactivity of co-micelles of functional/cationic surfactants: 1-cetyl-3-(2-amino-2-hydroxyiminoethyl) and 1-cetyl-3-(2-hydroxyaminoethyl-2-onyl) imidazolium chlorides (**XXI**) toward the hydrolysis of 4-nitrophenyl esters of diethylphosphoric diethylphosphonic, and toluenesulfonic acids was investigated by Ukrainian team⁹¹ It was shown that the nucleophilicity of the functional groups in the surfactant does not undergo substantial changes with variation in the nature of the head group of the cationic surfactant and the fraction of functional detergent in the co-micelle.

Simanenکو *et al.*^{65, 92} performed a detailed kinetic analysis of nucleophilic cleavage of some phosphate and sulphur esters in the presence of novel functionalized surfactants **XXII**. The cleavage kinetics in micelles of functional detergents and combined micelles of functional detergents with cetyltrimethylammonium chlorides are adequately described in the simple framework of pseudophase partitioning model of micellar effect.



To estimate nucleophilicities of the functionalized surfactants, eq. (1.2) can be easily modified towards eq. (1.4):

$$k_{\psi} = \frac{k'_w + (k_{2,m}/V_m) K_s[M]}{(1 + K_s[M])} \quad (1.4)$$

Equation (1.4) made it possible to analyze the reactivities of the imidazolium and pyridinium surfactants bearing oxime moiety. The Bronsted plots for phosphorus and sulfur as electrophilic center show non-linearity similar to those observed in the case of non-micellizing oximes.

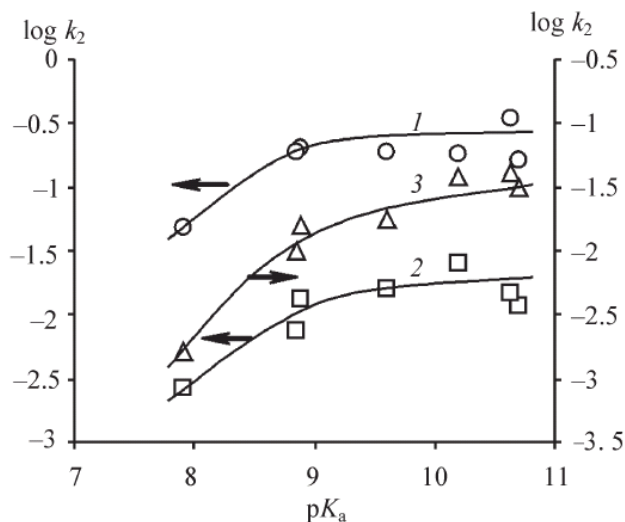
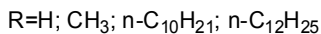
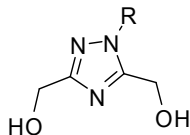


Figure 8. Bronsted plots for the series of oxime-functionalized surfactants in the reaction towards *p*-nitrophenyl esters of phosphonic 1 (arminum), phosphoric 2 (paraoxon), and 4-toluenesulfonic 3 acids⁸⁹.

Triazole based functionalized surfactants

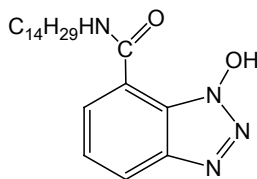
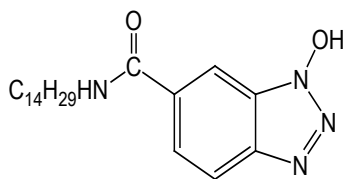
Hydroxy functionalized triazole based ligands (**XXIII**) were synthesized by Qui *et al.*⁹³ When R = H or CH₃, the catalytic activity was not much pronounced due to lack of hydrophobic character whereas in the case of the surfactants with

higher alkyl chain length showed enhanced activity of hydroxyl anion clearly indicating the role of hydrophobicity.



XXIII

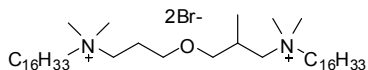
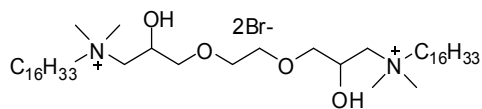
N-tetradecyl-1-hydroxy-1*H*-benzo[*d*][1,2,3]triazole-6-carboxamide and *N*-tetradecyl-1-hydroxy-1*H*-benzo[*d*][1,2,3]triazole-7-carboxamide (XXIV) having long alkyl chains were studied by Bhattachrya *et al.*^{30-31,78} These compounds along with their parent unsubstituted 1-hydroxybenzotriazole have been examined for the cleavage of *p*-nitrophenyl hexanoate (PNPH) and *p*-nitrophenyl diphenyl phosphate (PNPDPP) in comicelles with monovalent cetyltrimethylammonium bromide (CTAB) and the corresponding bis-cationic gemini surfactants 16-*m*-16, 2Br of identical chain lengths at pH 8.2.



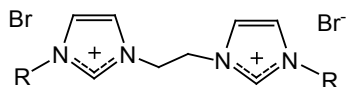
XXIV

Functionalized gemini surfactants

Ukrainian team⁹⁴ synthesized recently functionalized gemini surfactants (XXV) featuring a bridging unit (spacer) of hydroxyl groups. Modification of the spacer by the introduction of hydroxyl groups improves the solubility of these compounds in water since gemini surfactants with molecular formula m-s-m have relatively high Krafft temperatures and low solubility in water.¹⁰⁰



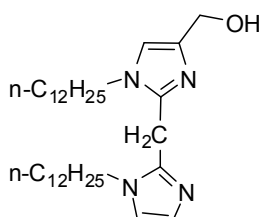
XXVa-b



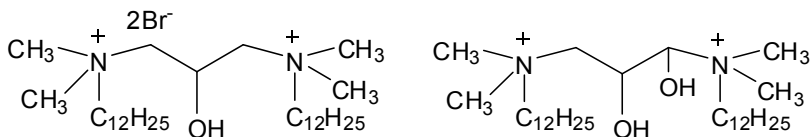
XXVc

Gemini surfactant micelles showed better catalytic activity towards ester cleavage than corresponding monomeric micelles and this was attributed to their better surface properties and lower critical micelle concentration.

With the extension of study of monomeric imidazolium surfactants, Tagaki *et al.*⁸⁴⁻⁸⁵ studied some gemini imidazolium based functional surfactants (**XXVI**). Micellization behaviour of gemini surfactants (**XXVII**) with hydroxyl substituted spacers of the type 1,3-bis(dodecyl-N,N-dimethylammonium bromide)-2-propanol and 1,4-bis(dodecyl-N,N-dimethylammonium bromide)-2,3-butanediol were studied by Saha *et al.*⁹⁵



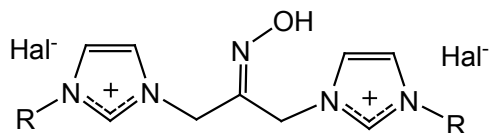
XXVI



XXVII

Finally, a series of imidazolium based Gemini surfactants with variable chain lengths (**XXVIII**) have been recently reported by Ukrainian team⁹⁹ to demonstrate fitting the Bronsted plot for oximate functionalized (monomeric)

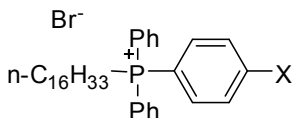
surfactants alone with high solubilization power and anomalously low CMC values.



XXVIII

Other cases

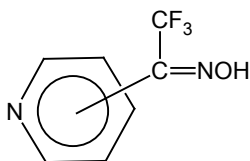
Phosphoester cleavage with functionalized quaternary phosphonium surfactants (XXIX) was reported by Jaeger *et al.*⁹⁶ These surfactants were evaluated as potential turnover catalysts for basic (0.01 M NaOH) hydrolysis of phosphate esters.



X= OH, OCOCH₃, OCH₃

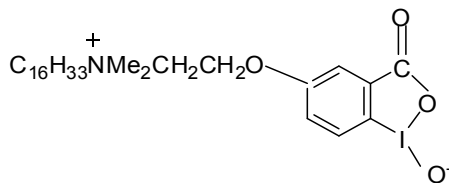
XXIX

Salvador *et al.*⁹⁷ have synthesized 2-, 3-, and 4-trifluoromethyl ketoxime isomers (XXX) of pyridine and N, N-dimethylaniline. They found that these nucleophiles were quite active in providing protection against either paraoxon or sarin. High reactivity of these compounds is due to the inductive effect of the CF₃ group. The inductive effect of the CF₃ group is sufficient to bring the pK_a value of the oximes in the range for maximal reactivation properties.



XXX

Moss *et al.*⁹⁸ reported that the iodosylcarboxylate functional surfactant (**XXXI**) comicellized with 5-fold excess of cetyltrimethylammonium chloride (cationic surfactant) afforded a kinetic advantage of 43600 fold in the cleavage of paraoxon. Such surfactants involved hydrolysis of substrate by nucleophilic substitution at phosphorus, followed by hydrolytic attack at central iodine to displace the P centre from iodosylcarboxylate.



XXXI

Nucleophilic reactivity of some oxime based functionalized surfactants as α -nucleophilic systems for cleavage of carboxylate (*p*-nitrophenyl acetate), phosphate (*p*-nitrophenyldiphenyl phosphate) and sulfonate (*p*-toluene sulfonate) esters has been studied in our laboratory.⁷⁹⁻⁸²

Conclusions

Owing to the rising threats of neurotoxic organophosphorus compounds, facile and efficient decontamination systems are required. Amphiphilic systems comprising of a surfactant and a nucleophilic moiety such as oximes, hydroxamates, peroxides etc. have witnessed increased scientific interest because of their various applications. Reactions of oximate ion with organic substrates in cationic micellar media are a convenient approach to detoxify the hazardous stockpiles of chemical warfare agents. Role of oximes as supernucleophilic systems for toxic ester cleavage is an important research problem and substantial efforts have been made in the thesis to address this issue.

The results are rationalized in terms of physicochemical properties and kinetic studies. Entry of oximate moiety into the head group cationic surfactants is potentially significant for dermatological applications. Also, such formulation increases oxime reactivity, solubilize the water-insoluble phosphates (phosphates and insecticides) and enhance the degradation reactions of the toxic esters and nerve agents. Despite the existence of many different oximes in use today against neurotoxic agents, it has not been reported yet any universal oxime, able to act efficiently against all the nerve agents. Further, such studies would also provide

a new field of useful research of academic interest. The present type of work motivates similar kinds of studies from different viewpoints. Such studies can be extended to other micellar systems with versatile hydrophobic and hydrophilic properties.

References

1. M. B. Mood, H. Saber, *Iran J. Med. Sci.* 37 (2012) 74.
2. J. Kassa, J. Z. Karasová, R. Pavlíková¹, F. Caisberger, J. Bajgar, *Acta Medica* 55 (2012) 27.
3. R. C. Gupta, *Toxicol. Applied Pharmacol.* 219 (2007) 95.
4. J. Bajgar, *Adv. Clin. Chem.* 38 (2004) 151.
5. T. R. Fukuto, *Environ. Health Perspect.* 87 (1990) 245.
6. J. Bajgar, J. Fusek, K. Kuca, L. Bartosova, D. Jun, *Mini Rev. Med. Chem.* 7 (2007) 461.
7. J. Misik, R. Pavlikova¹, J. Cabal, D. Josse, K. Kuca, *Mil. Med. Sci. Lett.* 81 (2012) 96.
8. R. Fornasier, U. Tonellato, *J. Chem. Soc., Faraday I* 76 (1980) 1301.
9. O. Soukup, Z. Kristofikov, D. Jun, V. Tambor, D. Ripov, K. Kuc, *Toxicol. Lett.* 212 (2012) 315.
10. M. Wandhammer, M. de Koning, M. Grol, M. Loiodice, L. Saurel, D. Noort, M. Goeldner, F. Nachon, *Chem. Biol. Interact.* (2012) doi: org/10.1016/j.cbi.2012.08.005.
11. M. Eddleston, L. Szinicz, P. Eyer, N. Buckley, *QJM.* 95 (2002) 275.
12. G. S. Andre, M. Kliachyna, S. Kodepelly, L. L. Leriche, E. Gillon, P. Y. Renard, F. Nachon, R. Baati, A. Wanger, *Tetrahedron* 67 (2011) 6352.
13. Z. Rappoport, J. F. Liebman, *The chemistry of Hydroxylamines, Oximes and Hydroxamic Acids*, John Wiley & Sons Ltd. (2009) ISBN: 978-0-470-51261-6.
14. B. B. Narakathu, W. Guo, S. O. Obare, M. Z. Atashbar, *Sens. Actuators B* 158 (2011) 69.
15. J. Kalisiak, E. C. Ralph, J. R. Cashman, *J. Med. Chem.* 55 (2012) 465.
16. Yun Chen, *Neuro. Toxicol.* 33 (2012) 391.
17. G. Mercey, T. Verdelet, J. Renou, M. Kliachyna, R. Baati, F. Nachon, L. Jean, P.Y. Renard, *Acc. Chem. Res.* 45 (2012) 756.
18. A. D. Pinheiro, G. O. Rocha, J. B. Andrade, *Microchem. J.* 99 (2011) 303.
19. J. S. V. Dyk, B. Pletschke, *Chemosphere* 82 (2011) 291.
20. J. Kassa, J. Misik, J. Z. Karasova, *Basic. Clin. Pharmacol. Toxicol.* (2012) doi: 10.1111/j.1742-7843.2012.00897.

21. S. M. Somani and J. A. Romano, *Chemical Warfare Agents: Toxicity at Low Levels*, CRC Press, Boca Raton, New York, London (2001).
22. B. M. Smith, *Chem. Soc. Rev.* 37 (2008) 470.
23. J. M. Collombet, *Toxicol. Applied Pharmacol.* 255 (2011) 229.
24. K. Musilek, M. Komloova, O. Holas, M. Harbinova, M. Pohanka, V. Dohnal, F. Nachon, M Dolezal, K. Kuca; *Eur. J. Med. Chem.* 46 (2011) 811.
25. P. K. Kanaujia, D. Pardasani, V. Tak, A. K. Purohit, D. K. Dubey, *J. Chromatogr. A* 1218 (2011) 6612.
26. M. L. Satnami, S. Dhritlahre, R. Nagwanshi, I. Karbhal, K. K. Ghosh, F. Nome, *J. Phys. Chem. B.* 114 (2010) 16759.
27. K. K. Ghosh, S. Kolay, S. Bal, M. L. Satnami, P. Quagliotto, P. R. Dafonte, *Colloid. Polym. Sci.* 286 (2008) 293.
28. R. A. Moss, H. Zhang, S. Chatterjee, K. K. Jespersen, *Tetrahedron Lett.* 34 (1993) 1729.
29. R. A. Moss, A. T. Kotchevar, B. D. Park, P. Scrimin, *Langmuir* 12 (1996) 2200.
30. S. Bhattacharya, P. V. Kumar, *Langmuir* 21 (2005) 71.
31. S. Bhattacharya, P. K. Vemula, *J. Org. Chem.* 70 (2005) 9677.
32. A. J. Kirby, B. S. Souza, M. Medeiros, J. P. Priebe, A. M. Manfredi, F. Nome, *Chem. Commun.* 12 (2008) 4428.
33. J. B. Domingos, E. Longhinotti, T. A. S. Brandao, L. S. Santos, M. N. Eberlin, C. A. Bunton, F. Nome, *J. Org. Chem.* 69 (2004) 7898.
34. F. Worek, A. Bierwisch, T. Wille, M. Koller, H. Thiermann, *Toxicol. Lett.* 212 (2012) 29.
35. T. S. Ribeiro, A. Prates, S. R. Alves, J. J. O. Silva, C. A. S. Riehl, J. Daniel F. Villar, *J. Braz. Chem. Soc.* 00 (2012) 1.
36. E. Buncel, C. Cannes, A. P. Chatrousse, F. Terrier, *J. Am. Chem. Soc.* 124 (2002) 8766.
37. Birendra Kumar, Manmohan L. Satnami, Kallol K. Ghosh and Kamil Kuca, *J. Phys. Org. Chem.* 25 (2012) 864.
38. S. Tiwari, S. Kolay, K. K. Ghosh, K. Kuca, J. Marek, *Int. J. Chem. Kinet.* 41 (2009) 57.
39. J. Acharya, A. K. Gupta, A. Mazumder, D. K. Dubey; *Toxicol. in Vitro* 22 (2008) 525.
40. C. A. Bunton, G. Savelli, *Adv. Phys. Org. Chem.* 22 (1986) 213.
41. H. Morawetz, *Adv. Catal.* 20 (1969) 341.
42. F. M. Menger, *Pure. Appl. Chem.* 51 (1979) 999.
43. K. Holmberg, *Curr. Opin. Colloid Surf. Sci.* 8 (2003) 187.

44. C. A. Bunton, F. Nome, L. R. Romsted and F. H. Quina, *Acc. Chem. Res.* 24 (1991) 7.
45. G. W. Wagner, Y. C. Yang, *Ind. Eng. Chem. Res.* 41 (2002) 1925.
46. J. M. Beck, C. M. Hadad, *Chem. Biol. Interact.* 175 (2008) 200.
47. K. Kim, O. G. Tsay, D. A. Atwood, D. G. Churchill, *Chem. Rev.* 111 (2011) 5345.
48. C. A. Bunton, Y. Ihara, *J. Org. Chem.* 42 (1977) 17.
49. E. Buncel, C. Cannes, A. P. Chatrousse, F. Terrier, *J. Am. Chem. Soc.* 124 (2002) 8766.
50. X. Han, V. K. Balakrishnan, G. W. VanLoon, E. Buncel, *Langmuir* 22 (2006) 9009.
51. V. K. Balakrishnan, E. Buncel, G. Vanloon, *Environ. Sci. Technol.* 39 (2005) 5824.
52. S. Couderc, J. Toullec, *Langmuir* 17 (2001) 3819.
53. M. Rojas, R. A. Moss, *Chem. Rev.* 102 (2002) 2497.
54. F. Mancin, P. Tecilla, U. Tonellato, *Eur. J. Org. Chem.* 104 (2000) 521.
55. J. Shobhat, D. Balasubramanian, *J. Phys. Chem.* 90 (1986) 2800.
56. F. Mancin, P. Scrimin, P. Tecilla, U. Tonellato, *Coord. Chem. Rev.* 253 (2009) 2150.
57. P. Madaan, V. K. Tyagi, *J. Oleo. Sci.*, 57 (2008) 197.
58. M. V. Bogotian, V. Cimpeanu, C. Deleanu, A. C. Corbu, G. Begatian T. S. Balaban *Arkivoc*, 21 (2005) 272.
59. J. K. Richard, S. Ginsburg, I. B. Wilson, *Biochem. Pharmacol.* 14 (1965) 1471.
60. W. Silwa, *Curr. Org. Chem.* 7 (2003) 995.
61. D. Sutton, N. Nasongkl, E. Blanco, J. Gao, *Pharm. Res.* 24 (2007) 1029.
62. X. Liu, L. Dong, Y. Fang, *J. Surfact. Deterg.* 14 (2011) 203.
63. C. A. Bunton, L. H. Gan, *J. Phys. Chem.* 87 (1983) 5491.
64. R. Fornasier, P. Scrimin, P. Tecilla, U. Tonellato, *J. Am. Chem. Soc.* 111 (1989) 224.
65. Y. S. Simanenکو, V. A. Savelova, T. M. Prokop'eva, V. A. Mikhailov, M. K. Turovskaya, E. A. Karpichev, A. F. Popov, N. D. Gillitt, C. A. Bunton, *Russ. J. Org. Chem.* 38 (2004) 1314.
66. B. Burczyk, K. A. Wilk, *Progr. Colloid. Polym. Sci.* 82 (1990) 249.
67. C. Biresaw, C. A. Bunton, *J. Phys. Chem.* 90 (1986) 5849.
68. R. Fornasier, D. Milani, P. Scrimin, U. Tonellato, *J. Chem. Soc., Perkin Trans. 2* (1986) 233.
69. J. Epstein, J. J. Kaminiski, N. Bodar, R. Eneves, J. Sowa, T. Higuchi, *J. Org. Chem.* 43 (1978) 2816.

70. R. Cibulka, F. Hampl, H. Kotoucova, J. Mazac, F. Liska, *Collect. Czech Chem. Commun.* 65 (2000) 227.
71. H. Kotoucova, R. Cibulka, F. Hampl, F. Liska, *J. Mol. Catal: A* 1 (2001) 3192.
72. R. Cibulka, F. Hampl, J. Smidrkal, F. Liska, *Tetrahedron Lett.* 40 (1999) 6849.
73. I. A. Belousova, I. V. Kapitanov, A. E. Shumeiko, V. A. Mikhailov, N. G. Razumova, T. M. Prokopeva, A. F. Popov, *Theor. Exp. Chem.* 44 (2008) 292.
74. R. Fornasier, P. Scrimin, P. Tecilla, U. Tonellato, *J. Am. Chem. Soc.* 111 (1989) 224.
75. F. Hampl, F. Liska, F. Mancin, P. Tecilla and U. Tonellato, *Langmuir* 15 (1999) 405.
76. S. Cheng, X. Zeng, X. Meng, X. Yu, *J. Colloid Interface Sci.* 224 (2000) 333.
77. S. Bhattacharya, K. Snehalatha, *Langmuir* 11 (1996) 4653.
78. S. Bhattacharya, N. Kumari, *Coord. Chem. Rev.* 253 (2009) 2133.
79. N. Singh, K. K. Ghosh, K. Kuca, J. Marek, *Indian J. Chem. Sec. B.* 51B (2012) 611.
80. N. Singh, K.K. Ghosh, K. Kuca, J. Marek, *Int. J. Chem. Kinet.* 43 (2011) 569.
81. S. Tiwari, K. K. Ghosh, K. Kuca, J. Marek, *J. Phys. Org. Chem.* 23 (2010) 519.
82. S. Tiwari, S. Kolay, K. K. Ghosh, K. Kuca, J. Marek, *J. Int. J. Chem. Kinet.* 41 (2009) 57.
83. U. Tonellato, *Colloids Surf. A* 35 (1989) 121.
84. K. Ogino, K. Shindo, T. Minami, W. Tagaki, T. Eiki, *Bull. Chem. Soc. Jpn.* 56 (1983) 1101.
85. T. Fujita, K. Ogino, W. Tagaki, *Chem. Lett.* (1988) 981.
86. X. Liu, L. Dong, Y. Fang, *J. Surfact. Deterg.* 14 (2011) 203.
87. Russ_J_Org_Chem, 2013, Vol. 49, No. 9, pp. 1291–1299.
88. I. V. Kapitanov, *Theor. Exp. Chem.* 47 (2011) 317.
89. I. V. Kapitanov, I.A. Belousova, M.K. Turovskaya, E.A. Karpichev, T.M. Prokop'eva, A.F. Popov, *Russ. J. Org. Chem.* 48 (2012) 651.
90. Y. S. Sadovskii, T. N. Solomoichenko, M. K. Turovskaya, I. V. Kapitanov, Z. P. Piskunova, M. L. Kostrikin, T. M. Prokopeva and A. F. Popov, *Theor. Exp. Chem.* 48 (2012) 122.
91. I. A. Belousova, E. A. Karpichev, T. M. Prokop'eva, L. V. Luk'yanova, V. A. Savelova, and A. F. Popov, *Theor. Exp. Chem.* 43 (2007) 247.

92. Y. S. Simanenko, E. A. Karpichev, T. M. Prokopeva, A. Lattes, A. F. Popov, V. A. Savelova, I. A. Belousova, *Russ. J. Org. Chem.* 40 (2004) 206.
93. L. G. Qiu, A. J. Xie, Y. H. Shen, *J. Mol. Catal. A: Chem.* 244 (2006) 58.
94. T. M. Zubareva, A. V. Anikeev, E. A. Karpichev, I. V. Kapitanov, T. M. Prokop'eva, and A. F. Popov, *Theor. Exp. Chem.* 47 (2011) 108.
95. A. K. Tiwari, Sonu, M. Sowmiya, S. K. Saha, *J. Mol. Liquids* 167 (2012) 18.
96. D. A. Jaeger and D. Bolikal, *J. Org. Chem.* 50 (1985) 4635.
97. R. L. Salvador, M. Saucier, D. Simon, R. Goyer, *J. Med. Chem.* 15 (1972) 646.
98. R. A. Moss, K. Y. Kim, S. J. Swarup, *J. Am. Chem. Soc.* 108 (1986) 788.
99. I. V Kapitanov, I.A. Belousova, A. E. Shumeiko, M. L. Kostrikin, T. M. Prokop'eva, A.F. Popov, *Russ. J. Org. Chem.* 49 (2013) 1291.
100. M. Ao, G. Xu, Y. Zhu, Y. Bai, *J. Coll. Int. Sci.* 326 (2008) 490.

Наукове видання

НОВІ ТЕНДЕНЦІЇ В СУПРАМОЛЕКУЛЯРНОЇ ХІМІЇ

(англійською мовою)

Збірник наукових праць

Підписано до друку 10.03.2014. Формат 60x84/16. Папір офісний.

Гарнітура Times New Roman. Друк-лазерний. Ум.друк.арк. 24.

Обл.-вид.арк. 25. Тираж 300.

Видавниче підприємство «Східний видавничий дім»
(Державне свідоцтво № ДК 697 від 30.11.2001)
83086, г. Донецьк, вул. Артема, 45
тел./факс (062) 338-06-97, 337-04-80
e-mail: svd@stels.net

О 80 Нові тенденції в супрамолекулярної хімії / [collected research papers]

Edited by V.I. Rybachenko.

Donetsk : «East Publisher House»

Ltd, 2014. – 356 с.

ISBN 978-966-317-208-8

Supramolecular chemistry it is interdisciplinary scientific field. The monograph presents various lines of research in the field of nanotechnology, interaction and self-organization of molecules.

Супрамолекулярная химия это междисциплинарное научное поле. В монографии представлены различные направления исследований в области нанотехнологий, взаимодействия и самоорганизации молекул.

УДК 541.1+547

О 80

